FEASIBILITY OF INDIVIDUALIZED AIRWAY SURGERY IN HORSES

A Thesis Submitted to the College of

Graduate and Postdoctoral Studies

In Partial Fulfillment of the Requirements

For the Degree of Doctor of Philosophy

In the Department of Large Animal Clinical Sciences

University of Saskatchewan

Saskatoon

By

MICHELLE LINDA TUCKER

PERMISSION TO USE

In presenting this thesis in partial fulfilment of the requirements for a Postgraduate degree from the University of Saskatchewan, I agree that the Libraries of this University may make it freely available for inspection. I further agree that permission for copying of this thesis in any manner, in whole or in part, for scholarly purposes may be granted by the professor or professors who supervised my thesis work or, in their absence, by the Head of the Department or the Dean of the College in which my thesis work was done. It is understood that any copying or publication or use of this thesis or parts thereof for financial gain shall not be allowed without my written permission. It is also understood that due recognition shall be given to me and to the University of Saskatchewan in any scholarly use which may be made of any material in my thesis.

Requests for permission to copy or to make other use of material in this thesis in whole or part should be addressed to:

Head of the Department of Large Animal Clinical Sciences
University of Saskatchewan
Saskatoon, Saskatchewan S7N 5B4

OR

Dean
College of Graduate and Postdoctoral Studies
University of Saskatchewan
Room 116 Thorvaldson Building, 110 Science Place
Saskatoon, SK, S7N 5C9, Canada

DISCLAIMER

Reference in this dissertation to any specific commercial products, process, or service by trade name, trademark, manufacturer, or otherwise does not constitute or imply its endorsement, recommendation, or favoring by the University of Saskatchewan. The views and opinions of the author expressed herein do not state or reflect those of the University of Saskatchewan, and shall not be used for advertising or product endorsement purposes.

ABSTRACT

This thesis describes a progressive series of studies that was conducted to investigate the use of benchtop and computational models in the investigation of multiple upper airway surgeries for recurrent laryngeal neuropathy (RLN) in horses. Overall, the objective was to build the knowledge of laryngeal conformation and fluid mechanics with various surgical procedures for application in patients as an evaluation for the surgery of best outcome and as a step toward patient-specific diagnosis and treatment of upper airway disorders.

The first study built upon a previously reported vacuum-based box setup that was used to compare RLN to four different surgical procedures within twenty-eight different equine larynges. Each larynx underwent these procedures in order and inhalation was simulated while measuring resistance to airflow (translaryngeal impedance). Two of the procedures, the combined laryngoplasty, ipsilateral ventriculocordectomy with arytenoid corniculectomy (LLPCOR) and laryngoplasty with ipsilateral ventriculocordectomy (LLP) were found to be significantly different from the RLN, arytenoid corniculectomy (COR) and partial arytenoidectomy (PA). The adapter used to mount the larynges was found to have a significant effect for the RLN, LLP and LLPCOR procedures. There was also a residual intraclass correlation of 27.6% in the final statistical model from individual laryngeal differences which were observed during the study.

The variation of laryngeal features observed during the first study led to questions about the interaction between these geometries and airflow development. To capture the three-dimensional geometry effectively, similar methodology was repeated with concurrent computed tomography (CT) scans. These scans were analyzed focusing on cross-sectional area and changes along the airstream. Each procedural run was analyzed and used to simulate a pipe constriction. Entrance and exit conformations were modeled with respect to the ratio of the inlet cross-sectional area (CSA), constriction CSA and the divergent CSA downstream. The entrance characteristics were found to be significant; specifically, the angle of constriction and the ratio of the larger and smaller areas had a significant effect on laryngeal impedance. A frictional coefficient was measured as a function of energy lost by air passing through the constricted area and was found to be significant. This confirmed the importance of detail in surgically addressing disease affecting the laryngeal entrance. To provide a more thorough analysis of geometry and flow application of computational fluid dynamics (CFD) analysis was next reasonable step.

The next study consisted of CFD analysis of the CT scans to determine the accuracy of CFD in reflecting the findings of the vacuum box airflow model. CFD provides a three-dimensional analysis of flow through complex geometries but also reduces the expense and intensive labor of complex flow experiments. Given these potential applications, this study reported the use of CFD to predict the procedure with the lowest impedance for each larynx. CFD results were compared to the measured values. Additionally, qualitative characteristics of the flow within the anatomical paradigm were examined. The CFD models corroborated the procedure of lowest impedance for 7 out of 10 of the larynges; 2 larynges had 2 procedures that were very close in impedance and the last larynx had unique collapse characteristics that may explain the lack of agreement. The measured pressure and impedance values showed a linear trend compared to the calculated values with measured impedance about 0.7 times that of the calculated (CFD) values. Qualitatively, areas of negative pressure and high velocity were noted in the higher impedance procedures and around tissue irregularities. While the CFD model was reasonably successful for the laryngeal study, demonstration of use in a more realistic equine patient application is needed.

The final study took an additional step toward the equine patient by incorporating an entire head with measured translaryngeal impedance similar to the previous studies. A cadaver head was used and RLN, LLP, LLPCOR, COR and PA were simulated and subjected to negative airflow. The impedance values measured during this study were higher than expected, but the computational model reported values that were similar to the previous literature. The observed flow characteristics showed some differences to previous studies but the CFD model clarified these differences by highlighting the differences in three-dimensional geometry between the heads used in each study. The PA was the lowest impedance procedure both as measured and as calculated. Thus, CFD continued to demonstrate a predictive capability when it comes to determining the procedure of lowest impedance for the whole equine upper airway.

Although there have been a large number of biomechanical models investigating the equine upper airway, they have not kept up with the technological advancements in human respiratory mechanics and CFD. CFD consistently confirmed the procedure of lowest impedance while incorporating individual patient geometry and can be performed much more efficiently than when the first equine application was reported over a decade ago. While more studies are needed, these models unquestionably provide a foundation for individual patient analysis in the future.

ACKNOWLEDGEMENTS

Firstly, I'd like to thank my committee for their persistence in guiding me through this program, Dr. James Carmalt (my supervisor), Dr. David Wilson, Dr. Donald Bergstrom, Dr. James Johnston and Dr. John Harding. Dr. Carmalt has my gratitude for his guidance, expertise and assistance throughout this large body of work, and serving as the sounding board for development of my ideas. It was his completion of a Ph.D. program that inspired me to pursue my own path. Dr. Wilson helped me not only to survive this program but also a global pandemic and held out hope for me when I had none left for myself. I would also like to recognize Arsh Brar who patiently aided my journey in computational fluid dynamics and Dr. Donald Bergstrom who also invested a lot of time and effort to that end. Shawn Reinink in the mechanical engineering department helped with equipment setup and dealt with every malfunction and inconvenience with the utmost of patience. I'd like to thank Drs. John Harding and Cheryl Waldner for serving as my graduate chairs and Dr. Waldner for her help with the statistics.

Drs. Joe Bracamonte, Travis Smyth, and Seiji Yoshimura also have my gratitude for making many of these projects possible by loaning their equipment, time and encouragement. Dr. Bracamonte first planted the idea that I could accomplish this monumental task and encouraged me to persist in finding a way forward even as obstacles presented themselves. He and Dr. Smyth helped me develop the momentum in the early stages that allowed me to forge ahead.

I would like to thank my ever-patient family, my parents John and Linda, and my brother Graham who have supported me in countless ways in pursuing this degree and my residency program. They have stuck with me through well over a decade of academic rigor in the pursuit of my passions. Additionally, so many of my friends have helped carry the burden of late nights and long days through their continued encouragement and advice: Dr. Valentina Ragno, Dr. Jennifer Abi-Younes, Dr. Margot Hayes, Dr. Sarah Khatibzadeh, Dr. Cheryl Ilienko, Dr. Amanda Trimble, Amy Boatman, Britney Ragland and Daniel Wildman Thrasher.

The Townsend Equine Health Research Fund also has my gratitude for providing funding toward this project and also for providing numerous scholarships to myself and other graduate students, easing our burden through this journey. I would also like to thank the clients who so selflessly donated their horses in order that we might be able to better help others. I hope that this work is worthy of their gift.

DEDICATION

"...to Him who is able to do immeasurably more than all we ask or imagine, according to His power that is at work within us."

Eph. 3:20

TABLE OF CONTENTS

PERMISSION TO USE i

DISCLAIMER ii

ABSTRACT iii

ACKNOWLEDGMENTS v

DEDICATION vi

LIST OF TABLES xii

LIST OF FIGURES xiv

LIST OF ABBREVIATIONS xx

CHAPTER ONE: LITERATURE REVIEW 1

1.2 Introduction 2

1.2 Anatomy 2

1.2.1 Laryngeal Anatomy 2

1.2.2 Pharyngeal Anatomy 5

1.3 Physiology 6

1.3.1 General Function 6

1.3.2 Swallowing 7

1.3.3 Airway Mechanics 7

1.4 Recurrent Laryngeal Neuropathy 9

1.4.1 Etiology/Incidence 9

1.4.2 Pathology 10

1.4.3 Diagnosis 12

1.4.4 Surgical Treatments 16

1.4.4.1 Laryngoplasty 16

1.4.4.1.1 Biomechanical Studies (*Ex Vivo*) 17

1.4.4.1.2 Outcomes 18
1.4.4.1.3 Recent Developments 21
1.4.4.1.4 Complications 21
1.4.4.2 Other Procedures 23
1.4.4.3 Partial Arytenoidectomy 23
1.5 Upper Airway Imaging 27
1.6 Airway Fluid Mechanics Models 28
1.6.1 Human Models 28
1.6.2 Canine Models 29
1.7 Computational Fluid Dynamics (CFD) Models 30
1.7.1 Human CFD Applications 30
1.7.2 Canine CFD Applications 33
1.7.3 Equine CFD Applications 35
1.8 Overarching Objectives and Hypotheses 36
CHAPTER TWO: EX VIVO EVALUATION OF ARYTENOID CORNICULECTOMY, COMPARED WITH OTHER AIRWAY INTERVENTIONS, PERFORMED ON CADAVERIC EQUINE LARYNGES WITH SIMULATED RECURRENT LARYNGEAL NEUROPATHY 39
2.1 Abstract 40
2.2 Introduction 41
2.3 Materials and Methods 42
2.3.1 Samples 42
2.3.2 Box Model Construct 42
2.3.3 Simulation of Left RLN 45
2.3.4 Simulation of Airway Interventions 47

2.3.5 Statistical Analysis 47
2.4 Results 48
2.5 Discussion 53
2.6 Acknowledgements 57
2.7 Addendum 57
CHAPTER THREE: COMPUTED TOMOGRAPHIC GEOMETRICAL ANALYSIS OF SURGICAL TREATMENTS FOR EQUINE RECURRENT LARYNGEAL NEUROPATHY 58
3.1 Abstract 59
3.2 Introduction 60
3.3 Materials and Methods 61
3.3.1 Specimens 61
3.3.2 Procedures 61
3.3.3 Statistical Analysis 67
3.4 Results 67
3.5 Discussion 72
3.6 Acknowledgements 77
3.7 Addendum 77
CHAPTER FOUR: COMPUTATIONAL FLUID DYNAMICS ANALYSIS OF UPPER AIRWAY PROCEDURES IN EQUINE LARYNGES 78
4.1 Abstract 79
4.2 Introduction 80
4.3 Materials and Methods 81
4.3.1 Experimental Data and Image Collection 81
4.3.2 Segmentation 83
4.3.3 Numerical Model 85

4.3.4 Boundary Conditions 85
4.3.5 Mesh Independence Study 85
4.3.6 Data Analysis 87
4.4 Results 88
4.4.1 Quantitative Results 88
4.4.2 Qualitative Results 88
4.4.2.1 Pressure 92
4.4.2.2 Velocity 92
4.4.2.3 Turbulent Kinetic Energy 92
4.5 Discussion 98
4.6 Acknowledgements 101
CHAPTER FIVE: COMPUTATIONAL FLUID DYNAMICS ANALYSIS OF AN EX VIVO UPPER AIRWAY MODEL OF THERAPEUTIC SURGERIES FOR EQUINE RECURRENT LARYNGEAL NEUROPATHY 102
5.1 Abstract 104
5.2 Introduction 105
5.3 Materials and Methods 107
5.3.1 Geometry 109
5.3.2 Mesh Independence Study 110
5.3.3 Assumptions 110
5.3.4 Governing Equations 111
5.3.5 Boundary Conditions 111
5.3.6 Numerical Solutions 111
5.3.7 Analysis 112
5.4 Results 112

5.4.1 Quantitative Results 112
5.4.2 Qualitative Results 123
5.5 Discussion 142
CHAPTER SIX: GENERAL DISCUSSION 145
6.1 Introduction/Background 146
6.2 Results: Physical Airway Models 147
6.3 Results: Computational Airway Model 150
6.4 Limitations and Future Research 153
6.5 General Conclusions 154
REFERENCES 156
APPENDIX A: ARTICLE PERMISSIONS 181

LIST OF TABLES

Table 1.1 Resting endoscopic grading system for RLN.....13

Table 1.2 Exercising endoscopic grading system for RLN.....15

Table 1.3 Laryngoplasty outcomes in chronological order.....20

Table 1.4 Partial arytenoidectomy outcomes in chronological order.....26

Table 2.1 Results for laryngeal airflow and pressures and relative laryngeal collapse in 28 cadaveric equine larynges with simulated states of left RLN alone and with subsequent airway interventions (LLP, LLPCOR, COR, and PA) 50

Table 2.2 Summary of the P values determined with the mixed-effects model controlling for repeated measures for each larynx to assess potential differences in results for predicted mean laryngeal impedance stratified by simulated state (RLN state alone and with each of LLP, LLPCOR, COR, and PA) and adapter size (2.54 cm vs 3.81 cm in diameter) for the 28 cadaveric equine larynges tested.....52

Table 3.1 Mean airflow and measured pressures for the RLN disease state and four surgical states (LLP, LLPCOR, COR, PA) 69

Table 3.2 Geometric assessment of larynges under airflow by procedure, reported as a mean and range values 70

Table 4.1 Procedure of lowest impedance for each larynx 90

Table 4.2 Resultant p-values between procedures from the mixed effects statistical model by procedure.....91

Table 4.3 Summary of qualitative results by larynx 97

Table 5.1 Experimental and computational results for pharyngeal pressure (kPa), flow rate (L/s) and impedance (kPa*s/L) by procedure. Tracheal pressure was measured experimentally and used as the boundary condition for the tracheal outlet for the computational model. Note that the procedure of lowest impedance in both instances is PA, in bold.....113

Table 5.2 Experimentally measured and CFD-model rima glottis area by procedure. The experimental rima glottis area was measured from the coinciding CT section while the CFD model rima glottis area was measured using SpaceClaim 114

Table 6.1 Procedure in order of measured impedance from least to most by larynx from the initial box study. Specimens that required the large (1.5") adapter size are in bold.....148

Table 6.2 Procedure in order of measured impedance from least to most by larynx from the second box (CT) study. Specimens that required the large (1.5") adapter size are in bold 151

LIST OF FIGURES

Figure 1.1 The equine laryngeal cartilages. Top right shows the view from the front, while the bottom left on this image represents the side view 4

Figure 2.1 Image of the box construct used in the present study to evaluate 28 cadaveric horse larynges for translaryngeal impedance following simulation of left RLN and subsequent airway interventions (LLP, LLPCOR, COR, and PA). Airflow (blue arrow), measured by the orifice plate, was through the airflow regulation valve and inlet portal, into the test box, through the cadaveric larynx and seated adapter (not shown), through the outlet portal, and through the pipe connected to the orifice plate, oscillating valve, and vacuum. The air pressure was measured separately as the pharyngeal (larger red star) and tracheal (small red star) pressure and the difference (Δ Pressure) taken during analysis. These values were recorded during testing cycles for each larynx, evaluated with a targeted maximum negative tracheal pressure in of –4.3 kPa and a maximum airflow rate of < 70 L/s 43

Figure 2.2 Representative images of a cadaveric horse larynx with simulated left RLN evaluated in the box construct described in Figure 1 in states of LLP at rest (A) and in maximally collapsed RLN alone (B) and RLN with either LLP (C), LLPCOR (D), COR (E), or PA (F). The basic lines and angles of measurements used to determine LQR overlay the image of the LLP state at rest (A) 46

Figure 2.3 Histogram of the predicted mean impedance stratified by adapter diameter (2.54 cm [gray shading] vs 3.81 cm [no shading]) for the 4 airway interventions described in Figure 2 when controlling for individual larynx and relative laryngeal collapse. Bars represent the 95% CI. 51

Figure 3.1 Instrumented box setup in CT. The experimental setup demonstrating the instrumented box in the CT gantry. Airflow in the image proceeded from left to right. PP-point of the "pharyngeal pressure" was measurement, just upstream of the laryngeal opening, TP-point of tracheal pressure measurement, O-orifice plate for airflow measurement, V-vacuum. 63

Figure 3.2 Larynx CT demonstrating cross-sectional areas of interest. CT images of a cadaveric horse larynx in a recurrent laryngeal neuropathy state (left image) that shows convergence and divergence of the airflow pathway as well as corresponding first, second, and third cross-sectional areas where they fall on the axial section (right images). The large arrow at the top of the left image shows the direction of airflow and the rostral aspect of the larynx. A = Right arytenoid cartilage. C = Cricoid cartilage. V = Ventricles 66

Figure 3.3 Conceptual model of a pipe demonstrating areas that reflect those measured in each equine airway. The large arrow at the top denotes the front of the larynx and the direction of airflow for the model. ∅ = Incident angle of the constricted region relative to the long axis of flow. A1, A2, and A3 = First, second, and third measured cross-sectional areas, respectively. D = Width at the most constricted portion of the airway. l = Distance along the long axis between the first and second cross-sectional areas. s = Length of the constriction, used to calculate the dimensionless orifice thickness or s/D 68

Figure 3.4 Predicted mean impedance by procedure, with 95% CIs. RLN = Recurrent laryngeal neuropathy. LLP = Left-sided laryngoplasty with ipsilateral ventriculocordectomy. LLPCOR = Left-sided laryngoplasty with ipsilateral ventriculocordectomy combined with corniculectomy. COR = Corniculectomy. PA = Partial arytenoidectomy.....71

Figure 3.5 Plot of incident angle versus log impedance. 73

Figure 4.1 Larynx in box geometry. The inlet on the left was defined as atmospheric pressure and flow proceeded into the box through the larynx to exit at the pipe outlet defined as the measured negative tracheal pressure 84

Figure 4.2 Planes generated for the independent mesh study and qualitative analysis. Planes in three orthogonal directions were generated in Fluent to analyze the flow characteristics in anatomical and geometrical areas of interest 86

Figure 4.3 Plot of CT versus CFD model derived rima glottis area. The CT-derived area was taken from the coronal plane, the first complete area of tissue. A similar plane was obtained in the 3D geometry in SpaceClaim following processing and the cross-sectional area measured.....89

Figure 4.4 LLP and COR sections inside the left arytenoid cartilage for pressure and velocity. The white region in the plane sections represents the laryngeal tissue, and the colored regions represent the region of airflow. A more gradual transition in pressure and velocity can be observed in the LLP section while the COR section reflects a more obstructive conformation where an abrupt change in pressure and velocity are present. 93

Figure 4.5A Sagittal velocity section (left) and cross-sectional rima glottis section for PA with velocity (right) and pressure (Figure 4.5B). Of particular note is the ventral obstruction in the sagittal image and the region of lower pressure and high velocity inside of the left arytenoid cartilage (on the right side of the cross-sectional images, denoted by the black arrow). 94

Figure 4.5B Cross-sectional rima glottis section for PA displaying the pressure distribution. Of particular note is the ventral obstruction in the sagittal image (Figure 4.5A) and the region of lower pressure and high velocity inside of the left arytenoid cartilage (denoted by the black arrow)...95

Figure 4.6 Dorsal transverse section of PA and three-dimensional rendering of the same larynx, top view. Both images represent a top perspective of the larynx showing increased turbulent kinetic energy downstream from tissue obstruction within the lumen and the three-dimensional rendering showing eddy formation in the same region. 96

Figure 5.1 Final geometrical model and horse head. Point A represents the area just outside of the nostrils where the pressure is atmospheric and there is minimal velocity. Point B is the area of pharyngeal pressure measurement. Point C is the area of surgical manipulation within the airway. Point D is where the tracheal pressure measurement occurs, upstream from the orifice plate and vacuum 108

Figure 5.2A Cross-sectional area along the upper airway by procedure. RLN had the lowest cross-sectional area in the laryngeal region and had the most variability across the cross-sectional areas in general 115

Figure 5.2B Cross-sectional area along the larynx by procedure. RLN has the lowest cross-sectional area at the region of the rima glottis while PA has a larger area through the length of the laryngeal region. The pharyngeal region is similar between procedures.....116

Figure 5.2C Area-averaged pressure along the upper airway by procedure. RLN had the lowest pressure in the region of the laryngeal opening. LLP was the second lowest. The remaining 3 procedures were more similar in their relative distribution. The LLPCOR procedure had increased negative pressure within the caudal portion of the larynx as it transitioned into the trachea 117

Figure 5.2D Area-averaged velocity along the upper airway by procedure. RLN had the highest velocity in the region of the laryngeal opening. LLP was the second highest. LLPCOR, COR and PA were more similar in their relative distribution 118

Figure 5.2E Area-averaged turbulent kinetic energy distribution along the upper airway by procedure. The turbulent kinetic energy was largely similar across procedures except in the caudal laryngeal/tracheal region where the cadaver model had compression of the caudal airway. In general, the pharyngeal and laryngeal regions are areas of increased turbulent kinetic energy as compared to the rest of the airway.....119

Figure 5.2F Area-averaged pressure along the larynx by procedure. As demonstrated with the larger-scale plot, RLN had the lowest pressure at the rima glottis, best characterized as one significant pressure drop across that region. LLP was the second lowest. LLPCOR, COR and PA were more similar in their relative distribution.....120

Figure 5.2G Area-averaged velocity along the larynx by procedure. RLN had highest velocity along the larynx, followed by the LLP procedure. The remaining 3 procedures were more similar in their relative distribution.....121

Figure 5.2H Area-averaged turbulent kinetic energy distribution along the larynx by procedure. Turbulent kinetic energy specifically within the larynx was higher for RLN, with the LLPCOR procedure being the second highest. All of the procedures showed increased turbulent kinetic energy at the laryngeal-tracheal junction.....122

Figure 5.3 Pressure and velocity distribution through the left parasagittal and ventral laryngeal planes for all procedures. Row (A) denotes the parasagittal left slice taken for each procedure while row (B) is the ventral laryngeal transverse section. Pressure is at the top while velocity is on the bottom. Air flows from left to right in the image, with the horse's left side up for the transverse sections, the nostrils to the left and the trachea to the right side of the images.....124

Figure 5.4 Laryngeal opening and mid-saccule cross-sectional planes by procedure. Row (A) denotes the laryngeal opening slice taken for each procedure while row (B) is the mid-saccule section. Pressure is at the top while velocity is on the bottom. These sections are perpendicular to airflow and captured straight on, so that the horse's left side is on the image right.....125

Figure 5.5A Pressure (top row), velocity (middle row), and turbulent kinetic energy (bottom row) for the nostril cross-sections by procedure 126

Figure 5.5B Pressure (top row), velocity (middle row), and turbulent kinetic energy (bottom row) for the mid-pharyngeal cross-sections by procedure 127

Figure 5.5C Pressure (top row), velocity (middle row), and turbulent kinetic energy (bottom row) for the laryngeal opening cross-sections by procedure.....128

Figure 5.5D Pressure (top row), velocity (middle row), and turbulent kinetic energy (bottom row) for the mid-saccule laryngeal cross-sections by procedure 129

Figure 5.5E Pressure (top row), velocity (middle row), and turbulent kinetic energy (bottom row) for the narrowest laryngeal cross-sections by procedure.....130

Figure 5.5F Pressure (top row), velocity (middle row), and turbulent kinetic energy (bottom row) for the caudal laryngeal cross-sections by procedure 131

Figure 5.5G Pressure (top row), velocity (middle row), and turbulent kinetic energy (bottom row) for the tracheal cross-sections by procedure.....132

Figure 5.5H Pressure (top row), velocity (middle row), and turbulent kinetic energy (bottom row) for the sagittal sections by procedure. The coloring is respective to the Figure 5.5A scales ….133

Figure 5.5I Pressure (top row), velocity (middle row), and turbulent kinetic energy (bottom row) for the sagittal sections by procedure. These are enlarged versions of Figure 5.5H, looking specifically at the larynx. The colors correspond to the respective scales in Figure 5.5A 134

Figure 5.5J Pressure (top row), velocity (middle row), and turbulent kinetic energy (bottom row) for the parasagittal sections by procedure. The top three rows are the left parasagittal plane; the bottom three rows are the right parasagittal plane. The colors correspond to the respective scales in Figure 5.5A 135

Figure 5.5K Pressure (top row), velocity (middle row), and turbulent kinetic energy (bottom row) for the parasagittal sections by procedure. The top three rows are the left parasagittal plane; the bottom three rows are the right parasagittal plane. These are enlarged versions of the same planes as Figure 5.5J, focused on the larynx. The colors correspond to the respective scales in Figure 5.5A.....136

Figure 5.5L Pressure (top row), velocity (middle row), and turbulent kinetic energy (bottom row) for the transverse sections by procedure. The top three rows are the mid-nostril transverse plane; the bottom three rows are the mid-pharyngeal transverse plane. The colors correspond to the respective scales in Figure 5.5A 137

Figure 5.5M Pressure (top row), velocity (middle row), and turbulent kinetic energy (bottom row) for the dorsal laryngeal transverse sections by procedure. The colors correspond to the respective scales in Figure 5.5A.....138

Figure 5.5N Pressure (top row), velocity (middle row), and turbulent kinetic energy (bottom row) for the dorsal laryngeal transverse sections by procedure. These are enlarged versions of the same planes as Figure 5.5M, focused on the larynx. The colors correspond to the respective scales in Figure 5.5A 139

Figure 5.5O Pressure (top row), velocity (middle row), and turbulent kinetic energy (bottom row) for the transverse sections by procedure. The top three rows are the mid-laryngeal transverse plane; the bottom three rows are the ventral laryngeal transverse plane. The colors correspond to the respective scales in Figure 5.5A 140

Figure 5.5P Pressure (top row), velocity (middle row), and turbulent kinetic energy (bottom row) for the transverse sections by procedure. The top three rows are the mid-laryngeal transverse plane; the bottom three rows are the ventral laryngeal plane. These are enlarged versions of the same planes as Figure 5.5O, focused on the larynx. The colors correspond to the respective scales in Figure 5.5A 141

LIST OF ABBREVIATIONS

3-D	Three-dimensional
CAD	Cricoarytenoideus dorsalis
CFD	Computational fluid dynamics
CI	Confidence interval
COR	Corniculectomy
CT	Computed tomography
LLP	Left-sided laryngoplasty with ipsilateral ventriculocordectomy
LLPCOR	Left-sided laryngoplasty with ipsilateral ventriculocordectomy combined with corniculectomy
LRQ	Left-to-right angle quotient
MRI	Magnetic resonance imaging
OSAS	Obstructive sleep apnea syndrome
PA	Partial arytenoidectomy
RLN	Recurrent laryngeal neuropathy

CHAPTER ONE:
LITERATURE REVIEW

1.1 Introduction

Obstructive upper airway disorders are complex and challenging across species, from horses to dogs and humans. The upper airway is the area of greatest resistance to airflow with variable levels of turbulence, making it a highly complex area of study. It consists of the inlet through the nares and mouth, leading into the naso- and oro-pharynx, the larynx and finally the trachea, which leads to the lower airways. Humans and dogs can breathe through either the mouth or nose, but the nose is considered preferable due to the filtering, humidification, and immunological functions (Dyce et al., 2010). Horses differ from humans and dogs in that they depend on the nostrils for airflow except in certain disease states which result in air flowing around the soft palate.

Within the same general problem of airway obstruction, each species has different outcome priorities. In the equine industry, athleticism is paramount. In human patients, fatigue, comfort and voice quality are important considerations. The vocal apparatus resides within the upper airway which is also in close proximity to the esophagus and thus complications associated with both of these structures can be anticipated with airway disease and surgical correction. In humans a change in voice quality or mucosal discomfort are considered suboptimal outcomes, while in equine patients, these do not appear to be clinically significant.

Despite these differences, surgical solutions are typically translatable between species. Much research has been devoted to improving patient outcomes from a biomechanical standpoint, with reported success rates of around 60-80% across species (Dinis et al., 2002; Ducharme et al., 2019). The use of advanced imaging and computational methods are contributing to the understanding of these diseases and the anatomical and physiological influences on the rest of the airway.

1.2 Anatomy

1.2.1 Laryngeal Anatomy

The equine larynx is comprised of the epiglottic cartilage, the paired arytenoid cartilages, the cricoid and the thyroid cartilage. These are primarily composed of hyaline cartilage, except the epiglottic cartilage and the corniculate process of the arytenoid cartilage, which are elastic cartilage (Ducharme 2019; Dyce et al., 2010). The junction between the cartilage types can be appreciated on palpation of the corniculate and body of the arytenoid cartilage upon dissection. The epiglottic

cartilage is leaf-shaped and sits in the ventral nasopharynx as the rostral-most cartilage of the larynx. The thyroid cartilage is shield-shaped and wraps in a hemi-circumferential shape along the ventral laryngeal lumen with a prominent, palpable ventral caudal notch that allows surgical access to the lumen through the cricothyroid ligament. The cricoid cartilage, in the shape of a signet ring, bounds the caudal larynx. The arytenoid cartilages are flat in the sagittal plane but have three (two dorsal and one ventral) prominences: the corniculate process rostrally and the muscular process caudally, and the cuneiform process. There are two arytenoid cartilages that are paired, mirror-images of each other **(Figure 1.1)**. An investigation into the mechanical properties of the cricoid and arytenoid cartilages demonstrated that the equine cricoid is composed of relatively stiff hyaline cartilage with an aggregate modulus of 2.29 MPa while the arytenoid body was 0.42 MPa, with the rostral aspect being approximately 20% stiffer than the caudal aspect (Passman et al., 2011). Over time, the cricoid cartilage stiffens, and mineralization of the laryngeal cartilages has been reported as another possible age-related change (Shapiro et al., 1979; Tulleners et al., 1988a; Taturniuk et al., 2009). Additionally, the cricoid cartilage has a relatively straight conformation as compared to other species with a variability of 3-19% reported in one study (Passman et al., 2011). Another study involving strictly Thoroughbred racehorses reported 7-35% variability across dimensions (Dahlberg et al., 2011). As far as the author is aware, this information has not been gathered for the other cartilages within the equine larynx.

The entrance to the esophagus lies dorsal to the larynx in the caudal pharyngeal region, shielded by the palatopharyngeal arch which surrounds the laryngeal opening. The esophageal adventitia is closely associated with the dorsal laryngeal anatomy (Brandenberger et al., 2018). The laryngeal muscles consist of intrinsic and extrinsic groupings. The intrinsic muscles lie between the cartilages and work to move the cartilages relative to each other. These include the cricothyroideus, cricoarytenoideus lateralis, cricoarytenoideus dorsalis, and thyroarytenoideus which are paired muscles, while the arytenoideus transversus muscle is unpaired. The thyroarytenoideus is comprised of separate vocalis and ventricularis components.

Figure 1.1 The equine laryngeal cartilages. Top right shows the view from the front, while the bottom left on this image represents the side view.

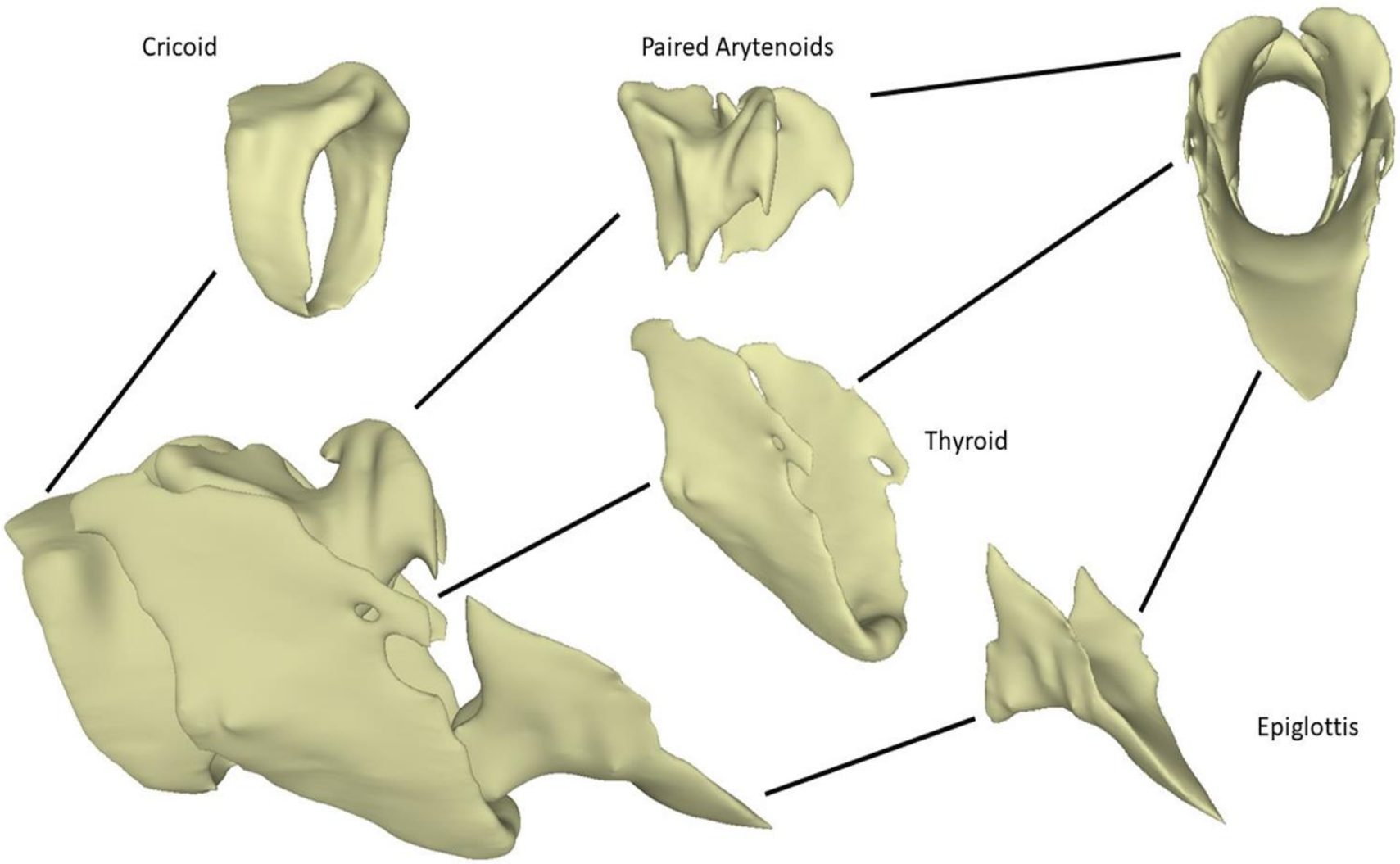

The larynx is innervated by the cranial laryngeal nerve and the caudal recurrent laryngeal nerve. The cranial laryngeal nerve is a direct branch of the vagus nerve and provides innervation to the cricothyroideus muscles and afferent stimulus from mechanoreceptors along the laryngeal mucosa. It is primarily responsible for elevation of the cricoid cartilage to increase the height of the rima glottis, tensing the vocal folds (Reesink et al., 2013). The remaining intrinsic muscles of the larynx are innervated by the recurrent laryngeal nerve, which branches from the vagus nerve distally. On the left it passes around the aortic arch, while on the right side the nerve passes around the right costocervical artery and then courses back up the neck to the larynx (Draper et al., 2018). The cell bodies of the nerve reside in the *nucleus ambiguus* lateral to the medulla oblongata in the brain (Cahill et al., 1986b). The muscles that receive innervation from this nerve are both adductors and abductors of the arytenoid cartilage. The cricoarytenoideus dorsalis (CAD) muscle is divided into two neuromuscular compartments, medial and lateral. The lateral compartment is more effective at increasing the rima glottis area when stimulated (Cheetham et al., 2008a).

The extrinsic muscles of the larynx are the thyrohyoideus, hyoepiglotticus, cricopharyngeus, thyropharyngeus and sternothyroideus. The thyrohyoideus muscle innervation was recently examined with a variety of innervations found between horses, and ranged from direct branches from just the first cervical nerve (C1) and combinations involving variations of an anastomotic branch between C1 and cranial nerve IX (Genton et al., 2021).

1.2.2 Pharyngeal Anatomy

The pharynx is comprised of muscle covered by mucosa and is separated into the oropharynx and nasopharynx by the soft palate, and the laryngopharynx which leads into the larynx (Budras et al., 2008; Dyce et al., 2010). The muscles of the nasopharynx and laryngopharynx originate on the hyoid, pterygoid and palatine bones, and insert on laryngeal cartilages to create these conduits. These are largely dependent upon muscle function to maintain patency. As with the larynx, its muscles are designated as being either intrinsic or extrinsic (Budras et al., 2008; Dyce et al., 2010). The palatine aponeurosis extends rostrally from the hamuli of the pterygoid bones, from the paired ends of the tensor veli palatini muscles (Budras et al., 2008; Dyce et al., 2010). More medially located are the levator veli palatini and the palatinus muscles. The palatinus muscles course laterally to contribute some fibers to the palatopharyngeal arch which can be seen endoscopically at the dorsolateral margins of the equine larynx. The palatopharyngeus muscle attaches on the palatine and pterygoid bones after arising from the palatine aponeurosis. The levator veli palatini extends from the lateral auditory canal

and petrous temporal bone to the dorsal soft palate. The tensor veli palatini originates from the lateral auditory canal, petrous temporal bone and pterygoid bone to support the lateral nasopharynx. The stylopharyngeus completes the intrinsic muscular grouping and has two muscle bellies. One portion originates on the stylohyoid bone and extends to the pharyngeal raphe, while the second portion substantiates the pharyngeal wall lateral to the larynx.

The extrinsic muscles consist of a paired series of muscles that assist in dilating the pharynx when negative airway pressure is experienced at exercise. The paired sternothyroideus, sternohyoideus, hyoepiglotticus, styloglossus, hyoglossus, thyrohyoideus, genioglossus, and geniohyoideus muscles comprise this group (Budras et al., 2008; Dyce et al., 2010).

The pharynx is innervated by branches of the trigeminal, vagus and glossopharyngeal nerves. The hypoglossal nerve innervates the geniohyoideus, hyoepiglotticus, styloglossus and hyoglossus and genioglossus muscles and has been experimentally demonstrated to provide a stabilizing effect on the pharyngeal wall (Cheetham et al., 2009). The mandibular branch of the trigeminal nerve provides sensory afferents to the pharyngeal wall and motor innervation to the tensor veli palatini muscle. The palatinus, palatopharyngeus and levator veli palatini muscles are supplied by the pharyngeal branch of the vagus nerve, which also provides sensory afferents (Budras et al., 2008; Dyce et al., 2010).

1.3 Physiology

1.3.1 General Functions

The nares, ethmoids, and pharynx to the level of the larynx assist in humidification, filtration, olfaction and protection of airflow as it passes down into the lungs. The pharynx and larynx participate in swallowing and maintain a patent airway. They facilitate food and water passage into the esophagus dorsal to the larynx while protecting the lower airways from these materials. Subsequently, some of the complications associated with surgery in this region result in aspiration of food and water due to disruption of the swallowing mechanism. For many years, the association between surgery and aspiration was unclear until the recent recognition of the insertion of the esophageal opening (*vestibulum esophagi*) adventitia on the muscular process of the arytenoid cartilage where surgery is performed. Inadvertent incorporation of, or damage to, the esophageal adventitia in this area is likely a significant cause of postoperative coughing and dysphagia (Brandenberger et al., 2018).

The upper airway also serves an important role in the immunological and functional protection of the lower airways. From a surgical standpoint this is rarely an important consideration, except in cases of infection of the upper airway, or lymphatic structures which become enlarged resulting in compression of the airway. Phonation also occurs within the larynx, via the vocal cords (Budras et al., 2008; Dyce et al., 2010).

The movement of air is the most important feature of the equine upper airway and surgical intervention requires careful evaluation as even small changes in the cross-sectional area may result in large mechanical differences and reduced postoperative outcomes.

1.3.2 Swallowing

The act of deglutition is a carefully orchestrated balance between guiding food and water into the dorsally located esophageal opening and at the same time protecting the ventrally located laryngeal opening. It is a sensitive mechanism requiring coordination of multiple muscle groups, through adequate neurological and mechanical function.

As the food bolus is moved into the caudal oropharynx, the tongue is elevated against the palate by the mylohyoid, styloglossal and hyoglossal muscles. The larynx is drawn rostrally by the hyoid apparatus and the epiglottis retroflexes dorsally. The caudal stylopharyngeus muscle contracts which draws the pharyngeal tissue over the bolus, allowing the cricopharyngeal muscles to initiate peristalsis which will be continued down into the esophagus (Dyce et al., 2010). This process becomes largely reflexive in nature once food has been drawn into the caudal portion of the mouth behind the tongue, and surgery within the laryngeal area has the propensity to disrupt this mechanism.

1.3.3 Airway Mechanics

Horses exhibit extremely high cardiopulmonary capabilities at exercise, especially compared to baseline values. At rest, horses have a resting respiratory rate of 6-14 breaths/minute with a minute ventilation of 67 L. The tidal volume is 5L and the expiratory: inspiratory ratio is 0.96-0.99. Peak inspiratory flow is 3.5 L/s while peak exhalation occurs at 5.7 L/s (Cheetham, 2019). The upper airway provides 80% of the total airway resistance to air movement, and the nares are the narrowest portion of the normal airway. At the larynx, the cross-sectional area is roughly 7% larger than the trachea, but in pathological states, this can become quite narrowed (Rakesh et al., 2008a). At exercise, the tracheal and pharyngeal pressures upon inspiration are negative 40-50 cm H_2O and negative 20-

26 cm H_2O, respectively, while during expiration they are positive at 15-28 cm H_2O and 10-24 cm H_2O in the trachea and pharynx respectively (Ducharme et al., 1994). The negative pressures generated during inspiration partly explain the tendency of the airway to collapse when there is a loss of neurological, or muscular, function.

At exercise, the horse is capable of large adaptations to allow peak performance. Minute ventilation increases to 1800L, tidal volume is 14-18L, and the respiratory rate increases to 120 breaths/min (Butler et al., 1993; Radcliffe et al., 2006) The Reynolds number is a measure of turbulence and indicates whether a given flow is expected to be laminar or turbulent based on the ratio of inertial and viscous forces on the fluid. These are calculated using the dynamic viscosity of the fluid (μ), the density (ρ), the length of the pipe (L), and the average velocity of the fluid (u) as shown below in **Equation 1.1**.

Equation 1.1 $$Re = \frac{\rho u L}{\mu}$$

A value of Re > 2000 is suggestive of turbulent flow, with even higher values representing a higher anticipated turbulent kinetic energy. In the horse, this results in an expected Reynolds number of 100,000 at exercise, indicating highly turbulent flows (Nielan et al., 1992; Rakesh et al., 2008b). At higher gaits such as the canter and the gallop, stride frequency is locked 1:1 with respiration which is thought to contribute to respiratory efficiency (Attenburrow, 1982). In some cases of upper airway abnormality, this ratio shifted to 2:1 (Fitzharris et al., 2015; Weishaupt et al., 1998). In horses, the oxygen consumption per unit body mass at exercise is over three times the amount expected based on the formula used in other mammals and coincides with increased respiratory and cardiovascular capacity (Evans et al., 1988a; Evans et al., 1988b). These changes in mechanics accommodate an increase in metabolism up to forty times the resting rate, which is largely due to tachycardia (Evans et al., 1988a; Thomas et al., 1981). Hemoglobin content of the blood, and by extension, oxygen content increases along with the difference in arteriovenous oxygen (Evans et al., 1988a). These changes were observed in unconditioned horses and a subsequent study demonstrated that conditioning changes cardiac output but does not appear to significantly affect the respiratory parameters that were observed (Evans, et al., 1988b). As an added measure, horses contract their spleen to expel red blood cells, increasing the number in circulation by as much as 50% of the original value and achieving a packed cell volume as high as 63% (Thomas et al., 1981; Weber et al., 1987).

These adaptations are impressive feats of physiologic response and further drive home the unique athleticism that these creatures exhibit.

1.4 Recurrent Laryngeal Neuropathy (RLN)

1.4.1 Etiology/Incidence

Equine RLN is one of the most common upper airway pathologies in the horse, affecting up to 35% of draft breeds, 25% of yearlings and approximately 5-10% of adult Thoroughbreds. one retrospective study of horses presenting for treadmill videoendoscopy, 65 out of the 192 horses with abnormalities were diagnosed with RLN (Tan et al., 2005). In horses presented to a referral center for poor performance, 42.6% (148 of 348 horses) had upper airway collapse with 34 horses having left arytenoid collapse on videoendoscopic exam (Martin et al., 2000). In another study of 744 Australian Thoroughbred racehorses examined following their race, 6.3% (47 horses) had upper airway abnormalities of which 1.6% exhibited laryngeal asymmetry (Brown et al., 2005a). It should be noted that this pool of horses was collected post-race and therefore represent horses that were performing well. One of the challenges of diagnosis is that there are varying degrees of severity of the disease, which is discussed in more detail below **(Section 1.4.3)**. Another study from New Zealand observing young racehorses (Thoroughbreds and Standardbreds) found a much higher prevalence of abnormalities, with 384 out of 452 horses displaying adequate arytenoid function upon the initial examination (Anderson et al., 1997). Subsequent examinations were performed with 29% receiving a better grade, and 28% worsening in the arytenoid function observed endoscopically at an exam performed at least 16 months later. This cohort of horses consisted of 2-4-year-old horses (Anderson et al., 1997). The potential for change in severity from one exam to the next creates uncertainty in the reported prevalence. The report of Thoroughbred yearlings where 25% had clinically important deficits has not been corroborated in older horses which suggests that some yearlings improved. Additionally, this disease may be underrecognized in some disciplines where a lesser severity of disease may not affect performance in a clinically significant manner. For example, the prevalence of the disease in jumping horses remains largely unreported as only the most severe cases will present clinically.

Multiple causes of RLN in horses have been documented, but the most common etiology is idiopathic (i.e. unknown) in 94% of cases. Some cases have resulted from trauma to the nerve due to physical or chemical disruption resulting in degeneration of the axon. The left recurrent laryngeal

nerve is longer than the right, which is thought to be associated with the prevalence of left-sided disease. Progression of the disease has been observed over time (Brakenhoff et al., 2006; Dixon et al., 2002). Hyperkalemic periodic paralysis, thiamine deficiency, and lead poisoning have been reported, while local damage, stretch and pressure causing nerve ischemia have been suspected in other cases (Carr et al., 1996; Loew et al., 1973; Rooney et al., 1970). Bilateral laryngeal paralysis has also been observed following anesthesia and may have been the result of patient positioning, but this seems unlikely (Dixon et al., 1993). Suspected organophosphate toxicity in four Thoroughbreds resulted in delayed bilateral laryngeal paralysis. Other neurological effects were also observed such as phrenic and digital nerve changes in one of the horses and spinal cord changes in two of the others (Duncan et al., 1985). This occurred three weeks following an acute gastrointestinal illness, but no other signs were observed. Finally, advanced liver disease has also been associated with the bilateral form of the disease (McGorum et al., 1999).

RLN is known to have a genetic predisposition, given different prevalence across breeds. Within a cross-sectional study of draft breeds, Belgian horses had a prevalence of 46%, Percherons 31%, and Clydesdales were the lowest at 17% (Brakenoff et al., 2006). More recently, a genetic locus, *LCORL/NCAPG*, was found on equine chromosome (ECA) 3 that is also associated with body size in horses (Boyko et al., 2014). Additionally, in draft horses a sex-specific localization was found on ECA15 for RLN (Brooks et al., 2018). The heritability is 0.4-0.61 and has been shown to correlate with a narrowed intermandibular space, with some evidence that RLN may be genetically eliminated from some breeds of horses (Gerber et al., 2015). This narrowed intermandibular space hypothesis is thought to originate from the time of the oral history of ancient Bedouin tribes and correlates with a smaller diameter airway (Cook, 1988). Surprisingly, zebras do not exhibit clinical or histological evidence of recurrent laryngeal neuropathy despite displaying some asymmetry between the left and right CAD muscles which would further point to genetic inheritance through human selection (Hahn et al., 2000).

1.4.2 Pathology

RLN is a bilateral mononeuropathy primarily affecting the left recurrent laryngeal nerve (Draper, 2018). The left nerve is the longer than the right, travelling from the base of the brain with the vagus nerve down the jugular furrow to branch off and encircle the aortic arch and then passing again through the neck up to the level of the larynx **(see Section 1.2.1)**. This pathway causes the ascending portion of the nerve to be relatively exposed within the jugular furrow of the neck. As a

result of this precarious anatomical position, recurrent laryngeal hemiplegia has been reported secondary to extravasation (leakage) of irritating substances into local tissues after injection of the jugular vein. Similarly, there is a risk of nerve laceration, injury during vascular injection, or damage secondary to local inflammation of the vein itself.

The histologic studies of horses affected with RLN would suggest that Wallerian degeneration occurs at the distal aspect of the nerve and proceeds proximally. Evidence of demyelination has been consistently observed across multiple studies (Cahill et al., 1986a; Duncan et al., 1974; Duncan et al., 1991). Additionally, it is known that the adductor muscle-innervating branch of the recurrent laryngeal nerve loses medium and large myelinated fibers first. These fibers could be explained by the increased length of these fibers which are about 5-7 cm longer than the nerves supplying the abductor muscles (Duncan et al., 1991). Degeneration has been documented within the central nerve fibers characterized by a consistent finding of axonal spheroids in the lateral cuneate nuclei in affected horses, without changes in the *nucleus ambiguus.* However, age was a significant confounding factor in this study as some of these findings can be a function of age alone, and not necessarily disease-dependent (Cahill et al., 1986b; Draper et al., 2018).

Nerve degeneration has been documented as early as two weeks of age in a population of male draft foals and may even suggest prenatal changes (Duncan, 1992). This finding was also supported by histopathologically-observed muscle changes (Duncan, 1992). There appears to be a cycle of denervation and re-innervation that characterizes the subclinical cases that have been examined (Cercone et al., 2019; Rhee et al., 2009a).

The pathophysiology of this disease ultimately results in decreased ventilation, increased lactate concentrations in the peripheral blood, and decreased performance (Christley et al., 1997). The larynx is already an area of increased resistance in the upper airway due to the slight narrowing compared to the pharynx. This narrowing results in increased velocity of air to maintain the volumetric mass flow. Higher velocity causes a more negative pressure, which encourages collapse of the structures. The cartilaginous and muscular structures become more important in maintaining patency, and when the CAD muscle becomes paralyzed, the left arytenoid cartilage collapses into the airway, but it is also “pulled” into the airway by the negative pressure within the lumen. The resultant collapse causes a more narrowed region within the larynx, necessitating increased velocities to maintain a similar volumetric flow, and more negative pressure development. The cross-sectional area becomes too narrow to support the airflow needed to maintain oxygenation at peak exercise, the

horse tires as peripheral blood lactate climbs with anaerobic respiration, and the horse ultimately fades down the track. Decreased performance and /or exercise intolerance is one of the most common complaints associated with RLN in racehorses.

1.4.3 Diagnosis

As RLN is a progressive disease, varying severities of the disease may be present which led to the development of a grading system for consistency between examiners and establishment of treatment guidelines. Multiple grading schemes were developed simultaneously which led to some controversy as to when the disease becomes performance-limiting and requires surgical intervention. This is typified by the disagreement surrounding the situation when asymmetry and asynchrony can be observed, and yet enough function remains to fully abduct the cartilage.

The most common and reliable method of diagnosis of RLN is videoendoscopy to directly observe the level of abduction of the arytenoid cartilage. Most grading systems use the right arytenoid cartilage position and movement for comparison. Initially, a simple 4-grade system was reported that used synchronicity and capability of left arytenoid abduction as criteria for categorization (Dixon et al., 2004; Rakestraw et al., 1991). This evolved into a 6-grade system that included 0 and 1 grades as normal to account for left arytenoid cartilages that “shivered”. It also further separated horses with asymmetry from horses with severe paresis, as these were previously within the same grade (Dixon et al., 2001). A 5-grade system was also simultaneously implemented among veterinarians in a different region to categorize 3,497 yearlings and was reported in the Havemeyer workshop proceedings (Lane et al., 2004). This workshop in 2004 resulted in the global consensus grading scheme for equine RLN for the standing endoscopic exam which is shown in **Table 1.1** (Dixon et al., 2004; Rakestraw et al., 1991).

Table 1.1 Resting endoscopic grading system for RLN. Havemeyer workshop consensus compiled from multiple grading systems developed over time (Dixon et al., 2004).

Grade	Description	Subgrade	Description
I	All arytenoid movements are synchronous and symmetrical; full arytenoid abduction can be achieved and maintained.		
II	Arytenoid cartilage movements are asynchronous and/or larynx is asymmetric at times, but full arytenoid cartilage abduction can be achieved and maintained.	A	Transient asynchronous flutter or delayed movements are seen.
		B	There is asymmetry of the rima glottidis much of time owing to reduced mobility of the affected arytenoid cartilage and vocal fold, but there are occasions typically after swallowing or nasal occlusion when full symmetrical abduction is achieved and maintained.
III	Arytenoid cartilage movements are asynchronous and/or asymmetric. Full arytenoid cartilage abduction cannot be achieved and maintained.	A	There is asymmetry of the rima glottidis much of the time owing to reduced mobility of the affected arytenoid cartilage and vocal fold, but there are occasions, typically after swallowing or nasal occlusion, when full abduction is achieved but not maintained.
		B	There is obvious arytenoid abductor muscle deficit and arytenoid cartilage asymmetry. Full abduction is never achieved.
		C	There is marked but not total arytenoid abductor muscle deficit and arytenoid cartilage asymmetry with little arytenoid cartilage movement. Full abduction is never achieved.
IV	Complete immobility of the arytenoid cartilage and vocal fold.		

A surgically relevant diagnosis of upper airway disease, and specifically RLN, is complicated. One study showed that 49% of the horses that had a normal standing videoendoscopic examination had abnormalities when repeated on a treadmill. However, 23% of horses diagnosed with grade II or III RLN on the resting exam were normal during the moving exam (Tan et al., 2005). These are contradictory findings as to whether the standing or treadmill dynamic exam is a more reliable measure of diagnosis. In another study of Standardbred and Norwegian Coldblooded Trotters, a large number of upper airway collapsing disorders were observed during treadmill videoendoscopy, of which only 25% were definitively diagnosed during the resting exam and 10.3% of them were diagnosed with RLN (Strand et al., 2012). A recent meta-analysis of the resting endoscopic exam found that it is 74.4% sensitive and 95.1% specific for predicting the presence of RLN at exercise (Elliott et al., 2019).

With the advent of dynamic over-ground endoscopy, in which the horse has the airway examination performed in its natural performance environment rather than on the treadmill, the classification scheme has further evolved to account for discrepancies observed between the standing endoscopic exam and dynamic exam. The standing exam lends some possibility to predict the dynamic exam findings in the cases of severe disease but more mild forms can be missed. An additional grading system was developed for dynamic endoscopy as for standing, reported in **Table 1.2** (Dixon et al., 2004; Rakestraw et al., 1991). Additionally, the complicated nature of upper airway diseases has become more apparent as we have come to recognize concurrent problems, such as aryepiglottic fold collapse, overlap of the dorsal corniculate processes, epiglottic retroversion, and intermittent soft palate displacement. These may occur together in various combinations and may manifest in a more obvious manner following surgery.

Transesophageal ultrasound has been investigated to assess early changes in CAD muscle volume and was strongly correlated with CAD muscle thickness at the midbody, however it may not be reliable at the individual level (Kenny et al., 2017). Use of ultrasound may allow correlation of size and echogenicity prior to neuromuscular deficits being observed endoscopically (Chalmers et al., 2015; Kenny et al., 2017).

Table 1.2 Exercising endoscopic grading system for RLN. Havemeyer workshop consensus developed by multiple experts in equine upper airway disease (Dixon et al., 2004).

Grade	Description
A	Full abduction of the cartilages observed during inspiration
B	Partial abduction of the left arytenoid cartilage between resting and full abduction positions
C	Abduction less than resting position; may cross the sagittal plane into the contralateral rima glottidis

1.4.4 Surgical Treatments

1.4.4.1 Laryngoplasty

The laryngoplasty was first reported in the English-speaking literature in 1970 as a treatment for RLN by using a suture to replace the function of the CAD muscle (Marks et al., 1970). The approach consists of a 10 cm longitudinal incision along the ventral aspect of the jugular furrow followed by dissection between the fascial planes dorsal to the omohyoideus and deep and ventral to the sternomandibularis muscles to the level of the larynx. During this approach the first cervical nerve is often encountered in the fascia between the linguofacial vein and omohyoideus muscle (Rossignol et al., 2018). The fascia above the cricopharyngeus and thyropharyngeus muscles can be dissected, creating a space dorsal to the larynx and extending caudally beyond the caudal aspect of the cricoid cartilage. The cricopharyngeus and thyropharyngeus muscles can be separated along the fascia in a dorsoventral plane. This allows exposure of the muscular process of the arytenoid cartilage. The suture bite in the cricoid cartilage should be placed medial to the notch, approximately 8 mm lateral to the sagittal ridge of the cartilage. Placing the bite medial to the notch helps to prevent lateral slippage which can result in laxity of the suture post-operatively, and decreased abduction of the left arytenoid cartilage over time (Dahlberg et al., 2011). A second bite is taken through the cricoid cartilage, 4 mm lateral to the first bite. Alternatively, a metallic button has been used to anchor the suture by threading the button onto the suture and passing both ends through the cricoid cartilage from ventral to dorsal simultaneously.

The arytenoid suture bite can be placed dorsoventrally or from the caudomedial to craniolateral direction through the muscular process of the arytenoid cartilage. As has been recently reported, the vestibulum esophagi lies close to the muscular process and the adventitia should be dissected free to avoid postoperative dysphagia and coughing (Brandenberger et al., 2018). The CAD tendon is transected by some surgeons to allow greater manipulation for suture bite placement, and to allow exposure for debridement of the cricoarytenoid joint for facilitated ankylosis. If two sutures are placed, one is placed more medial and dorsal, while the other is placed more lateral. Placing the suture dorsally has been shown to result in a greater level of abduction with the same level of applied force (Bishofberger et al., 2013). Additionally, a suture anchor may be used to provide greater mechanical advantage so that less force is required to achieve a similar level of abduction (Ahern et al., 2017). A Jamshidi needle has used to create a tunnel in the muscular process of the arytenoid

cartilage and the Scorpion Multifire ® laparoscopic device has been used in the cricoid cartilage when performing the standing laryngoplasty (Rossignol et al., 2015).

In addition to the laryngoplasty, a concurrent vocal cordectomy, ventriculectomy or ventriculocordectomy is frequently performed as it is thought to further increase the airflow through the larynx or to reduce noise. Multiple experimental studies have induced RLN in horses and then performed one of these additional procedures to attempt to decrease resistance as standalone procedures. Ventriculocordectomy under general anesthesia via laryngotomy was shown to reduce the level of certain sound formants and improved (decreased) the translaryngeal pressure drop caused by RLN, however it did not return the values to baseline (Brown et al., 2003). Laser-assisted left vocal cordectomy similarly improved the pressure drop but did not improve the noise made by horses after surgery (Brown et al., 2005b). In contrast, a later study of laser-assisted ventriculocordectomy found more promising results with exercise intolerance improving in 8 of 10 horses (Henderson et al., 2007) The use of ventriculectomy, vocal cordectomy and ventriculocordectomy have been advocated primarily as they reduce the number of collapsible structures in the airway. Additionally, their removal may facilitate prosthetic laryngoplasty by achieving greater abduction with lower suture tension (Perkins et al., 2011). However, there has been a recent recognition that removal of these structures may increase the likelihood of postoperative dysphagia and aspiration (Leudtke et al., 2020).

1.4.4.1.1 Biomechanical Studies (*Ex Vivo*)

Biomechanical testing associated with different suture material, bite placement in the cricoid and arytenoid cartilages, and suture retention have all been performed for the laryngoplasty procedure. #2 Ethilon, #5 Ethibond, Fiberwire, Fibertape, and #5 Ticron have all been biomechanically investigated (Ahern et al., 2010; Markwell et al., 2016). #5 Ethibond was found to have less cartilage fissure formation and less displacement than Fiberwire but the commercially supplied needle may have contributed to cartilage weakening before failure (Ahern et al., 2010). A separate study compared braided polyurethane elastomer (Lycra®) to #5 Ethibond and found that the elastomer pulled through the arytenoid cartilage muscular process more frequently and had greater displacement despite having a greater suture loop strength (Willsallen et al., 2015). Kelly et al. (2008) reported six separate biomechanical configurations of the suture construct with greater than 50% of failures occurring at the muscular process of the arytenoid cartilage and found that incorporating the spine of the arytenoid muscular process is mechanically stronger. For suture bite placement, a bone trocar,

trocar needle, and 16-gauge needle resulted in the same cartilaginous fissures that were observed with the curved trocar point needle (Boswell et al., 2000; Rossignol et al., 2006). The plastic sternal closure ZipFix® system was also shown to weaken the cartilage where the suture bite was placed, and had lower construct strength, despite the material being mechanically superior to suture (Markwell et al., 2016). A metal washer and steel cable were also tested against #5 polyester suture (Dagrofil) resulting in a much higher failure load but continued failure of the arytenoid muscular process over the cricoid cartilage was observed (Schumacher et al., 2000). Given these findings, various other strategies have been used for suture placement in the muscular process of the arytenoid cartilage and the cricoid cartilage, such as the FastTak® anchor system (Ahern et al., 2017). For the cricoid cartilage, a U-shaped bite, a metallic button, and a double-loop construct have also been investigated using cyclical testing with Fiberwire, Ethibond and Ethilon suture; a metallic button with Fiberwire suture was found to reduce loss of abduction and increase pull-out forces (Brandenberger et al., 2017).

The angle and level of force necessary to achieve, and maintain adequate abduction, has also been examined. A force of 11.86 N at angles of 0-30° relative to the lateral margin of the muscular process of the arytenoid best replicated the lateral muscle belly of the CAD muscle (Cramp et al., 2009). This study was the first to show that the level of abduction did not improve over 14.7 N for one suture. This is lower than 37.86 N which was reported by Lynch et al. (2020) but may be a function of the angle of suture placement within the larynges. Clamping of the arytenoid cartilage prior to tightening the suture was also tested, with no improvement in the level of abduction after cyclical testing (McClellan et al., 2014).

A dynamic laryngoplasty system has been reported using an inflatable balloon to adjust the laryngoplasty postoperatively, in an attempt to re-establish lost abduction (Ahern et al., 2018). This method demonstrated increased arytenoid abduction with increasing activation of the device and decreased translaryngeal impedance with increasing abduction when subjected to airflow (Ahern et al., 2018; Ahern et al., 2019). This system has not been tested in live patients to date.

1.4.4.1.2 Outcomes

Outcomes of the laryngoplasty procedure have been reported by various authors over the past 50 years, however variations in assessment of outcome prevent direct comparison between studies. Carpenter et al. (2009) reported that 84% of the horses that raced prior to surgery were able to return, with 62% of Thoroughbreds increasing their distance per start. Another report considered the

satisfaction of the clients with the procedure and reported a high positive outcome at 93% (Barnett et al., 2013a). This may suggest that clients are more satisfied with the surgical outcome than the postoperative assessment would predict, as in another report only 59% of Thoroughbreds had a reported improvement of performance index (Carpenter et al., 2009). Also, despite the high client satisfaction, repeat endoscopy demonstrated that 6 out of 41 horses had contamination of the trachea with food, while 2 had mucus (Barnett et al., 2013a). 78% of the horses had abnormalities at exercise such as axial deviation of the aryepiglottic fold and vocal fold collapse. Palatal dysfunction was also observed in 24% of horses at rest and 56% of horses at exercise which was not recognized preoperatively and suggests that this may occur as a sequala to laryngoplasty (Barnett et al., 2013a). This same group also demonstrated that lower levels of arytenoid abduction were less likely to be associated with coughing and dysphagia with less loss of abduction postoperatively (Barnett et al., 2013b). Evaluations were performed 6 weeks following surgery with 42% losing 1 grade of abduction, 27% two grades and 6% three grades (Barnett et al. 2013b). National Hunt racehorses were found to lose a grade of abduction by 6 days post-op in 41% of cases with even further loss at six weeks (Barakzai et al., 2009b). However, grade of postoperative abduction was not found to be significantly associated with performance. A summary of laryngoplasty assessment papers demonstrating the success rates reported through time can be found in **Table 1.3**.

A box construct was used in the above study to test the mechanics of airflow through equine larynges. Jansson et al. (2000) first demonstrated that a box with generated airflow can replicate the translaryngeal impedance previously reported in horses on a treadmill (Cheetham et al., 2008c). It also demonstrated that the cordopexy alone was not effective in improving impedance; and cordopexy with laryngoplasty was not significantly different from laryngoplasty alone (Jansson et al. 2000). The box model was further validated for running horses with cyclical flow, demonstrating similar pressures and flows to those reported for horses at exercise (Cheetham, et al., 2008c). This model has been used since to examine the effects of cricoarytenoid joint ankylosis via carbon dioxide laser and the effects after time to heal as well as the immediate in vitro effects of PMMA on the cricoarytenoid joint (Cheetham et al., 2008b; Hawkins et al., 2014). This model has some recognized limitations but has been well-established as an in vitro method for determining the improvement of translaryngeal impedance.

Table 1.3 Laryngoplasty outcomes in chronological order.

First Author	Year	Outcome Measure	Procedure	Success Rate	Population	#	Additional Findings
Speirs	1972	Return to racing	LP +/- VC	75%	Not Reported	8	
Goulden	1982	Reassessment/ owner questionnaire	LP/modified LP	44%	Standardbred, Thoroughbred racehorses, other breeds	68	
Bohanon	1990	Owner satisfaction	VeC +/- LP	87% VC alone	Draft breeds	21	
Russell	1994	Owner/Trainer satisfaction	LP w/bilateral VeC	60%	Variety of breeds, mixed workload	55	
Hawkins	1997	Racing performance	LP +/- VeC	77% returned to racing, 56% improved	Thoroughbred and Standardbred racehorses	176	81% owner satisfaction, 43 coughing, 26 nasal discharge
Strand	2000	Performance Index, racing	LP w/ bilateral VeC	94% made one start	Thoroughbred racehorses	52	Inexperienced horses performed better after surgery
Davenport	2001	Owner survey	LPw/ VCC	50% improved, 71% started	Thoroughbred racehorses	38	
Kidd	2002	Owner testimony	LP w/ VC, VeC	70%	Variety of breeds, mixed workload	80	
Kraus	2003	Exercise tolerance	LP w/ VC, VeC	92%	Draft breeds (hitch horses)	104	
Dixon	2003b	Owner survey	LP w/ VCC	91% full work	Variety of breeds, mixed workload	200	Noise less present in sport horses (76%) than racehorses (60%)
Barakzai	2009a	Individual Earnings	LP w/ VCC	78% raced, 47% improved	National Hunt racehorses	71	shorter career longevity, stainless steel implants
Witte	2009	Return to racing	LP w/ VC	68-72%	Thoroughbred racehorses	90	
Carpenter	2009	Racing/return to racing	LP w/ VC	73-84%	Thoroughbred and Quarterhorse racehorses	72	

LP-laryngoplasty, VeC-ventriculectomy, VC-vocal cordectomy, VCC-ventriculocordectomy, #-number of cases reported per study

1.4.4.1.3 Recent Developments

The standing (awake) laryngoplasty has been another landmark development in the treatment of RLN. Horses are heavily sedated, and aseptically prepared for surgery to allow the procedure to be performed standing. Local anesthesia is accomplished via local injection over the incision site or by performing a nerve block of the ventral branch of the second cervical nerve emerging from the first and second cervical vertebral junctions (Campoy et al., 2018; Rossignol et al., 2015). These can be located via ultrasonographic guidance within the fascial plane between the longus capitis and cleidomastoideus muscles (Campoy et al., 2018). An additional line block is performed caudal to the incision in the dorsoventral plane to block the third cervical nerve which supplies some sensory innervation to the area. This approach avoids the complications of general anesthesia (see below in section 1.4.4.1.4) during recovery and allows the surgeon to better determine if adequate abduction is being attained. Recumbent anesthesia necessitates use of an endotracheal tube which can obfuscate the observation of the arytenoid abduction as tension is applied to the laryngoplasty suture.

1.4.4.1.4 Complications

Reported complications of the laryngoplasty procedure include coughing, which can occur in up to 40% of cases, dysphagia, loss of abduction, chondritis, and over-abduction. Approximately 17% of horses required revision of the surgery due to over-abduction or under-abduction, which can increase the probability of postoperative infection or colic due to a second surgical event (Dixon et al., 2003a). Over-abduction can result in dysphagia with aspiration pneumonia and this can lead to decreased performance, even death (Barakzai et al., 2015). Increased lower airway inflammation has been noted in horses post-laryngoplasty, in addition to the partial arytenoidectomy, which suggest that both surgeries negatively impact lower airway health (Radcliffe et al., 2006). Coughing has been reported as a complication of laryngoplasty and was reported in 26% of horses, incisional seroma occurred in 7%, and incisional infection was present in 2% of horses in one study that reported on 230 racehorses undergoing laryngoplasty with or without ventriculectomy (Hawkins et al., 1997).

Chondritis has been reported postoperatively and is suspected to occur secondary to intraluminal penetration and subsequent infection. The presence of the suture material in the surgical site makes this surgery particularly prone to infection and thus strict asepsis should be maintained. Observing suture bites via an endoscope placed just outside the larynx will assist in identifying penetration of the laryngeal or tracheal lumen, in which case the suture can be replaced. Frequently,

a concurrent ventriculocordectomy or ventriculectomy is performed and there was concern about whether these incisions should be closed following surgery. Primary closure did not result in a significantly increased complication rate, but the use of suture for skin closure was 7.9 times more likely to become infected compared to staples (Lindegaard et al., 2016). Fistula formation has also been observed six months to three years following laryngoplasty which was suspected to have formed secondary to the use of elastic material and complicated removal due to the brittle nature of the material (Bienert-Zeit et al., 2014). Suture pull-through in the muscular process of the arytenoid cartilage can also be very serious. One case of potential contamination that resulted in muscular process pull-through revealed necrosis, granulation tissue and inflammation. Spontaneous failure of the prosthesis ultimately resulted in patient death during a subsequent anesthetic recovery with associated cardiomyopathy, pulmonary congestion, edema and hemorrhage (Hardcastle et al., 2012).

Concern about the tension and possible failure of the suture has led to studies about the tension that develops from swallowing or coughing. Witte et al. reported on the effects of coughing and swallowing on the laryngoplasty suture based on the force that the suture experiences (Witte et al., 2010a; Witte et al., 2010b). 19 N was experienced in the stall with spontaneous swallowing while 26 N occurred with induced swallowing; 12 N occurred with coughing. Coughing and spontaneous swallowing were not significantly different but spontaneous and induced coughing caused significantly different force levels on the suture, however the previously discussed biomechanical studies would suggest that these physiological functions are not a significant cause of suture failure or pullout. Fusion of the cricoarytenoid joint to reduce tension on the prosthesis has been performed with a CO_2 laser which resulted in greater maintenance of abduction when the larynges were mechanically tested postoperatively (Parente et al., 2011). Additionally, polymethylmethacrylate (PMMA) injected into the cricoarytenoid joint reduced the force on the laryngoplasty suture when tested under dynamic airflow and maintained arytenoid abduction under negative airflow when the laryngoplasty suture was cut (Cheetham et al., 2008b; Witte et al., 2010b).

Dorsal displacement of the soft palate has been recognized with increased frequency in horses undergoing laryngoplasty for RLN. In one study, 46% of the horses examined with dynamic endoscopy following laryngoplasty had DDSP at exercise, and 17% at rest (Barnett et al., 2014). Disruption of the cranial laryngeal nerve branch within the cricopharyngeus and thyropharyngeus muscle aponeurosis was theorized to cause this complication, but there were some horses where the aponeurosis was not disrupted during the surgery (Barnett et al., 2014). Right RLN has been reported

following a left laryngoplasty in a colt following intense vocalization which resulted in pulmonary edema and necessitated an emergency tracheotomy. The right RLN resolved spontaneously within six weeks (Canada et al., 2017).

In horses undergoing general anesthesia for a laryngoplasty, routine complications that are common to any surgical procedure may occur. During the procedure hypoxemia, hypoventilation, hypothermia, and hypotension and even death may occur. During or following recovery from general anesthesia spinal myelopathy, myopathy, peripheral neuropathy, colic, and catastrophic fracture may occur which have not been reported in the same frequency in standing procedures (Ducharme et al., 2019; Rossignol et al., 2015).

1.4.4.2 Other Procedures

As the laryngoplasty is continually modified, another surgical option for young horses includes reinnervation of the CAD muscle using a nerve muscle pedicle graft or a nerve implantation (Ducharme et al., 1989; Fulton et al., 1991). A neuroprosthesis has also been proposed to regain function in some horses with some functioning nerve still present (Cheetham et al., 2011; Ducharme et al., 2010). A nerve-muscle pedicle graft has also been proposed employing the first cervical nerve or the spinal accessory nerve in an attempt to-reinnervate the left dorsal cricoarytenoid muscle. The lateral belly is recommended based on the angle and force to achieve abduction (Cramp et al., 2009). Additionally, new methods of address postoperative dysphagia have been reported, such as vocal fold bulking and esophageal release (Ludke et al., 2020).

1.4.4.3 Partial Arytenoidectomy

The subtotal and partial arytenoidectomy procedure have also been reported as a treatment for RLN (Speirs, 1986). The subtotal arytenoidectomy removes the arytenoid body while leaving the muscular process and corniculate processes intact within the patient. Clinically however the subtotal arytenoidectomy was found to have decreased improvement of laryngeal impedance and was no longer used in clinical patients thereafter (Belknap et al., 1990). This result could have been anticipated given that the corniculate process of the arytenoid cartilage tends to collapse into the upper airway with RLN.

The partial arytenoidectomy differs from the subtotal in that it involves removal of the entire arytenoid cartilage except the muscular process, thereby removing the corniculate process. The partial

arytenoidectomy improved the translaryngeal impedance over RLN but did not return it to normal at high flow rates in an experimental study (Lumsden et al., 1994; Radcliffe et al., 2006). The partial arytenoidectomy continues to be used in clinical patients as it has a reasonable success rate and has been shown to improve laryngeal impedance (Radcliffe et al., 2006).

Indications for a partial arytenoidectomy procedure include RLN with complications such as suture pullout with severe cartilage fracture, infection from an attempted prosthesis, and arytenoid chondritis. Arytenoid chondritis may occur separately from RLN or as a sequela to cartilage disruption during the laryngoplasty.

Intraoperative complications of the arytenoidectomy procedure include difficulty in removing the cartilage and accidental mucosal penetration in a case where closure is desired. Induration of the arytenoid cartilage muscular process has been reported (Tulleners et al., 1988a) and causes difficulty in removing the body of the arytenoid cartilage as osseous-like material forms in the junction of the muscular process of the arytenoid cartilage and the body.

The partial arytenoidectomy is performed via a ventral midline skin incision from 2 cm caudal to the cricoid cartilage rostral to the base of the basihyoid bone. The paired sternohyoid and sternothyroid muscles are separated down to the level of the cricothyroid ligament. A linear incision approximately 4-5 cm in length is created through the cricothyroid ligament. The corniculate process of the arytenoid cartilage is first removed by sharp transection through the adjoining cartilage and mucosa. Forceps are used to grasp the corniculate process for manipulation to allow dissection of the soft tissue attachments around it. Next, incisions are made through the laryngeal mucosa using the created entry on the dorsal, rostral and caudal aspects of the arytenoid cartilage body. Dissection between the mucosa and cartilage is performed with scissors to maintain a flap to cover the area where the cartilage is removed. Dissection is then performed along the lateral aspect of the cartilage to remove it from the surrounding tissues. Once the muscular process is encountered along the lateral border, it is transected to allow removal of the cartilaginous body of the arytenoid cartilage. Following removal, the medial mucosa is used to close the surgical wound using 4-0 suture in a continuous pattern. If closure of the laryngotomy is selected, the mucosa, cricothyroid ligament, muscle layers, subcutaneous and skin layers are closed in a continuous fashion.

There is some debate about whether this incision should be closed, as it is a contaminated procedure given the entry into the laryngeal lumen. As previously discussed, the laryngotomy incision

may also be left open to heal by second intention with minimal consequence (Lumsden et al., 1994; Radcliffe et al., 2006). Expedited healing has been observed with closure but it does not necessarily decrease granulation and dorsal dehiscence was observed in the majority of horses in one study (Tulleners et al., 1988b). At times, granulomatous lesions have arisen which were treated with laser or sharp excision and resulted in a good outcome. As with the laryngoplasty, a standing arytenoidectomy procedure has been reported with good outcomes in horses and represents one of the next areas in the development of this procedure (Gray et al., 2019).

Postoperative complications consist of dysphagia, coughing, infection of the surgical site, lateral wall collapse within the larynx. Unfortunately, as these procedures consist of cartilage removal, they are irreversible and severe complications may be difficult to address. In one report, transection of the transverse arytenoid ligament resulted in dysphagia, and 5 horses experienced coughing and 9 had nasal discharge out of 22 horses that underwent partial arytenoidectomy (Speirs 1986). A summary of studies of partial arytenoidectomy outcomes can be found in **Table 1.4**.

To better understand RLN, the surgical procedures used to address this problem, and the mechanics behind air movement within the larynx, some ex vivo models have sought to replicate exercise conditions in horses. Both cadaveric and computational methods have been previously reported, contributing to the understanding of the role of pressure, velocity, and turbulence within the dynamic situation of equine airflow. Advanced imaging has contributed significantly to the understanding of the structure of the equine airway and possible influences on airflow.

Table 1.4 Partial arytenoidectomy outcomes in chronological order.

First Author	Year	Outcome Measure	Procedure	Success Rate	Number	Breed	Comments
Speirs	1986	Exercise tolerance	PA	91%	22	Variety	Serious complications in 9/22
Barnes	2004	Racing/earning money	PA (open)	61-78%	27	Thoroughbred	
Parente	2008	Racing	PA	63-82%	73	Thoroughbred	Return to preoperative level of work
Witte	2009	Racing and earnings	PA	62-75%	45	Thoroughbred	RLN and arytenoid chondritis included

RLN-recurrent laryngeal neuropathy; PA-partial arytenoidectomy

1.5 Upper Airway Imaging

Multiple diagnostic techniques have been used to evaluate RLN. Computed tomography (CT), magnetic resonance imaging (MRI) and transesophageal ultrasound have been used to assess the laryngeal region in horses. CT and transesophageal ultrasound have been used to compare the left and right CAD muscles in clinically affected RLN patients to demonstrate that significant differences between sides are a strong indicator of clinically relevant disease. The volumetric assessment of these muscles using three-dimensional reconstruction showed strong correlation with *ex vivo* measurements of muscle volume in one study (Kenny et al., 2017). In another study, the cross-sectional area of the left and right CAD muscles when expressed as a ratio demonstrated a that a decreasing ratio was associated with increasing grade of disease via transcutaneous ultrasonography (Satoh et al., 2019). Disease progression was also associated with increased echogenicity. Additionally, experimentally induced right laryngeal neuropathy was associated with decreased neural density within the muscle on the affected side, and a greater collagen/fat percentage compared to the normal side via both transcutaneous and transesophageal ultrasonography (Chalmers et al., 2015)

CT has also been used to examine the conformation of the equine cricoid cartilage, which showed significant morphological differences between animals within the same breed (Dahlberg et al., 2011).The size of the equine CAD muscle has been examined using CT with the finding that grade 4 RLN had significantly smaller muscles sizes and horses with grade C on the dynamic exam had more collagen in the left than the right CAD muscle (Tulloch et al., 2014)

Three-dimensional reconstruction of the larynx has been performed using CT to examine the pitch, roll and yaw of the arytenoid cartilage with varying degrees of tension along the suture (Perkins et al., 2010). The medial belly of the CAD muscle was found to prevent collapse of the arytenoid into the airway while the lateral belly was primarily responsible for pitch, which represents most of the observed arytenoid motion (Lynch et al., 2020; Perkins et al., 2010). A recent additional study examined the effects of suture tension on these three variables but also on translaryngeal impedance with different levels of airflow (Lynch et al., 2020). There was no benefit above 50% of the maximal suture force and no significant difference in the placement of the suture bite in the muscular process of the arytenoid cartilage (Lynch et al., 2020).

Advanced imaging techniques have been demonstrated to significantly affect decision-making in the veterinary and human sinonasal surgeries and continue to provide insight into diagnosis, pathology and treatment. Three-dimensional renderings of the equine sinus anatomy led to greater understanding of the sinonasal communications that explain the pathology and better elucidate the treatment of equine sinus disease (Brinkschulte et al., 2014). This was also shown in human studies of the role of three-dimensional imaging in the decision for sinus surgery and approximation laryngoplasty (Anzai et al., 2004; Nerukar et al., 2012). As these imaging modalities are further used to characterize RLN, they will likely be relied upon more and more in making decisions regarding surgery for equine obstructive airway diseases.

1.6 Airway Fluid Mechanics Models

1.6.1 Human Models

The earliest models of human airways were performed by taking casts of cadaver airways and then using these to create *ex vivo* models. Clear panels were originally observed with smoke passed through the cast to determine the pattern of flow through human airways (Proetz, 1951). Casts of cadavers were also created to generate models of the human nasal passage to perform laser anemometry which resulted in inhalation and exhalation velocity profiles of the human nose. This study suggested that the shape of the human nasal passage plays a large role in the air velocity and that fluid mechanics may explain a variety of pathologies in the human nasal passage (Girardin et al., 1983). This evolved into a simplified computer-generated "nose like" geometrical model that was made increasingly more complex to describe the flow fields throughout the human nose (Elad et al., 1993). Upscaled human nasal models have been constructed from CT scans to examine flow patterns using hot-wire anemometry to develop velocity profiles within the nasal passage (Hahn et al., 1993). While these types of model do not consider the compliance of tissues, mucus, and other factors, it contributed to the understanding of flow patterns through the upper airway (Hahn et al., 1993).

Human glottic models have also been created to better understand the simplified components of airflow through the vocal folds using other domestic animals and simplified models (Alipour et al., 1996). Canine larynges and a plexiglass replica have been used to model the human vocal folds mechanically and computationally. These three models had strong agreement for flow characteristics and demonstrated transition from laminar to turbulent flow as air crossed the glottis.

While the objective of this study was to study human phonation, the convergence and divergence of the anatomy are similar to obstructive disorders in the human, canine, and equine airways (Alipour et al., 1996). One interesting observation was the attachment of flow to one wall of the model independent of the presence of geometrical symmetry. Preferential flow attachment in this scenario, termed the Coanda effect, results in higher velocity and lower pressures on the wall and a post-glottic jet formation which was characterized for various conformations (Scherer et al., 2001). It is thought to occur at the false vocal folds and larynx downstream (Erath et al., 2006b). This was further characterized with concurrent computational models. Asymmetry can result in pressure differences between walls that are up to 25% of the total pressure difference across the channel and may play a role in some of the unilaterally-dominant diseases observed (Erath et al., 2006a). Pressure differences between sides have been further explored in the context of surgical impacts of procedures such as the of medialization of the glottic folds (Zhang et al., 2019).

1.6.2 Canine Models

Laryngeal hemiplegia is also a significant problem in the canine species, for which lateralization of the arytenoid cartilage is performed to replicate the dorsal cricoarytenoid muscle as occurs in horses. However, dogs are anatomically more akin to humans in that oral and nasal breathing can be interchanged and the larynx is more recessed caudally. A common problem following the canine "tieback" is the lack of epiglottic-glottic seal or LEGS, which results in aspiration of food and water. In one study, increased lateralization resulted in increased rima glottis area but the caudal movement of the arytenoid associated with the tieback procedure resulted in a greater lack of seal (Guillemot et al., 2015). This is consistent with the findings in the equine patient in that higher levels of arytenoid abduction may result in aspiration, and further demonstrates the need for an improved understanding of this complex structure across species.

The canine larynx has been used in *ex vivo* models due to its similarity to the human counterpart in the study of fluid-structure interactions. Velocity profiles of the canine larynx showed that the posterior portion of the velocity increased first and also allowed capture of profiles with different degrees of abduction of the arytenoid cartilages and confirmed the previous computed models (de Luzan et al., 2020). This study was the first of its kind to demonstrate near-glottal flow, which is paramount to sound formation.

1.7 Computational Fluid Dynamics (CFD) Models

1.7.1 Human CFD Applications

CFD analysis has been performed on human upper airways from the nasal passages to the trachea, with applications from determining pathogenesis to diagnosis and treatment of complex airway disorders. CT scans of patients have been used to create 3D computer geometries of the airway and then to perform a wide variety of analyses (Kimbell et al., 2009; Mylavarapu et al., 2013). Modelling prior to surgery can be used to determine which stenosis is the most important and to assess which surgical procedure will best alleviate the patient's problem (Mylavarapu et al., 2013). This allows direst comparison of different surgical methods within the paradigm of a particular conformation. The complication rates associated with human upper airway obstructive disorders range from 60-80% which are similar to the reported rates for equine patients (Dinis et al., 2002; Ducharme et al., 2019). This may be drastically improved by applying these novel types of analysis in complicated cases where the most significant obstruction may not be apparent (Mylavarapu et al., 2013).

However, CFD is inexact in that it relies on mean estimation of the turbulent flow that occurs within a structure, and model verification and validation must be performed for each application. Each mesh and model configuration has different merits and each aspect of the human airway (upper versus lower) requires validation and comparison to real-life results. In one study of the effects of mesh type on the solution of flow in bifurcating models of human lower airways, a structured hexahedral mesh was the most accurate and had solution time that was 3 times less than the flow adaptive tetrahedral, unstructured tetrahedral and hybrid grid mesh types (Longest et al., 2007). Comparison of three different turbulence models for the human upper airway model between Large Eddy Simulation (LES), standard κ-ω, and the Spalart-Allmaras model demonstrated that the standard κ-ω model was the most consistent with a physical replica due to the treatment of near-wall conditions (Mylavarapu et al., 2009). The human nasal passage has been modeled using DNS, standard κ, and LES models with additional confirmation that the κ model provides the superior near-wall treatment for the computational costs (Li et al., 2017). Each turbulence model balances accuracy versus computational cost depending on the anticipated flow characteristics (Versteeg et al., 2007). Once rigid, simplified structures are validated, complexity can be added. Liquid (respiratory mucus) was added with wall compliance and was found to

dampen the forces along the respiratory wall in a simple geometry (Pirnar et al., 2017). Wall shear stress contributes to stenosis/post-stenosis flow separation as demonstrated in the cardiovascular discipline and likely influences respiratory airflow but this remains to be proven (Plesniak et al., 2004). Once the proper calculation of the effect of these types of forces has been established, a simplified version can then be added to later computations, increasing model accuracy.

CFD simultaneously compares multiple levels of the upper airway such as the nasal valve and the pharynx. These are areas of important constriction with significant influence on airflow in obstructive sleep apnea syndrome (OSAS) that previously were not well understood. Maximal velocity occurs at the nasal valve which directs flows vertically, then toward the floor along the nasal septum. This creates a swirling effect in the pharynx which contributes to collapse in OSAS (Sung et al., 2006). Schwab et al. (1993) reported on significantly decreased retropalatal area in apneic versus mildly apneic patients on CT scans further contributing to this effect. An additional low Reynolds κ-ϵ model from an OSAS patient CT demonstrated that pharyngeal narrowing causes a "pharyngeal jet", an uneven velocity profile, and increased aerodynamic force on the velopharynx (Jeong et al., 2007). This results in collapsing forces that are over 17 times greater than the opening force on the nasopharynx side. While muscle function was not included, this disparity in force caused by shape of the airway overpowers the muscular forces needed to maintain airway patency (Jeong et al., 2007).

One of the largest applications of CFD in humans to date is obstructive sleep apnea syndrome (OSAS). One of the first major studies compared side-by-side collapsing pressure changes with mandibular advancement, uvula excision, and palatal resection procedures (Huang 2005a). This group further built on this model by incorporating muscular function (Huang et al. 2007). First, a two-dimensional model of the upper airway was created. Muscular function was simulated with the genioglossus muscle in the tongue based on EMG readings from asleep patients. The mechanical collapse of the palate and the tongue were predicted based on the negative pressure values calculated in the pharynx during sleep. This study confirmed the inefficacy of palatal or glossal implants. The predicted pressures of the model supported the reported values from patient mechanical studies, establishing model validity. The application of CFD in this case allowed the assessment various surgical alterations without varying treatments between clinical patients. Prior to modelling, mandibular advancement oral devices resulted in complete success rates of only 35-

40% in these patients with no understanding of the varied response to treatment (Chan et al., 2007). Alternatively, the benefits of surgery were demonstrated using CFD in nine different OSAS patients with improved soft palate and tongue base areas (Ito et al., 2011; Sittitavornwong et al., 2013). Simultaneously, CFD was also performed to analyze the oral devices for OSAS in seven patients with variable responses to treatment and found that enlargement of one region of the airway was not as predictive as CFD (Zhao et al., 2013). Thus, CFD was able to explain the differences between temporary oral device and surgery successes in OSAS patients despite previously observed changes in cross-sectional areas.

CFD has also been useful in identifying the confounding effects of OSAS predispositions and comorbidities. The male predisposition to OSAS was proven by the finding that the longer airway in males contributed to less stability and greater propensity for collapse (Malhotra et al., 2002). Obese adolescent females also underwent awake dynamic MRI with CFD analysis to investigate the correlation of obesity with OSAS. The pharyngeal dilator muscles in these patients overcompensated resulting in an increased cross-sectional area while awake, which may explain the predisposition to collapse during sleep (Wootton et al., 2016). Adenotonsillectomy has been proposed as a possible treatment option in obese adolescent OSAS patients. Computed upper airway pressure differentials were more strongly correlated to apnea-hypopnea index (AHI) than simple change of anatomical areas, and means that CFD is a stronger predictor of clinical success in adolescent obese patients as well. (Luo et al., 2014).

As an added benefit, CFD has been substituted for experiments that cannot or should not be performed in humans, like modelling toxic gas inhalation. Hydrogen sulfide nasal extraction and effects between individual adults and children have been modeled to determine toxic levels of exposure (Schroeter et al., 2006b; Schroeter et al., 2010). Nasal spray deposition has also been modeled which allowed a range of variables to be tested such as particle size, actuator insertion depth and angle, velocity and the effect of simultaneous inhalation to determine the spread of particulates such as medications within the nostril (Kimbell et al., 2007; Kimbell 2009; Schroeter et al., 2006a). CFD eliminates the time and financial investment of repeated experimentation on a human subject for each of these variables. This provides valuable information about medication delivery into the upper or lower airways without the labor intensive or radioactive agent-based models used previously (Kimbell et al., 2007; Martonen et al., 2002; Vinchurkar et al., 2012). CFD

validation similarly was performed using combined single photon emission CT in asthmatic patient lungs (De Backer et al., 2010). This is especially useful in predicting "hot spots" throughout the airways making the previous radioactive particle studies obsolete (De Backer et al., 2010). This greatly expands the ability to study these diseases with minimal ethical concerns.

Surgical planning, symptom, and outcome justifications in other portions of the airway have been performed using CFD analysis. One report looked at the effect of stenting on tracheal stenosis (Taherian et al., 2017). Multiple other studies have examined the effect of airflow and jet formation on vocal and ventricular folds, which can affect voice quality (Sadeghi et al., 2019). Ventricular pressures decreased while glottic resistance increased with inclusion of the vocal folds in the model. Another laryngeal model implemented varying glottic closure angles with time to examine backflow and vortex formation. Even with time-based variation, the pharyngeal flow did not significantly affect the flow patterns observed (Renotte et al., 2000). Most exciting is the potential shown in nasal surgery. The individual patient response to septal variation on a specific patient outcome has been investigated and demonstrates the potential of CFD to break down the "one surgery fits all" ideology (Kim et al., 2013). Advanced imaging can be used to measure the changes in cross-sectional area with surgical interventions, which was previously thought to directly correlate to resistance, but this is not always the case (De Backer et al., 2008). The use of CFD in diagnosis, understanding of pathology, and surgical planning is the future of nasal surgery in human patients and is expected to improve outcomes due to the exploration of a variety of manipulations and the use of individual patient geometry from advanced imaging to drive decision-making (Rhee 2009b; Rhee et al., 2011).

1.7.2 Canine CFD Applications

CFD models of the canine upper airway have been performed with specific attention to the nasal passage anatomy as it relates to olfaction. It was determined from these models that unique aspects of the canine morphology contribute to an increased olfactive potential, as the caudal portion of the nasal cavity contains an extra shelf of bone that redirects a separate stream of air into the olfactory recess allowing it to pass over the highly complex ethmoturbinates (Craven et al., 2007; Craven et al., 2009). This flow is laminar in the case of sniffing inhalation and does not participate in exhalation, which allows for a prolonged exposure to particles. Laminar airflow through the olfactory region is expected to deposit more soluble particles near the rostral areas of

the olfactory recess (dorsal meatus and nasal septum) whereas particles of lesser solubility travelled more uniformly along the recess. This likely contributes to the remarkable scent capabilities of dogs and other macrosmatic species (Lawson et al., 2012). Additionally, it was demonstrated that the left and right nostrils maintain separate streams, potentiating accurate localization of an odorant source. A vorticial pattern of airflow was observed outside the nares as a function of the lateral nasal meatus, which was shown to maintain a continuous stream of new odorants entering the olfactory path with a reach of approximately 1 cm rostral to the nares (Craven et al., 2010). This is consistent with the observed behavior that a dog holds its nose just above the ground when sniffing. Further investigation also demonstrated the odorant localization effect is consistent with the olfaction neuron distribution within the ethmoid region.

Brachycephalic obstructive airway syndrome (BOAS) in dogs is another complex upper airway problem due to the involvement of multiple anatomical structures. The nares, soft palate, larynx and trachea may all be involved alone, or in many combinations causing extreme difficulty and even distress when breathing. Multiple surgical procedures have been reported to address each of these areas but little is known about how each influence breathing beyond superficial improvement in the patient's quality of life. Hostnik et al. (2017) measured airway resistance based on CFD analysis of CT images in a group of English bulldogs. In 19 of 21 patients, the nasal passage was the region of greatest resistance and therefore represented an area of high potential for intervention. The maximal local resistance within the upper airway was not necessarily reflective of the total air passage resistance between patients. Another report confirmed these findings and compared mesocephalic and dolichocephalic models. The median airway resistance and pressure difference were most different between breeds in the regions from the nares to the larynx but were similar in values from the larynx to the trachea, except for the English Bulldog (Fernandez-Parra et al., 2019). Another study examined French bulldogs and the pre-operative versus post-operative CFD models for nostril stenosis and found that mild cases are not significantly influenced by rhinoplasty, while severe cases improved with a wedge-resection rhinoplasty (Khoa et al., 2021). These models indicated that for patients with BOAS syndrome, likely the nasal passage is the area of most influence, however CFD analysis may have an application in determining the area of highest resistance and interventional effects in canine patients in the future.

1.7.3 Equine CFD Applications

Previous computational models of the equine upper airway have been performed to better understand airflow using a Thoroughbred horse head (Massie 2015; Rakesh et al., 2008a). The first model used airflow mechanics data from previous studies of exercising horses to develop boundary conditions for the model, and both inhalation and exhalation at exercise were modeled (Rakesh et al., 2008a). The cross-sectional areas were reported for the equine upper airway with a 7% decrease in size noted between the rima glottis and trachea which had not been reported previously. The nasopharynx and larynx were found to be areas of concentrated high turbulence and negative pressure (Rakesh et al., 2008a). This parallels models of the human airway that have reported a higher turbulence intensity in the anterior portion of the nasal passage with high flow rates in the middle and inferior portions and a high level of turbulence in the pharynx (Li et al., 2017).

The model was created using CT images that were analyzed slice-by-slice for the flow area using Mimics to create the object file. The object file was then edited in Magics and meshed and analyzed in Fluent (Rakesh et al., 2008b). CFD analysis was performed using a κ-ϵ model for turbulence and assuming an isothermal, incompressible, and unsteady flow with the Reynolds-Averaged Navier Stokes equations (Rakesh et al., 2008b). This model is the most researched and it balances computational expenditure with a reasonable amount of complexity (Versteeg et al., 2007). Pressure boundaries were used at the inlet and outlet as measured from exercising horses-atmospheric at the nares and maximal negative pressure of -4300 Pa within the trachea but using experimental values from within the equine trachea. The discretized equation solution used pressure-implicit with splitting of operators or PISO scheme and the convection terms were solved using a second-order upwind scheme. The computed model was verified by comparison with experimental curves for pressure, flow rate and velocity in an exercising horse during inhalation and exhalation (Rakesh et al., 2008b). Additionally, turbulent kinetic energy was spatially plotted within the model of the equine upper airway (Rakesh et al., 2008b). This model was later used to examine three levels of abduction of the laryngoplasty and the effects on airflow through the upper airway (Rakesh et al., 2008c). One reported hurdle of this method of modeling is the amount of time and work required to produce segmented three-dimensional models of the equine upper airway. One report has demonstrated that the use of semi-automatic segmentation can be used in

equine sinuses, reducing the amount of time and effort required to produce an anatomically meaningful model (Brinkschulte et al., 2013).

In addition to using the upper airway model to investigate the cross-sectional area of the laryngoplasty, a nasal model was created from an equine nasal passage mold to investigate creation of a mask to study respiratory mechanics in exercising horses (Massie, 2015). The mask allowed measurement of tidal volume, expiratory flow, inspiratory flow, and ventilation of horses at exercise. A three-dimensional model was created from MRI images of a horse head in addition to casts of the nasal passages for creation of a CFD model (Massie, 2015). A simplified model was also three-dimensionally printed to allow experimental data collection to confirm the computational results. Ultimately, this allowed selection between four possible mask designs to minimize interference in respiration while allowing measurement of the above variables. An SST κ-ω model was used with velocity and mass flow rate boundary conditions (Massie, 2015). Good agreement was found between the computational and experiment values during this investigation. The κ-ω model on a simplistic level better models near-wall conditions and avoids the wall-dampening functions necessary for other models in low Reynolds number applications (Versteeg et al., 2007). It should be noted that turbulence model selection is based on geometrical application, level of anticipated turbulence and outcome measure of interest and that model validation and calibration within each field is developed with experience.

1.8 Overarching Objectives and Hypotheses

The complex nature of equine RLN and upper airway collapse necessitates creative solutions to address this disease. While the literature primarily focuses on the pathological basis, diagnosis and certain treatment conditions, a gap between the interaction of the laryngeal anatomy, fluid mechanics, and airway obstruction remains. Some basic models have explored these principles, looking primarily at simplistic variables such as translaryngeal impedance and rima glottis area to assess surgical success or failure. While these parameters are loosely correlated with improved performance, there are a number of aspects of equine respiration that remain unknown.

In contrast, the human and canine fields have gone through an evolution of model development, beginning with simple concepts which are then expanded into more complex scenarios. Particular aspects of the airway geometry are then further explored as questions arise,

such as the interaction between pharyngeal length, jet formation and vocalization. This type of model development and progression has not occurred in the equine field to the same extent, which may explain some of the continued gaps in knowledge about the mechanisms of equine upper airway disease and its treatment.

Furthermore, human and canine models of obstructive airway disease have progressed dramatically with CFD analysis. It has led to multitudinous insights about the pathological basis of upper airway obstructive disorders, the influence of comorbidities on disease severity, and the influence of surgery. In the human field a large volume of literature has contributed to the validation and application of CFD in patients and it has become a useful adjunct to the respiratory surgeon. It is applied to the diagnosis of clinically significant obstructions and surgical procedure selection and refinement. Ultimately, this is leading to an individualized approach to diagnosis and surgery.

This thesis aims to address some of the gaps in equine airflow model development by examining a previously published model and examining the laryngeal geometry as it relates to collapse. Next, to apply CFD to this model and a horse head model to evaluate the role of CFD in model analysis and potential patient applications. Additionally, the aim of this thesis is to demonstrate that individual variability between patients with RLN warrants further investigation and to propose CFD as a potential avenue to address individual patient needs.

Objectives:

1) Replicate a previously-published laryngeal impedance model and implementation for investigation of a novel upper airway procedure.
2) Contribute to further equine airway model development by identifying and reporting important variables associated with equine airway fluid mechanics.
3) Develop the application of CFD to the equine upper airway as it relates to multiple laryngeal procedures and provide a general assessment of the accuracy of this model as a potential predictive tool for application to clinical patients.

It was hypothesized that incorporation of three-dimensional laryngeal geometry in ex vivo equine models would provide greater insights into surgical manipulations in equine patients with

RLN beyond the current recommendations. Secondly, that CFD could be used as a predictive tool for individual equine patients, as demonstrated through cadaveric testing to experimentally corroborate the surgical procedure with the lowest translaryngeal impedance.

CHAPTER TWO:

EX VIVO EVALUATION OF ARYTENOID CORNICULECTOMY, COMPARED WITH OTHER AIRWAY INTERVENTIONS, PERFORMED ON CADAVERIC EQUINE LARYNGES WITH SIMULATED RECURRENT LARYNGEAL NEUROPATHY

This chapter presents a preliminary fluid mechanics investigation of a new proposed procedure for equine recurrent laryngeal neuropathy, the arytenoid corniculectomy. This was compared with currently accepted procedures of the laryngoplasty and partial arytenoidectomy in addition to a combined laryngoplasty/corniculectomy procedure using an ex vivo model that measured laryngeal impedance. The corniculectomy was significantly different from the laryngoplasty and combined laryngoplasty/corniculectomy procedure, but was not different from the disease state and the partial arytenoidectomy procedures.

The corniculectomy procedure may represent a viable alternative procedure for instances where corniculate process collapse is observed in horses post-laryngoplasty. Individual variation was found to have a large contribution to the variability observed in this study, which could not be accounted for by other factors. Individual variation may play a role in the varied success observed postoperatively in horses with obstructive upper airway disease.

Full citation: Tucker ML, Sumner D, Reinink SK, Wilson DG, Carmalt JL. Ex vivo evaluation of arytenoid corniculectomy, compared with three other airway interventions, performed on cadaveric equine larynges with simulated recurrent laryngeal neuropathy. Am J Vet Res. 2019; Dec 80 (12):1136-1143.

Author Contributions: Tucker and Carmalt were responsible for the study design, data collection and analysis. Wilson contributed to grant authorship and study design. Sumner and Reinink contributed to the fluid mechanical study design components and provided editorial assistance to the manuscript. Tucker authored the manuscript with editorial assistance from Carmalt, Sumner, Reinink and Wilson.

2.1 Abstract

Laryngoplasty is the procedure of choice for left recurrent laryngeal neuropathy (LRLN), however partial arytenoidectomy (PA) has also been successful. Removal of the corniculate process of the arytenoid cartilage is simple and less invasive than a PA. The objectives of this study were to compare laryngeal impedance, in terms of air flow and pressure, following arytenoid corniculectomy (COR) versus 3 other airway interventions (left-sided laryngoplasty with ipsilateral ventriculocordectomy [LLP], LLP combined with COR [LLPCOR], and partial arytenoidectomy [PA]) performed on cadaveric equine larynges with simulated left recurrent laryngeal neuropathy (RLN) and to determine whether relative laryngeal collapse correlated with the interventions performed. Twenty-eight cadaveric equine larynges were collected from horses with no history of upper airway disease. Each larynx in states of simulated left RLN alone and with airway interventions in the order LLP, LLPCOR, COR, and PA was evaluated in a box model construct that replicated upper airway flow mechanics consistent with peak exercise in horses. Results for impedance, calculated from airflow and pressure changes, were compared between states for each larynx. Multivariable mixed-effects analysis controlling for repeated measures within larynx was performed to calculate the predicted mean impedance for each state. The tracheal adapter diameter, individual larynx properties, airway intervention, and relative laryngeal collapse significantly affected laryngeal impedance. The LLP and LLPCOR interventions had the lowest impedance, whereas the COR and PA interventions did not differ substantially from the simulated left RLN state. Residual intraclass correlation of the model was 27.6 %. Although impedance was higher for the simulated left RLN with the COR intervention state than with the LLP intervention state, given the clinical success of PA for treating RLN in horses and the similar results for the COR and PA intervention states in the present study, the use of COR warrants further investigation. The residual interclass correlation suggested that individual laryngeal variation affected impedance and may have a clinical effect.

2.2 Introduction

Since the first report of laryngoplasty by Marks et al. in 1970, many studies have been performed on suture material, placement, and the biomechanical strength of the constructs (Ahern et al., 2017; Brandenburger et al., 2017; Kelly et al., 2008; Willsallen et al., 2015). Laryngoplasty with ipsilateral ventriculocordectomy remains the surgery of choice for RLN in horses, yet important obstacles to success remain. The incidence of coughing, postoperative loss of abduction, and the precision required to place the suture for optimal abduction still present challenges (Barnett et al., 2013a; Barnett et al., 2013b). A 2013 study shows that of 41 horses with long-term follow-up after laryngoplasty, 3 (7%) had chondritis and 32 (78%) had abnormalities noted during dynamic endoscopy, most notably continued soft tissue collapse (Barnett et al., 2013a). Although many improvements have been made, laryngoplasty continues to be a difficult procedure with frequent suboptimal outcomes. The partial and subtotal arytenoidectomy procedures were proposed as treatments of last resort when laryngoplasty fails (Speirs, 1986; White et al., 1980). Removal of cartilage has less risk of infection, compared with the placement of a prosthesis, but may cause irreversible destabilization of the airway. Additionally, reasonable success with removal of cartilage can be achieved with less precision than placement of a prosthesis. Subtotal arytenoidectomy, a less extensive procedure, did not improve the airway impedance of exercising horses with RLN (Belknap et al., 1990). Partial arytenoidectomy allowed 14 out of 18 (78%) racehorses to return to performance in one study however, coughing, nasal discharge, and dysphagia were observed in some cases (Speirs, 1986). Partial arytenoidectomy has also been shown to have comparable rates of return to performance as laryngoplasty in racehorses (Witte et al., 2009). The arytenoid cartilage consists of both hyaline and elastic cartilage, with the elastic portion comprising most of the corniculate process (Fulton et al., 2012). This process collapses into the airway during dynamic endoscopy in horses with RLN. Removal of this portion of the arytenoid cartilage, here termed COR, is expected to improve airway impedance without destabilizing the airway as occurs with PA. Further, COR does not require prosthesis placement, obviates the need for precise abduction and possible subsequent failure, and reduces the amount of soft tissue available to collapse into the airway (Barnett et al., 2013a).

The primary objectives of the study reported here were to compare laryngeal impedance, in terms of air flow and pressure, following COR versus three other airway interventions (LLP,

LLPCOR, and PA) performed on cadaveric equine larynges with simulated left RLN and to determine whether COR performed to remove the corniculate process of the left arytenoid cartilage (left COR) would provide similar improvement in laryngeal impedance as would LLP. The secondary objective was to determine whether relative laryngeal collapse correlated with the intervention procedures. The primary hypothesis of this study was that the improvement in laryngeal impedance after left COR in this model of left RLN in horses would be equivalent to the improvements following either LLP or LLPCOR, but greater than the improvement with PA and that the relative collapse of the cross-sectional area of the rima glottis measured from digital videos during simulated airflow would not differ significantly between the COR and LLP interventions.

2.3 Materials and Methods

2.3.1 Samples

Larynges were collected from cadavers of horses euthanized for reasons unrelated to upper respiratory illness. The intrinsic laryngeal musculature was left intact on each larynx, and the larynges were dissected from the thyrohyoid bones to the fifth or sixth tracheal ring caudal to the cricoid cartilage. The isolated larynges were preserved in gauze saturated in saline (0.9% NaCl) solution to prevent desiccation during frozen storage. Larynges were frozen within 2 hours after euthanasia of donor horses, stored at –20°C, then thawed at 23°C for 20 hours prior to use. After thawing, the remaining extrinsic musculature, esophagus, and tracheal rings beyond the third ring were trimmed. The cricoarytenoideus dorsalis muscles were left intact bilaterally to simulate intact, diseased muscle.

2.3.2 Box Model Construct

A box with outer dimensions of 21.5 X 21.5 X 47.0 cm was built of 0.64 cm thick clear acrylic sheets and had 2 circular portals (an inlet and an outlet) of 5.08 cm in diameter as previously described and shown in **Figure 2.1** (Cheetham et al., 2008c; Hawkins et al., 2014; Jansson et al., 2000). For testing each larynx, the specimen was mounted in the box with either a 2.5 cm or 3.81 cm diameter polyvinyl chloride adapter for best fit inserted into the tracheal lumen and secured with releasable nylon cable ties. The other end of the adapter connected to the outlet portal of the box. The epiglottis was maintained in extension with a nail fixed in the foam base support in the box.

Figure 2.1 Image of the box construct used in the present study to evaluate 28 cadaveric horse larynges for translaryngeal impedance following simulation of left RLN and subsequent airway interventions (LLP, LLPCOR, COR, and PA). Airflow (blue arrow), measured by the orifice plate, was through the airflow regulation valve and inlet portal, into the test box, through the cadaveric larynx and seated adapter (not shown), through the outlet portal, and through the pipe connected to the orifice plate, oscillating valve, and vacuum. The air pressure was measured separately as the pharyngeal (larger red star) and tracheal (small red star) pressure and the difference (Δ Pressure) taken during analysis. These values were recorded during testing cycles for each larynx, evaluated with a targeted maximum negative tracheal pressure in of –4.3 kPa and a maximum airflow rate of < 70 L/s.

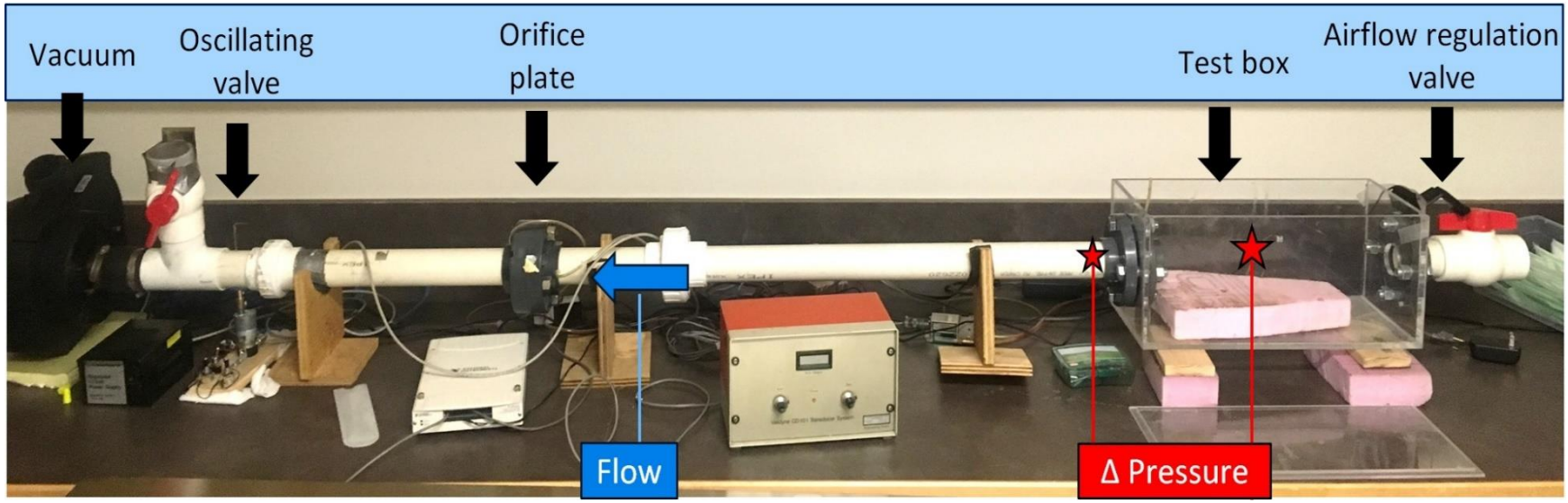

The air pressure within the lumen of the trachea (tracheal air pressure) and that in the box (pharyngeal air pressure) were each measured with a separate differential pressure transducer (Model P55D, Validyne Engineering, Northridge, CA; Model DP103-14, Validyne Engineering, Northridge, CA) connected to polyurethane tubing placed behind the third tracheal ring in the adapter and another length of tubing placed in the box. The measurements were taken relative to the air pressure in the room, then the difference between the tracheal and pharyngeal air pressures (each relative to the pressure in the room) was used to calculate the change in pressure across the larynx. Upstream of the inlet portal, an airflow regulation valve was used to adjust airflow into the box. Downstream of the outlet portal, a butterfly valve within the pipe was attached to a direct current motor with manually adjustable speed that was used to cycle the air flow at 2 Hz. An orifice plate conforming to ISO standard 5167 was used to measure airflow 71 cm upstream from the vacuum and approximately 115 cm downstream from the rima glottis (ISO 5167, 2003). The air pressure difference across the orifice plate was measured with a differential pressure transducer (Model P55D, Validyne Engineering, Northridge, CA) and from this pressure difference, the airflow rate was calculated per ISO 5167-1 (ISO 5167, 2003). The minimum and maximum airflow rates were tested in steady-state conditions to confirm accurate measurement during airflow oscillation. The airflow through the construct was adjusted to target a maximum negative pressure in the tracheal lumen of –4.3 kPa and a maximum airflow rate < 70 L/s for each cycle, consistent with parameters in horses at maximal exercise (Nielan et al., 1992). Once the airflow was adjusted to maintain these parameters for each trachea in each intervention state, data were collected for ≥ 20 seconds.

Tracheal air pressure and pharyngeal air pressure and flow were recorded and monitored for each test (simulated RLN alone and with each intervention state [LLP, LLPCOR, COR, and PA]) performed on each larynx. The flow oscillation frequency was monitored by performing a Fourier transform on the flow measurement in real time, and the rotational speed of the butterfly valve was adjusted to ensure the flow oscillation frequency was maintained at 2Hz. Data acquisition was performed at 100 Hz with a USB analog-to-digital converter (USB-6221 National Instruments, Austin, TX). These were simultaneously monitored and recorded with an individualized algorithm created in commercial software (LabView, National Instruments, Austin, TX.). The laryngeal impedance was calculated from the difference in pressure (pharyngeal air pressure minus tracheal air pressure) divided by the airflow measured for the given duration.

Each test was recorded with a digital camera, (Logitech C920 Pro HD Webcam, Logitech; Newark, CA) and video analysis of the resulting digital images was conducted by one of the authors (MLT). The point of maximal collapse was determined by scrolling through the frames for 3 cycles and determining when relaxation began, then selecting the frame prior to initiation of relaxation. This image was saved and imported into the imaging software (ImageJ, National Institutes of Health, Bethesda, MD) **(Figure 2.2)**. The length of the right corniculate process was measured manually on the physical specimen and the digital image to create the scale for each image. Similarly, measurements between the right and left thyrohyoid joints on the physical specimen and the digital image were obtained to verify the scale of each image. The scale was used to measure the open area of the rima glottis by tracing along the internal border of the arytenoid cartilages, the laryngeal saccules, and the epiglottis in digital images. This was the area through which active airflow was expected to occur. For each larynx, 3 measurements of area were taken, and the mean was calculated for each tested simulated state. In addition, still images were taken when the larynx was not subjected to a vacuum so that the LRQ could be calculated in the LLP state; this still image was also used to measure the open area of the rima glottis, and this measurement was used as the baseline area. Relative laryngeal collapse was defined as the mean luminal area of each tested state divided by the baseline open rima glottis area from the still images (reported as a percentage). Each larynx was in turn secured in the box for testing first in the simulated state of left RLN alone, then in intervention states in the order of LLP, LLPCOR, COR, then PA before moving on to the next specimen.

2.3.3 Simulation of Left RLN

To imitate right arytenoid abduction and left RLN in each isolated larynx, a standard right-sided laryngoplasty was performed and the left arytenoid cartilage was unaltered. For the laryngoplasty, a single suture of size 5 polyester suture material (Ethibond Excel, Ethicon US LLC, Bridgewater, NJ) was placed approximately 10 mm from the caudal edge of the cricoid cartilage medial to the most prominent palpable notch, when present, and 8 mm from the caudal edge of the muscular process of the arytenoid cartilage, engaging the spinous process. Maximal abduction of the right arytenoid cartilage was achieved by pulling the suture as tightly as possible before securing it with a knot.

Figure 2.2. Representative images of a cadaveric horse larynx with simulated left RLN evaluated in the box construct described in Figure 1 in states of LLP at rest (A) and in maximally collapsed RLN alone (B) and RLN with either LLP (C), LLPCOR (D), COR (E), or PA (F). The basic lines and angles of measurements used to determine LQR overlay the image of the LLP state at rest (A).

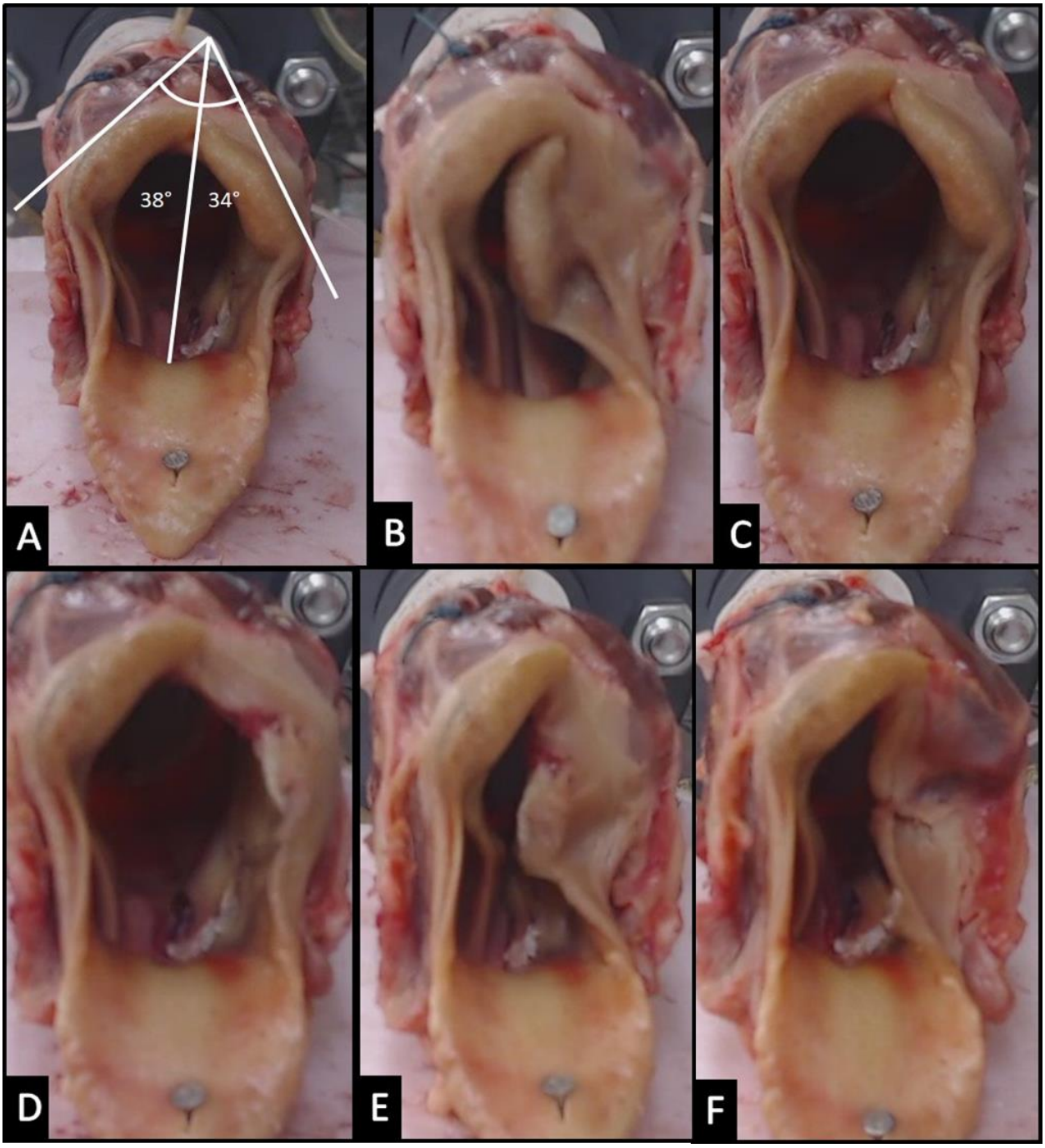

2.3.4 Simulation of Airway Interventions

Once left RLN had been simulated in an isolated larynx and tested in the construct, an LLP was performed on that same larynx. A continuous suture pattern of 4-0 poliglecaprone 25 suture material (Monocryl, Ethicon US LLC, Bridgewater, NJ) was used to suture the mucosal aperture, and cyanoacrylate glue was placed along the rostral border of the saccule to seal it. The laryngotomy was left open to replicate the clinical situation immediately after surgery.

To use the LRQ method to compare the left and right sides of the larynx with LLP, a picture of each larynx was taken with a camera mounted above the testing box, 32 cm from the larynx opening and angled downward at 67.5° as previously described (Ahern et al., 2018; Perkins et al., 2011; Witte et al., 2010a). The picture was subsequently imported into imaging software (ImageJ, National Institutes of Health, Bethesda, MD) with which the distance from the junction of the ventral aspect of the laryngeal saccules to the junction of the tips of the corniculate processes of the arytenoid cartilages was measured and one-third this length was then added to the dorsal aspect of this line **(Figure 2.2)**. The angles between this line and a line drawn tangential to the dorsal edge of each corniculate process was measured, and the LRQ calculated. An LRQ of 0.88 was attempted; however, an LRQ between 0.85 and 0.95 was considered acceptable.

After testing was completed for the larynx with simulated left RLN and LLP intervention, an LLPCOR was performed by incising the arytenoid cartilage on the left side at the junction of the elastic and hyaline cartilage of the corniculate process in the transverse plane. The mucosa was fixed to the remaining cartilage with cyanoacrylate glue, and the larynx was tested again.

Next, the suture in the left side of the larynx was cut and removed, thus resulting in a replication of the laryngeal anatomic configuration following a simple left COR. The larynx was then tested in this configuration. Finally, a PA was performed by removing the remaining portion of the left arytenoid cartilage, leaving the muscular process as previously described (White 1980), and the larynx was tested.

2.3.5 Statistical Analysis

Twenty peaks of airflow and each pressure were included in statistical analysis for each test, but only if the corresponding peak tracheal pressure along the curve fell within the range of –4.0 to –4.6 kPa. When oscillation of the tissue resulted in an inability of the orifice plate to give

a meaningful flow value, commercially available software (Microsoft Excel, version 1810, Microsoft Corp, Redmond, WA) was used for interpolation with a curve of best fit derived from the method of least squares to determine the data at the peak of the curve (Johnson et al., 2005). The apex of each peak was determined, and the mean peak value was calculated for tracheal pressure, pharyngeal pressure, and airflow for each tested simulated state in each larynx. A multivariable mixed-effects linear regression model was used to compare results for each of the simulated states (RLN alone and with each of LLP, LLPCOR, COR, and PA), controlling for multiple tests on each larynx. Measurements for laryngeal impedance were logarithmically transformed to normalize the data during analyses. Horse breed and age, adapter size (2.54 cm vs 3.81 cm), LRQ, surgical procedure (LLP, LLPCOR, COR, and PA), whether the set required interpolation, airflow adjustment, use of nonconsecutive peak air pressures, and percentage of visibly open area of the rima glottis were included in the model, with nonsignificant factors removed. The mixed-effects model accounting for repeated measures for each larynx was used to determine the predicted mean impedance of each simulated state, correcting for individual larynx and relative laryngeal collapse. Statistical analyses were performed with commercial software (Stata, version 14.0, StataCorp, College Station, TX), and values of $P < 0.05$ were considered significant.

2.4 Results

Twenty-eight larynges were collected from cadavers of horses euthanized for reasons unrelated to upper respiratory illness. During testing of each larynx in each simulated state, the air pressures, airflow, and airflow oscillation frequency were continuously monitored to allow adjustment of peak air pressure, flow, and butterfly valve frequency. Airflow ranged from 10.4 to 85 L/s, and peak negative tracheal air pressure ranged from –4.07 to –4.54 kPa **(Table 2.1)**. Air pressure in the construct was adjusted when testing each larynx until the peak negative tracheal air pressure was approximately –4.30 kPa. Nonconsecutive peaks were occasionally used. Two tests (the LLP and LLPCOR states on larynx 9) resulted in insufficient peaks falling within the acceptable range of –4.0 to –4.5 kPa, and the missing 20 peaks for the tests were determined by interpolation with a curve of best fit derived from the method of least squares to determine the data at the peak of the curve (Johnson, 2005).

When corrected for individual larynx and relative laryngeal collapse, the predicted mean laryngeal impedance was significantly ($P < 0.01$) greater for larynges fit with the 2.54 cm adapter versus those fit with the 3.81 cm adapter when tested in the simulated states of RLN (0.170 kPas/L [95% CI, 0.142 to 0.203 kPas/L] and 0.122 kPas/L [95% CI, 0.092 to 0.161 kPas/L], respectively), LLP (0.094 kPas/L [95% CI, 0.078 to 0.112 kPas/L] and 0.046 kPas/L [95% CI, 0.035 to 0.059 kPas/L], respectively), and LLPCOR (0.094 kPas/L [95% CI, 0.079 to 0.112 kPas/L] and 0.052 kPas/L [95% CI, 0.040 to 0.068 kPas/L], respectively). However, the predicted mean laryngeal impedance did not differ significantly ($P = 0.875$ and $P = 0.115$, respectively) between larynges fit with the 2.54-cm adapter versus those fit with the 3.81-cm adapter when tested in the simulated states of COR (0.151 kPas/L [95% CI, 0.128 to 0.179 kPas/L] and 0.148 kPas/L [95% CI, 0.113 to 0.192 kPas/L], respectively) or PA (0.139 kPas/L [95% CI, 0.119 to 0.164 kPas/L] and 0.109 kPas/L [95% CI, 0.084 to 0.141 kPas/L], respectively; **Figure 2.3; Table 2.2**). In addition, the predicted mean impedance did not substantially differ among the RLN alone, COR, and PA simulated states for either adapter size, but was significantly ($P < 0.01$) higher for those simulated states than for the simulated states of LLP and LLPCOR, regardless of adapter size. The predicted mean impedance did not differ substantially between the simulated states of LLP and LLPCOR for either adapter size. Residual intraclass correlation of the model was 27.6%, which suggested that individual laryngeal variation affected airway impedance because this remained once all the other factors had been accounted for.

The mean LRQ was 0.88 (range, 0.81 to 0.94), and the overall mean video-derived measurement of the open area of the rima glottis was 6.43 cm^2 (range, 1.06 cm^2 [a larynx with RLN simulated state alone] to 16.84 cm^2 [a larynx with RLN and LLP simulated states]). The mean relative collapse of the rima glottis area differed significantly among airway intervention states ($P < 0.001$) and after controlling for adapter size ($P = 0.004$). Specifically, the mean relative collapse of the rima glottis area was 35.0% (95% CI, 31.7% to 38.3%) for the COR, 51.2% (95% CI, 45.7% to 56.7%) for the PA, 66.6% (95% CI, 61.0% to 72.2%) for the LLPCOR, and 71.4% (95% CI, 65.1% to 77.7%) for the LLP.

Table 2.1 Results for laryngeal airflow and pressures and relative laryngeal collapse in 28 cadaveric equine larynges with simulated states of left RLN alone and with subsequent airway interventions (LLP, LLPCOR, COR, and PA). Data reported as the mean (range).

Simulated State	Airflow (L/s)	TP (kPa)	PP (kPa)	Relative Laryngeal Collapse (%)
RLN	25.0 (10.4 to 52.8)	–4.28 (–4.13 to –4.49)	-0.157 (-0.47 to -0.05)	0.27 (0.12 to 0.50)
LLP	53.3 (12.3 to 85.0)	–4.22 (–4.08 to –4.45)	-0.853 (-2.97 to -0.04)	0.71 (0.21 to 0.94)
LLPCOR	50.3 (20.7 to 80.8)	–4.24(–4.07 to –4.46)	-0.782 (-2.96 to -0.103)	0.67 (0.27 to 1.03)
COR	26.8 (10.9 to 48.5)	–4.30 (–4.11 to –4.54)	-0.252 (-2.20 to -0.07)	0.32 (0.12 to 0.54)
PA	32.5 (14.2 to 53.3)	–4.27 (–4.12 to –4.47)	-0.270 (-0.16 to -2.36)	0.51 (0.20 to 0.86)

TP - Tracheal air pressure; PP- Pharyngeal air pressure

Figure 2.3 Histogram of the predicted mean impedance stratified by adapter diameter (2.54 cm [gray shading] vs 3.81 cm [no shading]) for the 4 airway interventions described in Figure 2.2 when controlling for individual larynx and relative laryngeal collapse. Bars represent the 95% CI.

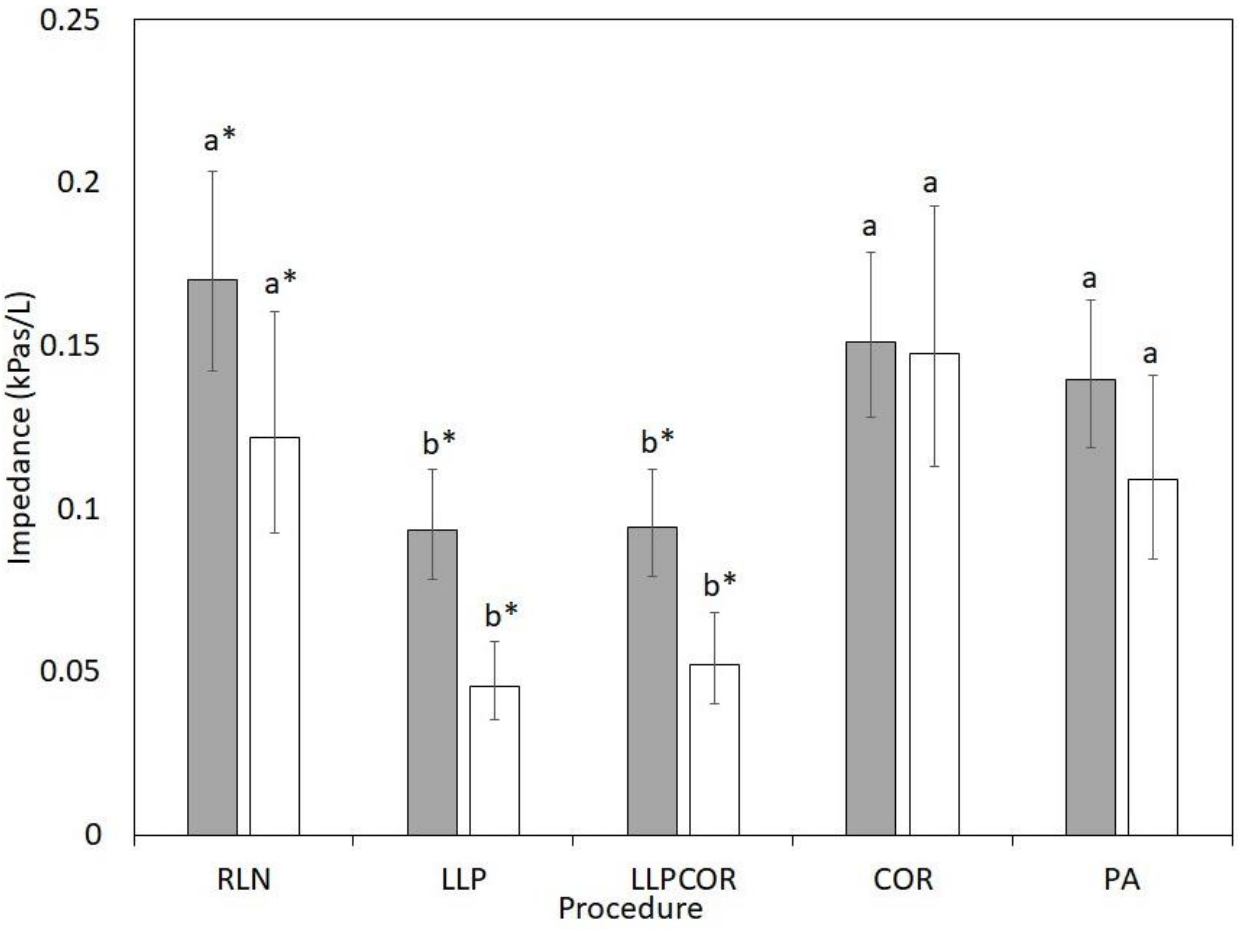

*Significant ($P < 0.01$) difference between larynges fit with the 2.54-cm versus 3.81-cm adapter within a specific procedure group.

[a,b]Procedures with different superscripts differed significantly ($P < 0.05$).

Table 2.2 Summary of the P values determined with the mixed-effects model controlling for repeated measures for each larynx to assess potential differences in results for predicted mean laryngeal impedance stratified by simulated state (RLN state alone and with each of LLP, LLPCOR, COR, and PA) and adapter size (2.54 cm vs 3.81 cm in diameter) for the 28 cadaveric equine larynges tested.

Adapter Diameter	**Simulated State**				
Simulated State	**RLN**	**LLP**	**LLPCOR**	**COR**	**PA**
2.54 cm					
LLP	**<0.01**	---			
LLPCOR	**<0.01**	0.934	---		
COR	0.24	**<0.01**	**<0.01**	---	
PA	0.93	**<0.01**	**<0.01**	0.44	---
3.81 cm					
LLP	**<0.01**	---			
LLPCOR	**<0.01**	0.378	---		
COR	0.213	**<0.01**	**<0.01**	---	
PA	0.482	**<0.01**	**<0.01**	0.05	----

*P < 0.05 was considered significant and are denoted in bold lettering

2.5 Discussion

The box model used in the present study has been validated to yield comparable values for pharyngeal and tracheal air pressures and airflow as measured in exercising horses (Cheetham et al., 2008c). Results of the present study indicated similar laryngeal impedance values for the simulated RLN alone and with LLP intervention as previously reported by other *ex vivo* models (Cheetham et al., 2008c; Jansson et al., 2000), which further supported the replicability of this model. Hawkins et al. reported different values for impedance in 2013, compared with other ex vivo studies (Cheetham et al., 2008c; Jansson et al., 2000), but included surgeries and postoperative healing in live horses before the animals were euthanized and the larynges tested. The validity of the box model construct used in the present study was further supported with our results for the simulated RLN alone and with LLP intervention, which were similar to pressure and flow measurements obtained from different portions of the upper airway during exercise in horses that underwent airway surgeries (Belknap et al., 1990; Lumsden et al., 1994; Radcliffe et al., 2006; Williams et al., 1990a; Williams et al., 1990b).

The box model yielded a wide range of results for airflows for the simulated states tested; however, this was unavoidable given the variation in the open area of the rima glottis across the different states. The adapters that were used to accommodate different laryngeal diameters in the present study were not used in previous studies but best replicated the tracheal diameter with the associated larynx. Incising the tracheal rings to force fit a 5 cm diameter pipe end is one potential solution to avoid airflow losses associated with the change in diameter from the larynx to the downstream components of the testing system. However, doing so may stretch the soft tissues and interfere with the abduction of the arytenoid cartilages. The placement of the adapters in the present study was observed to avoid interference with the soft tissues of each larynx but allowed the tracheal mucosa to form a seal with the pipe connected to the vacuum. Thus, our model resulted in a controlled change in diameter, replication of the patient geometry, and inclusion of the adapter as a factor within the statistical model.

Laryngoplasty improves laryngeal impedance to the pre-RLN state; however, studies (Lumsden et al., 1994; Radcliffe et al., 2006) of the PA have yielded conflicting results. Results of the present study indicated that PA did not improve airway impedance as well as LLP, and that results for COR were not meaningfully different from those of PA. Additionally, the predicted

mean impedance for the simulated RLN state alone was consistently an order of magnitude higher than that of the LLP intervention state, which was consistent with findings in another study (Jansson et al., 2000). Further, the impedances for the PA and COR intervention states were not meaningfully different from the RLN state alone, which indicated that laryngeal collapse in this model was dissimilar to that observed in live horses. This finding was inconsistent with findings in an in vivo study that shows horses with induced RLN treated with a modified PA returned to pre-RLN impedance values (Radcliffe et al., 2006). Additionally, Lumsden et al. (1994) also demonstrated improved impedance with PA; however, impedance was measured across the entire upper airway.

The subtotal arytenoidectomy has also been evaluated in live horses; however, subtotal arytenoidectomy did not improve the laryngeal negative air pressure beyond that of the RLN state (Belknap et al., 1990). In the present study, air pressure was controlled while the airflow was altered, and substantial drops in flow were observed for the RLN simulated state alone and for the COR and PA intervention states. In contrast, the subtotal arytenoidectomy has been largely abandoned and involves removal of the arytenoid cartilage excepting the corniculate and muscular processes. This outcome is not unexpected given that the corniculate process collapses into the airway during peak exercise in horses with RLN. In another study (Davidson et al., 2011) of PA, postoperative morbidity was reduced by reevaluation and removal of the remaining collapsing portions of the aryepiglottic fold. This finding suggests that targeted removal of the collapsing portions of the airway would be beneficial to improve airway mechanics, as with the COR procedure. The conformation of the laryngeal entrance to the airway could be adjusted during a standing endoscopic COR, and, given the differences between results observed in live horses versus the box model for these arytenoid procedures, further investigation into the usefulness of COR is warranted.

A study by Jansson et al. (2000) measured cross-sectional area of the rima glottis in horses to compare cordopexy, cordopexy and laryngoplasty, and laryngoplasty. The areas ranged from 3.80 to 10.10 cm^2; however, the measurements were calculated on the basis of airflow, translaryngeal pressure difference, and density, whereas the values in the present study were measured from still digital images. In the present study, some differences between larynges (eg, larynx length and angle) could not be controlled; therefore, the internal scale of the right arytenoid

of each larynx was used. The percentage of reduction in area was calculated to avoid error resulting from laryngeal size variation. The force of the vacuum was observed to pull the larynx caudally along its long axis, despite the epiglottic anchor. Nonetheless, the relative laryngeal collapse and impedance for the COR intervention state were markedly greater than those in the LLP intervention state in the present study. Measuring cross-sectional areas within larynges is intricate, and, as has been previously demonstrated, flows within this region are complex and interaction between patient geometry and flow development warrants further investigation (Rakesh et. al., 2008a).

Our results indicated that approximately 28% of the variation within our statistical model could have been attributed to the difference between individual larynges. This indicated that factors intrinsic to individual larynges and not captured in our model affected airway impedance. Similarly, other studies (Compostella et al., 2012; Davidson et al., 2011; Witte et al., 2010b) have also alluded to this unquantified aspect. For instance, Witte et al. reported that some larynges required an unusually great force to achieve a similar amount of abduction, and other authors have commented that the stability of the cartilage is a contributing factor to the performance of the horse following laryngoplasty (Compostella et al., 2012; Davidson et al., 2011; Witte et al., 2010b). In the present study, results for the LLPCOR intervention state indicated improved laryngeal impedance and open area of the rima glottis in some larynges and worsened impedance in others, compared with results for the respective larynges with the LLP intervention state. This finding suggested that for some larynges, corniculate process collapse may have resulted in suboptimal LLP performance and less improvement of impedance, compared with the simulated RLN state alone. Historically, failure of laryngoplasty has been blamed, in part, on the lack of cartilaginous stiffness of the arytenoid cartilages. Indeed, arytenoid corniculate process flexibility was proposed as one of the reasons for failure of improvement of a horse's performance in the face of adequate arytenoid abduction observed during resting examination (Barnett et al., 2013a; Davidson et al., 2011). Additionally, induction of dorsal displacement of the soft palate, concurrent soft tissue collapse, and arytenoid chondritis have also been observed postoperatively in horses that underwent laryngoplasty, indicating that further intervention may be required in particular cases (Barnett et al., 2013a; Davidson et al., 2011).

Results of the present study indicated that neither COR nor PA improved impedance as well as LLP. These findings regarding PA conflicted with its reported clinical success and by extension also suggested that COR may have different clinical success in exercising horses than observed in the present study. The variation in results attributed to individual larynx properties in the present study were consistent with findings in other studies (Compostella et al., 2012; Davidson et al., 2011; Witte et al., 2010b) in which individual horses had various soft tissue conformations and collapse after surgery.

2.6 Acknowledgments

The authors would like to acknowledge Dr. Cheryl Waldner for her assistance in coding and development of statistical analysis for this manuscript.

2.7 Addendum

The abstract of this chapter was revised to reflect the format of the thesis and to maintain the cohesiveness of the document. Minor revisions to the manuscript were made to improve content and readability as compared to the original publication.

CHAPTER THREE:

COMPUTED TOMOGRAPHIC GEOMETRICAL ANALYSIS OF SURGICAL TREATMENTS FOR EQUINE RECURRENT LARYNGEAL NEUROPATHY

This chapter expands upon the findings of the previous chapter by incorporating a simultaneous computed tomographic (CT) capture of the disease and surgical procedures for each larynx. Mechanical airflow testing was performed as before on ten different larynges but with steady airflow to facilitate image capture. The CT scans were then used to establish the three-dimensional geometry and changes by procedure. This provided a unique opportunity to explore the relationship between changes in laryngeal diameter and translaryngeal impedance.

The theme of individual larynx geometry contributing to impedance outcome persisted through this study. This study established how laryngeal airflow may fit within the fluid dynamics discipline in regards to basic flow models. Reducing the larynx to a basic duct flow model to describe the unique turbulent flow behavior is an important step in determining flow characteristics. This study explored the anatomical characteristics of intraluminal constriction that lay the basic foundation.

Full citation: Tucker ML, Wilson DG, Reinink SK, Carmalt JL. Computed Tomographic Geometrical Analysis of Surgical Treatments for Equine Recurrent Laryngeal Neuropathy. Am J Vet Res. 2022. Mar Doi:10.2460/ajvr.21.03.0040

Author Contributions: Tucker, Reinink, Carmalt were responsible for the study design, data collection and analysis. Wilson contributed to grant authorship and study design. Reinink contributed to the fluid mechanical study design components and provided editorial assistance to the manuscript. Tucker authored the manuscript with editorial assistance from Carmalt, Reinink and Wilson.

3.1 Abstract

Three-dimensional analysis of the upper airway in humans has led to a unique understanding of obstructive airway disorders. Similarly, 3-D models of the equine airway may contribute significantly to the understanding of the responses to surgery within individual patients. The objectives of this study were to characterize the 3-D geometry of the equine larynx replicating laryngeal hemiplegia and 4 surgical interventions by use of CT under steady-state airflow conditions. Secondly, to use fluid mechanic principles of flow through a constriction to establish the relationship between measured airflow geometries with impedance for each surgical procedure. While CT scans were performed, inhalation during exercise conditions was replicated for each of the following 5 conditions: laryngeal hemiplegia, left laryngoplasty with ventriculocordectomy, left laryngoplasty with ipsilateral ventriculocordectomy and arytenoid corniculectomy, corniculectomy, and partial arytenoidectomy for each of ten cadaveric equine larynges. Laryngeal impedance was calculated, and selected cross-sectional areas were measured along each larynx for each test. Measured areas and constriction characteristics were analyzed with respect to impedance using a multilevel, mixed-effects model. Incident angle, entrance coefficient, outlet coefficient, friction coefficient, orifice thickness, and surgical procedure were significantly associated with upper airway impedance in the bivariable model. The multivariate model showed a significant influence of incident angle, entrance coefficient, and surgical procedure on impedance; however, the orifice thickness became nonsignificant within the model. Laryngeal impedance was significantly associated with the entrance configuration for each procedure. This suggested that the equine upper airway, despite having a highly complex geometry, adheres to fluid dynamic principles applying to constrictions within pipe flow. These underlying flow characteristics may explain the clinical outcomes observed in some patients, and lead to areas of improvement in the treatment of obstructive upper airway disease in horses.

3.2 Introduction

Equine upper airway diseases that restrict airflow continue to present a complex problem for veterinary surgeons. Reported postoperative success rates range from 60 to 80%, with a trend toward improvement over time (Barnes et al., 2004; Compostella et al., 2012; Speirs, 1986; Witte et al., 2009). Multiple investigations regarding the fluid mechanics of the equine upper airway have been performed to evaluate the effect of surgical interventions on air movement. Both in vivo and ex vivo studies (Cheetham et al., 2008c; Derksen et al., 1986; Jansson et al., 2000; Tucker et al., 2019; Williams et al., 1990a; Williams et al., 1990b) have reported the impedance of the airway as an outcome measure to predict clinical improvement in patients. Specifically, equine recurrent laryngeal neuropathy (RLN) has been investigated with correlating measurements of the visual appearance of the larynges, such as the amount of arytenoid abduction and the cross-sectional area (CSA) of the rima glottis (Ahern et al., 2018; Hawkins et al., 2014; Perkins et al., 2011; Tucker et al., 2019).

Measurement of the visible CSA of the rima glottis has been generally accepted but recent studies (Ahern et al., 2018; Perkins et al., 2011) have reported different methodologies for camera placement and angulation (Tucker et al., 2019). In one study, the distance from the camera was challenging to quantify given the varying laryngeal lengths within a standardized box (Tucker et al., 2019). Ultimately, this introduces a potential source of error based on the measurement of a two-dimensional area from a 3-D structure and fails to address the effective flow area caudal to the rima glottis where ventricular dilation occurs. Rima glottis CSA measurement simulates the intraoperative endoscopic image of the larynx conformation during a laryngoplasty procedure but does not provide adequate understanding of the collapse that may occur when the horse is exercising at maximal effort (Tucker et al., 2019).

The previous study (Tucker et al., 2019) yielded questions regarding the geometry associated with the airways and the development of flow within them. In the discipline of fluid mechanics, airflow within a pipe with a constricted region has been studied to determine how the narrowed region (orifice) affects flow and pressure (Adam et al., 2019; Fossa et al., 2002). Flow development for a given orifice is strongly correlated with energy loss and pressure drop, due to irregularities in the flow caused by the orifice shape (Fossa et al., 2002). In human airways, idealized versions of the vocal folds demonstrated airflow separation, wherein the jet of air breaks

into eddies as it emerges into an expanded area. This separation may explain clinical phenomena in these patients, such as changes in voice quality during speech (Johnstone et al., 2004; Scherer et al., 2001). Similarly, some of the postoperative complications observed in equine patients and outcomes of ex vivo airway studies may be explained by fluid flow phenomena.

The objectives of this study were to characterize and report the 3-D geometry of the equine larynx while replicating left laryngeal hemiplegia (RLN), left laryngoplasty with ipsilateral ventriculocordectomy (LLP), left laryngoplasty with ventriculocordectomy combined with left arytenoid corniculectomy (LLPCOR), left arytenoid corniculectomy (COR), and left partial arytenoidectomy (PA) by use of CT while simulating inhalation during exercise. A second objective was to examine these geometries within the paradigm of fluid dynamic principles for airflow through constrictions within a circular pipe. The first hypothesis was that despite concurrent airflow and subsequent motion, CT images of sufficient quality could be captured for analysis. The second hypothesis was that the experimental impedance for various laryngeal configurations would correspond with constriction and divergence geometrical characteristics, namely, the angle of incidence, frictional loss factor, dimensionless orifice thickness, and inlet and outlet area ratios.

3.3 Materials and Methods

3.3.1 Specimens

Ten larynges from equine cadavers with no reported history of upper airway disease were collected as previously described (Tucker et al., 2019). These were preserved in saline (0.9% NaCl) solution–saturated gauze wraps and frozen at –20 °C within 2 hours after euthanasia by placement in a freezer until the time of use. The larynges were thawed in a room at 23 °C for 20 hours to allow trimming of the excess tracheal rings and esophagus, leaving the cricoarytenoideus dorsalis (CAD) muscles bilaterally intact prior to experimentation.

3.3.2 Procedures

An instrumented box of the exact dimensions and construction was used as reported previously and larynges were similarly mounted using a polyvinyl chloride pipe adapter with diameter of 2.5 or 3.81 cm with nylon cable ties, and a nail to anchor the epiglottis to a foam board during each testing period (Tucker et al., 2019). Adapter size was chosen based upon the tightness

of fit within the trachea. Separate differential pressure transducers were connected to polyurethane catheter tubing within the tracheal lumen (Model P55D, Validyne Engineering, Northridge, CA) and the inside of the box (Model DP103-14, Validyne Engineering, Northridge, CA). Each pressure was measured relative to the pressure within the room. An inlet airflow regulation valve was used upstream to adjust flow; steady flow was maintained during each testing period and was measured using an orifice plate according to ISO standard 5167 with a third differential pressure transducer (Model DP103-14, Validyne Engineering, Northridge, CA) to measure the pressure drop across the plate (ISO 5167, 2003).

Airflow was adjusted by an assistant to blind the author to the pressure differentials generated by each laryngeal simulation, with the goal of a tracheal pressure of –4.3 kPa and maximal airflow of 70 L/s as has been reported for a horse at maximal exertion (Nielan et al., 1992; Rakesh et al., 2008a). Flow was adjusted to achieve the desired tracheal pressure using a downstream valve to regulate the vacuum. Airflow and pressure within the box and trachea were measured for each simulation for each larynx while the CT was performed. A USB analog-to-digital converter (USB-6221; National Instruments, Austin, TX) was used to acquire data at 100 Hz, which were recorded using commercial software (LabView; National Instruments, Austin, TX). The difference between the 2 pressures was divided by the flow at the time to yield laryngeal impedance which was reported for each test. A mean value was calculated for each of these values over a 10-second period, given that flow and pressure were controlled in a steady-state fashion. Data were collected to obtain consistent measurements for at least 20 seconds corresponding with a CT scan, which was performed in conjunction with airflow **(Figure 3.1)**. Helical scans were performed at 1-mm slice thickness with settings of 120 kVp, 200 mAs, and 0.64-mm pitch on a machine (Toshiba Aquilon One; Canon Medical Systems, Markham, ON, Canada) with a scan speed of 1 mm/s.

Figure 3.1 Instrumented box setup in CT.

The experimental setup demonstrating the instrumented box in the CT gantry. Airflow in the image proceeded from left to right.

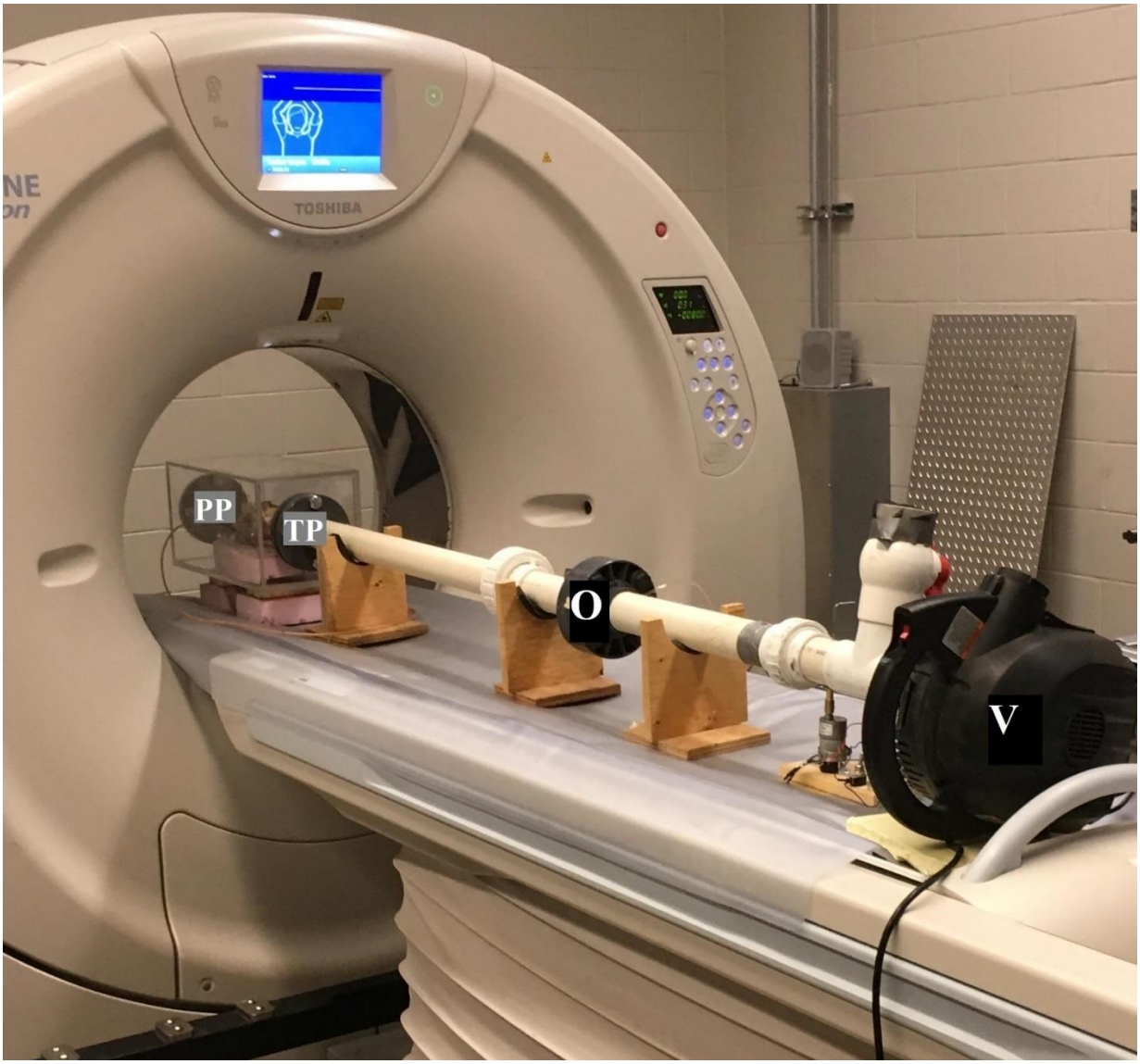

PP-point of the “pharyngeal pressure” was measurement, just upstream of the laryngeal opening; TP-point of tracheal pressure measurement; O-orifice plate for airflow measurement; V-vacuum

Each larynx underwent testing while replicating the disease state and then 4 different sequential surgical interventions. Left RLN (disease) was replicated by placing a nylon suture (#5 Ethibond Excel; Ethicon US LLC, Bridgewater, NJ) from the right cricoid cartilage to the arytenoid cartilage and allowing the left arytenoid cartilage to collapse under airflow. The cricoid bite was taken 5 to 10 mm lateral to the sagittal ridge of the cricoid cartilage, so that the suture would fall within a palpable notch when possible. The arytenoid bite was taken through the muscular process of the right arytenoid cartilage in a dorsomedial to ventrolateral direction. This was tied with a surgeon's throw with 5 more throws to replicate maximal abduction of the right arytenoid cartilage. Each larynx was tested in this configuration, and then an LLP procedure was performed. A continuous pattern of 4-0 poliglecaprone 25 (Monocryl; Ethicon US LLC, Bridgewater, NJ) was used to close the left ventriculocordectomy incision. The left-to-right quotient (LRQ) was measured by capturing a digital still image of the larynx and measuring the angle from midline for both the left and right arytenoid corniculate processes, as has been reported (Tucker et al., 2019). An LRQ of 0.85 to 0.95 was considered acceptable to replicate clinically satisfactory abduction. The larynx was tested again, and then an LLPCOR procedure was performed by incising through the mucosa and cartilage, removing the corniculate process of the left arytenoid cartilage. The mucosal edges were adhered to the cartilage using cyanoacrylate glue to replicate postoperative healing. The larynx was tested and a COR procedure was imitated by cutting and removing the left laryngoplasty suture. Following testing, a PA procedure was subsequently performed by removing the body of the arytenoid cartilage as described by White et al, and the mucosal edges were glued (White et al., 1980). A final test with airflow was performed. With each test, a concurrent CT scan was performed.

Digital video using a USB camera (Logitech C920 Pro HD Webcam, Logitech; Newark, CA) was obtained for comparison with the CT images. Still frames were captured from those videos for analysis of the rima glottis areas as performed previously (Tucker et al., 2019). Open-source software (ImageJ; National Institutes of Health, Bethesda, MD) was used to perform the measurements using the right arytenoid cartilage to provide a scale along with the thyrohyoid width. Three measurements were taken of each rima glottis area excluding the saccules and averaged to represent the CSA as measured from the video for the RLN, LLP, LLPCOR, and COR states.

From each CT examination, the image was balanced within the transverse plane using the caudal aspect of the cricoid cartilage. Three separate areas were measured for each specimen based on the coronal plane cross section. The first area was measured where a complete ring of tissue was first present along the longitudinal axis of the larynx; this was comparable to the rima glottis area for the video measurements. For the PA procedure frequently the first CSA of complete tissue was present more caudally due to the loss of the left corniculate process and arytenoid body, and this was recorded as the second area. In the other procedures, the second area was taken by finding the halfway point along the saccules within the dorsal plane, which largely coincided with the point of maximal constriction along the larynx. Lastly, a third area was measured at the level of the cricoid, which corresponded with the loss of intraluminal soft tissue within the airway in the scan **(Figure 3.2)**. These were captured, transferred into open-source imaging software (ImageJ; National Institutes of Health, Bethesda, MD), and the intraluminal area measured using the scale present within the CT image. Each of these areas was measured in triplicate, and the mean value was reported.

Based on the areas, inlet and outlet ratios were calculated for each procedure within each larynx and reported as σ_1 (inlet coefficient) and σ_2, (outlet coefficient) respectively. The first area divided by the second was used to calculate the σ_1, and the second area divided by the third for the σ_2 (Adam et al., 2019). In instances with the PA procedure where the first area was not present, only σ_2 was recorded. The length of the larynx between areas was also measured using the measured distance between the individual CT slice images to calculate the angle of incidence of airflow. Using the first and second areas measured, these were used to create a theoretical conceptual model with perfectly circular areas. The radii of such circles were then calculated, and the angle required to cone down between areas was taken by taking the inverse tangent of the difference between the radii divided by the length between them. Additionally, the length of the constricted region (s) of each larynx was measured, and the constriction diameter (D) calculated from the second measured area. These were used to calculate the dimensionless orifice thickness, s/D (Fossa et al., 2002).

Figure 3.2 Larynx CT demonstrating cross-sectional areas of interest. CT images of a cadaveric horse larynx in a recurrent laryngeal neuropathy state (left image) that shows convergence and divergence of the airflow pathway as well as corresponding first, second, and third cross-sectional areas where they fall on the axial section (right images). The large arrow at the top of the left image shows the direction of airflow and the rostral aspect of the larynx.

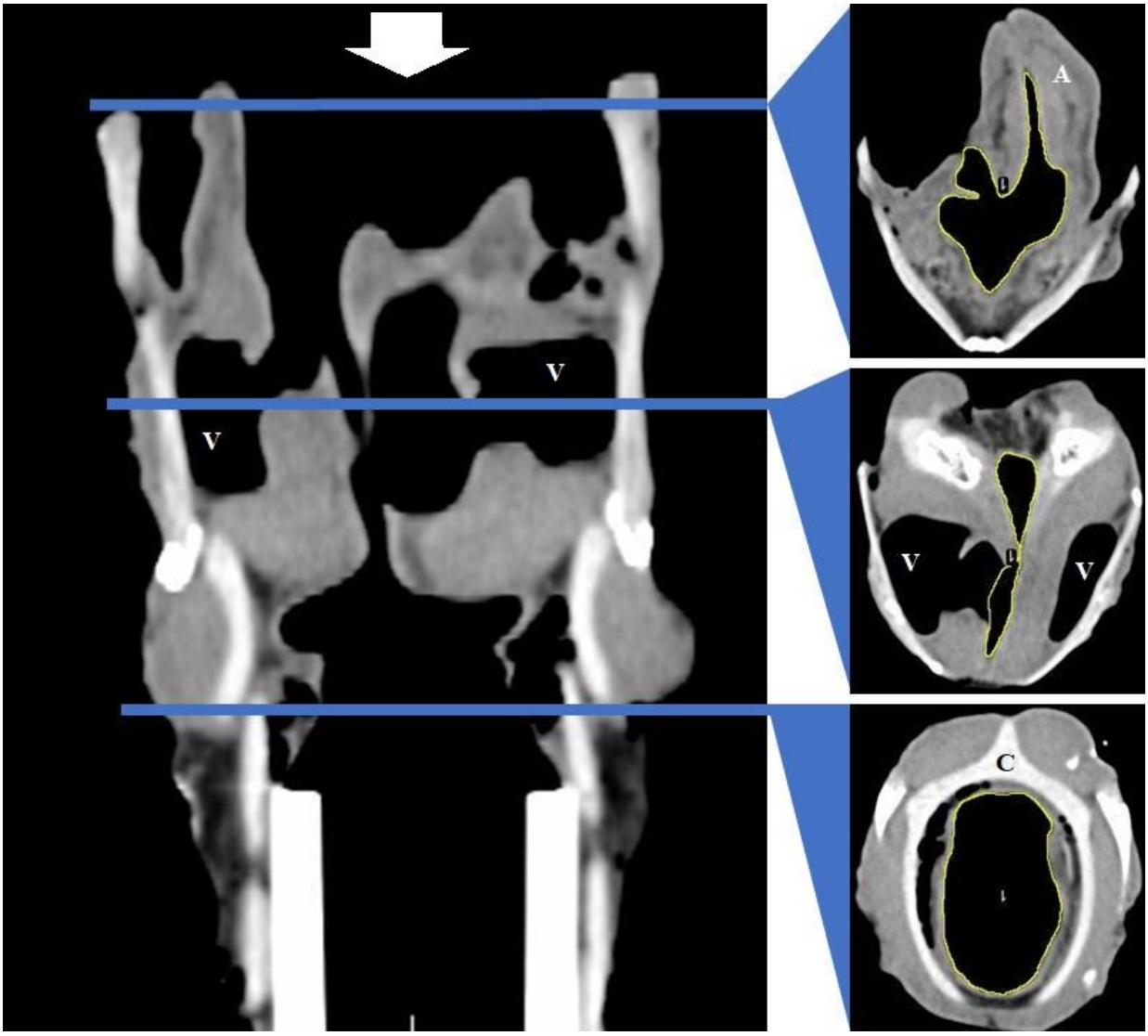

A- Right arytenoid cartilage; C -Cricoid cartilage; V - Ventricles

The friction coefficient (K) was calculated using the difference in total pressure across the larynx, which represents the energy lost as the air flows through it (Fossa et al., 2002). This total pressure difference was calculated using the measured tracheal and pharyngeal pressures, and the dynamic pressure upstream and downstream of the larynx as follows:

Equation 3.1

$$K = \frac{|\Delta P_{total}|}{\frac{1}{2}\rho V^2}$$

where ΔP_{total} is the change in total pressure, static and dynamic, across the larynx (the difference between the total tracheal pressure and the total "pharyngeal pressure" which is the pressure in the box), ρ is the density of air which was assumed to be 1.2 kg/m^3 for the conditions of the box, and v is the velocity calculated by dividing the measured flow rate through the box by the cross-sectional area of the larynx. The conceptual pipe constriction model is shown **(Figure 3.3)**.

3.3.3 Statistical analysis

Data were imported into a commercial statistics package for analysis (Stata version 14.0; StataCorp, College Station, TX). Variables were initially screened using bivariable analysis, and when the *P* value was < 0.2, they were subsequently considered in the multivariable analysis. A multilevel, mixed-effects model controlling for individual larynx was used using a backward stepwise approach to examine the effects of the significant variables on impedance.

3.4 Results

A mean negative tracheal pressure of 4.3 kPA was maintained for each procedure **(Table 3.1)**. During data analysis for each test for each larynx, a 10-second period of steady flow was chosen, and the mean value was used to reflect the measured tracheal and box (pharyngeal) pressures. For the LLP procedure, the LRQ ranged from 0.85 to 0.95, with a mean of 0.89. Predicted mean impedance by procedure was graphically displayed **(Figure 3.4)**. The frictional loss coefficient (K) in increasing order was LLP, LLPCOR, PA, COR, and RLN, which represented increasing amount of work done by the patient to breathe, respectfully. The geometrical measurements, including the areas, incident angle, inlet and outlet ratios, and dimensionless orifice coefficients were also summarized **(Table 3.2)**. The first and second measured areas showed the most variation between procedures, which coincided with σ1, the ratio of these areas.

Figure 3.3. Conceptual pipe model.

Conceptual model of a pipe demonstrating areas that reflect those measured in each equine airway. The large arrow at the top denotes the front of the larynx and the direction of airflow for the model.

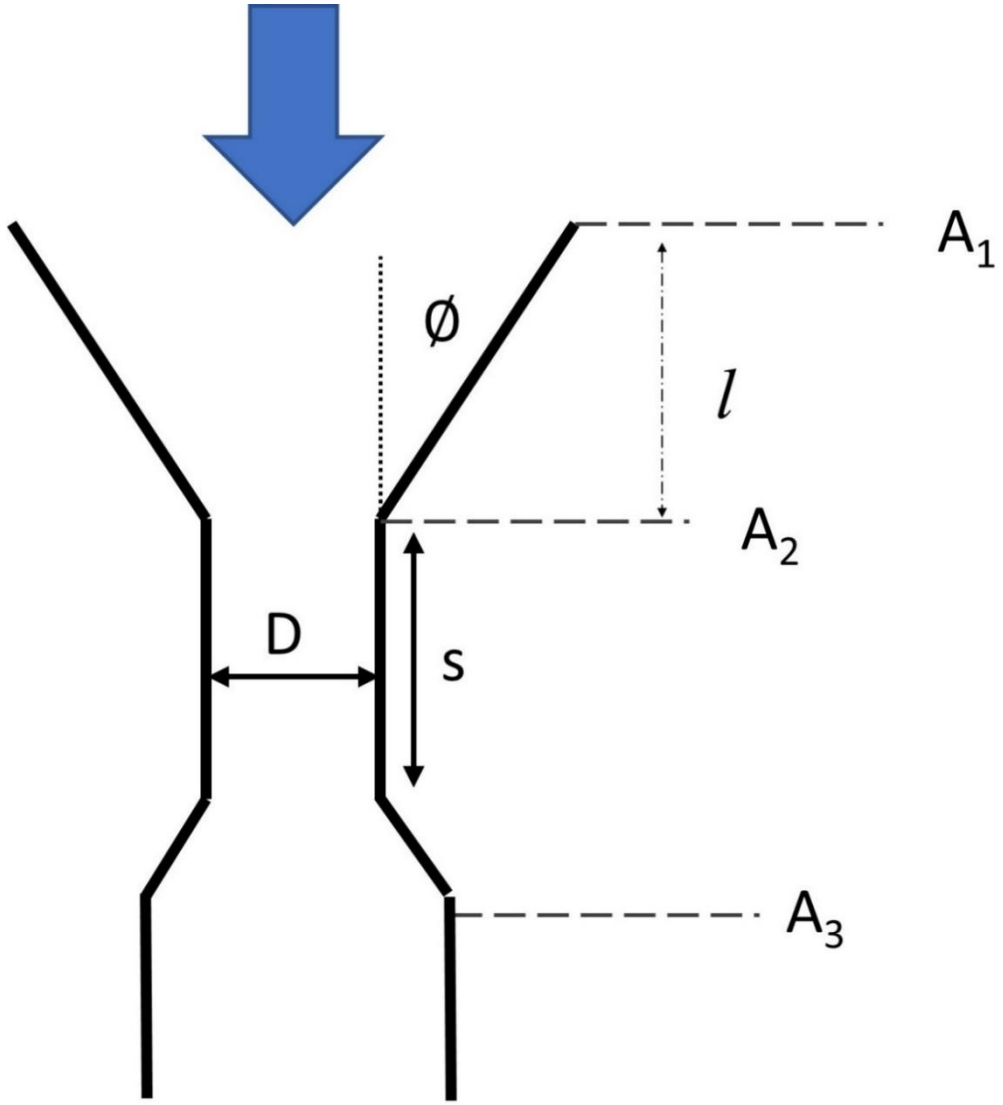

Ø - Incident angle of the constricted region relative to the long axis of flow; A1, A2, and A3 - First, second, and third measured cross-sectional areas, respectively; D - Width at the most constricted portion of the airway; *l*- Distance along the long axis between the first and second cross-sectional areas; s - Length of the constriction, used to calculate the dimensionless orifice thickness or s/D

Table 3.1 Mean and range of airflow and measured pressures for the RLN disease state and four surgical states (LLP, LLPCOR, COR, PA).

Simulated State	Airflow (L/s)	TP (kPa)	PP (kPa)	K
RLN	20.2 [5.59-33.4]	4.34 [4.20-4.44]	0.43 [0.06-1.07]	18.4 [0.38-81.1]
LLP	39.3 [20.1-54.5]	4.37 [4.25-4.66]	1.38 [0.53-3.13]	1.88 [0.029-5.82]
LLPCOR	37.9 [14.2-53.5]	4.33 [4.27-4.53]	1.30 [0.29-3.01]	2.40 [0.091-8.01]
COR	22.5 [5.7-37.8]	4.30 [4.24-4.35]	0.53 [0.063-1.70]	12.5 [0.18-54.0]
PA	24.6 [12.54-35.7]	4.32 [4.26-4.38]	0.55 [0.22-1.00]	6.50 [0.18-28.6]

The reported pressures are negative relative to atmospheric.

RLN- Recurrent laryngeal neuropathy; LLP - Left-sided laryngoplasty with ipsilateral ventriculocordectomy; LLPCOR- Left-sided laryngoplasty with ipsilateral ventriculocordectomy combined with corniculectomy; COR - Corniculectomy; PA - Partial arytenoidectomy;
TP - Tracheal air pressure; PP -Pharyngeal air pressure; K - Frictional loss coefficient

Table 3.2 Geometric assessment of larynges under airflow by procedure, reported as mean and range values.

Simulated State	A1 (cm^2)	A2 (cm^2)	A3 (cm^2)	σ_1	σ_2	Angle (deg)	s/D
RLN	8.73 [5.70-11.23]	4.9 [1.924-8.56]	15.8 [10.51-19.29]	2.01 [1.01-3.23]	0.32 [0.14-0.70]	14.54 [0.24-28.47]	1.88 [1.25-2.70]
LLP	12.83 [3.70-21.84]	10.4 [3.66-21.30]	16.3 [11.44-20.88]	1.32 [0.61-2.40]	0.62 [0.29-1.02]	6.42 [-8.74-16.02]	1.35 [0.75-2.04]
LLPCOR	12.37 [7.05-19.2]	9.8 [3.56-18.50]	16.0 [11.19-19.87]	1.53 [1.10-2.35]	0.60 [0.30-0.98]	10.53 [-1.54-25.08]	1.16 [0.69-1.91]
COR	8.77 [6.01-11.45]	5.3 [2.65-6.99]	15.4 [10.62-19.20]	1.72 [1.20-2.27]	0.35 [0.25-0.57]	16.17 [11.79-24.33]	1.39 [1.03-2.30]
PA	9.33 [8.10-10.92]	8.3 [4.51-13.90]	15.3 [10.6-18.95]	1.29 [1.10-1.58]	0.54 [0.4-0.86]	7.06 [-17.30-26.20]	1.02 [0.32-1.62]

A1, A2, and A3 = First, second, and third cross-sectional areas. D = Constriction diameter. s = Length of constricted region. σ1 = Inlet coefficient. σ2 = Outlet coefficient.

Figure 3.4 Predicted mean impedance by procedure, with 95% CIs.

RLN = Recurrent laryngeal neuropathy; LLP = Left-sided laryngoplasty with ipsilateral ventriculocordectomy; LLPCOR = Left-sided laryngoplasty with ipsilateral ventriculocordectomy combined with corniculectomy; COR = Corniculectomy; PA = Partial arytenoidectomy.

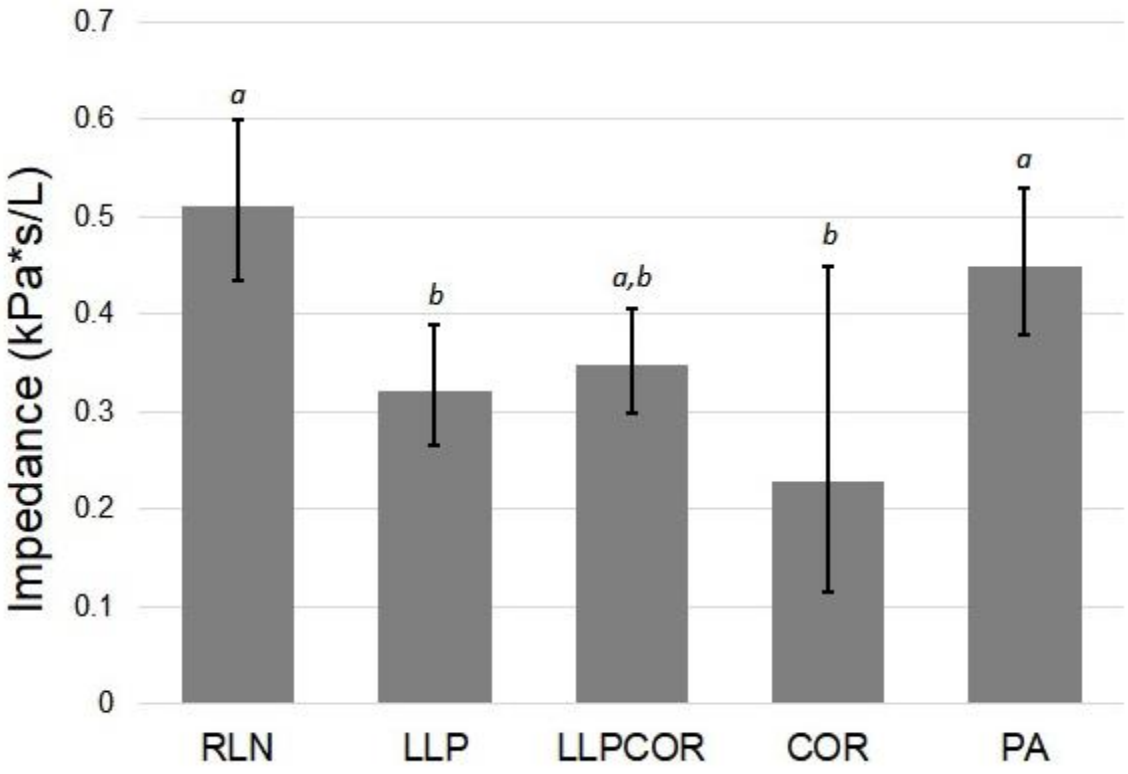

[a,b]Mean values with different letters are significantly ($P < 0.05$) different from each other.

The dimensionless orifice ratio, s/D, did not show any correlation in procedure order, compared with the other variables. The CT areas were plotted with the areas measured from the digital videos and showed a trend toward correlation.

All CT images captured allowed areas to be measured even with vibrations of the tissues noted during testing **(Figure 3.2)**. Incident angle was exponentially associated with the logarithmic transformation of the impedance **(Figure 3.5)**.

From the bivariable analysis, procedure, σ1, σ2, K, and s/D were significant ($P < 0.001$). These variables were included in the initial multivariable model, and then a backward elimination approach was used to determine which variables were significant with respect to impedance. The multivariable mixed-effects model showed a significant effect of procedure, incident angle, and inlet ratio on impedance. There was a residual intraclass correlation of 86%. Impedance was significantly different between the RLN state and PA procedure compared with the LLP and COR procedures, while the LLPCOR was not significantly different from the other 4 states **(Figure 3.4)**. Thus, the LLP and COR procedures had the least resistance to airflow over the RLN and PA.

3.5 Discussion

The box model has been previously published as a controlled method for comparing between degrees of abduction of the laryngoplasty, new surgical prototypes, and other upper airway procedures (Ahern et al., 2018; Cheetham et al., 2008c; Hawkins et al., 2014; Jansson et al., 2008; Tucker et al., 2019). Compared with the previous studies, similar magnitudes of impedance were reported for the replicated disease and procedures (Cheetham et al., 2008c; Jansson et al., 2008; Tucker et al., 2019). The COR and LLP procedures had significantly lower impedance to airflow than the RLN state and the PA procedure in the present study. The friction coefficients reported for each procedure in **Table 3.1** reflected previous findings, with increased energy loss associated with the RLN, COR, and PA procedures over the LLP and LLPCOR procedures. This value reflects energy lost with air movement across the larynx and relates to the work done by the patient during breathing. Compared with previous research, the RLN impedance reported here was much higher but this may be explained by having different populations of larynges and a different airflow model (dynamic versus static). A static airflow model was necessary in this instance to ensure clear CT images for analysis.

Figure 3.5 Plot of incident angle versus log impedance.

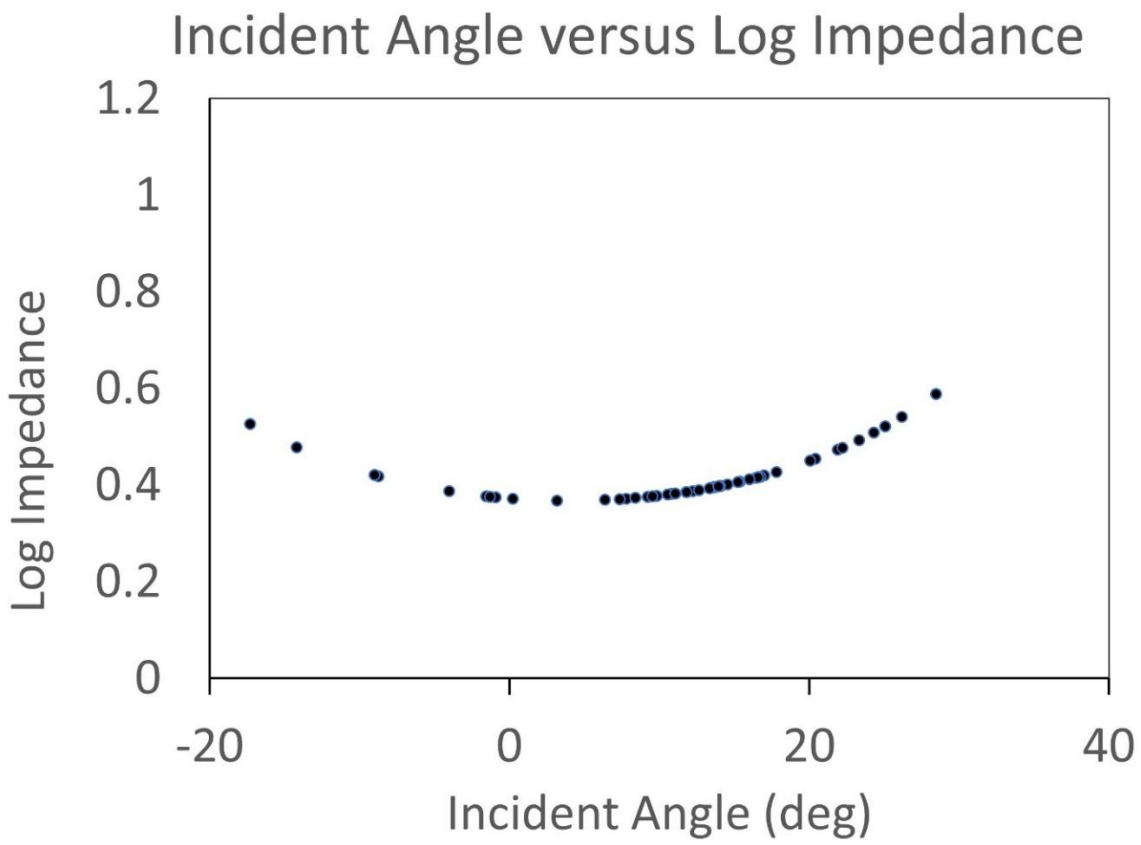

Three-dimensional imaging affords greater insight into the diagnosis and treatment of upper airway obstructive disorders in horses. Using CT imaging and markers, one study (Perkins et al., 2010) found that the arytenoid cartilage moves about 3 axes during abduction, with the primary movement of interest due to rocking from the lateral belly of the CAD muscle. More recently, Lynch et al. (2020) related this motion to varying levels of force on the laryngoplasty suture while also replicating inhalation within a larynx. That report also demonstrated insignificant gains in arytenoid angle and airflow beyond approximately 50% of the maximal suture abduction force (Lynch et al., 2020). Uniting the anatomical configuration of arytenoid abduction with the CSAs along the larynx and fluid mechanics will lead to a more accurate awareness of airflow as it relates to patient outcomes. CT, MRI, and transesophageal ultrasound have also led to insights about the pathology and diagnosis of RLN. Decreased CAD muscle volume, muscle belly CSA, neuronal density and percentage of collagen and fat have all been associated with progressively decreased arytenoid abduction (Chalmers et al., 2012; Kenny et al., 2017; Pekarkova et al., 2009). While these efforts focused on diagnostic capabilities and decreasing CAD muscle function, the present study demonstrated the possible therapeutic potential of these imaging modalities beyond diagnosis alone.

The literature reporting the box model concludes that while it does not exactly capture the clinical scenario, it does duplicate respiratory mechanics that have been experimentally confirmed in adult horses (Cheetham et al., 2008c; Jansson et al., 2008; Tucker et al., 2019). Complete paralysis of the CAD muscle as occurs with advanced RLN is successfully duplicated, and previous research found that measured CSA of the rima glottis is significantly associated with impedance. However, it raised some questions about the validity of this measure. The ventricles within the larynx lie caudal to the rima glottis, but may collapse with severe disease, further narrowing the effective CSA of airflow. Area measurements from both the CT images and digital video showed a trend toward correlation in the present study, but outlying values raised questions about why these differences in measurement might have occurred. One consideration is that the arytenoid cartilages are angled differently within the coronal plane between larynges. Dependence upon a scale measurement within digital imaging software versus CT images may also influence measurement accuracy. As the ability to improve image analysis improves with technology, this is likely to be the more consistent methodology for future studies.

Form within the upper airway significantly affects function, especially with equine performance. While decreased CSA has been the primary focus, there are other factors that have not been examined previously, such as the length over which airway constriction occurs, and the outflow conformation. Within a constricted region of a pipe the ratio of the constriction to original pipe diameter, angle of the inlet, and thickness of the constriction are significantly associated with increasing turbulence in fluid mechanics. The area ratios observed here indicate that the level of constriction, relative to the patient's initial pharyngeal and tracheal diameters, significantly affect impedance. The replicated disease and procedures in the present study demonstrated a thick orifice conformation, $\sigma_1 > 0.5$ (Fossa et al., 2002). This means that airflow within the constricted portion of the larynx is expected to reattach to the walls before exiting into the trachea, which could increase wall stress experienced by the caudal larynx. In patients with a longer larynx, this equates to a greater propensity for collapse with higher velocities closer to the caudal portion of the arytenoid cartilages. Given the proposed cycle of collapse causing increased air velocity and negative pressure resulting in more collapse, this may represent a potential area of intervention. The incident angle of airflow demonstrated an exponential relationship with impedance, which is also expected for flow within a pipe. There is an ideal angle of approach to a narrowed region that reduces the amount of flow disturbance. Clinically this means that in a horse with a wide pharynx and a narrower trachea, a greater degree of abduction may be advantageous in creating a smoother transitional zone as air flows into the larynx. These regions are known to have a significant effect on flow development in fluid mechanics but have not been examined in the horse to the author's knowledge.

In the human airway surgery literature, experimental simplified models based on actual patient conformations have been fundamental to understanding the fluid mechanics before incorporating complexities such as tissue elasticity, muscular function, and fluid-structure interactions (Geng et al., 2020; Johnstone et al., 2004; Scherer et al., 2001). The areas, ratios, and orifice thickness reported in this paper may be used to develop similar models for horses. By contrast, the vocal folds of humans have been extensively researched due to their direct influence on speech quality, but unanticipated impacts on airflow were also discovered (Scherer et al., 2001). Recirculation regions and flow separation were observed in both symmetrically and in asymmetrically angled models (Erath et al., 2006a). These recirculating areas may contribute to more stress on the larynx due to increased velocity profiles (Erath et al., 2006a). Given that within

the human airway these regions represent a significant constriction, the same may be true in a horse with RLN such that the airflow in the region is heavily influenced by small conformational changes. The present study demonstrated that the point of maximal constriction occurs at the level of the ventricles which likely play a significant role in arytenoid collapse. The 2000 study by Jansson et al. also revealed that a laryngoplasty with cordopexy did reduce the drop in pressure and increased the airflow across the larynx, but this was not found to be significant. In cases of inadequate abduction, removal of the ventricle and vocal fold may therefore improve laryngeal CSA and airflow. Further investigation regarding the role of the ventricle in equine airflow is warranted.

The present study reported a 3-D, stressed image of the upper airway that is unlikely to be possible in equine patients for the foreseeable future. It sets the foundation for basic configurational analysis of the equine upper airway; however, there are many areas where further investigation is needed. The LLP and LLPCOR improved impedance significantly over the RLN state, and the fluid mechanics reported here would suggest that a COR procedure may be advantageous in horses with an elongated laryngeal region. Additionally, creating a smooth “funneling” transition from pharynx to trachea should be prioritized to maximize postoperative airflow while minimizing the work of breathing.

3.6 Acknowledgments

The authors would like to acknowledge Dr. Cheryl Waldner for her assistance in coding and development of statistical analysis for this manuscript.

3.7 Addendum

The abstract of this chapter was revised to reflect the format of the thesis and to maintain the cohesiveness of the document. Minor revisions to the manuscript were made to improve content and readability as compared to the original publication. Supplementary material was incorporated into the main body of the manuscript.

CHAPTER FOUR:

COMPUTATIONAL FLUID DYNAMICS ANALYSIS OF UPPER AIRWAY PROCEDURES IN EQUINE LARYNGES

The previous study raised questions about the three-dimensional interaction of equine laryngeal geometry and flow. Computational fluid dynamics analysis provides a finite solution of fluid mechanic characteristics throughout a given volume. It can be used in a predictive manner to anticipate changes in airflow associated with changes in geometry.

This study sought to unite the three-dimensional fully complex equine larynx geometry with three-dimensional flow characteristics using CFD on each of the procedures for each larynx. It also served as an initial investigation into the use of CFD as a predictive tool in equine airflow, especially when comparing between procedures within one larynx which represented an individual patient. While the previous study focused on cross-sectional area, CFD analysis is more comprehensive in capturing the tissue changes that occurred between procedures and the influence within larynx on pressure and velocity in fully-developed flow. This better informs the decisionmaker about why certain procedures may have a lower impedance over another and the anatomical regions that are most critical to flow development.

Full citation: Tucker ML, Bergstrom D, Wilson DG, Carmalt JL. Computational fluid dynamic analysis of upper airway procedures in equine larynges. Anticipated 2022.

Author Contributions: Tucker, Bergstrom, Carmalt were responsible for the study design, data collection and analysis. Wilson contributed to grant authorship and study design. Bergstrom contributed to the fluid mechanical study design components and provided editorial assistance to the manuscript. Tucker authored the manuscript with editorial assistance from Carmalt, Bergstrom and Wilson.

4.1 Abstract

Computational fluid dynamics (CFD) has been a very useful adjunct analysis used in the planning of upper airway surgery in humans, where it is used to study the projected influence of the surgical procedures on post-operative airflow. This technology has only been reported twice in an equine model, with only select aspects of airflow mechanics examined. The reported study seeks to widen this application to the variety of procedures currently used to treat equine recurrent laryngeal neuropathy (RLN). The first objective of this study was to characterize the three-dimensional geometry of equine larynges replicating RLN and four subsequent surgical procedures under airflow conditions. The second objective was to determine the accuracy between a CFD model and measured airflow characteristics in equine larynges. The last objective was to explore the anatomic distribution of modelled areas of pressure, velocity, and turbulence associated with the disease (RLN) and each surgical procedure performed. Ten equine cadaveric larynges were placed in an instrumented box to replicate inhalation airflow while undergoing a concurrent computed tomographic exam. The pressure upstream and downstream (outlet) were measured simultaneously. Image segmentation was then performed to generate stereolithography files which were smoothed and remeshed, then used for CFD modelling. CFD analysis using the experimentally measured outlet pressure were performed. The procedural order and calculated laryngeal impedance were then compared to the experimentally obtained values. The CFD model agreed with the experimental portion of the study in predicting the surgical procedure resulting in the lowest post-operative impedance in 9/10 larynges. Numerically, the CFD calculated laryngeal impedance was approximately 0.7 times that of the experimental calculation. Areas of low pressure and high velocity were observed around tissue irregularities within the lumen of the larynx. Peaks were associated with RLN and the corniculectomy and partial arytenoidectomy surgical procedures. CFD modelling of the equine larynx reliably calculated the lowest impedance of the different surgical procedures. Future development of the CFD technique to this application may improve numerical accuracy.

4.2 Introduction

Partial upper airway obstruction as a result of equine recurrent laryngeal neuropathy (RLN) results in decreased performance and represents a complex surgical problem. While there have been a large number of studies looking at the laryngoplasty and partial arytenoidectomy (PA) surgical techniques and their effects on performance, there are still many suboptimal postoperative outcomes (Compostella et al., 2012; Davidson et al., 2010). Ex vivo models have contributed significantly to the refinement of these procedures, and further exploration of how laryngeal manipulation influences airflow development.

In particular, the equine "laryngeal box" flow system has explored the influence of various surgeries on overall airflow through the larynx. It allows for a controlled environment in which the effect of laryngoplasty, cricoarytenoid joint stabilization, vocal cordopexy, PA, and the arytenoid corniculectomy surgeries have been studied (Ahern et al., 2019; Cheetham et al., 2008c; Gray et al., 2021; Hawkins et al., 2014; Jansson et al., 2000; Tucker et al., 2019). This system was used to prove that the translaryngeal impedance was related to prosthesis shortening and arytenoid abduction and demonstrated the mechanical advantage of cricoarytenoid joint stabilization. Despite this, a recurring theme of "individual variability" was observed across the studies. While the box system continues to be used as a preliminary testing mechanism for new surgical ideas, it does not completely capture the intricacies of laryngeal mechanics nor the outcomes observed in individual clinical patients.

The benefit of combining computational fluid dynamics (CFD) to clinical knowledge is exemplified within human respiratory surgery. CFD studies have led to a greater understanding of the relationship between the geometry of the upper airway and obstructive airway disorders, such as the pharyngeal length and increasing degrees of collapse (Jeong et al., 2007; Kim et al., 2013; Sung et al., 2006; Taherian et al., 2017; Wootton et al., 2016). This has allowed surgeons to make better decisions regarding treatment type, and expected procedure efficacy, for complicated problems such as obstructive sleep apnea syndrome and nasal septal deviation; even going so far as to develop individualized patient treatments (Jeong et al., 2007; Kim et al., 2013; Sittitavornwong et al., 2013; Sung et al., 2006; Taherian et al., 2017; Wootton et al., 2016).

Similarly, an equine upper airway CFD model that replicated the anatomy from nares to trachea has been reported. The model replicated the inhalation and exhalation cycles of an

exercising horse with the anticipated air velocity and volumetric flow rates, demonstrating validity in the application of the equine patient (Rakesh et al., 2008a; Rakesh et al., 2008b). A follow up study demonstrated the use of the model to investigate equine surgeries and found that 88% arytenoid abduction was an acceptable level to potentially improve performance in horses (Rakesh et al., 2008c). A different group used CFD to test variations of an equine metabolic nasal mask design and to ensure that the mask would function as desired without significantly increased airway impedance (Massie, 2015). While CFD provides more specific and comprehensive information about the fluid mechanics in the equine subject, its continued validation and advancement are needed in this field to widen its applications.

The objectives of this study were to generate a clinically accurate CFD model of ten different equine larynges replicating RLN and four therapeutic surgeries based on an *ex-vivo* box model. Secondly, to determine the reliability of the CFD model in predicting which surgical procedures would generate the lowest impedance to airflow and compare the results to those measured from the box model. Thirdly, to examine the morphological impacts of RLN and four different surgical interventions on pressure, velocity and turbulent kinetic energy. The first hypothesis was that the CFD model would be able to accurately predict the surgical procedure generating the lowest impedance compared to the experimental data for a specific larynx as the comparison. The second was that the peak negative pressure concentration, peak velocity, and peak turbulence would occur in those surgical procedures that created the highest impedance and the generated the most collapse of the laryngeal tissue.

4.3 Materials and Methods

4.3.1 Experimental Data and Image Collection

Ten larynges were collected from equine cadavers with no reported history of upper airway disease as previously described (Tucker et al., 2019). Each larynx was collected within two hours of euthanasia along with the esophagus and surrounding tissues and wrapped in saline-soaked gauze. They were placed in a freezer at -20˚C until the day before testing. Thawing occurred over 20 hours by placing the laryngeal specimens in a room at 23˚C. Just prior to testing, the esophagus, excess tracheal rings, and remaining extrinsic musculature were removed from each specimen. Four to five tracheal rings were left *in-situ* to allow overlap with a polyvinyl chloride

adapter for insertion into an instrumented box. The adapter facilitated attachment of each laryngeal specimen to the box outlet which was 5.08 cm in diameter. Each trachea was matched to a corresponding adapter of either 2.54 or 3.81 cm in diameter and fixed with plastic cable ties to create a seal (Tucker et al., 2019). The epiglottis was anchored to foam in the bottom of the box to prevent dorsal movement and retroversion into the airflow during testing.

Pressure transducers (Model P55D, Validyne Engineering, Los Angeles, CA) were used to measure the pressure within the box and the tracheal adapter at 100Hz while an orifice plate (ISO 5167, 2003) was used to measure the flow rate of air through the trachea using an additional transducer (Model DP103-14, Validyne Engineering, Los Angeles, CA; Tucker et al., 2019). The flow rate was recorded for a minimum of 30 seconds using an analog-to-USB adapter (USB-6221, National Instruments, Austin, TX) for each laryngeal trial and monitored using a commercial software (LabView; National Instruments, Austin, TX). Pressure within the trachea and box were recorded, along with flow rate, as previously described (Tucker et al., 2019). Concurrent digital video recording was performed using a USB camera (Logitech C920 Pro HD Webcam, Logitech, Newark, CA) during the simultaneous computed tomographic (CT) exam. Helical CT scans were performed at 200 mAs, 120 kVp with a 0.64 mm pitch with 1 mm slice thickness at a scan speed of 1 mm/s using a Toshiba Aquilon One (Canon Medical Systems, Markham, ON, CA).

Each larynx underwent the same testing sequence, resulting in 5 different trials per larynx. First, left RLN was imitated by performing a right laryngoplasty with a single piece of #5 Ethibond suture (Ethibond Excel, Ethicon US LLC, Bridgewater, NJ). The cricoid cartilage bite was performed from ventral to dorsal, approximately 10 mm rostral to the caudal border and medial to any palpable notches within 10 mm from the sagittal ridge. The arytenoid bite was placed into the spine of the muscular process in a dorsomedial to ventrolateral direction. Tension was placed to ensure maximal abduction of the right arytenoid cartilage and a surgeon's throw was performed followed by three square throws, ensuring that tension was maintained. The larynx was tested with the right arytenoid cartilage abducted and the left arytenoid cartilage allowed to collapse. Once adequate data was collected, a left laryngoplasty with ipsilateral ventriculocordectomy (LLP) was performed using a roaring burr to exteriorize the left ventricular mucosa for excision (Brown et al., 2003) The remaining mucosa was glued using cyanoacrylate glue to minimize excessive tissue collapse and replicate the postoperative mucosal healing. Following the airflow trial, a left

arytenoid corniculectomy was performed by excising the corniculate process of the left arytenoid (LLPCOR). Once this was tested, the left laryngoplasty suture was cut and removed from the larynx, imitating a simple corniculectomy with ipsilateral ventriculocordectomy procedure (COR). This was tested and then a PA procedure was performed by removing the body of the left arytenoid cartilage, followed by a final round of testing (Speirs, 1986).

4.3.2 Segmentation

The DICOM files from the CT scans were imported into Fiji (ImageJ National Institutes of Health, Bethesda, MD) for segmentation. Automatic segmentation was performed using the 3D viewer plugin, examined slice-by-slice, then exported as binary stereolithography file (.stl) files. These were then imported into Ansys® SpaceClaim (Ansys 2021 R1, ANSYS, Inc., Canonsburg, PA) to remove plastic cable ties from the laryngeal geometry, in addition to artifact elements from the metal anchor used to pin the epiglottis and any unattached artifacts. The CT resulted in mirror image geometry, which was flipped and imported as a stereolithography file (.stl) into MeshLab (MeshLab version 2020.12, Visual Computing Lab, CNR-ISTI, Pisa, Italy). The non-manifold vertex and face filters were applied to clean the mesh, and the HC Laplacian smooth function was applied for twenty iterations until the geometry appeared smooth (Massie, 2015; Vollmer et al., 1999). The remesh filter was applied to minimize the file size associated with the mesh. The mesh was exported as an .stl file which was reintroduced into SpaceClaim. The sharp edge detection tool and mesh editing tools were used to clean the geometry further until the faceted body could be converted into a solid body. This was adjoined with the computer-aided design (CAD) geometry for the box and inlet and outlet pipes to replicate the experimental system. The inlet and outlet were labelled in SpaceClaim and the geometry subsequently imported into Ansys® Fluent (Ansys 2021 R1 build 10179, ANSYS, Inc., Canonsburg, PA) for meshing and computation **(Figure 4.1)**.

A mesh independence study was performed to determine optimal mesh size for the variables of interest, namely the calculated within-box pressure, calculated airflow rate and laryngeal impedance as in section 4.3.5. The resulting ideal mesh size was 11 million cells or greater. A local size element of 0.25 mm was used for the surface mesh around the larynx, while 0.5-15 mm was used throughout the box and pipe with a growth rate of 1.2. Smooth transition boundary layers were applied with 5-layer depth. A polyhedral mesh was generated using the meshing tool under these conditions for each procedure for each larynx.

Figure 4.1 Larynx in box geometry.

The inlet on the left was defined as atmospheric pressure and flow proceeded into the box through the larynx to exit at the pipe outlet defined as the measured negative tracheal pressure.

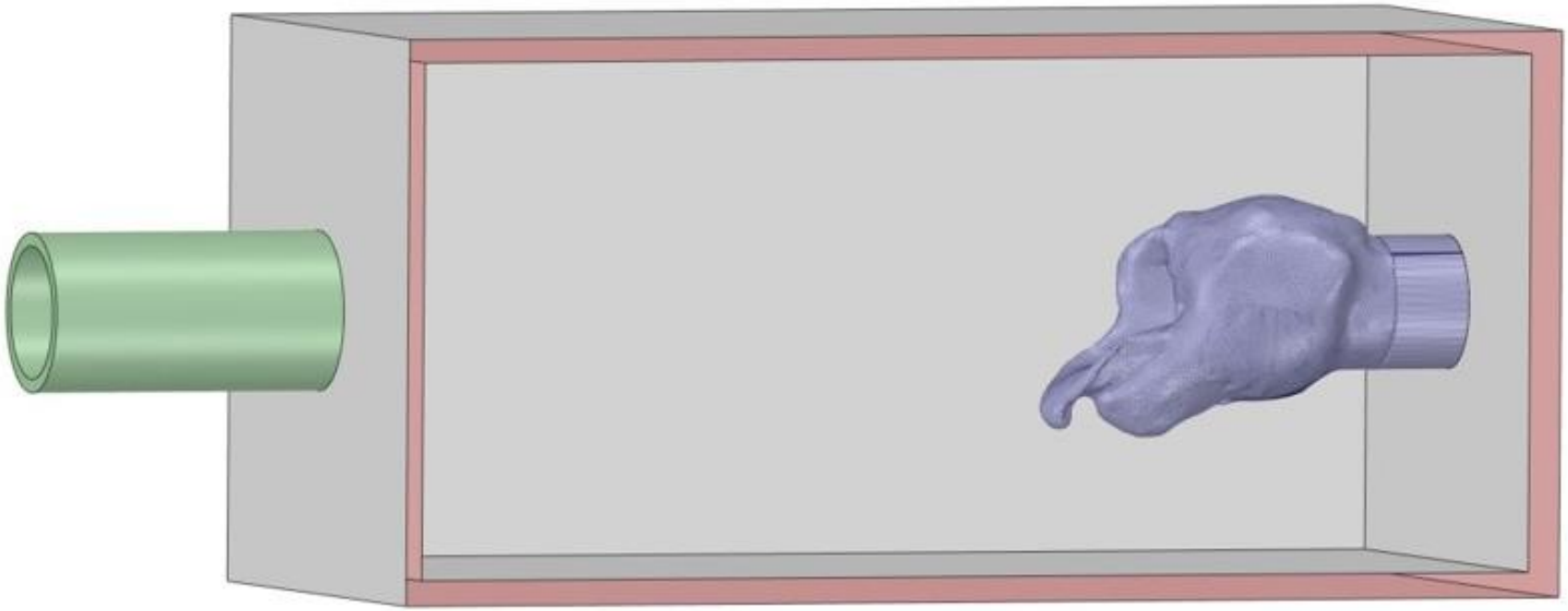

4.3.3 Numerical Model

The calculations were performed using Fluent using the finite volume method. Air was assumed to be incompressible with density 1.225 kg/m^3 and viscosity 1.789x 10^{-5} kg/(m*s). Rigid walls were assumed with dry conditions and no respiratory mucus as has been previously reported (Massie, 2015; Rakesh et al., 2008b). This circumvented the need for a complex fluid-fluid interaction model. A realizable κ-ε turbulence model was solved using the Semi-Implicit Method for Pressure Linked Equations (SIMPLE) method for the Reynolds-Averaged Navier Stokes (RANS) equations. A standard wall function was implemented.

4.3.4 Boundary Conditions

Each case was set up as a pressure differential problem. At the inlet of the pipe, atmospheric pressure of 0 Pa was used. For the outlet pipe, the opening pressure was defined as the measured tracheal pressure for that treatment/larynx, which was on average -4300 Pa. Zero velocity was assumed along the walls. The walls were defined as "no slip" with a smooth transitional boundary mesh. Calculations were performed on a 16-core, 4.30 GHz AMD Ryzen Threadripper processer (Advanced Micro Devices, Santa Clara, CA) with 128GB RAM.

4.3.5 Mesh Independence Study

The mesh independence study was conducted using the RLN state for the fifth larynx, which was anticipated to exhibit high resistance with resultant complex flows. Planes of interest were generated parallel to the axial, sagittal and transverse planes to capture the average and minimum pressure for each plane, with mesh sizes of 1.5, 3, 5.8, 11.5 and 17.9 x10^6 cells to determine the change between each of the increases in size and the trend of the solutions. The planes of interest are shown in **Figure 4.2**. The variables of greatest clinical interest were pressure, flow rate, and impedance. These changed in clinically insignificant proportions between the 11 and 17 million cell models (4-5%, 0.004%, and 1.4% respectively). The computer was unable to proceed with calculations above 17 million mesh elements. The 11 million cell model took less than an hour to run 1000 iterations in most instances. This was sufficient to achieve stable residual reduction of more than 10^{-2} in the majority of the calculations performed.

Figure 4.2 Planes generated for the independent mesh study and qualitative analysis.

Planes in three orthogonal directions were generated in Fluent to analyze the flow characteristics in anatomical and geometrical areas of interest.

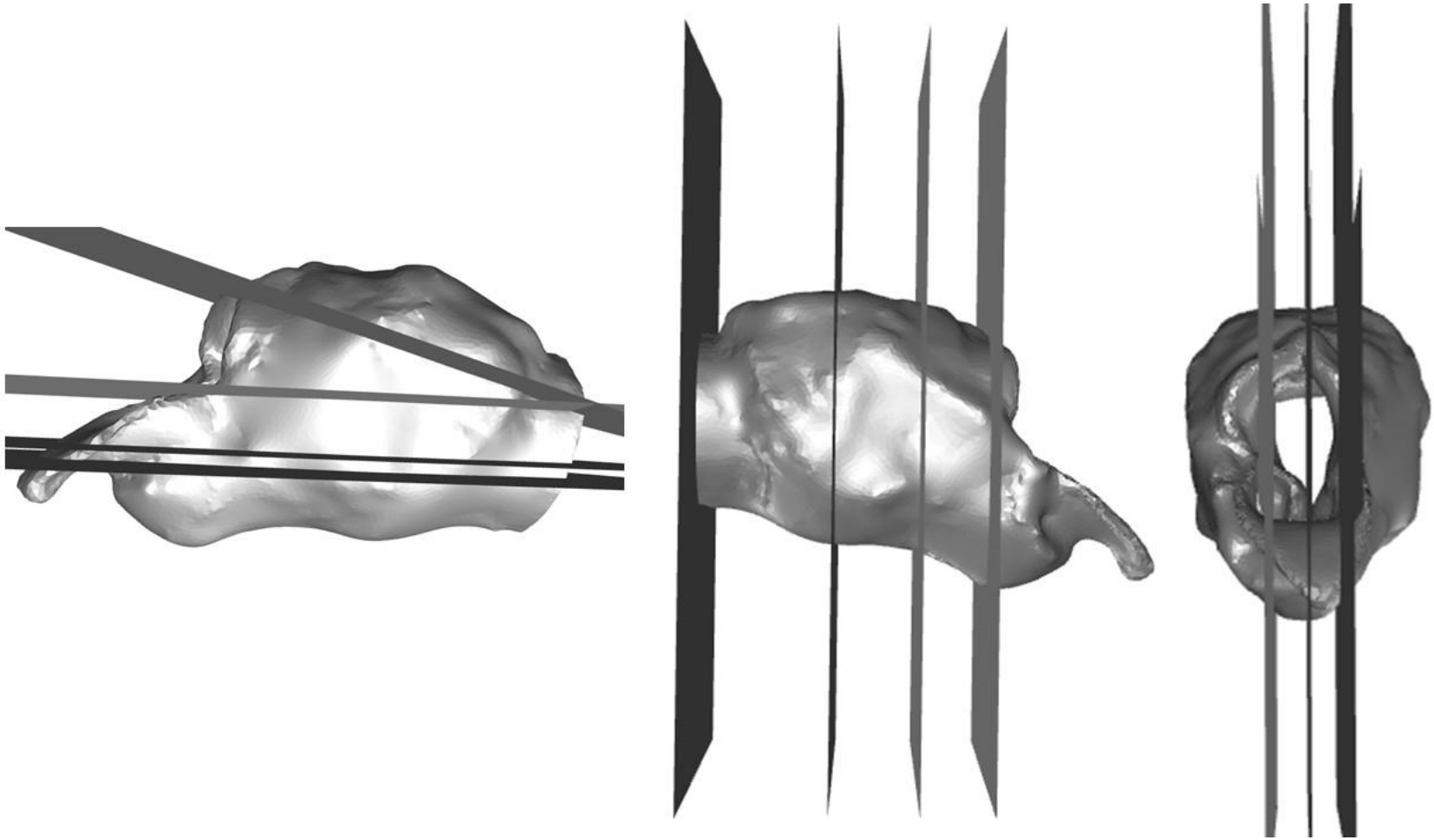

4.3.6 Data analysis

For each of the five tests for each larynx the computational result was analyzed for the given impedance across each larynx. This was calculated by taking the area-averaged box pressure just upstream from the larynx and subtracting this from the area-averaged outlet pressure divided by the calculated air flow rate, as shown in the equation that follows.

Equation 4.1

$$Impedance = \frac{P_{Box} - P_{Trachea}}{Flow\ Rate}$$

A mixed effects statistical model was performed examining the effect of larynx and procedure on the CFD-derived impedance using larynx number as a subject-level effect. Subsequent pairwise comparisons were then performed using Tukey-Kramer between procedures (SAS 9.4, SAS Institute Inc., Cary, NC) with significance set at $p < 0.05$.

Qualitative analysis of the velocity, pressure, and turbulent kinetic energy production was performed for each procedure within larynx by creating planes of interest as for the mesh independence study. Three sagittal planes, four transverse, and four cross-sectional planes were generated to examine the flow characteristics within the larynges. Each of these planes was cropped to focus on the mechanics of the laryngeal region for comparison. The sagittal planes were generated at midline, then a parasagittal left and parasagittal right plane to examine the effects just inside the walls on the left and right side of the larynx. Transverse planes were generated to divide the larynx in half, then mid-saccule, and an additional dorsal and ventral plane halfway between the limits of the lumen and the existing planes, and slightly angled to incorporate the trachea. Cross-sectional planes were generated at the laryngeal opening, mid-saccule, and caudal to the saccules and a fourth plane within the trachea. For each larynx, the pressure, velocity and turbulent kinetic energy color scale was normalized to determine the influence of each procedure within larynx. When characteristics were seen that warranted closer examination, the three-dimensional streamline (velocity, turbulent kinetic energy) or wall renderings (pressure) were referenced to further characterize the flow effects.

4.4 Results

4.4.1 Quantitative Results

The rima glottis cross-sectional areas were compared between CT measurements and the final geometry for all procedures across all larynges and showed a strong trend toward a 1:1 correlation. This indicates that the methods used to produce the three-dimensional models here were effective in appropriately capturing the geometry for numerical analysis **(Figure 4.3)**.

For 7 out of 10 larynges, the CFD model determined that the same surgical procedure generated the lowest impedance that was reported experimentally. For 2 of the larynges, there were two procedures where the CFD and experimental "procedure of choice" were different, but looking at the impedance values, the difference is 0.02 or much less. The procedure of choice by larynx along with the experimentally measured and CFD-calculated impedance are listed in **Table 4.1**. For one larynx, the computational model and experimental measurement resulted in different procedures of lowest impedance, but computationally there were two procedures that were close in impedance.

In comparing experimental versus computed values for flow rate, pharyngeal pressure, and impedance, plots were performed to compare the experimental and CFD results. A strong correlation was observed between experimental- and CFD-derived impedance, flow rate and pharyngeal pressure. The mixed effects statistical model was constructed accounting for larynx and procedure and examining the effects on CFD calculated impedance. RLN was found to be significantly different from the surgical procedures, LLP was significantly different from COR but there were no other significant differences between surgical procedures. The resultant p-values from the Tukey-Kramer pairwise comparisons are shown in **Table 4.2**.

4.4.2 Qualitative Results

All of the slices from each procedure for each larynx were placed side-by side and compared as reported below. Trends across larynges are reported as follows for pressure, velocity and turbulent kinetic energy.

Figure 4.3 Plot of CT versus CFD model derived rima glottis area.

The CT-derived area was taken from the coronal plane, the first complete area of tissue. A similar plane was obtained in the 3D geometry in SpaceClaim following processing and the cross-sectional area measured.

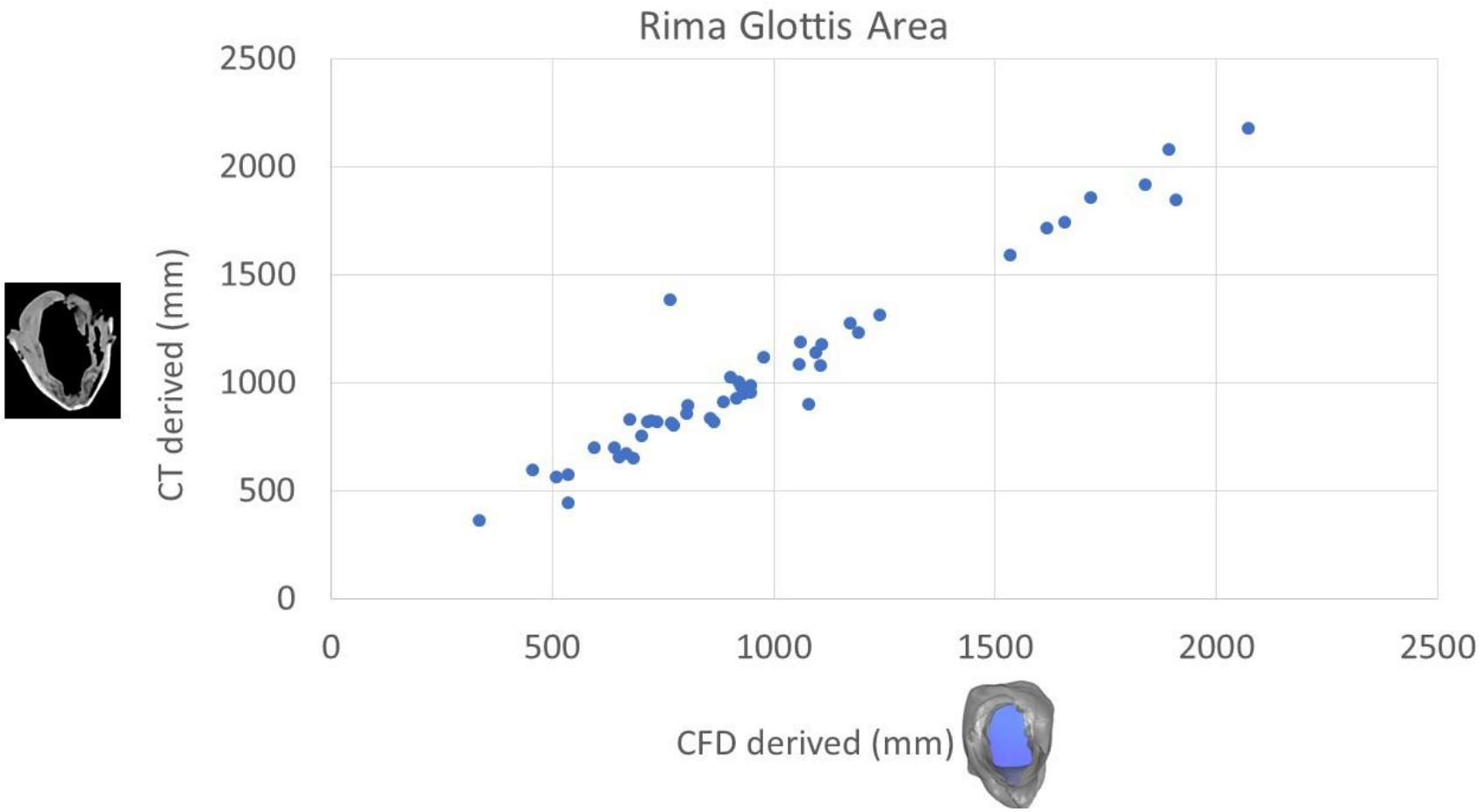

Table 4.1 Procedure of lowest impedance for each larynx.

		Impedance (kPa*s/L)	
Larynx #	**Surgical Procedure**	**CFD**	**EXP**
1	**LLP**	0.177	0.195
2*	**LLP**	0.026	0.024
2*	**LLPCOR**	0.026	0.026
3**	**LLPCOR**	0.109	0.169
3**	**PA**	0.107	0.201
4	**LLP**	0.030	0.041
5	**LLPCOR**	0.058	0.084
6	**LLP**	0.039	0.048
7	**LLP**	0.055	0.080
8*	**LLP**	0.067	0.099
8*	**LLPCOR**	0.065	0.118
9	**LLPCOR**	0.051	0.093
10	**LLP**	0.038	0.045

EXP-experimentally measured laryngeal impedance

*For larynges 2 and 8 there were two procedures with lowest impedances that differed by less than 0.02.

**For larynx 3, the CFD and EXP impedance did not agree for the “best” procedure so both are reported for comparison.

Table 4.2 Resultant p-values between procedures from the mixed effects statistical model by procedure.

Simulated State	PA	COR	LLPCOR	LLP	RLN
RLN	**<0.0001***	**0.0054**	**<0.0001***	**<0.0001***	**---**
LLP	0.4114	**0.0169***	0.9997	----	
LLPCOR	0.5236	0.270	----		
COR	0.5558	-----			
PA	---				

*Significantly different impedances between these two procedures with $p < 0.05$

4.4.2.1 Pressure

Pressure for the LLP and LLPCOR procedures was uniformly distributed across the opening and from rostral to caudal, as demonstrated in **Figure 4.4**. This was consistent across larynges. RLN, COR, and PA demonstrated a more abrupt change in pressure associated with the rapid change from a large to small luminal diameter.

4.4.2.2 Velocity

A uniformly increased velocity through the lumen was observed for the LLP and LLPCOR procedures, while a higher peak velocity was observed for the RLN, COR and PA procedures. **Figure 4.4** demonstrates the difference between these groupings with relevant cross-sections from the LLP and COR states. Occasional areas of focused negative pressure and high velocity were noted with particular laryngeal geometries, as shown in **Figures 4.5A and B**.

4.4.2.3 Turbulent Kinetic Energy

Regions of increased turbulent kinetic energy were observed often caudal to the saccules, and were associated with inconsistencies of the lumen, such as irregularity in the tissue margins, especially when perpendicular to the plane of flow **(Figure 4.6)**. Concentrated areas of increased turbulent kinetic energy were not always observed with more obstructive procedures. Larynges 3 and 5 had greater turbulence in the rostral portions of the LLP and LLPCOR procedures compared to their cohorts. A brief summary of the observations for pressure, velocity, and turbulent kinetic energy for each larynx by procedure can be found in **Table 4.3**.

Figure 4.4 LLP and COR sections inside the left arytenoid cartilage for pressure and velocity.

The white region in the plane sections represents the laryngeal tissue, and the colored regions represent the region of airflow. A more gradual transition in pressure and velocity can be observed in the LLP section while the COR section reflects a more obstructive conformation where an abrupt change in pressure and velocity are present.

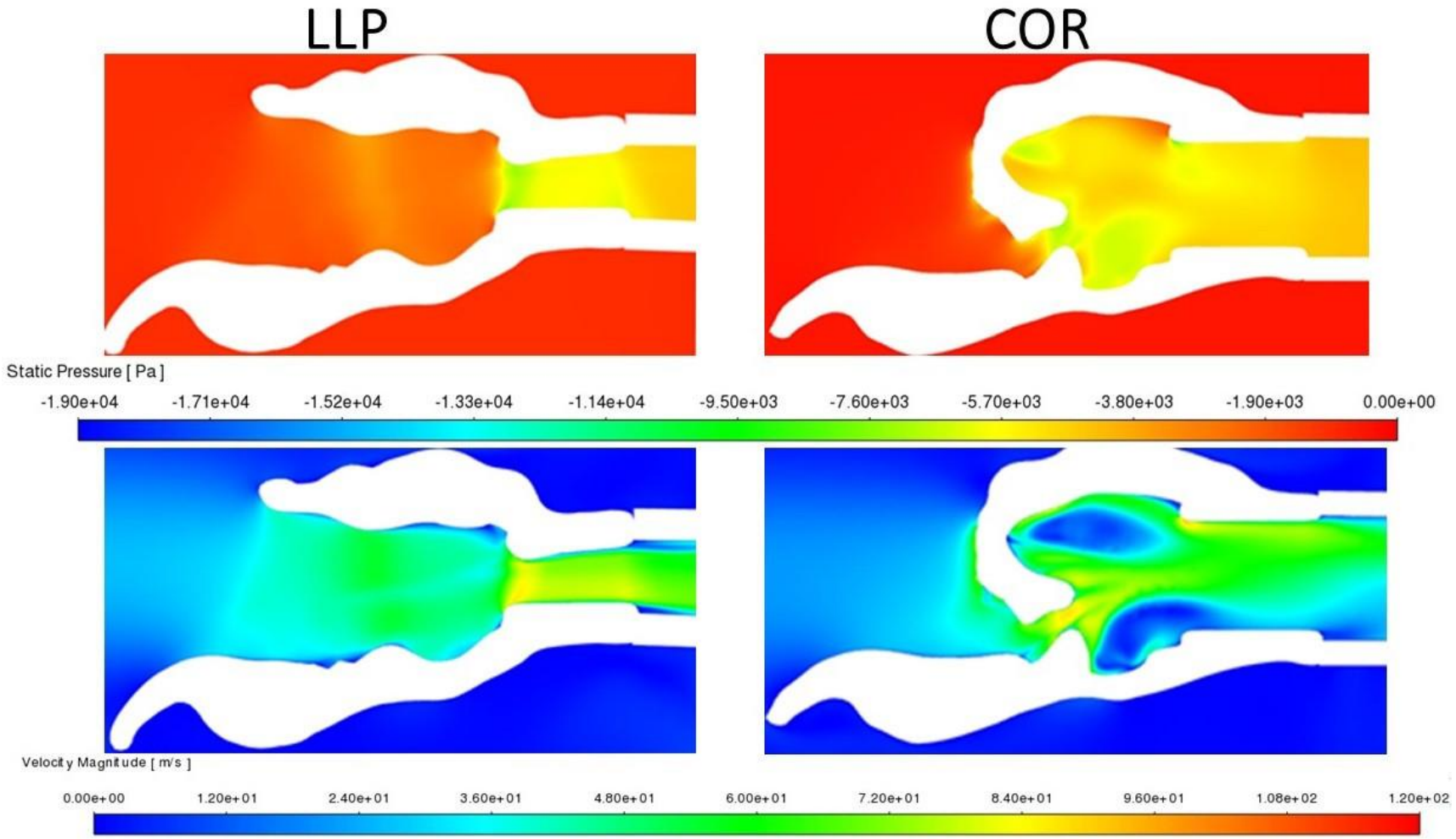

Figure 4.5A Sagittal velocity section (left) and cross-sectional rima glottis section for PA with velocity (right) and pressure (Figure 4.5B).

Of particular note is the ventral obstruction in the sagittal image and the region of lower pressure and high velocity inside of the left arytenoid cartilage (on the right side of the cross-sectional images, denoted by the black arrow).

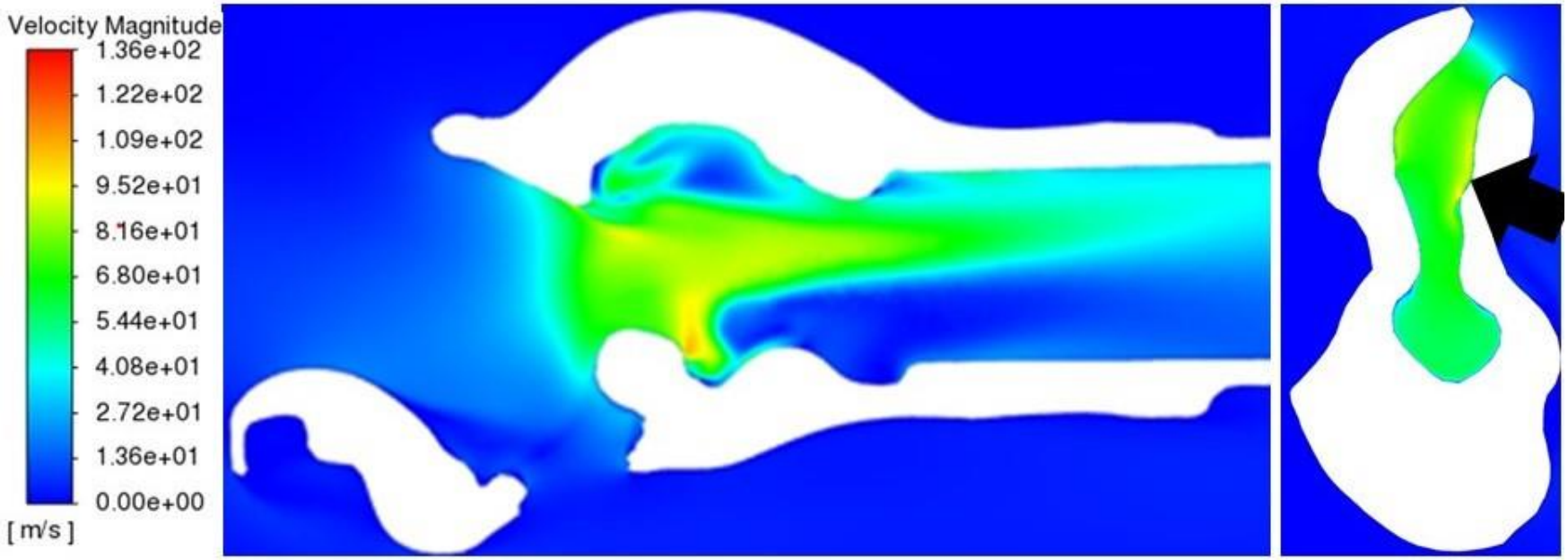

Figure 4.5B Cross-sectional rima glottis section for PA displaying the pressure distribution. Of particular note is the ventral obstruction in the sagittal image (Figure 4.5A) and the region of lower pressure and high velocity inside of the left arytenoid cartilage (denoted by the black arrow).

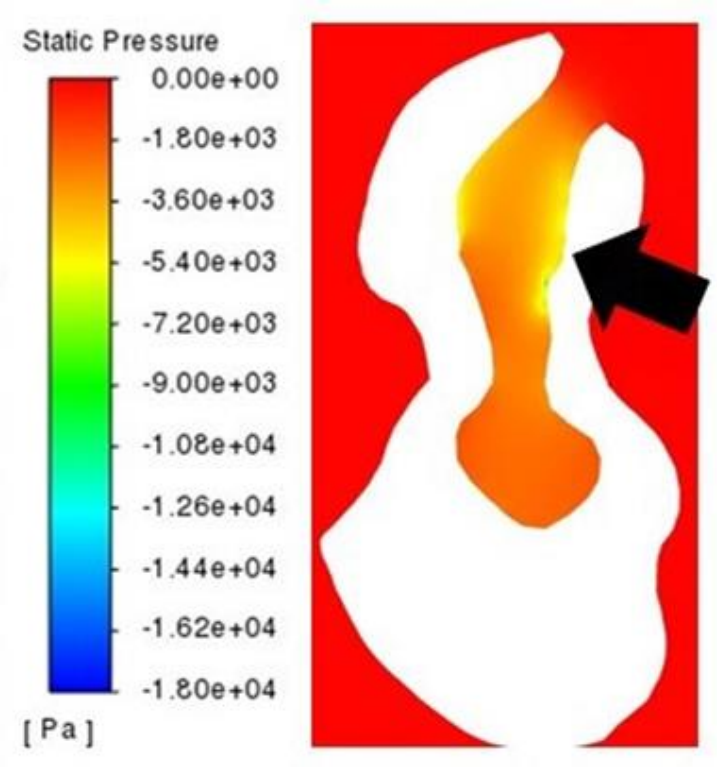

Figure 4.6 Dorsal transverse section of PA and three-dimensional rendering of the same larynx, top view. Both images represent a top perspective of the larynx showing increased turbulent kinetic energy downstream from tissue obstruction within the lumen and the three-dimensional rendering showing eddy formation in the same region behind the obstruction.

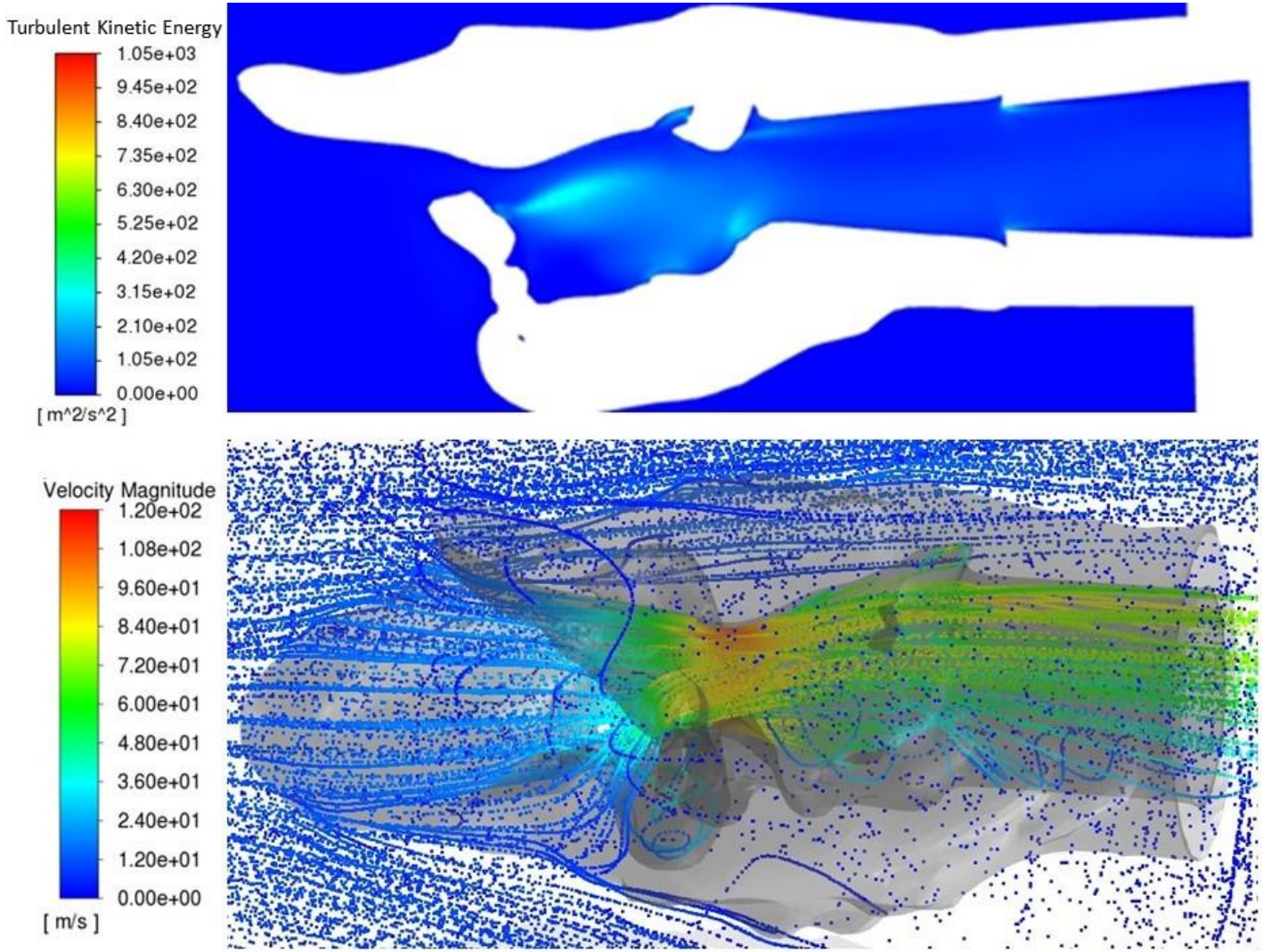

Table 4.3 Summary of qualitative results by larynx.

Larynx #	Pressure	Velocity	Turbulent Kinetic Energy
1	LLP, PA: right peak LLP: right arytenoid; mid saccule LLPCOR, PA: peak left arytenoid	RLN: jet formation, right side higher than left LLP, LLPCOR, PA: increased velocity COR: right side has higher than the left	LLP, LLPCOR, PA: increased caudal larynx
2	LLP/LLPCOR: more uniform COR: spike PA: High pressure inside left	LLP, LLPCOR: more uniform RLN, COR, PA: spikes	RLN, COR, PA: increased PA: most, caudal portion
3	LLP increased	LLP increased more caudal, dorsal left arytenoid wall LLP/LLPCOR increased, COR lower	LLP increased turbulence LLPCOR caudal PA on left
4	COR: peak inside left arytenoid	RLN: high COR: highest with caudal narrowing PA: flow separation from wall	COR/ PA: more caudal mixing
5	LLP: peak inside left arytenoid LLPCOR: inside aryepiglottic fold	LLP, LLPCOR-high caudal and inner left arytenoid, ventral decreased	RLN, LLP LLPCOR increased caudally LLP: rostrally
6	COR: low inside the left arytenoid LLP, LLPCOR: more uniform	COR higher caudal velocity, on right side LLP, LLPCOR, PA more uniform	RLN, COR: ventrally
7	COR: low inside the left arytenoid	LLPCOR: Coanda effect transverse section COR: high mid-saccule, dorsally, narrowing caudally	LLP, LLPCOR increased RLN, COR, PA-dorsally
8	LLP, LLPCOR: low right ventral arytenoid	LLPCOR, COR: velocity increased dorsally LLP: increased dorsally left arytenoid	LLP, LLPCOR: increased caudally
9	LLP, LLPCOR: low inside left arytenoid COR: caudal arytenoid ventrally LLPCOR, PA: increased dorsally	LLP: lower velocity LLPCOR, COR: caudal arytenoid high velocity PA: high velocity right side, central lumen	LLP: caudal to saccule PA: dorsal left arytenoid
10	LLP/LLPCOR: uniform RLN/COR: inside left arytenoid	RLN, COR, PA: high velocity mid-saccule, caudal LLP/LLPCOR: distribution throughout	COR: high dorsal and ventral LLP/LLPCOR: low, uniform

RLN = Recurrent laryngeal neuropathy. LLP = Left-sided laryngoplasty with ipsilateral ventriculocordectomy. LLPCOR = Left-sided laryngoplasty with ipsilateral ventriculocordectomy combined with corniculectomy. COR = Corniculectomy. PA = Partial arytenoidectomy

4.5 Discussion

The CFD model generated in this study agreed with the experimental data in predicting the surgical procedure with the lowest impedance in 9 out of 10 larynges. The statistical findings for this study differed from that of **Chapter 3** (focused solely on cross-sectional area) in that the CFD results indicated a significant difference between LLPCOR and PA versus RLN (Tucker et al., 2022). Additionally, the LLP versus COR procedures were found to be significantly different for the CFD impedance results, while a significant difference was not found between PA versus LLP and COR (Tucker et al., 2022). Thus, the CFD model could be developed further in future applications to achieve greater numerical accuracy. However, it is important to consider that there has been significant variability in reported translaryngeal impedances across studies (Ahern et al., 2019; Gray et al., 2021; Hawkins et al., 2014; Jansson et al., 2000; Tucker et al., 2019). Clinically, this CFD model provided useful information about which surgical procedure would be expected to have the greatest influence on airflow impedance, and anatomically, where airflow mechanics may contribute to collapse. Within the CFD model, air was observed to recirculate around the larynx within the box, which was expected from previous experiences with the laryngeal box system. This is obviously not reflective of the airflow within an equine patient, which represents an area of potential improvement. Inclusion of more components of the upper airway would establish more clinically-realistic inlet boundary conditions, given that in the live animal, air travels through the nostrils, around the nasal turbinates and ethmoids and then enters the pharynx, which is an area of a high level of mixing and recirculation (Rakesh et al., 2008a). Unquestionably this presents a very different computational problem as compared to the experimental scenario replicated in the current study. However, isolating the larynx in this study afforded a controlled mechanism by which to compare the different surgical procedures and to examine the accuracy of the CFD model as it pertained to the airflow.

It is not entirely clear why larynx 3 **(Table 4.1)** had a different outcome but it had distinct features. This larynx was unique in that collapse the ventral corniculate processes of the arytenoids was observed together with the aryepiglottic folds. This level of flaccidity has been observed in clinical patients, so this result is not unlike some of the cases that may be encountered in clinical practice (Barnett et al., 2013a). In these cases, cartilage biomechanics may play a role in the level of collapse observed. Another larynx (5) in this study exhibited a similar shape of aryepiglottic

fold and corniculate collapse but to a lesser degree. An associated region of peak negative pressure concentration was observed inside the aryepiglottic fold, which raises the question of whether the collapse or the negative pressure occur first. It is important to identify regions of high resultant negative pressures, as airway compliance in that region will subsequently determine whether collapse occurs.

Additionally, an increased amount of turbulence was observed in the rostral portions of the LLP and LLPCOR procedures for these larynges, concentrated around the aryepiglottic fold. From a clinical standpoint, these patients would receive additional revisional procedures to address this collapse, most likely resection of the aryepiglottic fold on the left side (King et al., 2001). It is also important to note that these larynges were isolated and this level of collapse may not have been observed in the presence of a more anatomically correct pharynx to larynx transition. The importance of the entry of airflow was established in a previous study, and by extension more upstream effects within an anatomically correct geometry may be anticipated (Tucker et al., 2022).

The qualitative observations of this study suggest a number of points regarding clinical upper airway surgery. The presence of irregularity in luminal tissue was associated with increased turbulent kinetic energy along with negative pressure development which can precede collapse. In general, the LLP and LLPCOR consistently generated the lowest impedance, and showed the most uniform distributions of pressure and velocity whereas procedures creating the more obstructive conformations generated highly variable pressure and velocity. This finding suggests that surgery should aim to maintain a funnel-like transitional entrance into the proximal trachea to facilitate airflow in this region.

Collapse that results in an obstruction perpendicular to the main axis of flow should be addressed surgically. It results in a region of recirculation and negative pressure on the downstream wall producing further collapse of the affected tissue into the airway. The PA trial for some of the larynges in this study exhibited this flow pattern **(Figure 4.4)**. This corroborates the report of horses that have presented for poor performance or noise after a PA procedure that were observed to have collapsing tissue at the surgical site (Davidson et al., 2010). Increased turbulent kinetic energy is consistent with mixing and eddy formation and represents energy lost to these flow patterns and a concurrent loss of effective airflow (Faizal et al., 2021a; Faizal et al. 2021b). Higher levels of air mixing and eddy formation are also strongly correlated with severity of obstruction

(Faizal et al., 2021a; Faizal et al. 2021b). Accordingly, revisional surgery may be a worthwhile pursuit in cases with continued postoperative noise and poor performance as has also been suggested clinically (Davidson et al., 2011; Gray et al., 2019) Another consistent feature of the PA was negative pressure and high velocity inside the left wall of the larynx. These flow characteristics are consistent with collapse of the ipsilateral aryepiglottic fold along with other tissue structures reported in horses following PA (Davidson et al., 2011). Interestingly, it occurs predominantly on the left side. The Coanda effect, or flow adherence predominantly to one side of a biconvex constriction, even in symmetrical situations, results in increased velocity and negative pressure and may explain asymmetrical mechanics (Erath et al., 2006b). Further investigation of the role of entrance effects on these flow patterns is warranted in future studies.

The ventricular saccules contributed greatly to the flow characteristics observed in many larynges. This was most likely a function of the *ex vivo* nature of this study, but concurrent ventricular collapse has been observed in dynamic endoscopic videos of horses with RLN and following LLP (Davidson et al., 2010; Davidson et al., 2011). There has been an ongoing discussion within the equine surgical community about the necessity of performing a concurrent ipsilateral ventriculocordectomy with the laryngoplasty. It has been shown to reduce the noise associated with RLN (Brown et al., 2003; Kraus et al., 2003). Additionally, it may improve postoperative laryngoplasty patients that continue to experience suboptimal performance (Kraus et al., 2003). The vocal fold which resides at the rostral aspect of the ventricle seems to play an undefined yet important role in swallowing, given the recent report on bulking the fold as a technique to resolve postoperative dysphagia (Ludke et al., 2020). The results of this CFD study align with the clinical studies that suggest that the vocal fold and ventricle should be addressed to improve performance and noise (Davidson et al., 2010; Davidson et al., 2011; Kraus et al., 2003; Tate et al., 1993).

The CFD model showed a strong agreement with the laryngeal box system for comparing the relative efficacy of the equine laryngeal surgeries reported in this study. While CFD model development should continue for numerical accuracy, the realizable κ-ε turbulence model was able to distinguish relative impedance between procedures for larynges in the majority of cases, demonstrating possible usefulness in clinical applications. Additionally, insights into the important interaction of laryngeal geometry and airflow mechanics was further delineated.

4.6 Acknowledgments

The authors would like to acknowledge Dr. George E. Moore for his assistance in coding and development of statistical analysis for this manuscript.

CHAPTER FIVE:

COMPUTATIONAL FLUID DYNAMICS ANALYSIS OF AN EX VIVO UPPER AIRWAY MODEL OF THERAPEUTIC SURGERIES FOR EQUINE RECURRENT LARYNGEAL NEUROPATHY

The previous chapter reported the CFD analysis of the equine laryngeal vacuum box system. While this provided worthwhile information about how anatomic manipulation changes pressure and velocity distribution within the larynx, the larynges were analyzed outside of the normal upper airway anatomy. Previous models have reported significant swirling and mixing in the pharyngeal region and the entrance to the larynx was demonstrated to significantly impact translaryngeal impedance in Chapter 3. Thus, in order to further demonstrate the predictive capabilities of CFD, an entire equine head upper airway model was created and CFD analysis performed on the geometry which were compared with measured pressures and impedance.

This chapter reports the comparison of a cadaver head airflow study paired with CFD findings. The usefulness as a predictive tool for the procedure of lowest impedance was investigated, along with the numerical findings for impedance. This is further proof of concept that CFD may be applicable to individual patient airway geometry models to predict the procedure of lowest impedance for clinical patients. While the head model was somewhat unsuccessful in representing the reported values for horses at exercise in regard to pharyngeal pressure and impedance, the CFD analysis more accurately reflected this and led to some insights into aspects of the head model that may have caused these discrepancies.

Full citation: Tucker ML, Bergstrom D, Wilson DG, Carmalt JL. Computational fluid dynamics analysis of an *ex vivo* upper airway model of therapeutic surgeries for equine recurrent laryngeal neuropathy. Anticipated 2022.

Author Contributions: Tucker, Bergstrom, Carmalt were responsible for the study design, data collection and analysis. Wilson contributed to grant authorship and study design. Bergstrom

contributed to the fluid mechanical study design components. Tucker authored the manuscript with editorial assistance from Carmalt, Bergstrom and Wilson.

5.1 Abstract

Airway surgery in equine patients continues to present a challenge. While improvements in technique and procedures continue to be made, there is still a lot that is unknown about the specific influence that surgery has on obstructive airway disorders. Computational fluid dynamics (CFD) is gaining momentum as a useful mechanism for analyzing obstructive disorders and surgeries in the human field; it warrants further development for application in to the equine patient. The objective of this study was to apply CFD analysis to an equine head inhalation model replicating recurrent laryngeal neuropathy and four surgical techniques. CFD was hypothesized to corroborate the order of the different trials based on impedance and to provide a numerically similar impedance value to the experimental results. Additionally, it would provide insights into the fluid mechanical changes associated with each procedure on a finite scale. The CFD and experimental model resulted in the partial arytenoidectomy having the lowest impedance in this case. While this procedure did have the largest rima glottis area, the remaining procedural order was not dictated by rima glottis area. Recurrent laryngeal neuropathy and the combined laryngoplasty with corniculectomy showed negative pressure concentration on the luminal surface of the left arytenoid cartilage, which indicates a greater collapsing force on the tissues in this region. Narrowing within the caudal larynx in the region of the saccules showed increased negative pressure and higher velocities in the procedures with greater impedance while the partial arytenoidectomy had more uniform pressure and velocity. While this specific experimental head model contradicts previous flow studies, the CFD model reflected the experimental findings for procedure of least impedance and provided some insights as to why these discrepancies occurred for this particular case.

5.2 Introduction

Equine upper airway surgery continues to be a complex challenge despite extensive study over decades. Various surgical solutions have been used to address upper airway collapse syndromes such as recurrent laryngeal neuropathy (RLN) but many of these studies focus on biomechanical implant strength and simple flow impedance (Radcliffe et al., 2006). The laryngoplasty or "tie back" and the partial arytenoidectomy (PA) improve impedance and performance in horses with disease (Barnes et al., 2004; Radcliffe et al., 2006). The arytenoid corniculectomy (COR) was also investigated using the vacuum flow model but further exploration is needed regarding the applicability in clinical patients (Tucker et al., 2019). While the current *ex vivo* models provide useful information about the potential success of a surgery, they are limited in the level of detail about the flow mechanics which would provide further insight about the functionality in actual patients.

Computational fluid dynamics (CFD) modelling continues to evolve as a useful diagnostic and decisional tool in human respiratory surgery. It has been used to explore the relationship between complex human pharyngeal and laryngeal anatomy, vocalization, and obstruction (De Backer et al., 2007; Erath et al., 2006a; Huang et al., 2005a; Xu et al., 2006). The amount of anticipated negative pressure development along the wall dictates the collapsing forces that act on the airway walls (Huang et al., 2005b). Multiple mesh types and turbulence models have been used in the human literature and the influence of these different techniques has been demonstrated in a variety of applications (Longest et al., 2007; Xu et al., 2006). While airway CFD analysis continues to evolve, it has been shown to be very powerful in determining the regions of greatest resistance, how anatomical variations potentiate disease, and which surgical procedures are most effective (Huang et al., 2005a; Malhotra et al., 2002; Mylavarapu et al., 2013).

The use of CFD to evaluate surgical procedures in humans has led to insights into the interaction of surgical manipulations, airflow, and patient outcomes when addressing problems such as obstructive sleep apnea. This had led to a discussion about the application of CFD as a presurgical tool to aid in decision making as it relates to manipulation of airway geometry leading to decreased resistance and improved airflow (Malhotra et al., 2002; Huang et al., 2005a). One study compared the effects of a palatal stiffening, palatal resection and mandibular advancement for pharyngeal collapse and was able to demonstrate that these surgeries all improved the airway

mechanics in the patient geometries that were evaluated (Huang et al., 2005a). This type of analysis has been performed for only one specific procedure in horses to verify the level of airway opening required to see maximal improvement in airflow, but multiple procedures have not been compared.

An equine upper airway CFD model was previously reported over a decade ago and compared the differences between equine and human respiratory mechanics. Airflow during human breathing is primarily laminar/transitional and only turbulent with heavy effort or obstruction, while most equine respiration is turbulent (Rakesh et al., 2008a). Humans breathe roughly 12 times per minute with a tidal volume of about 0.5 L while horses breathe an average of 10 times per minute with a tidal volume of 5.5 L (Guyton et al., 1996; Radcliffe et al., 2006; Rakesh et al., 2008b). Human airway cross-sectional areas range from 50-177 mm^2 while the equine airway has been reported to range from 1127-4516 mm^2 (Guyton et al., 1996; Rakesh et al., 2008b). Reynolds numbers in the order of 100,000 have been reported based on these flow parameters within equine airways, making this a high turbulence model compared to human flows with Reynolds numbers of 900-1400, or transitional models (Allen et al., 2004; Rakesh et al., 2008b). While this initial comparison and model led to valuable insights regarding equine upper airway surgery, validation of the model through further iterations is needed.

A previous study examined the influence of RLN, left laryngoplasty with concurrent left ventriculocordectomy (LLP), laryngoplasty with left corniculectomy (LLPCOR), left arytenoid corniculectomy (COR) and PA on laryngeal impedance in an ex vivo model (Tucker et al., 2019). A follow up study looked at the geometrical changes associated with each surgical procedure on the larynges (Tucker et al., 2022). CFD was then performed to examine the flow patterns associated with each state within the larynx in the box model from Chapter 4. The objective of this study was to examine the influence of each procedure on flow development within the equine larynx in the context of the entire equine upper airway. The hypothesis was that the CFD model would confirm the experimentally derived results of surgical procedure effects on relative impedance. Additionally, the change of shape associated with each surgical procedure was hypothesized to influence the anticipated impedance of the larynx, the change in pressure, and the amount of flow separation observed downstream from the larynx as air moves into the trachea. Finally, the development of negative pressure and wall stress within the larynx would be influenced by the upstream pharyngeal geometry, as compared to the *ex vivo* model.

5.3 Materials and Methods

One equine cadaver head from a six-year-old Quarter Horse mare was obtained postmortem with the larynx in situ and four tracheal cartilage rings. The horse was humanely euthanized and had no history or signs of airway disease. The nostrils were sutured into the open/flared position to replicate muscular dilation that occurs while running. The horizontal portion of the mandible was removed to allow access to the soft palate by cutting through the lateral buccal cavity and performing bilateral ostectomies through the vertical ramus of the mandible. The soft palate and epiglottis were anchored using #2 nylon suture (Ethilon, Ethicon US LLC, Bridgewater, NJ) passed through the cartilage and the soft palate and tied to the hyoid apparatus which was left intact. The pharyngeal region was observed endoscopically during this process and also with airflow to determine whether collapse of the epiglottis or palate would occur during testing. The epiglottis was positioned to replicate the extension of the head that occurs when a horse extends its head during maximal exercise. The trachea was sealed over a portion of polyvinylchloride (PVC) pipe attached to a vacuum. The equine head anatomy is represented in **Figure 5.1**, along with points of interest. Point A corresponds to the room air which was used as a boundary condition in the later calculations. An orifice plate was placed approximately 60 cm downstream from the tracheal outlet to measure airflow, and the vacuum was placed another 30 cm downstream. This would be located to the right of the images shown in **Figure 5.1** below. This allowed air to be drawn in through the head to replicate inhalation. Polyethylene tubing ran from a connector within the PVC pipe to a pressure transducer to measure the pressure within the trachea relative to the room **(Point D, Figure 5.1)**. An additional set of tubing and a transducer were used to measure the pressure within the pharyngeal region by tunneling the tubing through a hole created using 14-gauge needle and mosquito hemostats **(Point B, Figure 5.1)**. Catheter placement into the pharynx was confirmed on endoscopic examination.

Figure 5.1 Final geometrical model with reference to the external view of a horse head.
Point A represents the area just outside of the nostrils where the pressure is atmospheric and there is minimal velocity. Point B is the area of pharyngeal pressure measurement. Point C is the area of surgical manipulation within the airway. Point D is where the tracheal pressure measurement occurs, upstream from the orifice plate and vacuum.

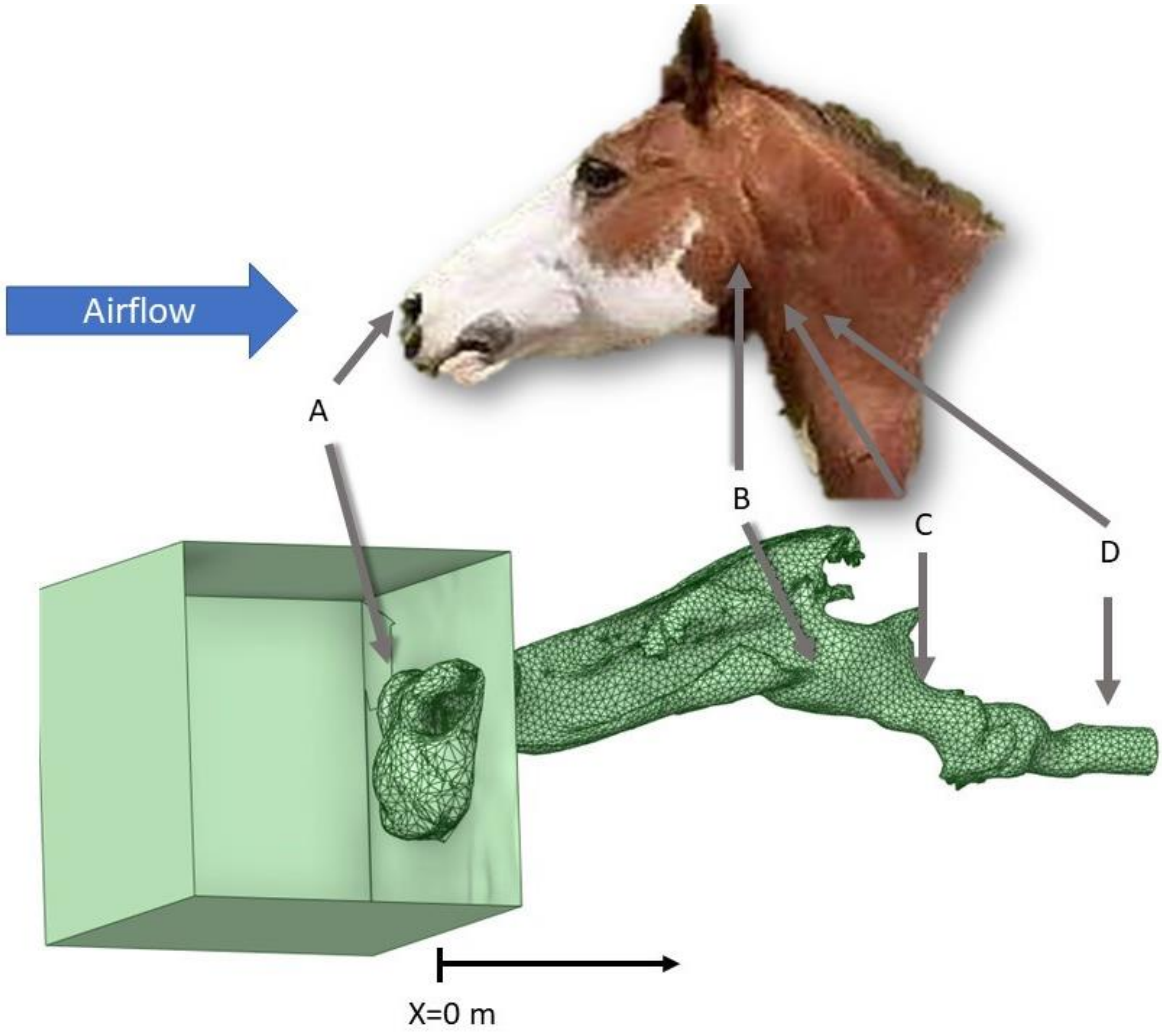

Five different scenarios were created in the upper airway, at point C as shown in **Figure 5.1**. The first replicated the disease state, in which the left arytenoid cartilage could collapse under airflow. A laryngoplasty was performed to replicate intact cricoarytenoideus dorsalis function on the right side of the larynx using #5 Ethibond (Ethibond Excel, Ethicon US LLC, Bridgewater, NJ) suture tied with a surgeon's throw followed by four subsequent throws, while the left arytenoid was left to collapse into the airway. This was tested with airflow with an induced tracheal pressure to replicate a horse with RLN. Next, left LLP was performed as has been recommended as the standard treatment for RLN using a laryngotomy approach to the ventricle with a roaring burr for exteriorization of the saccule (Brown et al., 2003). This was also tested with negative pressure generation. A left COR was then performed by removing the corniculate process of the left arytenoid cartilage as has been reported previously (Tucker et al., 2019). This was tested with the suture left intact, replicating a combined LLPCOR. The left suture was then cut to allow collapse of the arytenoid cartilage, replicating the plain COR procedure and was tested. Finally, left PA was performed by excising the left arytenoid body and tested (Speirs, 1986). Concurrent CT scans were performed to capture the three-dimensional geometry and anatomy of the head and airway under airflow conditions.

A Toshiba Aquilon One (Canon Medical Systems, Markham, ON, CA) was used to acquire CT scans with 1 mm slices, using a helical scanning algorithm. The scanning window could not extend from the nares to the trachea in one full run however the nostrils were scanned initially followed by the remaining head and this nostril geometry was unified with the head geometry on all subsequent runs.

5.3.1 Geometry

The CT scans from the head for each state were segmented using Fiji (ImageJ, National Institutes of Health, Bethesda, MD) an open-source software for the purpose of generating three-dimensional views from DICOM images. Using the segmentation editor, the area of effective airflow was outlined slice by slice. The sinuses were not included in the model to reduce the computational burden given that in previous studies no airflow was observed in the sinus regions (Rakesh et al., 2008a). The slices were then compiled into an .stl file using the 3D viewer plugin and smoothed in MeshLab (MeshLab version 2020.12, Visual Computing Lab; CNR-ISTI, Pisa, Italy). Unconnected vertices and facets were removed using the corresponding filters and the HC

Laplacian smoothing and remeshing filters applied as in Chapter 4 and as previously described (Vollmer et al., 1999; Massie 2015). The geometry was imported into Ansys® SpaceClaim (Ansys 2021 R1, ANSYS, Inc., Canonsburg, PA) for manipulations and correction of irregularity to create a watertight geometry. A box approximately 200 mm^3 was created in SpaceClaim to provide an inlet boundary away from the immediate nostril opening and a nose imprint was created in the box to simulate inhalation in a static room of air. It was then imported into Fluent (Ansys 2021 R1 build 10179, ANSYS, Inc., Canonsburg, PA) for meshing and a surface mesh was generated. A volumetric mesh was then applied, using a hexahedral mesh with approximately 10 million elements.

5.3.2 Mesh Independence Study

A mesh independence study was performed by generating a surface mesh using local sizing of 0.5 mm within the region of the larynx and pharynx. A maximum size of 20 mm was allowed but the mesh only reached this size in the box portion of the model. Five transitional boundary layers were used with a smooth transition. The maximal and minimal size were manipulated to generate mesh sizes of 1.7, 4.9, 6.9, 10 and 13.8 million cells respectively for the LLPCOR model. Planes of interest were generated parallel to the dorsal and axial planes and the area-averaged pressure for each plane within each mesh size was calculated and plotted. Peak minimum pressure for each plane was also plotted. Examining the area-averaged pressure and the peak minimum pressure for each plane, 10 million cells appeared to provide an appropriate balance between the anticipated calculation accuracy and the computational demand.

5.3.3 Assumptions

The density, temperature, and humidity of the air were held constant. The density of air was taken to be 1.204 kg/m^3 at 20˚C (Rakesh et al., 2008b). Uniformity was assumed. Wall rigidity was also assumed, with the soft tissues in the fully-developed flow state. This study sought to replicate the airway mid- to end-inhalation where the airway has accommodated the stress of negative pressure but airflow has not begun to decrease. Incompressible flow was also assumed.

5.3.4 Governing Equations

The Reynolds-averaged Navier-Stokes (RANS) and continuity equations were solved as below. Flow was assumed to be incompressible, isothermal, unsteady and entirely turbulent. As the flow is primarily horizontal, the effects of gravity were considered insignificant. This results in the following equations, as were reported in the previous models (Rakesh et al., 2008b):

Equation 5.1

$$\frac{\partial u_j}{\partial x_j} = 0$$

Equation 5.2

$$\frac{\partial u_i}{\partial t} + \frac{\partial u_i u_j}{\partial x_j} = -\frac{1\partial p}{\rho \partial x_i} + \nu \frac{\partial^2 u}{\partial x_j^2} - \frac{\partial u_j' u_i'}{\delta x_j}$$

The κ-ϵ realizable turbulence model was used for the Reynold's stress with standard wall functions used in the near wall region; a no-slip condition was assumed (Rakesh et al., 2008a).

5.3.5 Boundary Conditions

The nostrils were each defined as inlets while the trachea was treated as an outlet and the airway wall was defined as another boundary. Pressure within the trachea and atmospheric pressure outside of the nares were used as the outlet and inlet pressures respectively **(Points D and A, Figure 5.1)**. The measured pressures within the trachea from each CT scan were used. As described above, this pressure was measured just downstream from the fourth tracheal ring for each laryngeal procedure as in **Figure 5.1**.

5.3.6 Numerical Solution

Ansys Fluent was used to implement the finite volume method to solve the model equations. Convection was modeled using a second-order upwind differencing scheme. Pressure was solved using standard interpolation, as has been previously reported and the discretized equations were solved using the pressure-velocity coupling scheme (Rakesh et al., 2008b). An AMD Threadripper Pro 3955WX Processor (4.30GHz) with 128 Gb of RAM was used to perform the simulations. Using 1000 iterations resulted in decreased continuity residuals of 10^{-2} or less. The average computation time for each simulation was about an hour and a half.

5.3.7 Analysis

Each procedural run was divided into cross-sectional planes 4 mm apart starting with the box edge as x=0 m within the model and pressure, velocity, and turbulence were taken as an area-average. Within the pharyngeal and laryngeal regions at around x=0.36-0.48 m, planes were added to create 1 mm spacing to better examine the changes within that region in regard to each procedure. Translaryngeal impedance was taken by calculating the area-averaged pressure in the region of the pharynx where the catheter was present minus the input trachea value from the experimental measurement divided by the volumetric flow rate reported at the problem outlet as in the equation below.

Equation 5.3

$$\frac{|P_{pharynx} - P_{trachea}|}{Flow\ Rate}$$

Separate planes were generated to perform the qualitative analysis. Planes parallel to sagittal were generated focusing on characteristics just inside the left and right side of the larynx. Transverse planes were generated to look at the characteristics of the ventral larynx, mid-larynx, dorsal larynx, mid-pharynx and mid-nostrils. Cross-sections were also captured mid-nostrils, mid-pharynx, at the laryngeal opening, mid-saccule, at the narrowest portion of the larynx, at the caudal dilation corresponding to the cricoid level and finally a section at the level of the trachea. The larynx was specifically examined in the larger planes by focusing them in the region of the larynx to observe changes in pressure, velocity and turbulent kinetic energy.

5.4 Results

The head model replicated flow in the equine upper airway from nares to trachea.

5.4.1 Quantitative Results

Both the experimental and CFD scenarios resulted in PA as the lowest impedance procedure, but the reported impedances were very different (83-87%) for all procedures. Measured tracheal pressure, pharyngeal pressure, flow rate, impedance and rima glottis area are reported in **Table 5.1**. The rima glottis area was measured using the CT cross-sectional images and the final SpaceClaim geometries. These areas are reported in **Table 5.2**. The LLPCOR procedure showed the largest difference in rima glottis areas. The plots of pressure, velocity and turbulent kinetic energy along the upper airway and specifically within the larynx are shown in **Figures 5.2 A-H**.

Table 5.1 Experimental and computational results for pharyngeal pressure (kPa), airflow (L/s) and impedance (kPa*s/L) by procedure. Tracheal pressure was measured experimentally and used as the boundary condition for the tracheal outlet in the computational model. Note that the procedure of lowest impedance in both instances is PA, in bold.

	Experimental				CFD		
Simulated State	**TP (Pa)**	**PP (Pa)**	**Airflow (L/s)**	**Impedance (kPa*s/L)**	**PP (Pa)**	**Flow Rate (L/s)**	**Impedance (kPa*s/L)**
RLN	-8258	-563.5	10.8	0.712	-1379.5	57.7	0.1193
LLP	-8409	-243.5	10.5	0.774	-1292.6	55.1	0.1292
LLPCOR	-7500	-117.8	8.8	0.837	-1357.4	58.7	0.1046
COR	-7319	-70.2	9.95	0.728	-1010.9	50.5	0.1249
PA	-7106	-108.4	10.1	**0.695**	-1424.4	61.8	**0.0919**

CFD-Computational fluid dynamics results; TP - Tracheal air pressure; PP -Pharyngeal air pressure; RLN- Recurrent laryngeal neuropathy; LLP - Left-sided laryngoplasty with ipsilateral ventriculocordectomy; LLPCOR- Left-sided laryngoplasty with ipsilateral ventriculocordectomy combined with corniculectomy; COR - Corniculectomy; PA - Partial arytenoidectomy

Table 5.2 Experimentally measured and CFD-model rima glottis area by procedure.
The experimental rima glottis area was measured from the coinciding CT section while the CFD model rima glottis area was measured using SpaceClaim.

	Rima Glottis Area (mm^2)		
Simulated State	**Experimental**	**CFD**	**% difference**
RLN	1218	1169	4.1
LLP	1122	1159	3.3
LLPCOR	1482	1314	11.4
COR	1247	1172	6.0
PA	1671	1593	4.6

CFD-Computational fluid dynamics results; RLN- Recurrent laryngeal neuropathy; LLP - Left-sided laryngoplasty with ipsilateral ventriculocordectomy; LLPCOR- Left-sided laryngoplasty with ipsilateral ventriculocordectomy combined with corniculectomy; COR - Corniculectomy; PA - Partial arytenoidectomy

Figure 5.2A Cross-sectional area along the upper airway by procedure.

RLN had the lowest cross-sectional area in the laryngeal region and had the most variability across the cross-sectional areas in general.

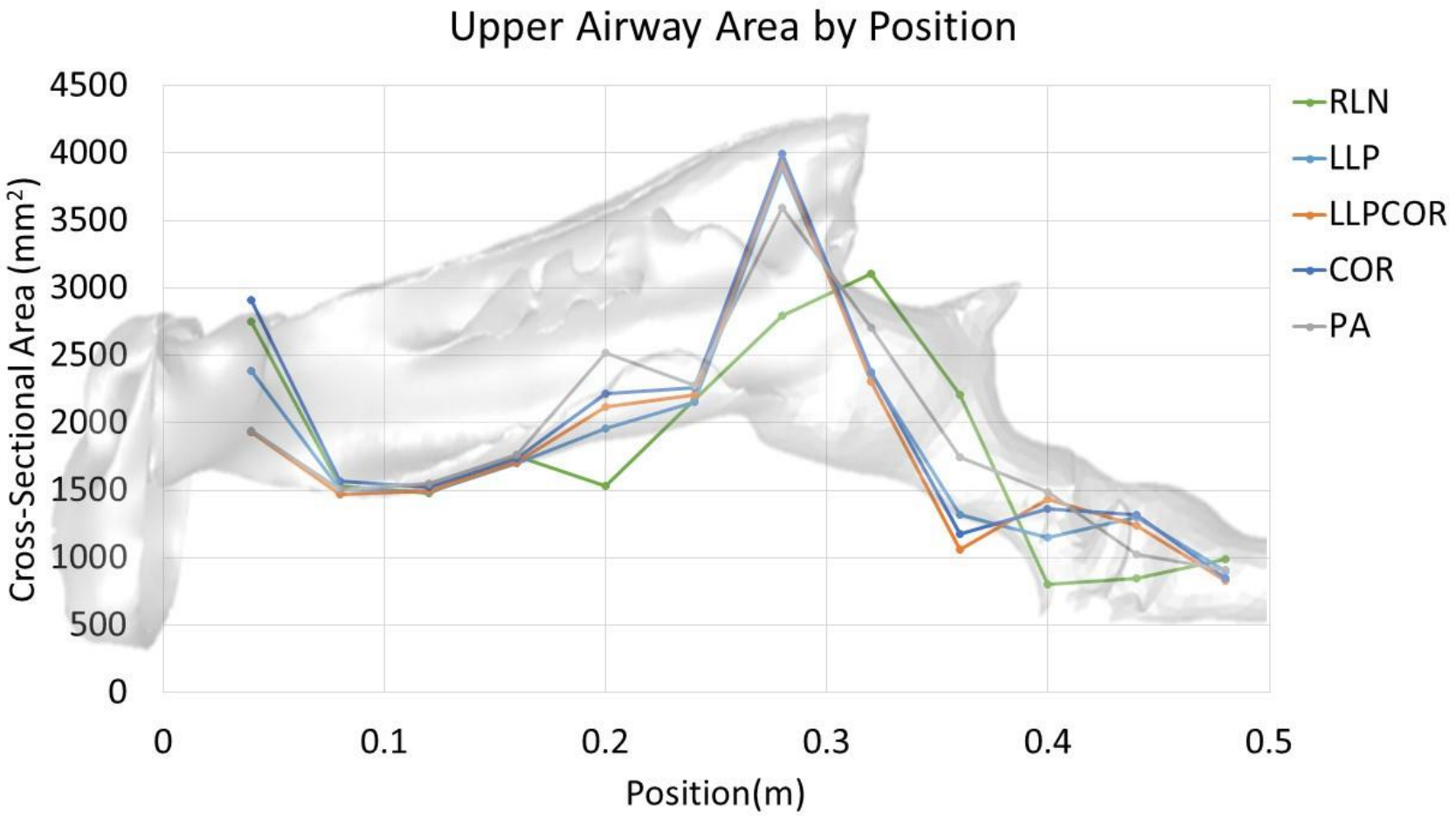

Figure 5.2B Cross-sectional area along the larynx by procedure.

RLN has the lowest cross-sectional area at the region of the rima glottis while PA has a larger area through the length of the laryngeal region. The pharyngeal region is similar between procedures.

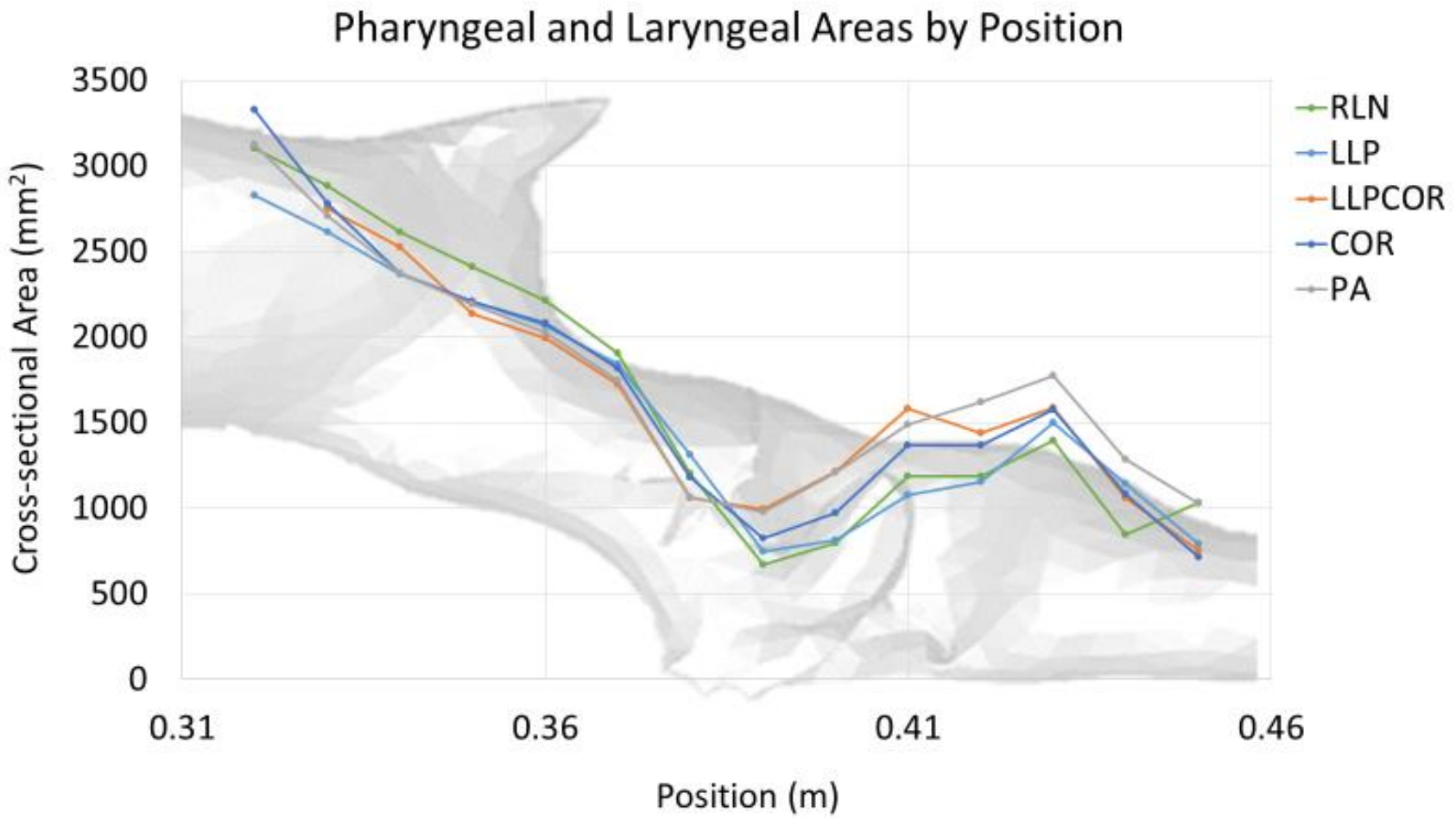

Figure 5.2C Area-averaged pressure along the upper airway by procedure.

RLN had the lowest pressure in the region of the laryngeal opening. LLP was the second lowest. LLPCOR, COR, and PA were more similar in their relative distribution. The LLPCOR procedure had increased negative pressure within the caudal portion of the larynx as it transitioned into the trachea.

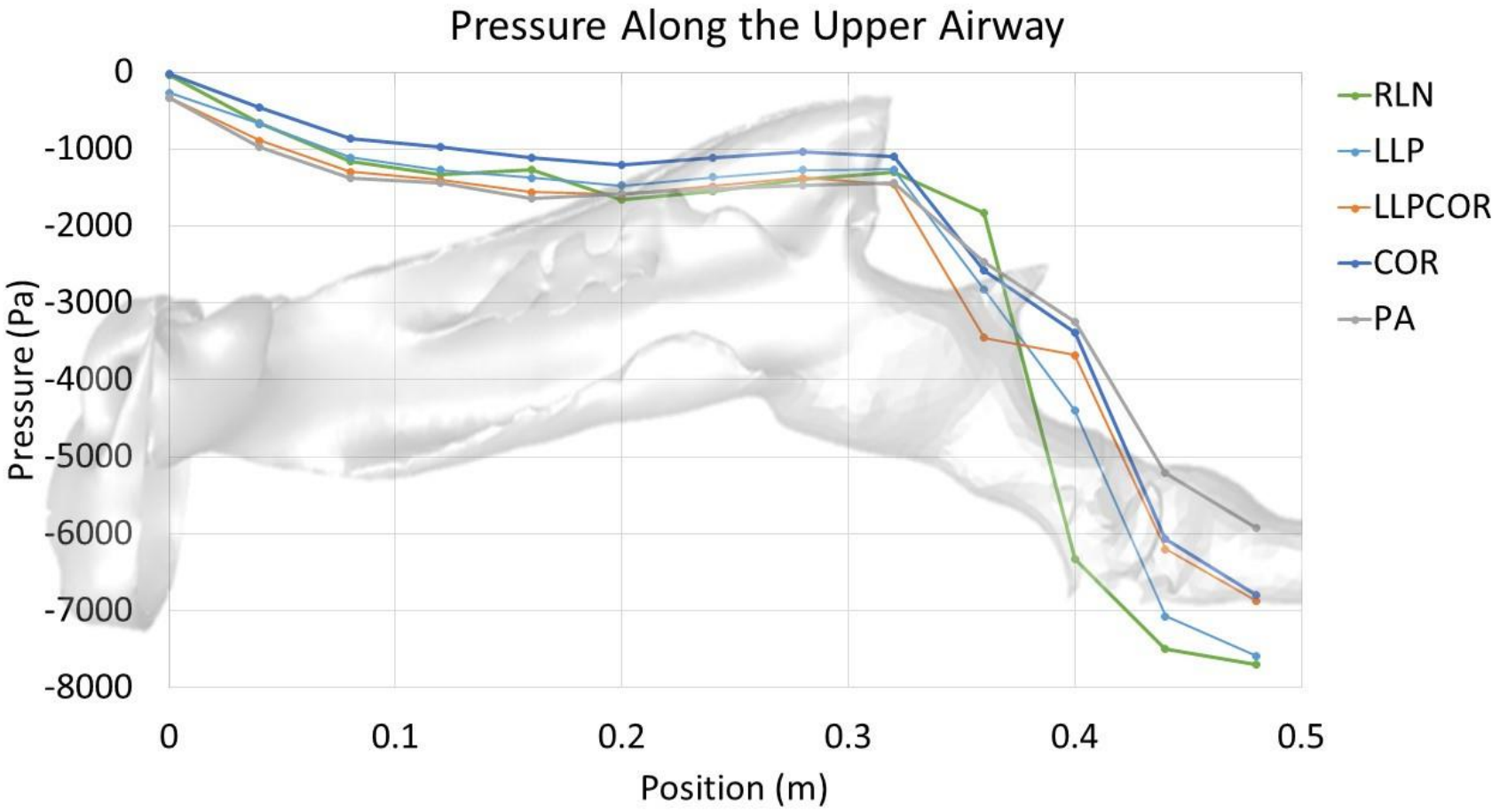

Figure 5.2D Area-averaged velocity along the upper airway by procedure.

RLN had the highest velocity in the region of the laryngeal opening. LLP was the second highest. The remaining 3 procedures were more similar in their relative distribution.

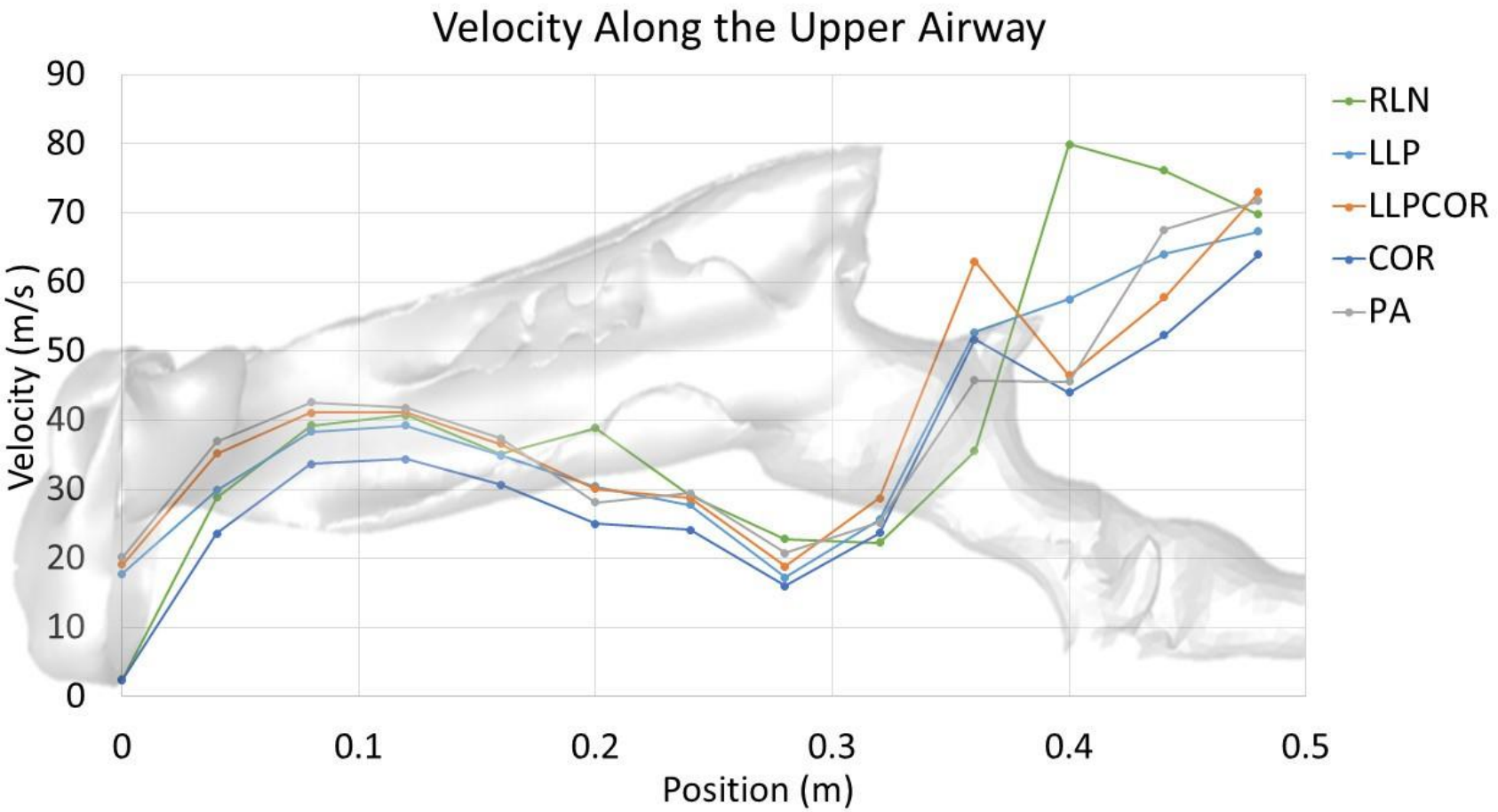

Figure 5.2E Area-averaged turbulent kinetic energy distribution along the upper airway by procedure.

The turbulent kinetic energy was largely similar across procedures except in the caudal laryngeal/tracheal region where the cadaver model had compression of the caudal airway. In general, the pharyngeal and laryngeal regions are areas of increased turbulent kinetic energy as compared to the rest of the airway.

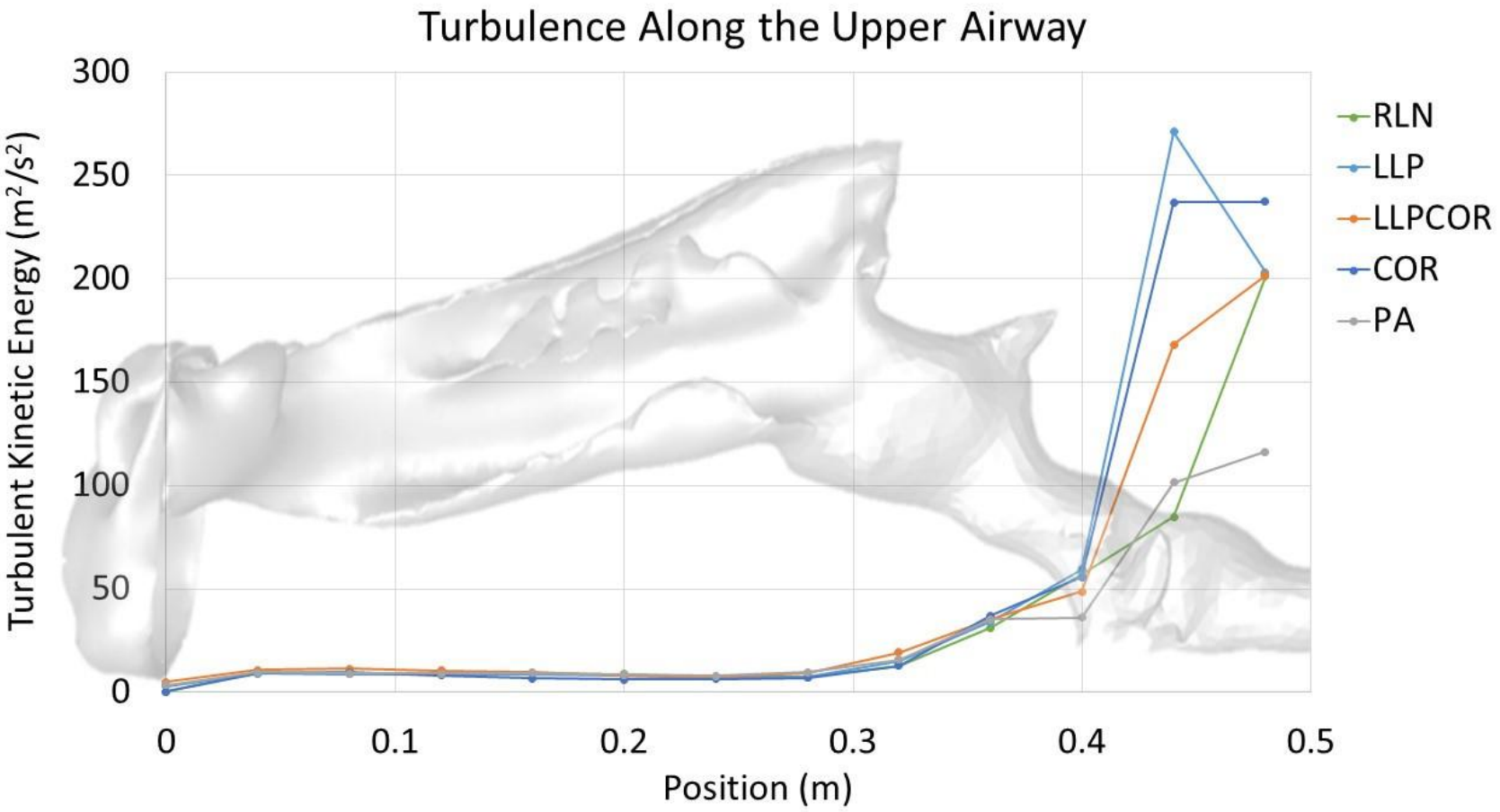

Figure 5.2F Area-averaged pressure along the larynx by procedure.

As demonstrated with the larger-scale plot, RLN had the lowest pressure at the rima glottis, best characterized as one significant pressure drop across that region. LLP was the second lowest. LLPCOR, COR, and PA were more similar in their relative distribution.

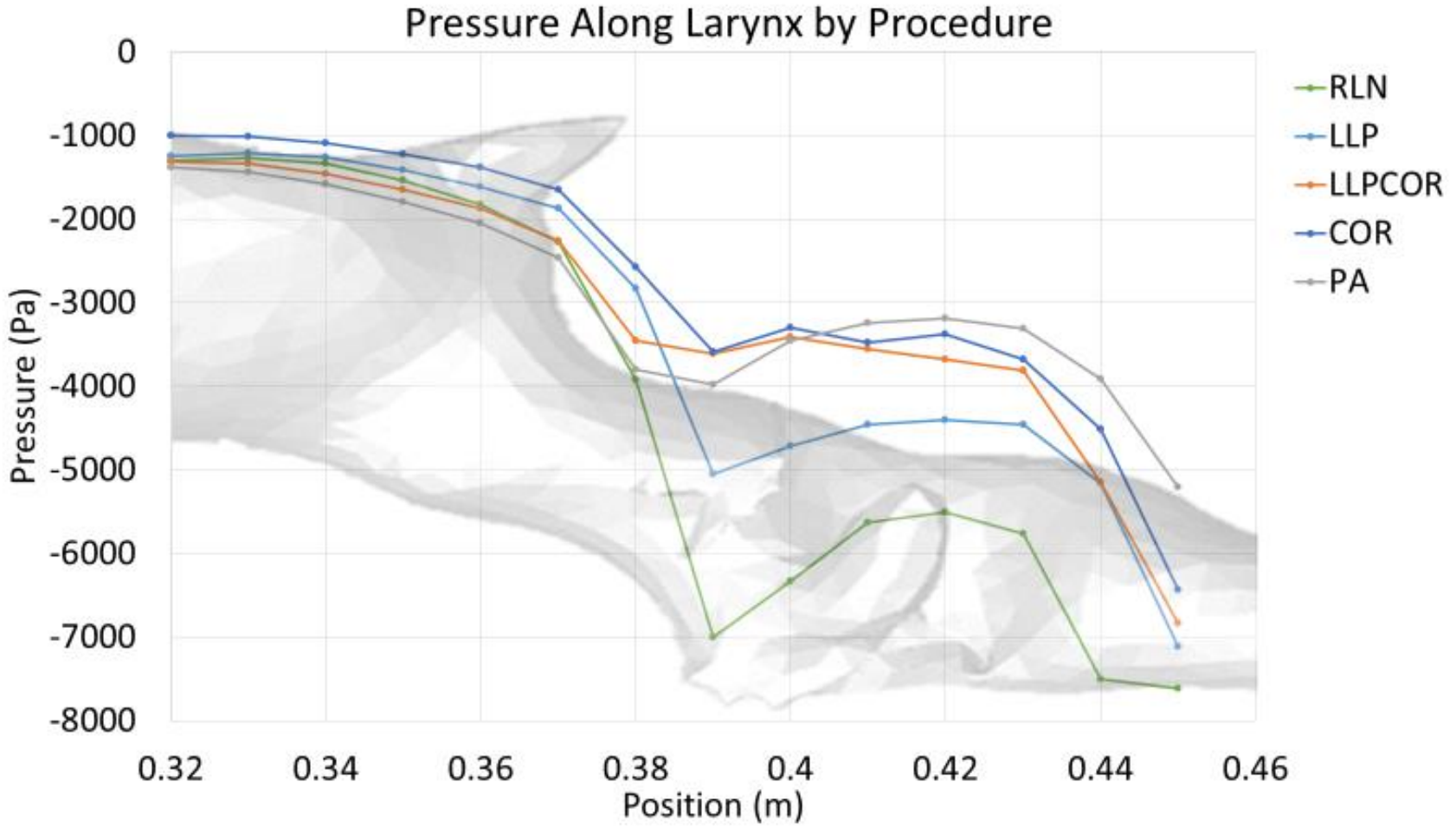

Figure 5.2G Area-averaged velocity along the larynx by procedure.

RLN had highest velocity along the larynx, followed by the LLP procedure. The remaining 3 procedures were more similar in their relative distribution.

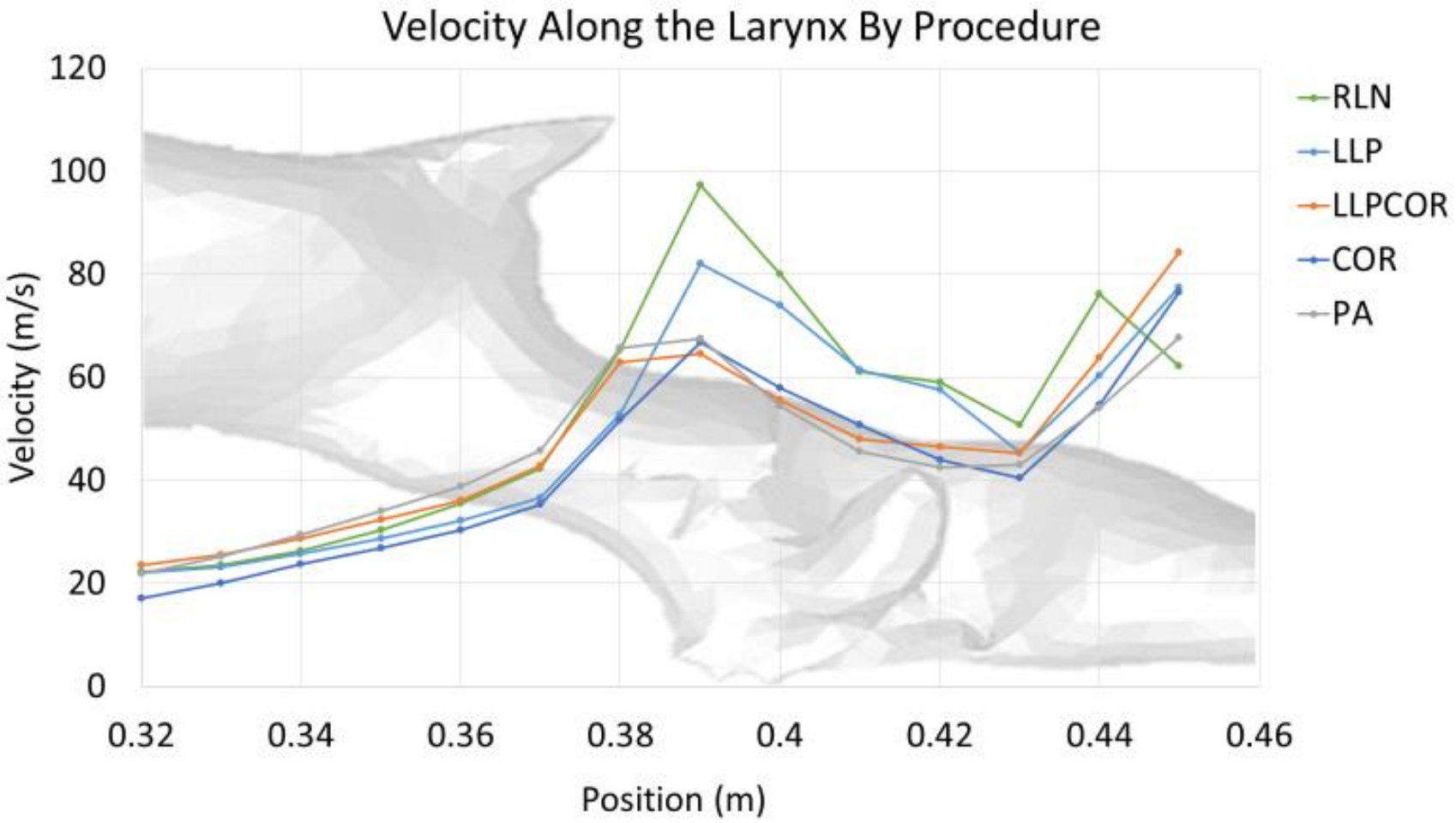

Figure 5.2H Area-averaged turbulent kinetic energy distribution along the larynx by procedure.

Turbulent kinetic energy specifically within the larynx was higher for RLN, with the LLPCOR procedure being the second highest. All of the procedures showed increased turbulent kinetic energy at the laryngeal-tracheal junction.

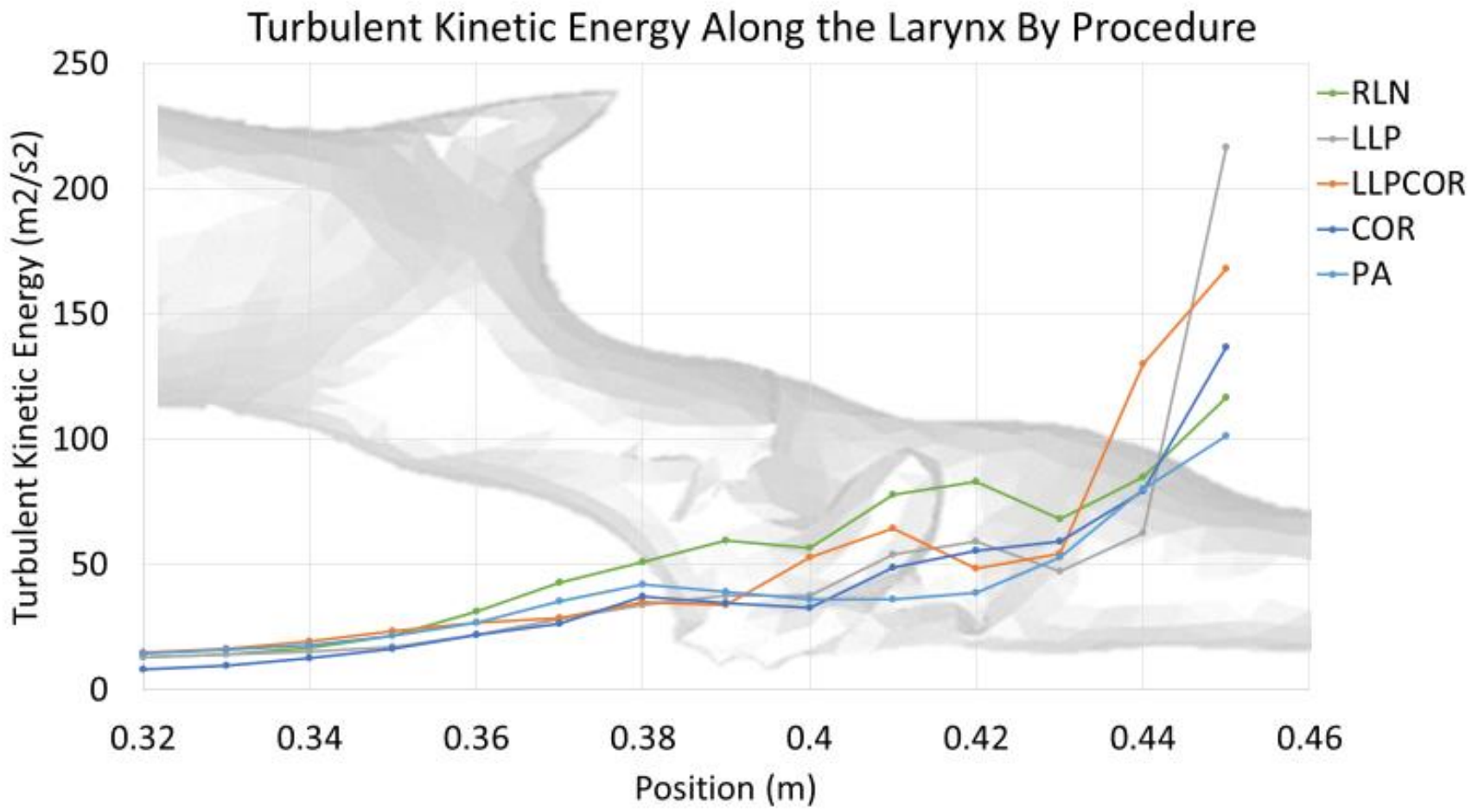

5.4.2 Qualitative Results

There were similar nostril and pharyngeal characteristics across procedures. The parasagittal section observed just inside the left arytenoid cartilage demonstrated higher negative pressure within the RLN, LLP, LLPCOR, COR and PA procedures. It was most pronounced for RLN. Within the transverse planes, there were lower pressures and higher velocities observed for the RLN and LLP procedures. The LLPCOR, COR and PA procedures appeared to be more uniform. All of the procedures showed a narrowed conformation ventrally caudal to the saccules, but this seemed more exaggerated some procedures than others. This is shown in **Figure 5.3**.

The cross-sectional planes at the laryngeal opening showed narrowing for RLN, coinciding with more negative pressures and high velocities. At the mid-saccule region, there was more negative pressure observed inside the left wall of RLN and LLPCOR. The removal of the arytenoid body in the PA procedure expanded this region on the left side and therefore less air velocity and less negative pressures were observed. Even caudal to the saccules, there was a similar trend of less negative pressure and less high velocity in the narrowest portion of the PA procedure. These are shown in **Figure 5.4**.

All of the planes captured and examined can be found in **Figures 5.5 A-P**. Pressure, velocity and turbulent kinetic energy were all examined in cross-sectional, sagittal and transverse planes; all were adjusted to the same color scale for each of the planes as reported by procedure. Differences in the shape of the planes are a function of position of the head within the CT.

Figure 5.3 Pressure and velocity distribution through the left parasagittal and ventral laryngeal planes for all procedures.
Row (A) denotes the parasagittal left slice taken for each procedure while row (B) is the ventral laryngeal transverse section. Pressure is at the top while velocity is on the bottom. Air flows from left to right in the image, with the horse's left side up for the transverse sections, the nostrils to the left and the trachea to the right side of the images.

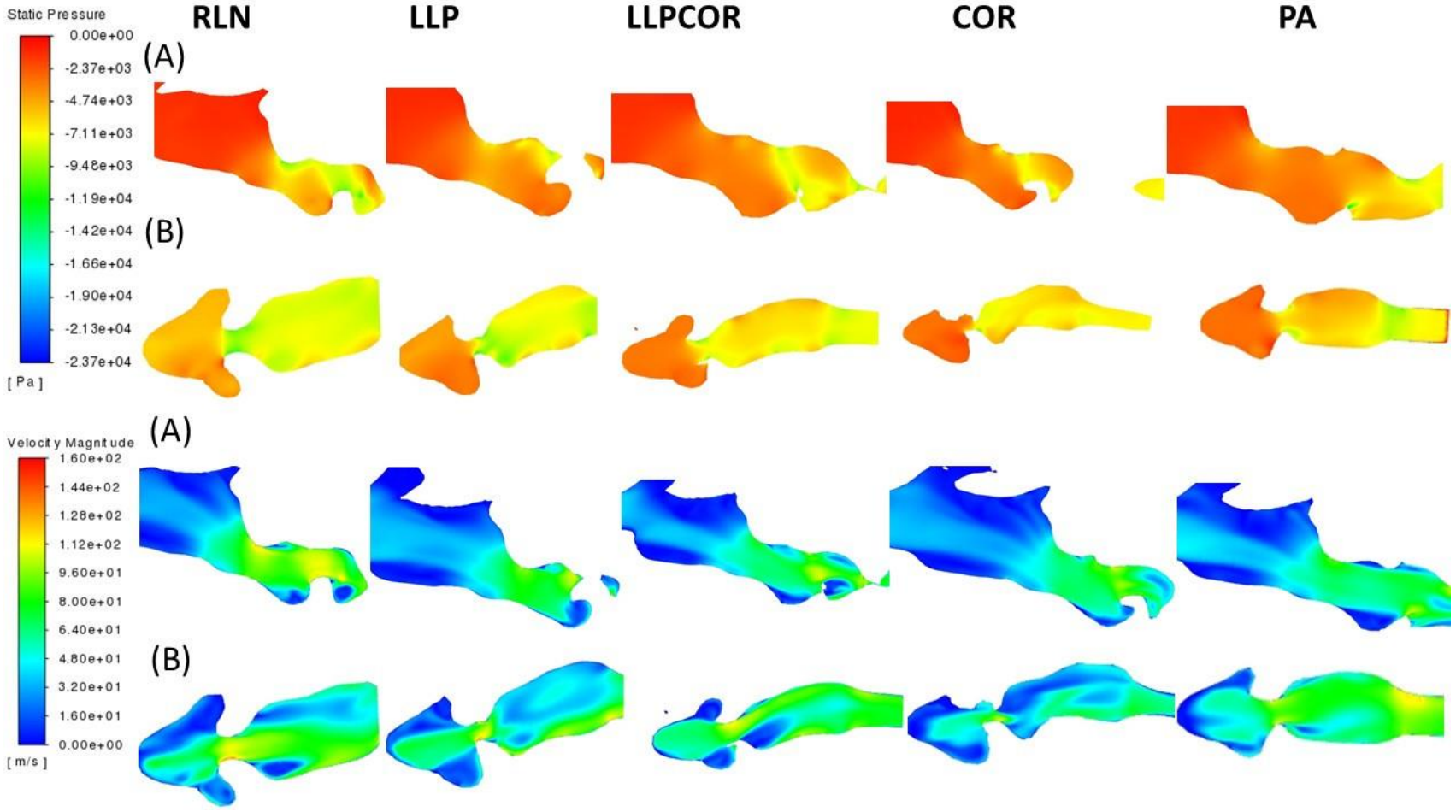

Figure 5.4 Laryngeal opening and mid-saccule cross-sectional planes by procedure.

Row (A) denotes the laryngeal opening slice taken for each procedure while row (B) is the mid-saccule section. Pressure is at the top while velocity is on the bottom. These sections are perpendicular to airflow and captured straight on, so that the horse's left side is on the image right.

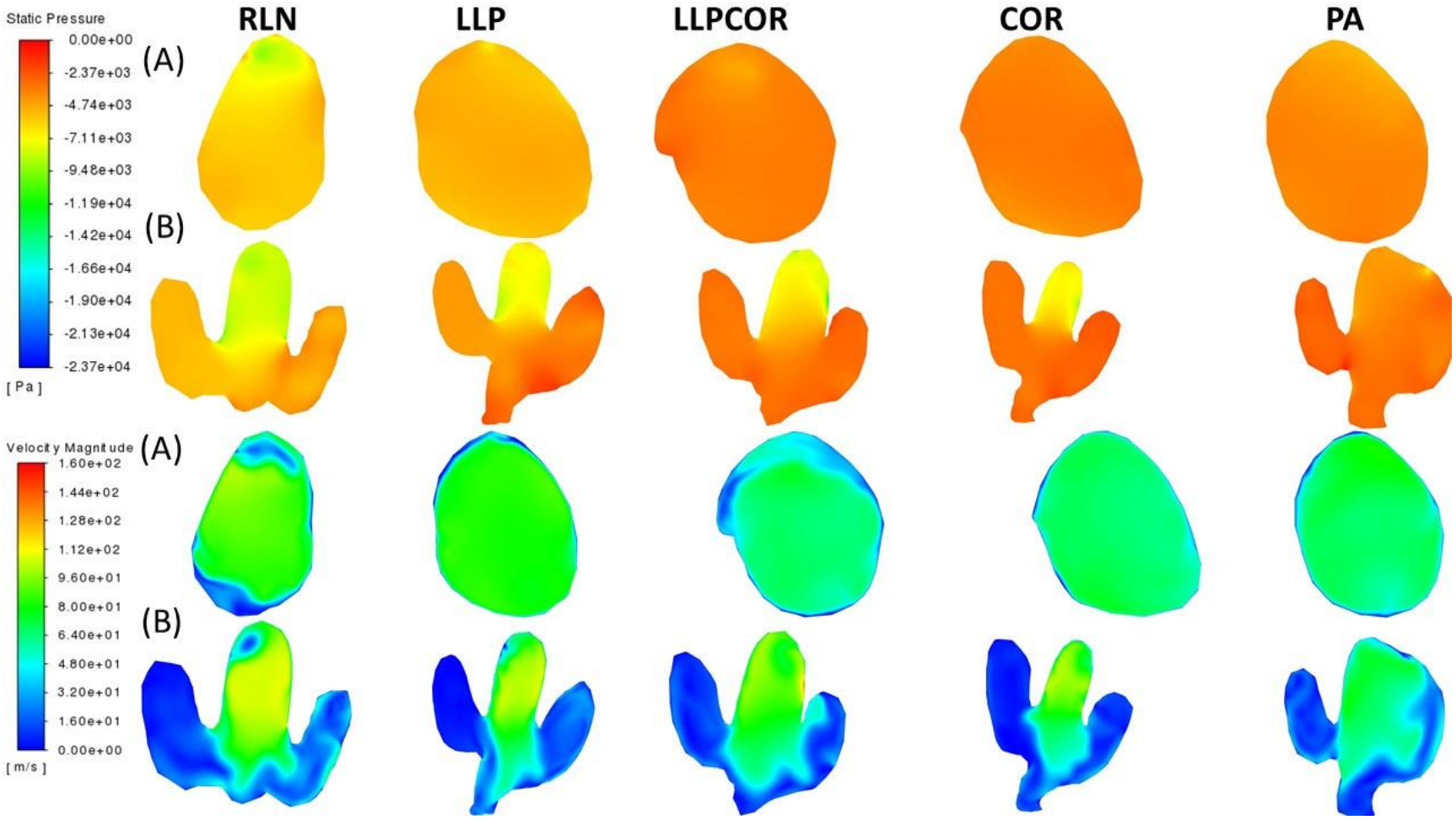

Figure 5.5A Pressure (top row), velocity (middle row), and turbulent kinetic energy (bottom row) for the nostril cross-sections by procedure.

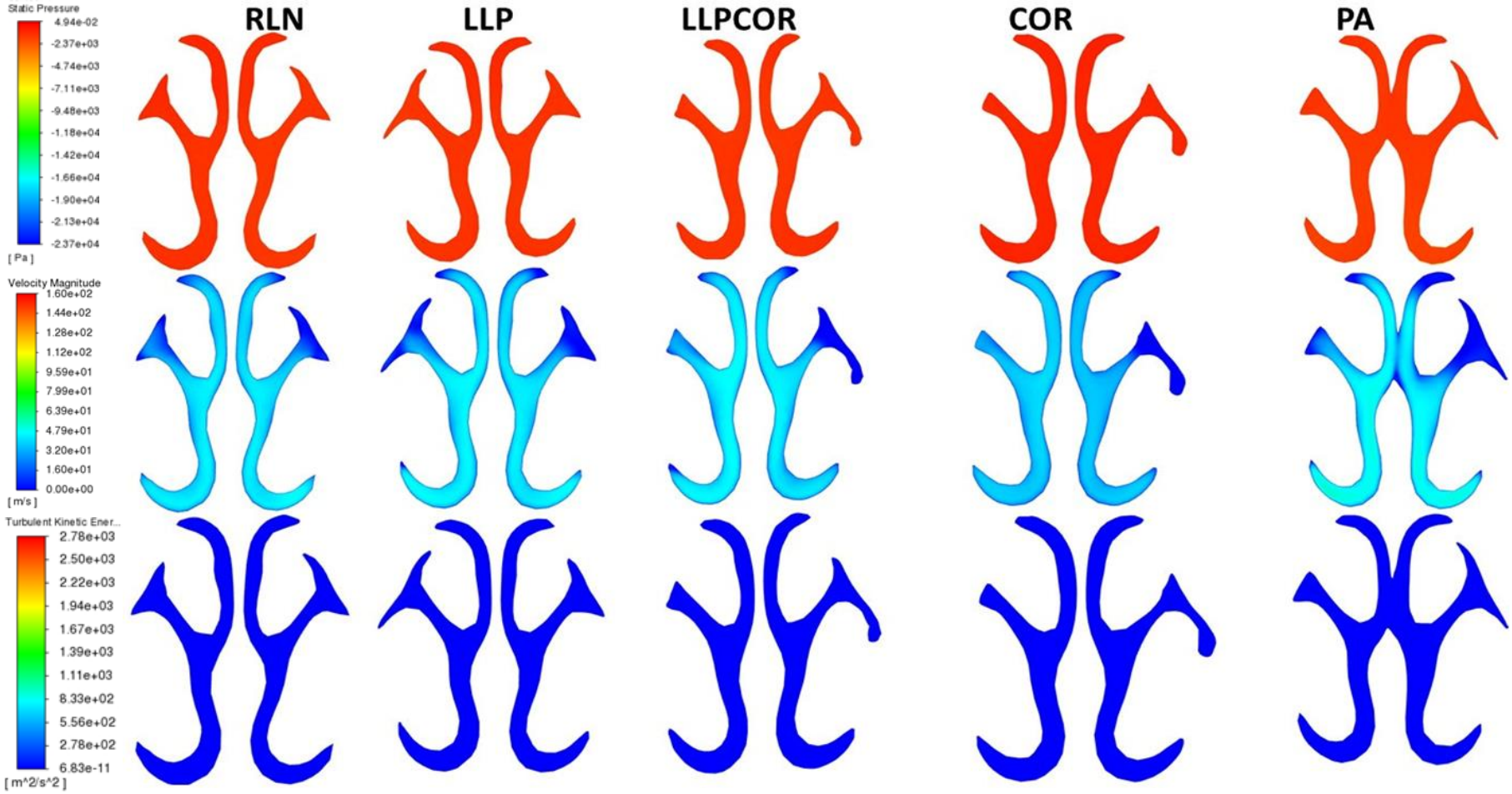

Figure 5.5B Pressure (top row), velocity (middle row), and turbulent kinetic energy (bottom row) for the mid-pharyngeal cross-sections by procedure.

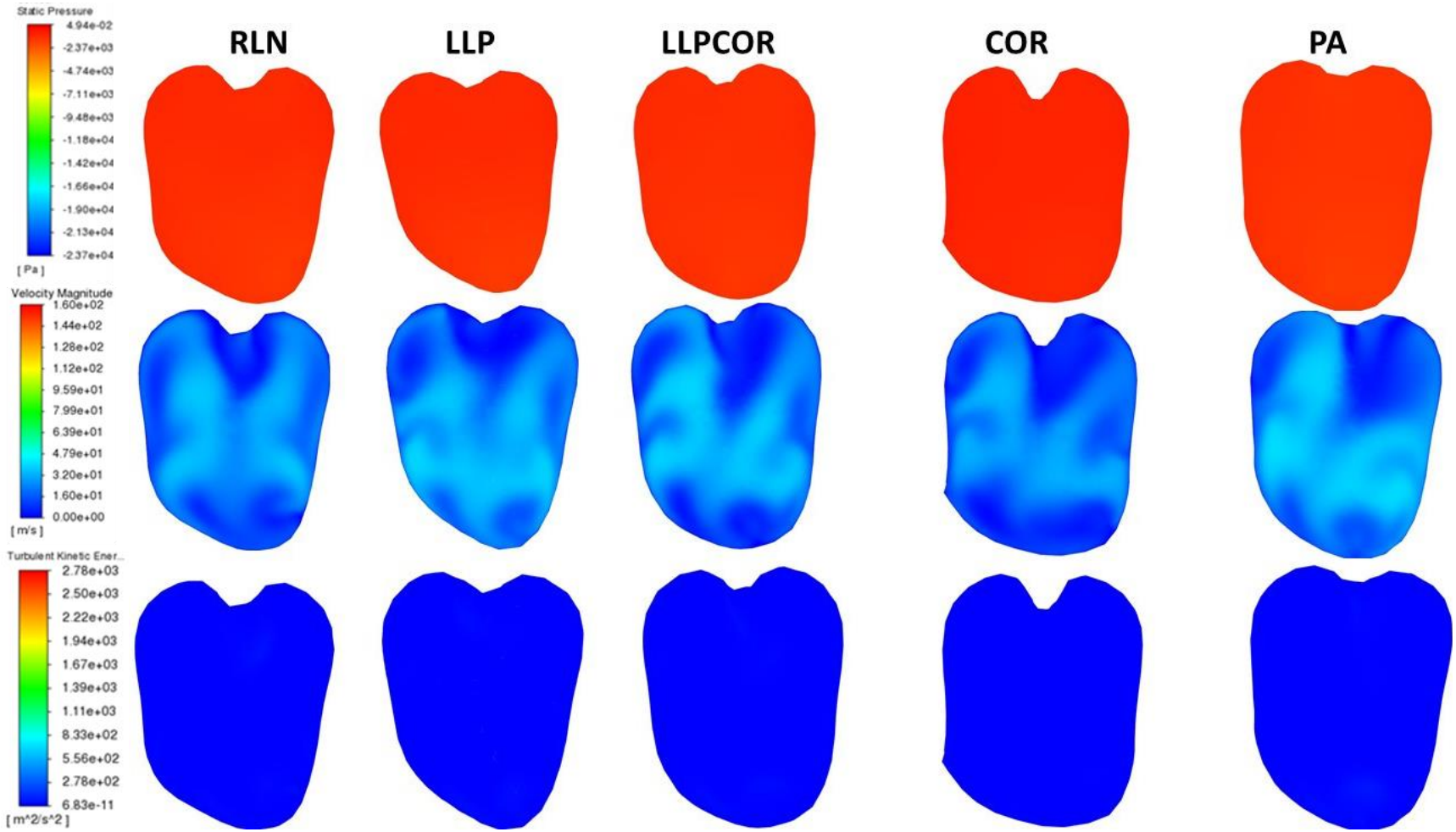

Figure 5.5C Pressure (top row), velocity (middle row), and turbulent kinetic energy (bottom row) for the laryngeal opening cross-sections by procedure.

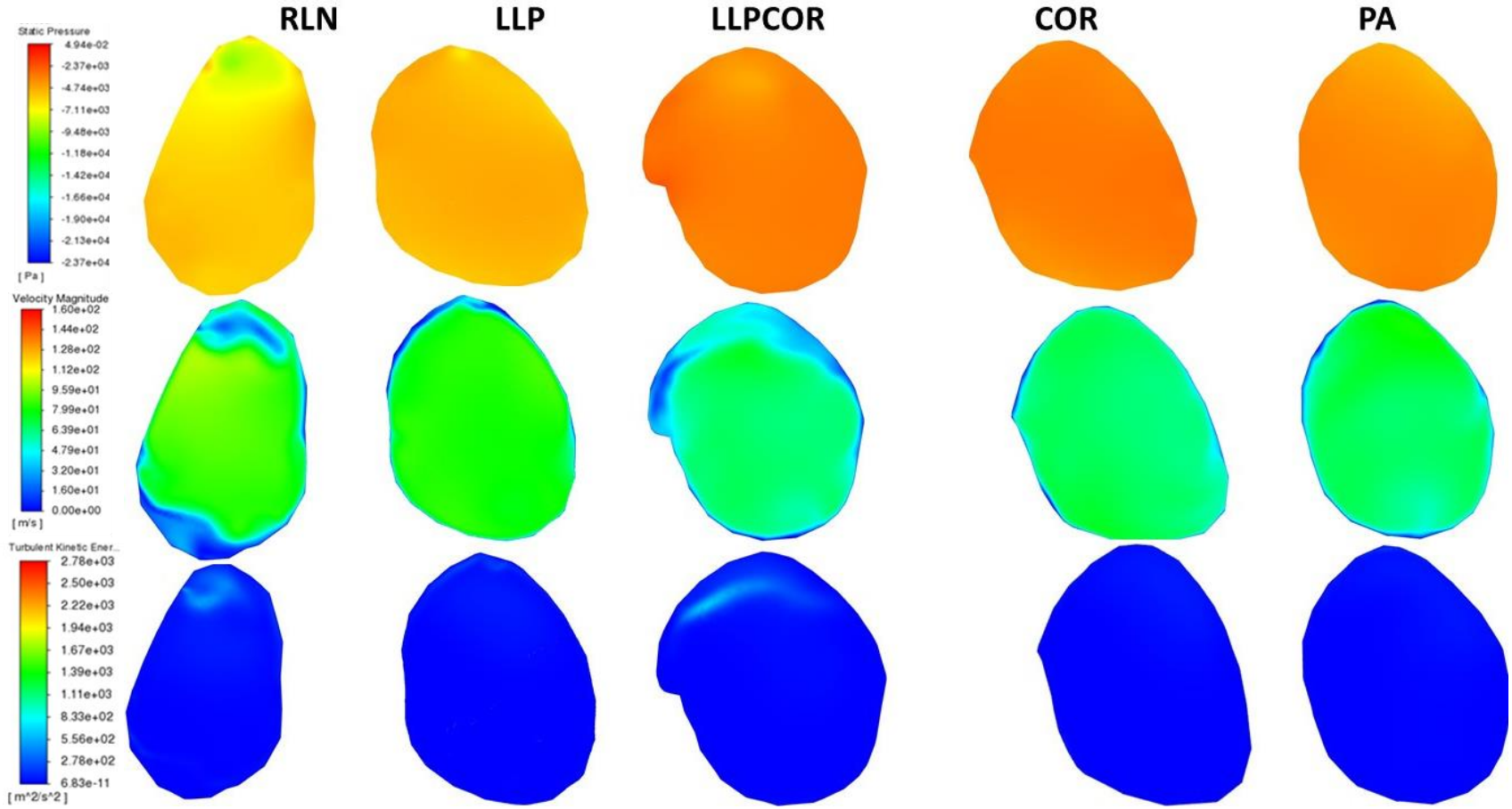

Figure 5.5D Pressure (top row), velocity (middle row), and turbulent kinetic energy (bottom row) for the mid-saccule laryngeal cross-sections by procedure.

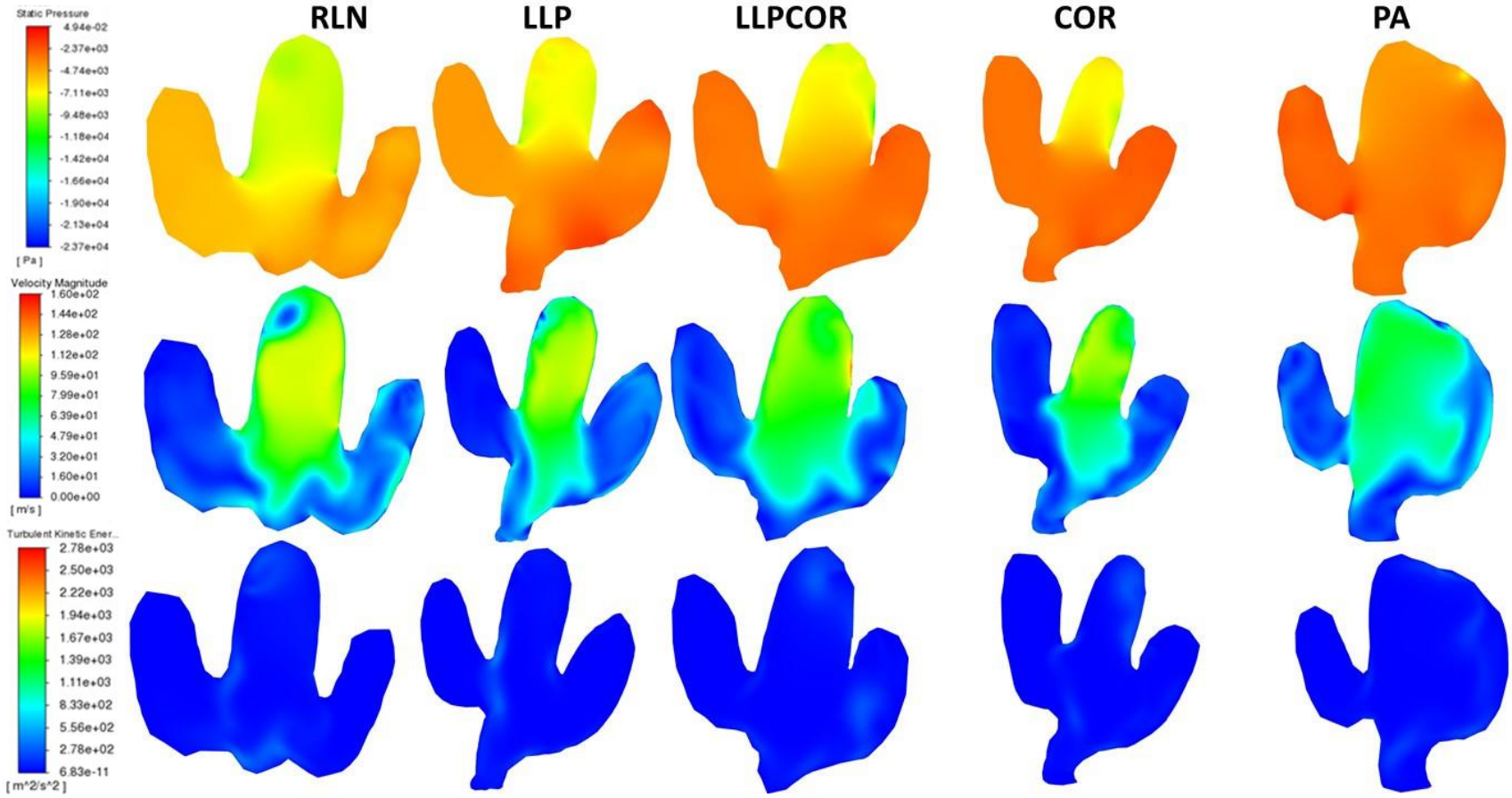

Figure 5.5E Pressure (top row), velocity (middle row), and turbulent kinetic energy (bottom row) for the narrowest laryngeal cross-sections by procedure.

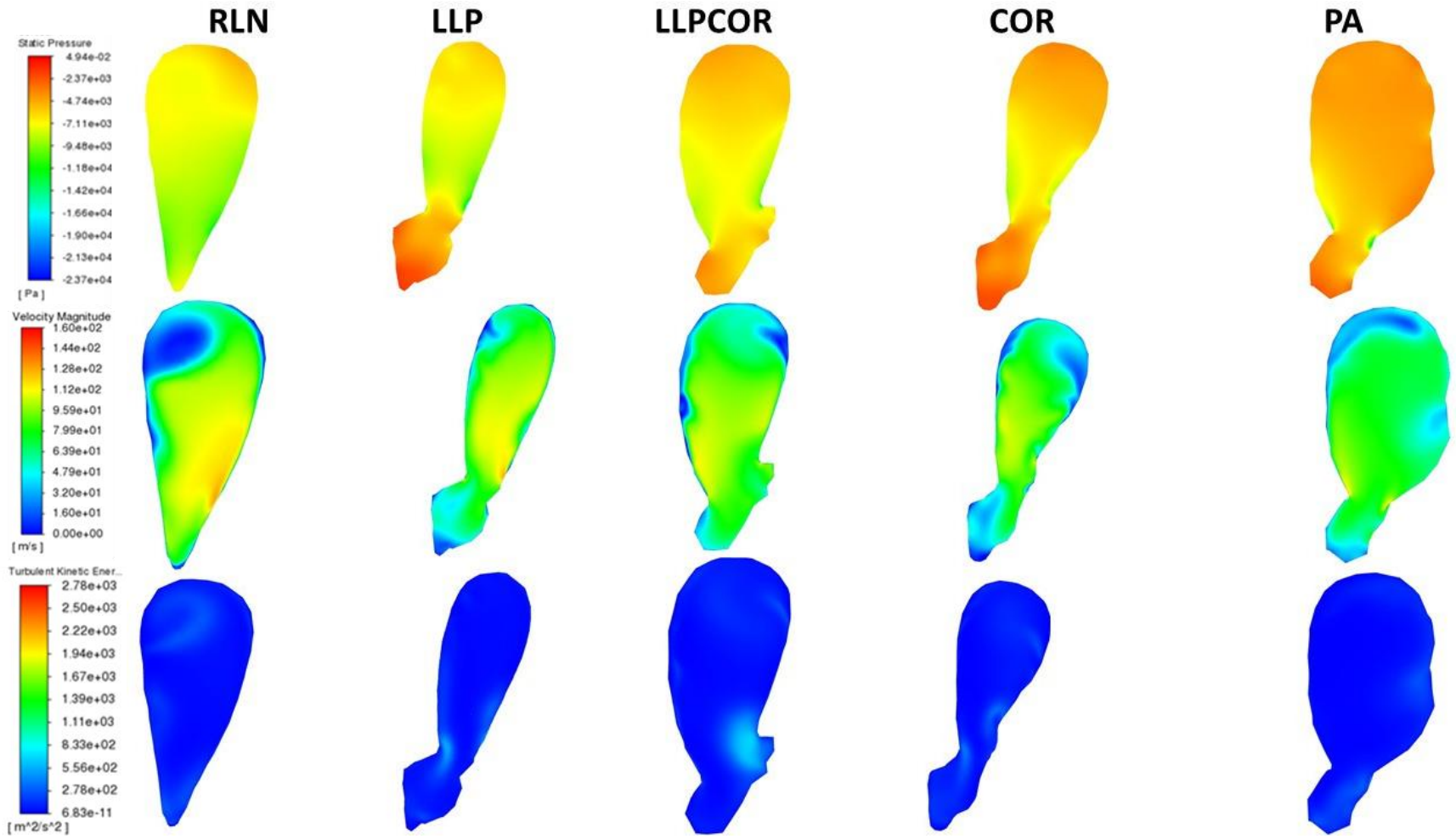

Figure 5.5F Pressure (top row), velocity (middle row), and turbulent kinetic energy (bottom row) for the caudal laryngeal cross-sections by procedure.

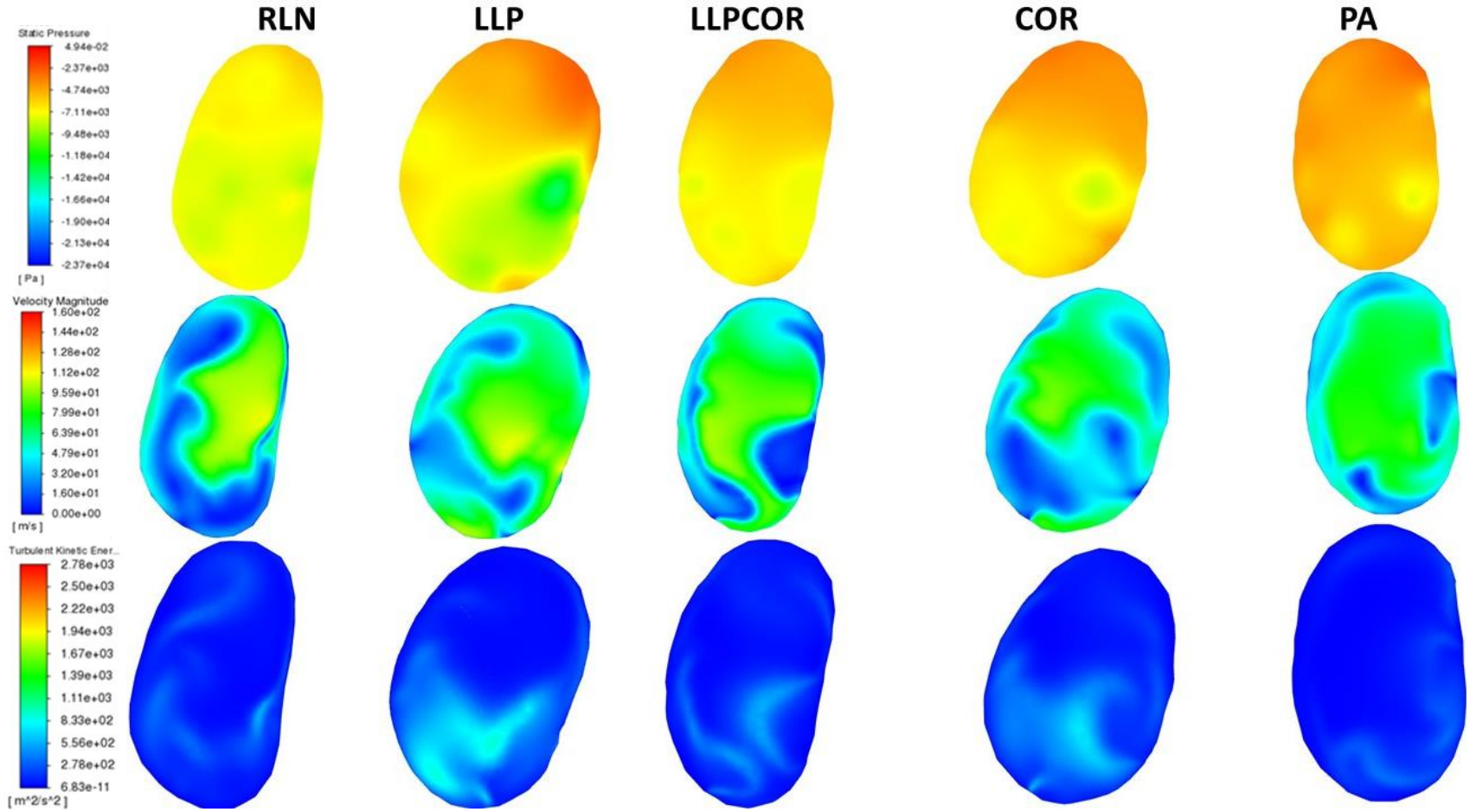

Figure 5.5G Pressure (top row), velocity (middle row), and turbulent kinetic energy (bottom row) for the tracheal cross-sections by procedure.

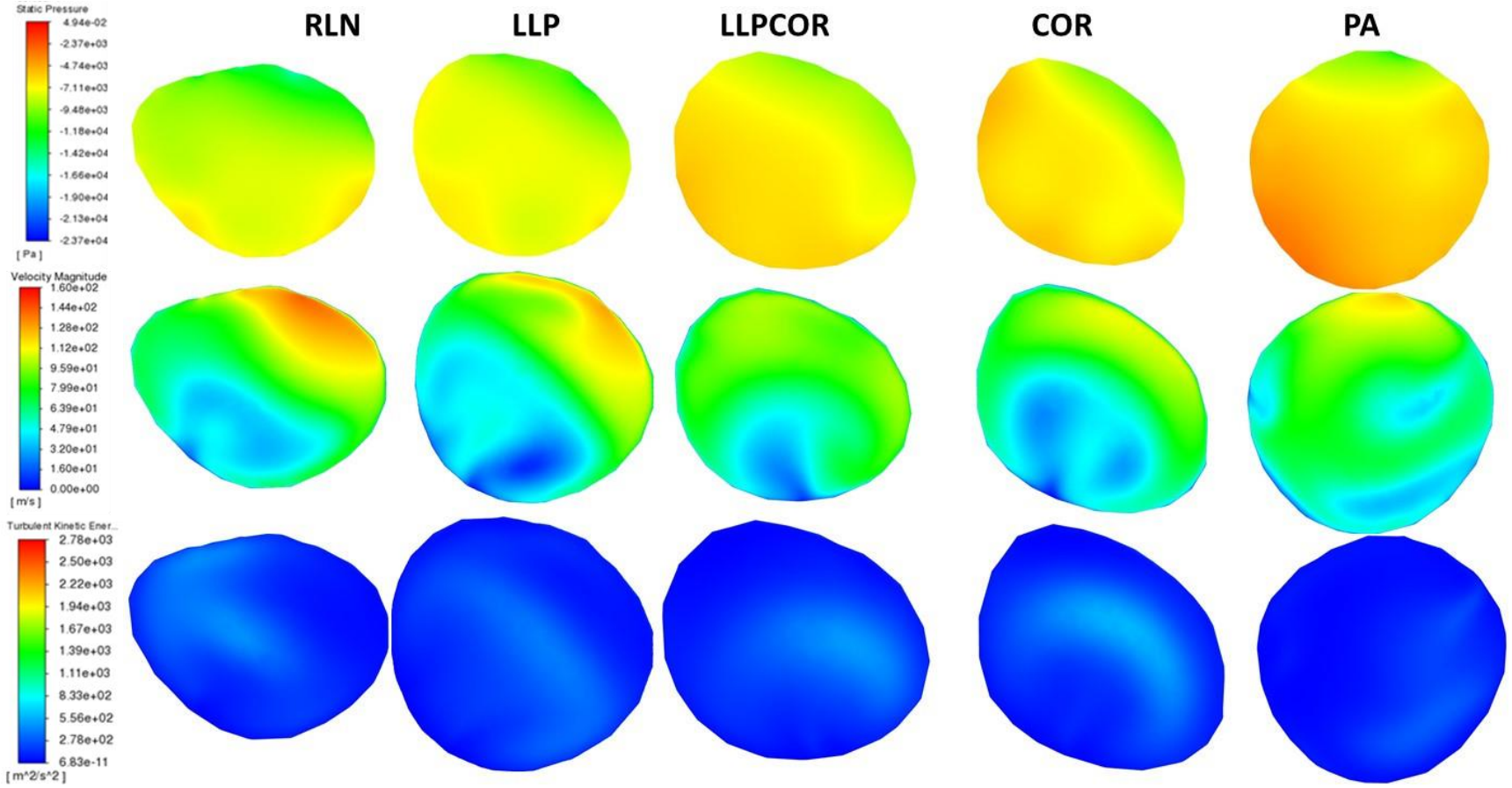

Figure 5.5H Pressure (top row), velocity (middle row), and turbulent kinetic energy (bottom row) for the sagittal sections by procedure. The colors correspond to the respective scales in Figure 5.5A.

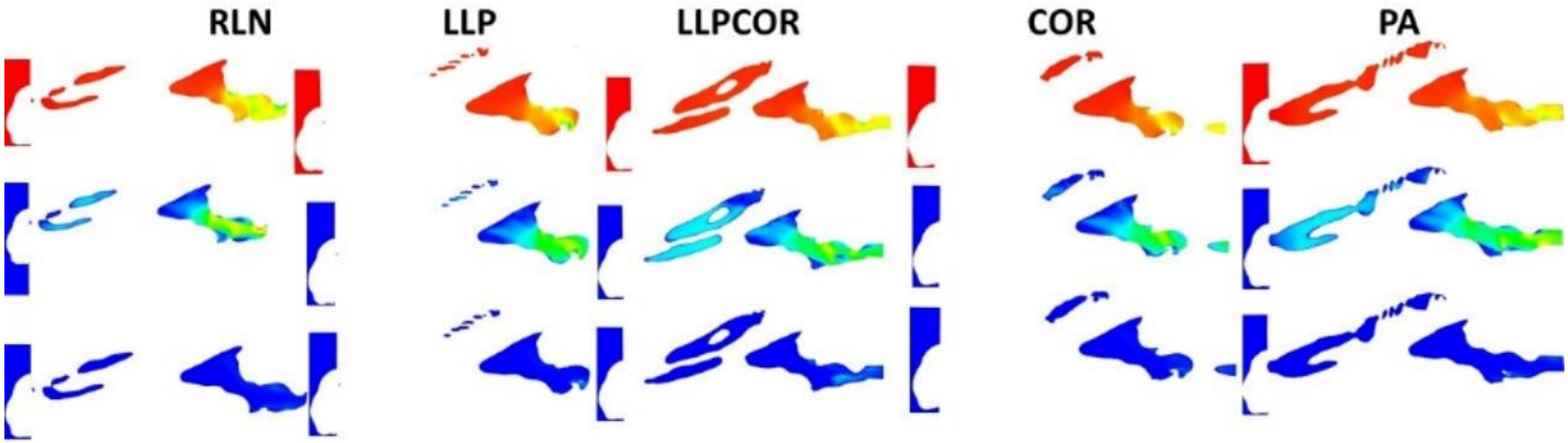

Figure 5.5I Pressure (top row), velocity (middle row), and turbulent kinetic energy (bottom row) for the sagittal sections by procedure. These are enlarged versions of Figure 5.5H, looking specifically at the larynx. The colors correspond to the respective scales in Figure 5.5A.

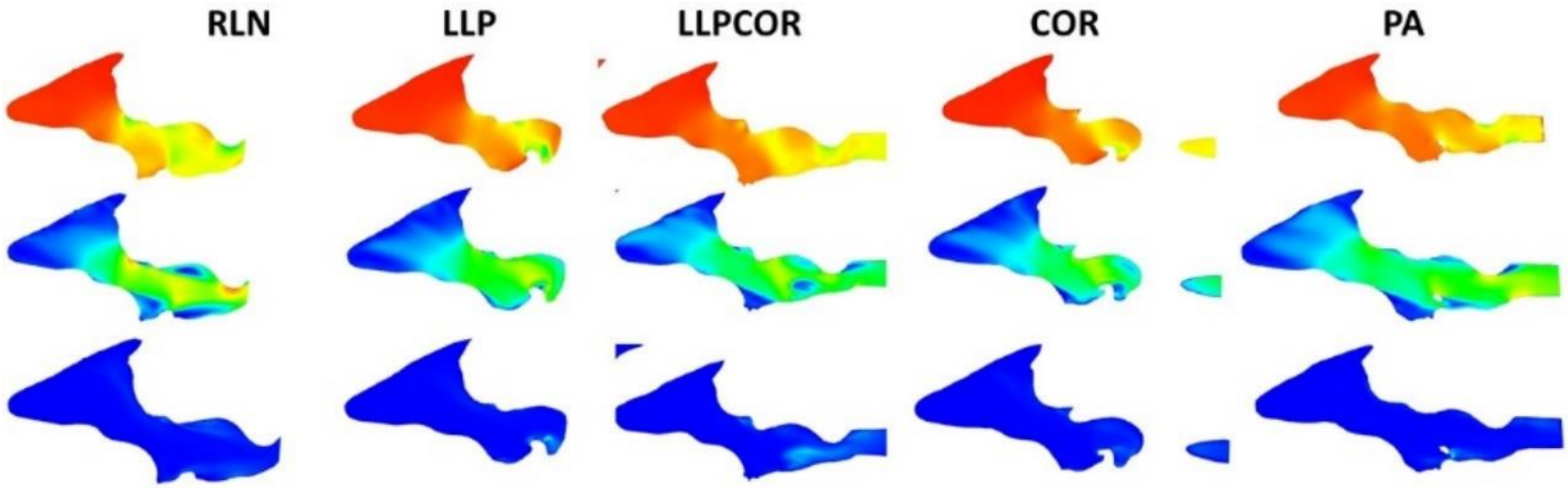

Figure 5.5J Pressure (top row), velocity (middle row), and turbulent kinetic energy (bottom row) for the parasagittal sections by procedure. The top three rows are the left parasagittal plane; the bottom three rows are the right parasagittal plane. The colors correspond to the respective scales in Figure 5.5A.

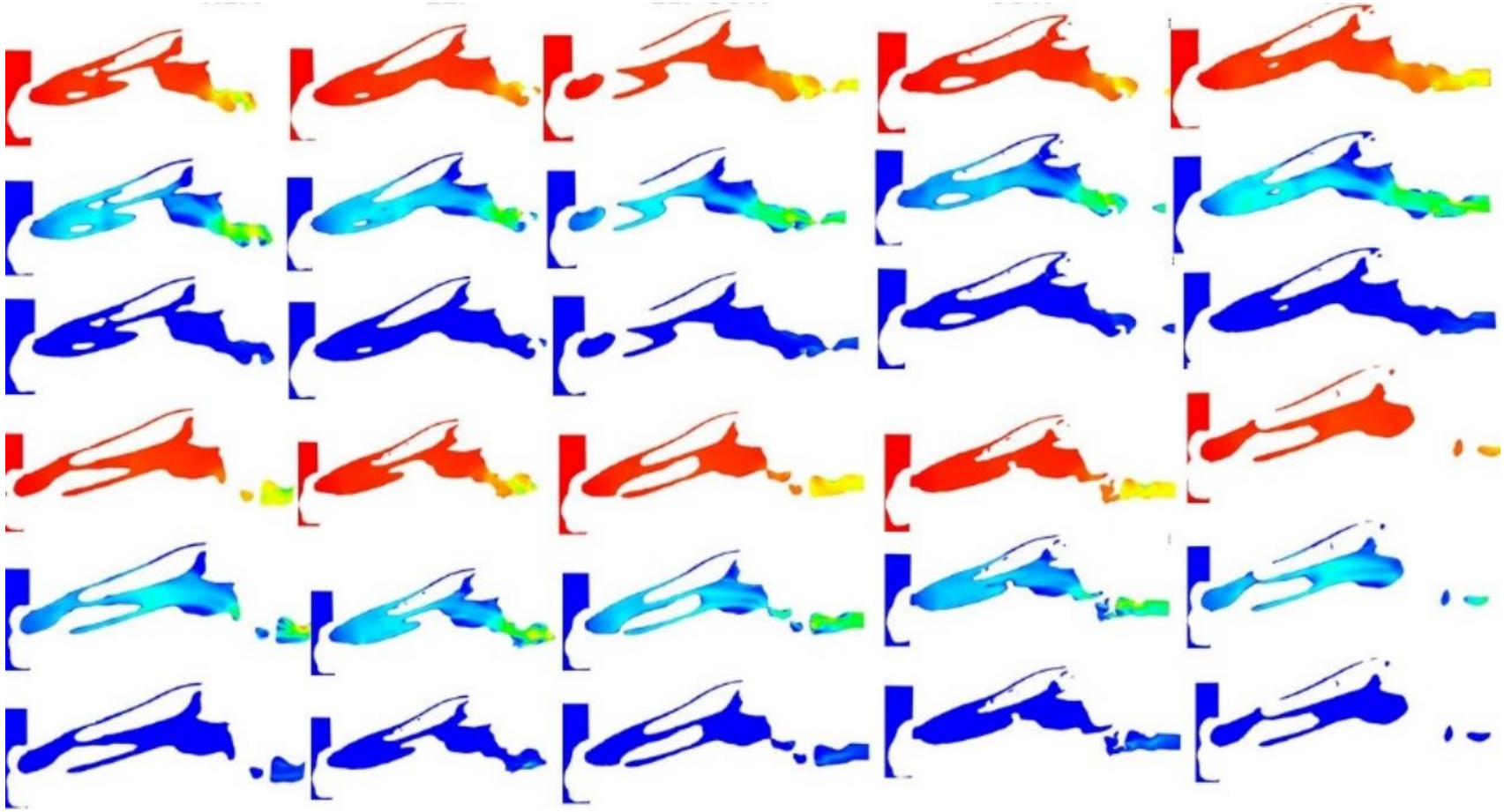

Figure 5.5K Pressure (top row), velocity (middle row), and turbulent kinetic energy (bottom row) for the parasagittal sections by procedure. The top three rows are the left parasagittal plane; the bottom three rows are the right parasagittal plane. These are enlarged versions of the same planes as Figure 5.5J, focused on the larynx. The colors correspond to the respective scales in Figure 5.5A.

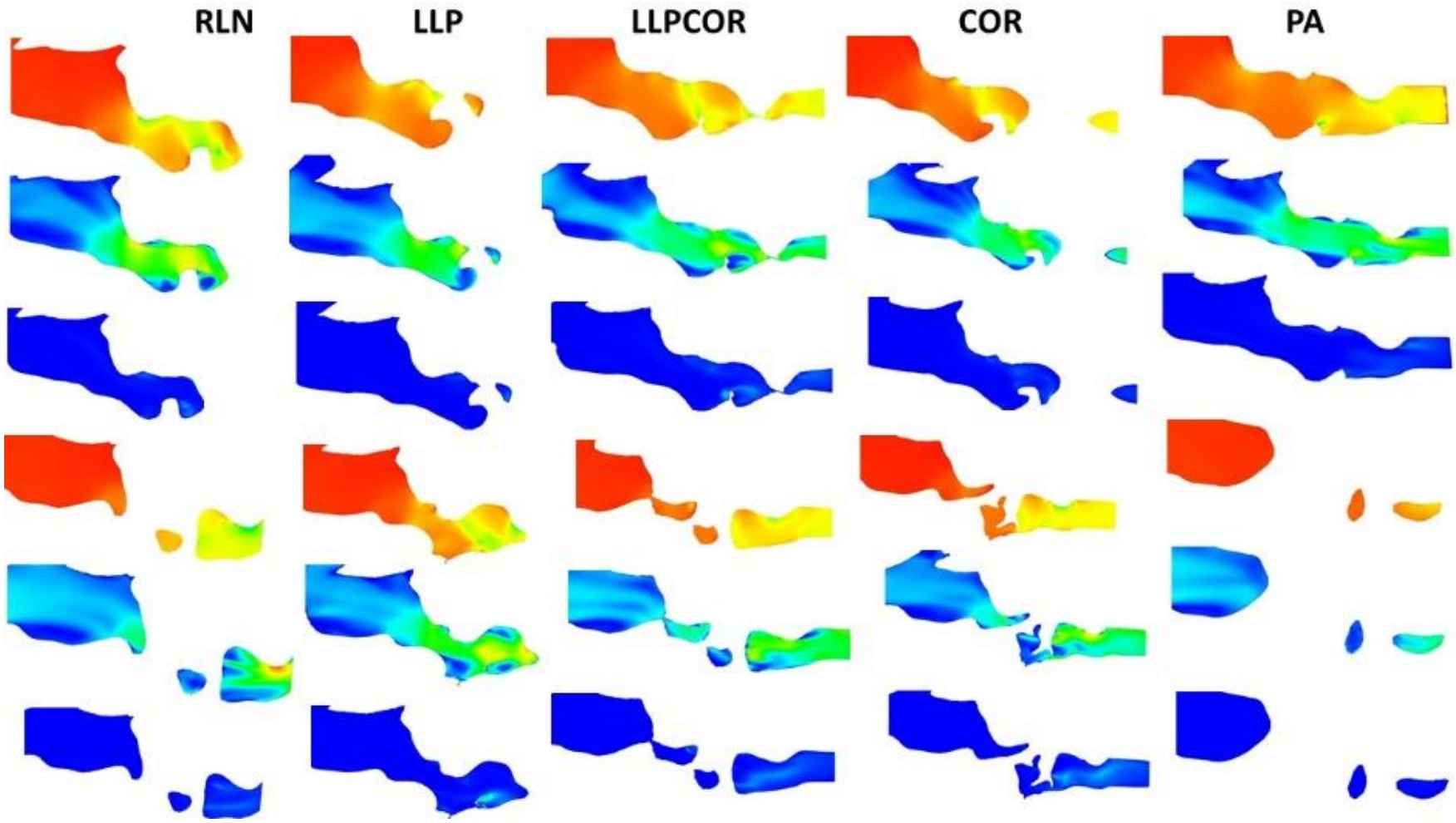

Figure 5.5L Pressure (top row), velocity (middle row), and turbulent kinetic energy (bottom row) for the transverse sections by procedure. The top three rows are the mid-nostril transverse plane; the bottom three rows are the mid-pharyngeal transverse plane. The colors correspond to the respective scales in Figure 5.5A.

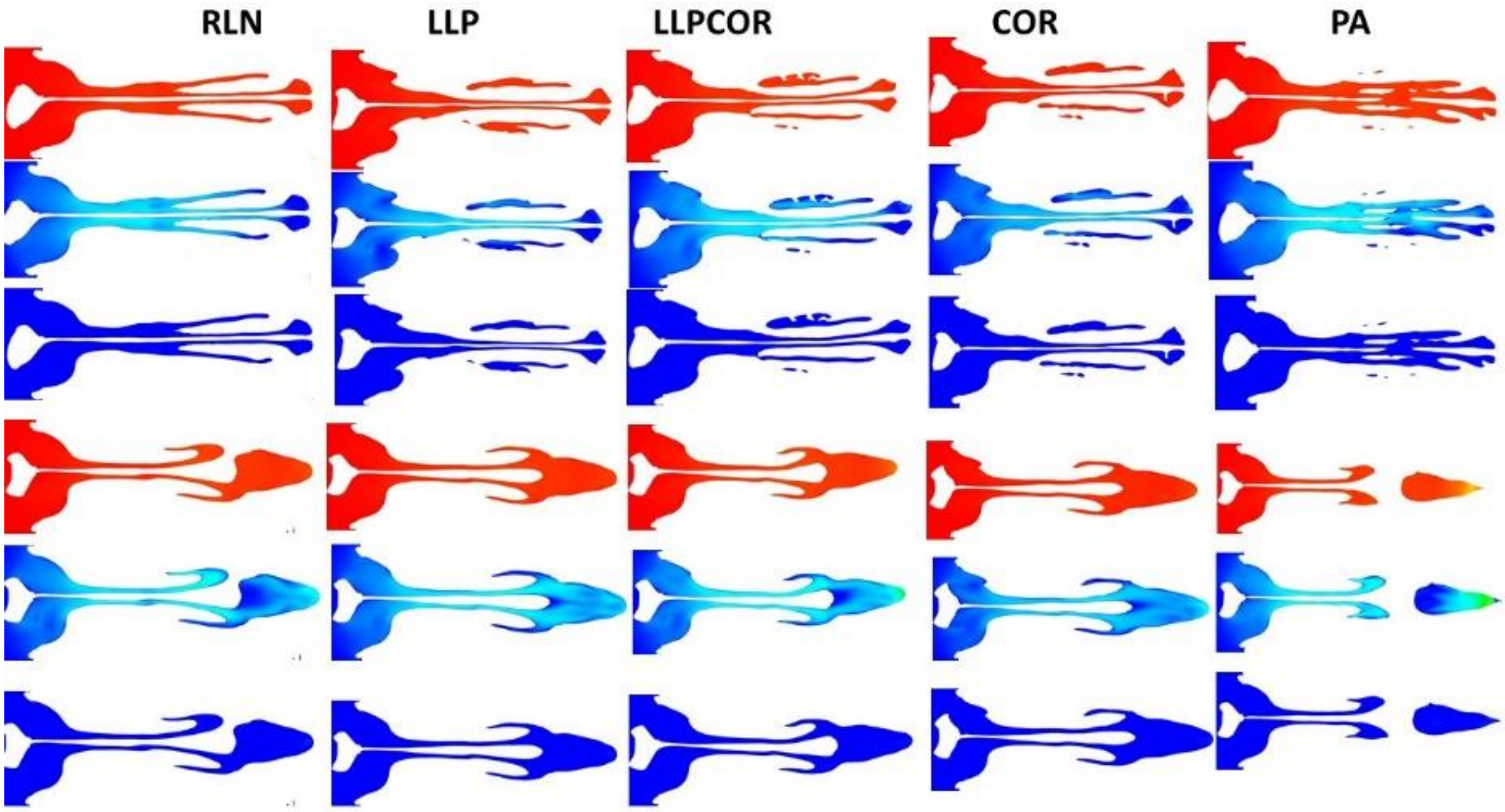

Figure 5.5M Pressure (top row), velocity (middle row), and turbulent kinetic energy (bottom row) for the dorsal laryngeal transverse sections by procedure. The colors correspond to the respective scales in Figure 5.5A.

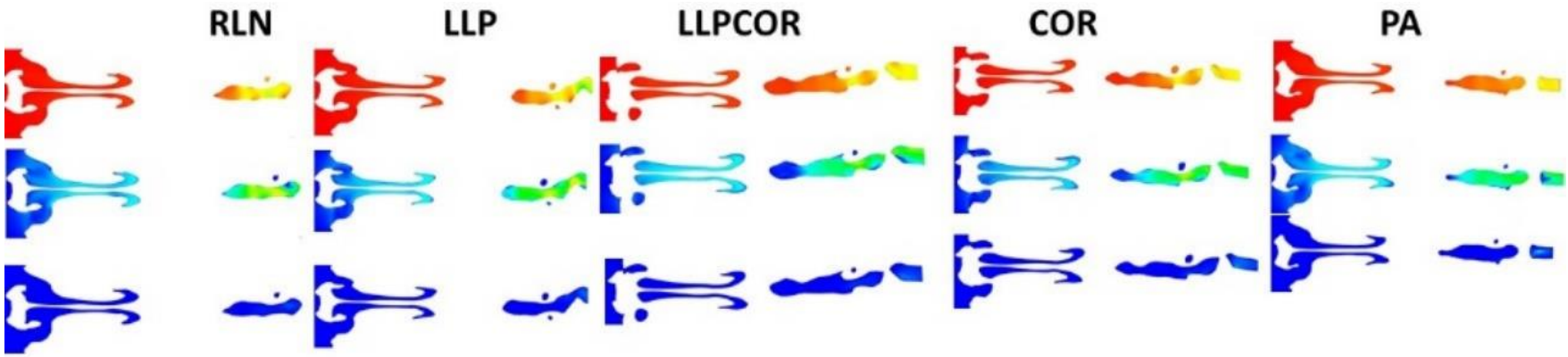

Figure 5.5N Pressure (top row), velocity (middle row), and turbulent kinetic energy (bottom row) for the dorsal laryngeal transverse sections by procedure. These are enlarged versions of the same planes as Figure 5.5M, focused on the larynx. The colors correspond to the respective scales in Figure 5.5A.

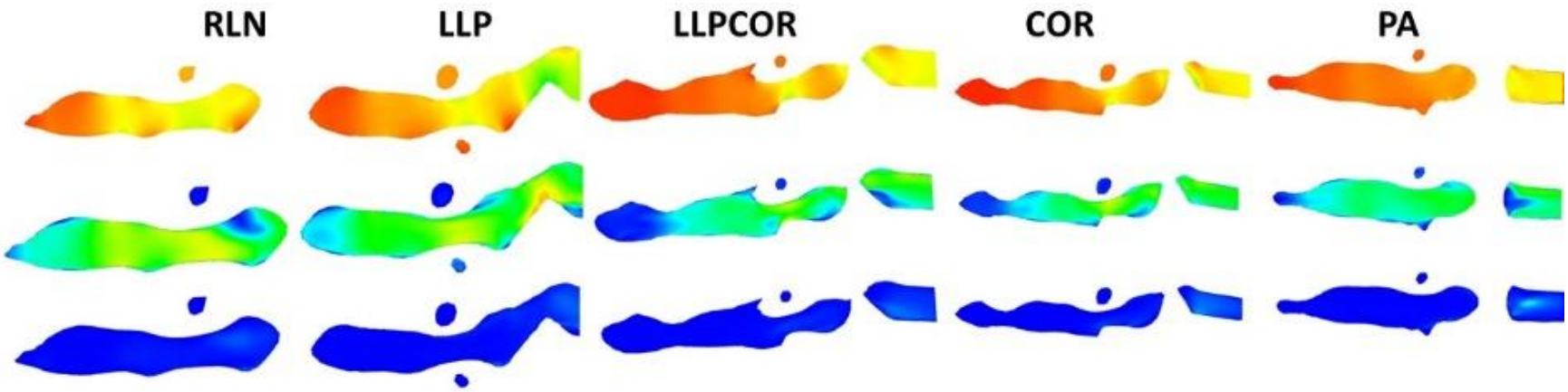

Figure 5.5O Pressure (top row), velocity (middle row), and turbulent kinetic energy (bottom row) for the transverse sections by procedure. The top three rows are the mid-laryngeal transverse plane; the bottom three rows are the ventral laryngeal transverse plane. The colors correspond to the respective scales in Figure 5.5A.

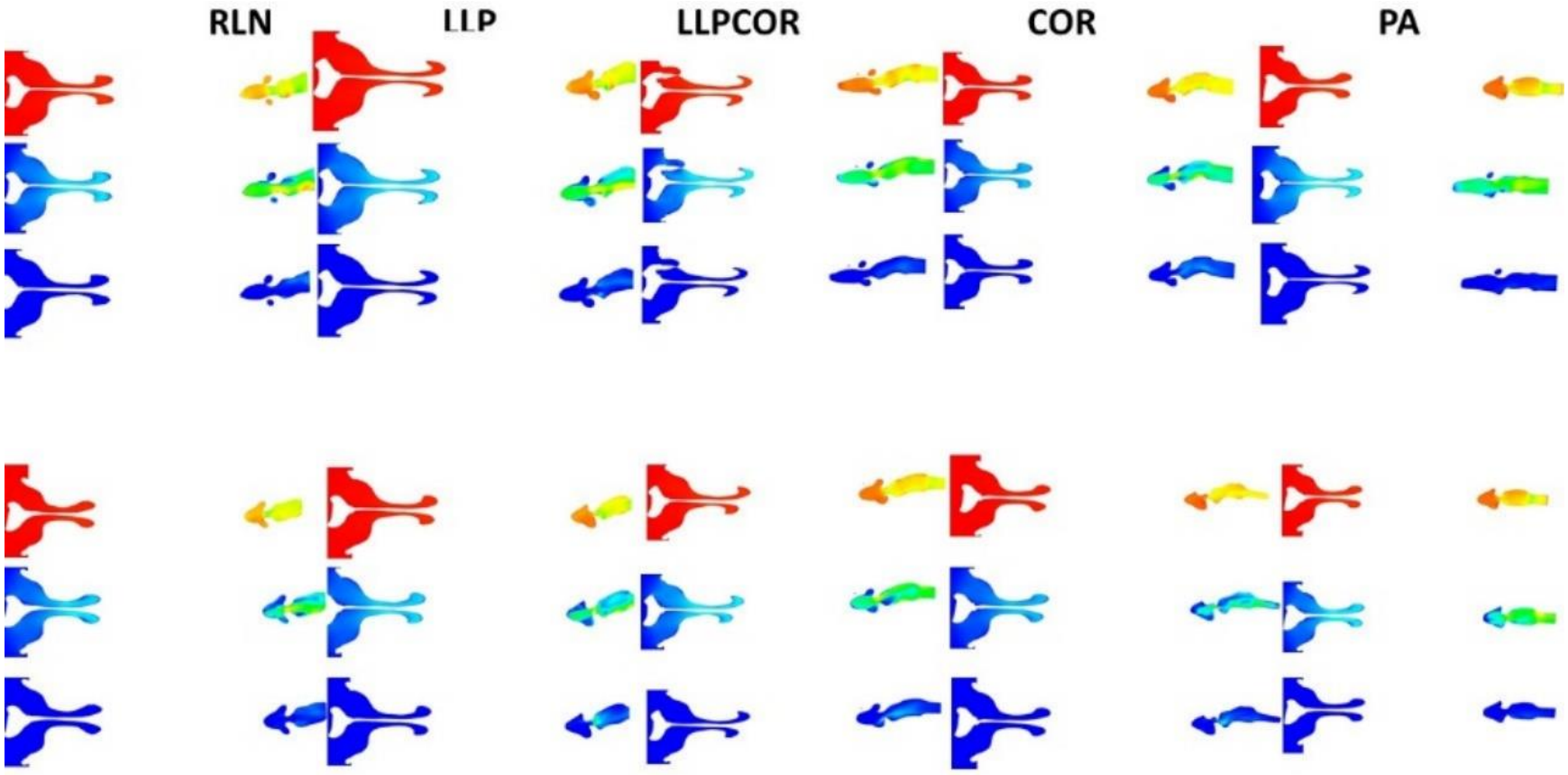

Figure 5.5P Pressure (top row), velocity (middle row), and turbulent kinetic energy (bottom row) for the transverse sections by procedure. The top three rows are the mid-laryngeal transverse plane; the bottom three rows are the ventral laryngeal plane. These are enlarged versions of the same planes as Figure 5.5O, focused on the larynx. The colors correspond to the respective scales in Figure 5.5A.

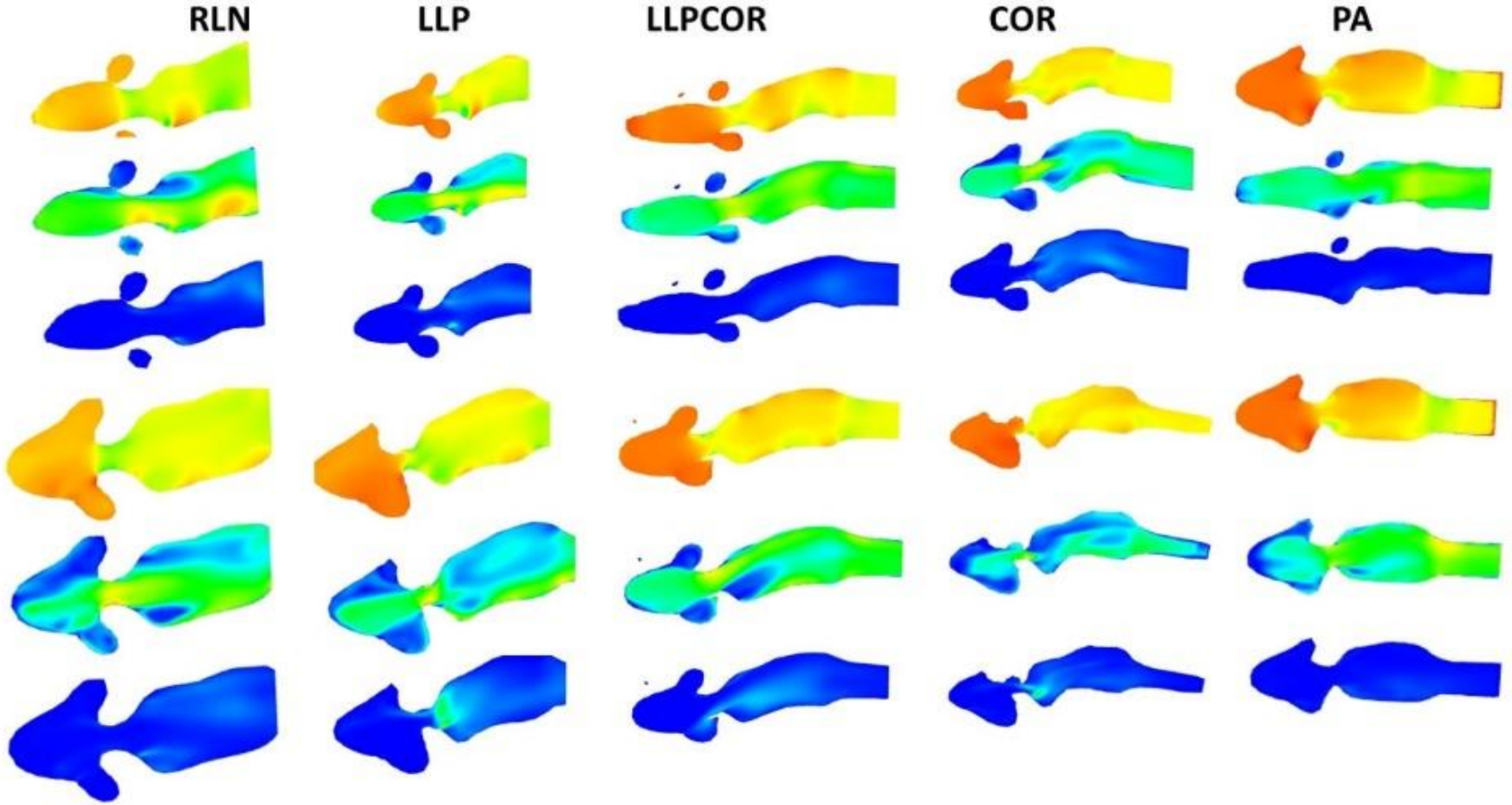

5.5 Discussion

The experimental and CFD models agreed in regards to the procedure of lowest impedance for this horse model but had slight differences in overall procedure order. Numerical comparison showed a larger disparity between the impedance values for the laryngeal region between the experimental and computational values than would be expected based on previously reported equine and human models (Li et al., 2017; Rakesh et al., 2008a; Rakesh et al., 2008b). The flow rates reported from the experimental portion of the study were lower than expected. This may have been a measurement error from small-scale oscillations in the flow brought about by passing through the tissues which may have disrupted the orifice plate measurements. The CFD model reported values that were much closer to the anticipated values for flow rate and may therefore be more accurate in this case.

There was a high impedance reported between the pharynx and the tracheal outlet, both numerically and relative to the impedance over different portions of the airway. Multiple studies have reported that 50% of the upper airway resistance should be attributable to the nasal passage but that was not the finding in this case. There are a number of factors that may explain this (Art et al., 1988; Bayly et al., 1997; Rakesh et al., 2008a). Throughout each of these studies, different breeds were used. In this study, a Quarter horse was used as the model while the previous study used a Thoroughbred horse (Rakesh et al., 2008a). It is also important to consider the application as the current study sought to establish a truly inhalation-based model by subjecting the head to negative airflow after stabilizing the collapsible portions of the airway. This may have resulted in a higher impedance in the regions of collapsible tissues. Rakesh et al. (2008a) also found that there was a constriction at the caudal nasal region where air dropped into the pharynx, which resulted in high pressure and turbulence. The horse used for this study did not have the same narrowed region, and even from the original CT images there was significant overlap between the caudal nasal passage and the pharynx in the current study model. Some of the earlier studies reporting higher nasal resistance also incorporated transducer catheter placement in the pharynx and did not report specific placement within that region. Pharyngeal resistance changes from rostral to caudal, enough to influence the reported proportional resistance and to explain the disparity between studies (Art et al., 1988; Derksen et al., 1986). The current study correlates more closely with a previous fiberglass model that found the nares, pharynx and larynx each contributed around thirty

percent of the airway resistance (Bayly et al., 1997). Additionally, the tracheal pressures were much higher than in some reports but it has been demonstrated that horses compensate for upper airway resistance through greater pull from the lower airways, within the ranges reported here for tracheal pressure (Williams et al., 1990a).

This study follows a similar theme to the work performed in Chapter 4. In the other study, the equine larynx was modelled in isolation. A similar jet effect from the caudal nostrils into the larynx was observed as before; however, the anatomical change in direction ventrally from the ethmoid region, dropping into the pharynx, and then subsequently into the larynx is much more abrupt than the straight box model. A funneling effect of the pharynx was observed as documented in Chapter 4. There appeared to be less abrupt changes in the airway which may be a function of the geometry construction. In this study, the channel of airflow was traced by hand to establish the geometry for airflow while in the previous study, the tissues were isolated. Segmentation by hand was necessary in this case as the shape/contour of sinuses and conchal bullae were expected to confound the process of semi-automated segmentation. Across both studies, the RLN and COR procedures were more obstructive and characterized by higher negative pressures and velocities. The saccules also influenced flow as shown in **Figure 5.3**. There is a pattern of a sudden change in pressure and velocity over a short distance with the higher impedance procedures as has been noted in the other study. Unique to this study, the LLP and LLPCOR procedures did not reduce impedance as effectively and PA was the lowest impedance procedure. One explanation for this was that the head was oriented in the upright position which may have resulted in compression of the ventral airway structures and less airway space. The PA may have resulted in a greater cross-sectional area in this region by simple tissue excision alone. The use of a cadaver head resulted in unexpected impedance results with LLP higher than that of the RLN state which would indicate the results are likely not reflective of results that would be seen in an actual patient. Narrowing of the airways at the level of the nostrils and in other regions may have played a role in these unexpected results and use of alive patient geometries would be beneficial for future studies.

One important outcome of this study which has been corroborated in other studies is that the PA did not have the lowest velocity or the highest negative pressure despite having the lowest impedance. Looking at the rima glottis region alone, the negative pressure for the PA is not the highest but as one proceeds caudally, the PA compensates in the more caudal regions of the larynx,

especially as the left ventricle region is incorporated into the cross-sectional area of flow. This coincides with the modified PA report that rima glottis area changes did not reflect the change in impedance with LLP and PA procedures (Radcliffe et al., 2006). Looking at one specific portion of the airway is not entirely predictive of the impedance and the use of CFD affords incorporation of the entire airway (Tucker et al., 2022). This finding has also been corroborated in multiple sleep apnea studies in humans where airway volume was correlated to impedance (Chang et al., 2018; De Backer et al., 2007).

While the experimental portion of the study did reflect the same findings for airflow and impedance as from other reports, the CFD results were much closer and provided information as to why the experimental discrepancy occurred. The different nasopharyngeal geometry of this patient compared to the previous study and the consistent expansion over distance afforded by the PA along with consistent pressure and velocity throughout the volume were all more apparent from the CFD analysis and explain the disparities. Capturing an accurate representation of the three-dimensional upper respiratory anatomy in the equine patient is a worthwhile pursuit given the potential insights that can be gleaned from the higher-level analysis of CFD. This study is unique in both the veterinary and human fields in seeking the validation of a CFD model based on experimental data obtained from a cadaveric model. More work is needed to calibrate the model for applications in clinical patients, but the potential benefits are limitless, given the continual advancement of computational and mechanical knowledge.

CHAPTER SIX:

GENERAL DISCUSSION

6.1 Introduction/Background

Equine recurrent laryngeal neuropathy (RLN) continues to present a significant problem within the racing industry. The advent of dynamic endoscopy, innovations in the biomechanical implants and developments in the implementation of the laryngoplasty have contributed to fewer postoperative complications. Despite these advances, surgical success rates appear to have plateaued at around 80%, mirroring that of human upper airway surgery (Dinis et al., 2002; Ducharme et al., 2019).

A number of fluid dynamic analyses have contributed to a greater understanding of the postoperative complications experienced by human patients with obstructive sleep apnea syndrome (OSAS), nasal obstructions and vocal fold procedures (Faizal et al., 2020; Ito et al., 2011). Likewise, CFD has been used in canine patients to explore fluid dynamic changes associated with brachycephalic syndrome and its associated surgeries (Khoa et al., 2021). Similar application of CFD to clinical equine patients has not yet been achieved.

A computational fluid dynamics (CFD) study was performed on a horse model over a decade ago looking at the influence of three different levels of laryngoplasty abduction on the fluid mechanics of the equine upper airway (Rakesh et al., 2008b). This lone study set the standard regarding assertions about the fluid dynamics within the equine upper airway (Rakesh et al., 2008c). Proper validation of a model necessitates intuitive evaluation, repeated confirmation, and agreement with subsequent experiments. CFD model confirmation has been performed through numerous parallel studies in human surgery but it has not been performed in the horse (Faizal et al., 2020). Computational methods and turbulence modelling have improved greatly since CFD was first implemented in the horse, which justifies the development and expansion of fluid calculations and their use in real-world equine clinical scenarios.

This thesis work aimed to establish surgical options for equine patients outside the typical RLN treatments and to continue the development and implementation of computational methods in solving complex equine airway problems. Review of the relevant literature regarding equine RLN along with canine and human upper airway CFD models was performed in Chapter 1.

6.2 Results: Physical Airway Models

Chapter 2 introduced a new surgical manipulation for equine RLN, the arytenoid corniculectomy, which was tested *ex vivo* against currently accepted surgical options. It employed a previously established box model to test equine larynges replicating RLN, a left laryngoplasty with ipsilateral ventriculocordectomy (LLP), combined left laryngoplasty, ventriculocordectomy and corniculectomy (LLPCOR), corniculectomy (COR), and partial arytenoidectomy (PA).

The COR procedure did not improve translaryngeal impedance as well as expected in the box model, however there are inconsistencies between this prototype and clinical success of other procedures, such as the PA. Impedance and collapse, or lack thereof, do not translate to optimal postoperative performance in horses. This was shown in one study of postoperative RLN cases with soft tissue collapse on dynamic endoscopy; owner satisfaction and performance were still high despite abnormalities noted on the follow-up exam (Barnett et al., 2013a; Compostella et al., 2012). Similarly, while the box model would indicate that the COR should not be used, it has been implemented in arytenoid chondritis cases with other procedures with some success (Piggott, 2021). The relationship between translaryngeal impedance, patient performance and client satisfaction warrants further investigation as the equine surgery community critically reflects on prioritizing the outcomes of upper airway surgery.

Another unexpected finding of this study was the intraclass correlation of 27.6% despite controlling for many patient variables and it represents uncaptured individualistic differences. The ordering procedures by impedance from least to most for each larynx provides some insight. There are two "categories" of procedures: LLP/LLPCOR versus COR/PA/RLN but there are many variations within these two groupings as shown in **Table 6.1.** The adapter size was also significant for RLN, LLP, and LLPCOR procedures, which represent both of the categories. This would suggest that the original width of the airway is important in highly obstructive and low obstructive states, but for procedures that are only partially obstructive, the airway diameter is less significant. Airway diameter has long been theorized to be associated with the level of clinical signs and performance observed in equine patients (Cook, 1988).

Table 6.1 Procedure in order of measured impedance from least to most by larynx from the initial box study. Specimens that required the large (1.5") adapter size are in bold.

Impedance Ranking

Larynx #	Least				Most
1	LLP	LLPCOR	PA	RLN	COR
2	LLP	LLPCOR	PA	COR	RLN
3	**LLP**	**LLPCOR**	**PA**	**RLN**	**COR**
4	LLP	LLPCOR	PA	COR	RLN
5	LLPCOR	LLP	PA	COR	RLN
6	LLP	LLPCOR	PA	RLN	COR
7	LLP	LLPCOR	PA	COR	RLN
8	LLP	LLPCOR	PA	COR	RLN
9	**LLP**	**LLPCOR**	**RLN**	**COR**	**PA**
10	**LLP**	**LLPCOR**	**COR**	**RLN**	**PA**
11	LLP	LLPCOR	PA	RLN	COR
12	LLP	LLPCOR	COR	PA	RLN
13	**LLP**	**LLPCOR**	**PA**	**RLN**	**COR**
14	**LLP**	**LLPCOR**	**PA**	**COR**	**RLN**
15	LLPCOR	LLP	PA	COR	RLN
16	**LLP**	**LLPCOR**	**RLN**	**PA**	**COR**
17	**LLP**	**LLPCOR**	**COR**	**PA**	**RLN**
18	LLP	LLPCOR	RLN	PA	COR
19	LLP	LLPCOR	PA	COR	RLN
20	PA	LLPCOR	COR	LLP	RLN
21	**LLP**	**LLPCOR**	**PA**	**COR**	**RLN**
22	LLP	LLPCOR	PA	RLN	COR
23	LLP	LLPCOR	PA	RLN	COR
24	LLPCOR	LLP	RLN	COR	PA
25	LLP	LLPCOR	PA	RLN	COR
26	LLP	LLPCOR	PA	COR	RLN
27	LLP	LLPCOR	PA	RLN	COR
28	LLP	LLPCOR	PA	RLN	COR

Ultimately during this analysis, it became clear that cross-sectional area (CSA) of rima glottis alone is not an adequate metric for determining the level of impedance. The CSA is evaluated clinically to assess disease and postoperative success, although it is not indicative of performance or client satisfaction, as mentioned above. The rima glottis area does not always reflect the changes in the laryngeal anatomy that are occurring caudally and the region of the saccules is inconsistently addressed across the literature.

However, the ventricles may still have a significant impact on impedance and performance (Henderson et al., 2007). This led to inquiries about how to best capture the three-dimensional laryngeal anatomy during collapse and constriction of the airway.

Constriction and its impacts on fluid flow development have been more thoroughly examined within pipe flow constructs in engineering disciplines. Characteristic variables related to the constriction within a pipe have been used to determine the impact on resistance to flow. An example is the incident angle at which the flow encounters the constriction. This angle, as well as the ratios of the expanded and constricted diameters and constriction length, significantly influences the energy lost across the constriction and is reflected in the upstream and downstream pressure differential (Fossa et al., 2002). Chapter 3 sought to bring together these fluid mechanics principles with three-dimensional laryngeal geometry to attempt to better explicate the variability in impedance which had been observed in Chapter 2. Once established, a simplified geometrical analysis of the surgical procedures was performed via CT exams and compared to a pipe constriction model.

Geometry of the collapsed equine airway is one piece of a very complex problem and it is difficult to isolate the effect of small changes on impedance from one larynx to another. While a simple pipe constriction seems like a gross oversimplification, simple geometrical models within the highly turbulent conditions of the equine airway need to be explored to verify future computational studies and to characterize the flow. The Venturi effect has long been cited as an explanation for the fluid mechanics observed in the equine upper airway, but this is a simplification as well (Cheetham, 2019). In looking to use simple features to describe the laryngeal geometry, wide ranges of values for area, area ratio and incident angle were found. These reported values can be used for comparison in future studies and for the development of future models as equine airflow mechanics continues to expand. The range of values found within the relatively small study

population demonstrates the complexity of the equine laryngeal geometry and further exemplifies the individuality that is observed between patients. This over-arching theme, which was identified in Chapter 2 was characterized further in Chapter 3 where six different variations in order of procedure by impedance was determined **(Table 6.2)**. These findings confirm the importance of individual variability and the subsequent difficulty in establishing the impact of a specific surgical manipulations will have on a generic equine upper airway.

6.3 Results: Computational Airway Models

Chapter 4 further emphasized the importance of individual variability by using CFD to incorporate the three-dimensional larynx geometry from CT scans into the analysis of the fluid mechanics of each surgical procedure. CFD juxtaposes the specific and yet extensive fluid mechanics characteristics with the laryngeal anatomy allowing a more in-depth analysis of the interaction between structure and fluid mechanics. CFD was found to be effective at determining procedural impedance for individual larynges. The numerical accuracy was not as high as would have been anticipated given reports in human respiratory surgery. Here, on average, a 20% difference in static pressure across multiple points of measurement has been reported (Mylavarpu et al., 2009). The difference between measured (experimental data) and CFD-calculated impedance in this body of equine work showed a linear trend closer to a 40% difference (factor of 1.4) between values. It is possible that a difference in model characteristics was responsible for the disparity of results. In the human study by Mylvarapu et al., (2009) the κ-ω model was the closest to the measured values for pressure at different points in a human pharyngeal mold. The κ-ω model was not used in this thesis as the κ-ε model had been previously was used in the equine pharyngeal/laryngeal models. Using the same model as that used historically permitted a closer comparison of findings between the current body of work and that of the original equine CFD work (Rakesh et al., 2008a); further its good agreement with equine exercise physiology study results suggests that it may be useful in “whole-body” real-world scenarios (Rakesh et al., 2008a).

Table 6.2 Procedure in order of measured impedance from least to most by larynx from the second box (CT) study. Specimens that required the large (1.5") adapter size are in bold.

	Impedance Ranking				
Larynx #	**Least**				**Most**
1	LLP	LLPCOR	PA	COR	RLN
2	LLP	LLPCOR	PA	RLN	COR
3	LLPCOR	LLP	PA	RLN	COR
4	**LLP**	**LLPCOR**	**COR**	**RLN**	**PA**
5	LLPCOR	LLP	PA	RLN	
6	LLP	LLPCOR	PA	COR	RLN
7	LLP	LLPCOR	PA	COR	RLN
8	LLP	LLPCOR	COR	PA	RLN
9	**LLPCOR**	**LLP**	**PA**	**COR**	**RLN**
10	**LLP**	**LLPCOR**	**PA**	**COR**	**RLN**

Chapter 4 also highlighted the importance of smoothing the laryngeal geometry. The *ex vivo* models do not capture the postoperative healed state and tend to have stray fragments of mucosa or muscle that collapse into the lumen. One exception was the box model application to equine larynges collected from horses that were kept alive and followed several months after surgery (Hawkins et al., 2014; Jansson et al., 2000). Despite model limitations in regard to postoperative healing, collapsing residual tissue has been cited as a reason for suboptimal postoperative noise and may possibly affect performance in actual patients (Davidson et al., 2010; Davidson et al., 2011). Thus, especially in the case of COR or PA procedures, using an extra-laryngeal approach as has been reported may warrant further investigation in achieving the overall goal of luminal smoothness (Hay et al., 1993).

This study resulted in the capture and analysis of 49 different laryngeal configurations. In the previous equine CFD model, three geometries were generated, manipulated and then unified with the head geometry (Rakesh et al., 2008c). In this study, the box CAD model was created and then the laryngeal geometries were unified in SpaceClaim. This may have resulted in some of the discrepancy between the benchtop and CFD results but also speaks to the versatility of this technology. To avoid complete geometry reconstruction within a specific patient for multiple scenarios this study serves as a reference point to determine how to best manipulate just the laryngeal geometry to reflect different surgical procedures for a predictive outcome. This ultimately can expedite the analysis and potentially reduce computational time as more direct correlations are made.

Chapter 5 introduced a full equine upper airway model and examined the effects of RLN and the previously mentioned surgical procedures within this context. While the entire equine upper airway has been modeled before, inhalation incorporated into the CFD model after geometry creation, and an educated guess was made for post-generation modifications (Rakesh, 2008a). The equine research community would benefit greatly from a realistic benchtop and CFD inhalation model that appropriately captures anatomical changes with muscular engagement at exercise and fatigue over time. In humans, patients may be cued to inhale, breath hold or exhale while undergoing a CT or MRI which facilitates the capture of the changing three-dimensional geometry through different phases of respiration (Faizal et al., 2020; Jeong et al., 2007).

Additionally, a more robust model may be developed by including an initial velocity field instead of relying on one to be generated. The model reported here for the equine head attempted to create one by moving the pressure inlet away from the nasal opening to simulate more realistic flow at the nares. The idea was to create a model similar to a horse inhaling in a room. No exploration to date of the velocity field in the equine upper airway outside of CFD models have been performed, and so the inlet conditions again represent an area where greater accuracy could be achieved.

6.4 Limitations and Future Research

The greatest limitation of this work is that it was performed on cadavers, and therefore the actual conformation of the live equine at exercise remains unexplored. As addressed in the respective chapters, obtaining a 3-D capture of the equine upper airway at exercise is likely not possible for the next several years. To properly bridge the gap between the cadaver and the patient, in vivo experiments with horses are needed. Additionally, only one example was used for the final model as in previous studies, and this should be expanded to create a more representative sample for the variations within and between breeds.

The basic evolution of an airway model for upper airway surgeries in horses exemplifies the continued validation that should occur within equine upper airway surgeries. Simplified *ex vivo* and CFD models that are properly developed may reduce the research costs associated with upper airway surgery in horses and lead to new insights in the way that new interventions are developed. Continued verification of the CFD model of the equine upper airway is necessary before significant clinical implementation can be anticipated, given the widespread investigation into human flows prior to its clinical implementation in that field (Faizal et al., 2020). Further branching into investigation of other portions of the airway and other disease states would also aid in the understanding of the interactions between different anatomical components. For example, there is a well-established but ambiguous connection between disorders of the soft palate, pharyngeal walls, and lower airway inflammation with RLN and a subsequent laryngoplasty.

It should also be noted that while there have been repeated studies of equine exercise physiology looking at pharyngeal pressure and flow, these studies have focused on two, maybe three points of measurement and lack detailed description of where these measurements are taken

(Derksen et al., 1986; Radcliffe et al., 2006). One outcome of this, and the previous, studies is that the pressure in the equine pharynx changes from rostral to caudal and from dorsal to ventral within the CFD simulation. Thus, an accurate description of where measurements are taken is recommended for future studies. Given the level of turbulence in the equine upper airway, multiple points of measurement would also be helpful for calibrating for future CFD models for comparison.

The equine upper airway is unique in that the levels of turbulence generated during exercise are not seen in the human or canine airway. Model validation in specific aspects of the human airway have been performed but these findings cannot be assumed to translate into equine airway applications due to the large difference in turbulent flow characteristics between these two species.

Noise continues to be debated among surgeons, as a high level of client satisfaction may be achieved despite high levels of abnormal respiratory noise remaining post-operatively. While noise is not related to performance, it may be related to the level of airway turbulence but this has yet to be established in the equine airway (Barnett et al., 2013a; Compostella et al., 2012).

6.5 General Conclusions

Equine surgeons are still in the early stages of their ability to manipulate the shape of the equine larynx. The use of various agents to bulk the vocal fold in dysphagic horses is a step toward the boundless possibilities that are available in the human respiratory discipline (Ludke et al, 2020). With more options comes greater complexity in the analysis of our interventional efficacy and greater potential for interactions between procedures that may have gone unrecognized previously. A greater ability to capture and analyze these changes is going to be critical to the forward movement of veterinary airway surgery.

Equine surgery is entering a new era. The generation that is currently reaching retirement entered the field when intuition and experience were the most important tools that a surgeon could wield, and these were absolutely critical to surgical practice. The upcoming generation is more familiar with advanced technologic techniques and evidence-based approaches and are therefore more rationalizing in their approach. This is demonstrated best in the advances in equine orthopedic surgery where once two orthogonal radiographs were sufficient, now three-dimensional imaging and customized drill guides are becoming standard of care. With these changes comes

increased diagnostic, prognostic and therapeutic capabilities but also a loss of some of the surgical art crafted by the initial founders. Some argue that this is leading to atrophy of the surgeon's ability to develop expertise-based intuition, while others argue that shift of the burden of actuarial knowledge frees up their cognitive power to better focus on more demanding tasks (Sutton et al., 2015). CFD is one of the tools that creates this potential by capturing the unique features of airflow in the individual patient. As the equine surgery community continues to try to improve postoperative success rates building upon what has already been done, CFD analysis provides an opportunity to critically analyze and characterize individual patient effects.

Ultimately, the continued advancement of equine surgery lies in the ability to address individual patient needs. This thesis demonstrates that advanced imaging and CFD can capture the unique features of individual equine airways and therefore drive the decision-making process in equine upper airway surgery.

REFERENCES

Adam NJ, De Cesare G, Schleiss AJ. 2019. Influence of geometrical parameters of chamfered or rounded orifices on head losses. J Hydraul Res. 57:263–271. Doi:10.1080/00221686.2018.1454518

Ahern BJ, Parente EJ. 2010. Mechanical evaluation of the equine laryngoplasty. Vet Surg. 39:661-666. Doi:10.1111/j.1532-950X.2010.00701.x

Ahern BJ, Van Eps EW, Boston RC, Franklin SH. 2017. In vitro comparison of 3 techniques of prosthesis attachment to the muscular process of the equine arytenoid cartilage. Vet Surg. 46:700-704. Doi:10.1111/vsu.12659

Ahern BJ, Lim Y, van Eps A, Franklin SH. 2018. In vitro evaluation of the effect of a prototype dynamic laryngoplasty system on arytenoid abduction. Vet Surg. 47:837-842. Doi:10.1111/vsu.12933.

Ahern BJ, Lukas E, Lam K, Wilke E, Bertin FR, Van Eps A, Franklin S. 2019. Evaluation of a prototype dynamic laryngoplasty system in vitro with an equine vacuum airflow system. Vet Surg. 48:173-179. Doi:10.1111/vsu.13137

Alipour F, Scherer R, Knowles J. 1996. Velocity distributions in glottal models. J Voice. 10:50-58. Doi:10.1016/S0892-1997(96)80018-X.

Allen GM, Shortall BP, Gemci T, Corcoran TE, Chigier NA. 2004. Computational simulations of airflow in an in vitro model of the pediatric upper airways. J Biomech Eng. 126:604-613. Doi:10.1115/1.1800554

Anderson BH, Kannegieter NJ, Goulden BE. 1997. Endoscopic observation on laryngeal symmetry and movements in young racing horses. NZ Vet J. 45:188-192. Doi:10.1080/00480169.1997.36024

Anzai Y, Weymuller EA, Yuch B, Maronian N, Jarvik JG. 2004. The impact of sinus computed tomography in treatment decisions for chronic sinusitis. Arch Otolaryng Head Neck Surg. 130:423-428. Doi:10.1001/archotol.130.4.423.

Art T, Serteyn D, Lekeux P. 1988. Effect of exercise on the partitioning of equine respiratory resistance. Eq Vet J. 20:268-273. Doi:10.1111/j.2042-3306.1988.tb01521.x.

Attenburrow DP. 1982. Time relationship between the respiratory cycle and limb cycle in the horse. Eq Vet J. 14:69-72. Doi:10.1111/j.2042-3306.1982.tb02340.x

Barakzai SF, Boden LA, Dixon PM. 2009a. Race performance after laryngoplasty and ventriculocordectomy in National Hunt racehorses. Vet Surg. 38:941-945. Doi:10.1111/j.1532-950X.2009.00600.x.

Barakzai SF, Boden LA, Dixon PM. 2009b. Postoperative race performance is not correlated with degree of surgical abduction after laryngoplasty in National Hunt Thoroughbred racehorses. Vet Surg. 38:934-940. Doi:10.1111/j.1532-950X.2009.00605.x.

Barakzai SF, Dixon PM, Hawkes CS, Cox A, Barnett TP. 2015. Upper esophageal incompetence in five horses after prosthetic laryngoplasty. Vet Surg. 44:150-155. Doi:10.1111/j.1532-950X.2014.12101.x

Barnes AJ, Slone DE, Lynch TM. 2004. Performance after partial arytenoidectomy without mucosal closure in 27 Thoroughbred racehorses. Vet Surg. 33:398–403. Doi:10.1111/j.1532-950X.2004.04058.x

Barnett TP, O'Leary JM, Parkin DH, Dixon PM, Barakzai SZ. 2013a. Long-term exercising video-endoscopic examination of the upper airway following laryngoplasty surgery: A prospective cross-sectional study of 41 horses. Eq Vet J. 45:593-597. Doi:10.1111/evj.12020

Barnett TP, O'Leary JM, Parkin TDH, Dixon PM, Barakzai SF. 2013b. Long-term maintenance of arytenoid cartilage abduction and stability during exercise after laryngoplasty in 33 horses. Vet Surg. 42:291-295. Doi:10.1111/j.1532-950X.2013.01109.x.

Barnett TP, O'Leary JM, Dixon PM, Barakzai SZ. 2014. Characterisation of palatal dysfunction after laryngoplasty. Eq Vet J. 46:60-63. Doi:10.1111/evj.12081.

Bayly WM, Slocombe RF. 1997. Airflow mechanics in models of equine obstructive airway disease under conditions simulating exercise. Res Vet Sci. 62:205-211. Doi:10.1016/S0034-5288(97)90191-0

Belknap JK, Derksen FJ, Nickels FA, Stick JA, Robinson NE. 1990. Failure of subtotal arytenoidectomy to improve upper airway flow mechanics in exercising Standardbreds with induced laryngeal hemiplegia. Am J Vet Res. 51:1481-1487. PMID:2396798

Bienert-Zeit A, Roetting A, Reichert C, Ohnesorge B. 2014. Laryngeal fistula formation after laryngoplasty in two Warmblood mares. Eq Vet Ed. 26:88-92. Doi:10/1111/eve.12066.

Bishofberger AS, Wereszka MM, Hadidane I, Perkins NR, Jeffcot LB, Dart AJ. 2013. Optimal tension, suture position, and number of prostheses required for maximal rima glottis area after laryngoplasty. Vet Surg. 42:280-285. Doi:10.1111/j.1532-950X.2013.01103.x

Bohanon TC, Beard WL, Robertson JT. 1990. Laryngeal hemiplegia in draft horses: A review of 27 cases. 19:456-459. Doi:10.1111/j.1532-950X.1990.tb01233.x.

Boswell JC, Schramme MC, Schumacher J, et al. 2000. An in vitro study of two surgical variables for suture placement through the muscular process of the arytenoid cartilage for prosthetic laryngoplasty in the horse. in Proceedings of the 9th Annual Scientific Meeting European College of Veterinary Surgeons, Berne, Switzerland, pp 168–170.

Boyko AR, Brooks SA, Behan-Braman A, Castelhano M, Corey E, Oliviera KC, Swinburne JE, Todhunter RJ, Zhang Z, Ainsworth DM, Robinson NE. 2014. Genomic analysis establishes correlation between growth and laryngeal neuropathy in Thoroughbreds. BMC Genom. 15:259. Doi:10.1186/1471-2164-15-259.

Brakenhoff JE, Holcombe SJ, Hauptman JG, Smith HK, Nickels FA, Caron JP. 2006. The prevalence of laryngeal disease in a large population of competition draft horses. Vet Surg. 35:579-583. Doi:10.1111/j.1532-950X.2006.00192.x

Brandenberger O, Rossignol F, Perkins JD, Lechartier A, Mespoulhes-Riviere C, Vitte A, Rossingol A, Ducharme N, Boening KJ. 2017. Ex vivo biomechanical stability of 5 cricoid-suture constructs for equine laryngoplasty. Vet Surg. 46:705-710. Doi:10.1111/vsu.12671.

Brandenberger O, Martens A, Robert C, Wiemer P, Pamela H, Vlaminck L, Barankova K, Haspeslagh M, Perkins JD, Ducharme N, Rossignol F. 2018. Anatomy of the vestibulum esophagi and surgical implications during prosthetic laryngoplasty in horses. Vet Surg. 47:942-950. Doi:10.1111/vsu.12944

Brinkshulte M, Bienert-Zeit A, Lupke M, Hellige M, Staszyk C, Ohnesorge B. 2013. Using semi-automated segmentation of computed tomography datasets for three-dimensional visualization and volume measurements of equine paranasal sinuses. Vet Radiol Ultrasound. 54:582-590. Doi:10.1111/vru.12080.

Brinkshulte M, Bienert-Ziet A, Lupke M, Hellige M, Ohnesorge B, Staszyk C. 2014. The sinonasal communication in the horse: examinations using computerized three-dimensional reformatted renderings of computed-tomography datasets. BMC Vet Res. 10:72. Doi:10.1186/1746-6148-10-72.

Brooks SA, Stick J, Braman A, Palermo K, Robinson NE, Ainsworth DM. 2018. Identification of loci affecting sexually dimorphic patterns for height and recurrent laryngeal neuropathy risk in American Belgian Draft Horses. Physiol Genomics. 50:1051-1058. Doi:10.1152/physiolgenomics.00068.2018.

Brown JA, Derksen FJ, Stick JA, Hartmann WM, Robinson NE. 2003. Ventriculocordectomy reduces respiratory noise in horses with laryngeal hemiplegia. Eq Vet J. 35:570-574. Doi:10.2746/042516403775467135

Brown JA, Hinchcliff KW, Jackson MA, Dredge AF, O'Callaghan RA, McCaffrey JR, Slocombe RF, Clarke AF. 2005a. Prevalence of pharyngeal and laryngeal abnormalities in Thoroughbreds racing in Australia, and their association with performance. Eq Vet J. 37:397-401. Doi:10.2746/042516405774480021.

Brown JA, Derksen FJ, Stick JA, Hartmann WM, Robinson NE. 2005b. Laser vocal cordectomy fails effectively reduce respiratory noise in horse with laryngeal hemiplegia. Vet Surg. 34:247-252. Doi:10.1111/j.1532-950X.2005.00037.x.

Budras KD, Sack WO, Rock S. 2008. Anatomy of the Horse. 5th Ed. Hanover, Germany: Schlütersche Verlagsgesellschaft mbH & Co. KG.

Bulter PJ, Woakes AJ, Anderson LS, Roberts CA, Marlin DJ. 1993. Stride length and respiratory tidal volume in exercising Thoroughbred horses. Resp Phys. 93:51-56. Doi:10.1016/0034-5687(93)90067-K.

Campoy L, Morris TB, Ducharme NG, Gleed RD, Martin-Flores M. 2018. Unilateral cervical plexus block for prosthetic laryngoplasty in the standing horse. Eq Vet J. Nov. 50:727-732. Doi:10.1111/evj.12956

Cahill JI, Goulden BE. 1986a. Equine laryngeal hemiplegia Part IV. muscle pathology. N Z Vet J. 34:186-190. Doi:10.1080/00480169.1986.35343

Cahill JI, Goulden BE. 1986b. Equine laryngeal hemiplegia Part V. Central nervous system pathology. N Z Vet J. 34:191-193. Doi:10.1080/00480169.1986.35344

Canada NC, McNally TP, Slone DE, Clark CK. 2017. Temporary right recurrent laryngeal neuropathy in a horse associated with a left prosthetic laryngoplasty procedure. Eq Vet Ed. 29:304-309. Doi:10.1111/eve.12441.

Carr EA, Spier SJ, Kortz GD, Hoffman, EP. 1996. Laryngeal and pharyngeal dysfunction in horses homozygous for hyperkalemic periodic paralysis. J Am Vet Med Assoc. 209:798-803. PMID: 8756883

Carpenter RS, McIlwraith CW, Hill AE. 2009. Racing performance in 72 racehorses treated with prosthetic laryngoplasty for laryngeal hemiplegia. J Eq Vet Sci. 29:584-589. Doi:10.1016/j.jevs.2009.05.012

Cercone M, Hokanson CM, Olsen E, Ducharme NG, Mitchell LM, Piercy RJ, Cheetham J. 2019. Asymmetric recurrent laryngeal nerve conduction velocities and dorsal cricoarytenoid muscle electromyelographic characteristics in clinically normal horses. Nature. 9:2713 Doi:10.1038/s41598-019-39189-z

Chalmers HJ, Yeager AE, Cheetham J, Ducharme N. 2012. Diagnostic sensitivity of subjective and quantitative laryngeal ultrasonography for recurrent laryngeal neuropathy in horses. Vet Radiol Ultrasound. 53:660–666. Doi:10.1111/j.1740-8261.2012.01974.x

Chalmers HJ, Viel L, Caswell JL, Ducharme N. 2015. Ultrasonographic detection of early atrophy of the intrinsic laryngeal muscles of horses. Am J Vet Res. 76:426-436. Doi:10.2460/ajvr.76.5.426.

Chan ASL, Lee RWW , Cistulli PA. 2007. Dental appliance treatment for obstructive sleep apnea. Chest. 132:693-699. Doi:10.1378/chest.06-2038.

Chang KK, Kim KB, McQuilling MW, Movahed R. 2018. Fluid structure interaction simulations of the upper airway in obstructive sleep apnea patients before and after maxillomandibular advancement surgery. Am J Orthod Dentofac Orthopod. 153:895-904. Doi:10.1016/j.ajodo.2017.08.027

Cheetham J, Radcliffe CR, Ducharme NG, Sanders I, Mu L, Hermanson JW. 2008a. Neuroanatomy of the equine dorsal cricoarytenoid muscle: Surgical implications. Eq Vet J. 40:70-75. Doi:10.2746/042516407X240465.

Cheetham J, Witte TH, Rawlinson JJ, Soderholm LV, Mohammed HO, Ducharme NG. 2008b. Intra-articular stabilisation of the equine cricoarytenoid joint. Eq Vet J. 40:584-588. Doi:0.2746/042516408X313643.

Cheetham J, Witte TH, Soderholm LV, Hermanson JW, Ducharme NG. 2008c. In vitro model for testing novel implants for equine laryngoplasty. Vet Surg. 37:588-593. Doi:10.1111/j.1532-950X.2008.00424.x.

Cheetham J, Pigott JH, Hermanson JW, Campoy L, Soderholm LV, Thorson LM, Ducharme NG. 2009. Role of the hypoglossal nerve in equine nasopharyngeal stability. J Appl Physiol. 107:471-477. Doi:10.1152/japplphysiol.91177.2008

Cheetham J, Regner A, Jarvis JC, Priest D, Sanders I, Soderholm LV, Mitchell LM, Ducharme NG. 2011. Functional electrical stimulation of intrinsic laryngeal muscles under varying loads in exercising horses. PLoS One. 6:e24258. Doi:10.1371/journal.pone.0024258

Cheetham J. 2019. Overview of upper airway function. In: Auer JA, Stick JA, Kummerle JM, Prange T. 2019. eds. Equine Surgery. 5th ed. St Louis: Elsevier Saunders; 678-682. Doi:10.1016/B978-0-323-48420-6.00046-6

Christley RM, Hodgson DR, Evans DL, Rose RJ. 1997. Cardiorespiratory responses to exercise in horses with different grades of idiopathic laryngeal hemiplegia. Eq Vet J. 29:6-10. Doi:10.1111/j.2042-3306.1997.tb01629.x

Compostella F, Tremaine WH, Franklin SH. 2012. Retrospective study investigating causes of abnormal respiratory noise in horses following prosthetic laryngoplasty. Equine Vet J Suppl. 44:27-30. Doi:10.1111/j.2042-3306.2012.00612.x

Cook WR. 1988. Diagnosis and grading of hereditary recurrent laryngeal neuropathy in the horse. J Eq Vet Sci. 8:432-455. Doi:10.1016/S0737-0806(88)80093-5

Cramp P, Derksen FJ, Stick JA, Fiejter-Rupp H, Elvin NG, Hauptman J, Robinson NE. 2009. Effect of magnitude and direction of force on laryngeal abduction: Implications for the nerve-muscle pedicle technique. Eq Vet J. 41:328-333. Doi:10.2746/042516409X388208.

Craven BA, Neuberger T, Paterson EG, Webb AG, Josephson EM, Morrison EE, Settles GS. 2007. Reconstruction and morphometric analysis of the nasal airway of the dog (Canis familiaris) and implications regarding olfactory airflow. Anat Rec. 290:1325-1340. Doi:10.1002/ar.20592.

Craven BA, Paterson EG, Settles GS, Lawson MJ. 2009. Development and verification of a high-fidelity computational fluid dynamics model of canine nasal airflow. J Biomech Eng. 131:091002. Doi:10.1115/1.3148202

Craven BA, Paterson EG, Settles GS. 2010. The fluid dynamics of canine olfaction: unique nasal airflow patterns as an explanation of macrosmia. J R Soc Interface. 7:933-943. Doi:10.1098/rsif.2009.0490.

Dahlberg JA, Valdes-martinez A, Boston RC, Parente EJ. 2011. Analysis of conformational variations of the cricoid cartilages in Thoroughbred horses using computed tomography. Eq Vet J. 43:229-234. Doi:10.1111/j.2042-3306.2010.00070.x

Davenport CLM, Tulleners EP, Parente EJ. 2001. The effect of recurrent laryngeal neurectomy in conjunction with laryngoplasty and unilateral ventriculocordectomy in Thoroughbred racehorses. Vet Surg. 30:417-421. Doi:10.1053/jvet.2001.25865.

Davidson EJ, Martin BB, Rieger RH, Parente EJ. 2010. Exercising videoendoscopic evaluation of 45 horses with respiratory noise and/or poor performance after laryngoplasty. Vet Surg. 39:942-948. Doi:10.1111/j.1532-950X.2010.00746

Davidson EJ, Parente EJ. 2011. Exercising videoendoscopic evaluation of 7 horses with abnormal respiratory noise and poor performance following partial arytenoidectomy. Equine Vet Educ. 23:626–629. Doi:10.1111/j.2042-3292.2011.00229.x

De Backer JW, Vanderveken OM, Vos WG, Devolder A, Verhulst SL, Verbraecken JA, et al. 2007. Functional imaging using computational fluid dynamics to predict treatment success of mandibular advancement devices in sleep-disordered breathing. J Biomech. 40:3708-3714. Doi:10.1016/j.jbiomech.2007.06.022.

De Backer JW, Vos WG, Verhulst SL, De Backer W. 2008. Novel imaging techniques using computer methods for the evaluation of the upper airway in patients with sleep-disordered breathing: A comprehensive review. Sleep Med. 12:437-447. Doi:10.1016/j.smrv.2008.07.009.

De Backer JW, Vos WG, Vinchurkar SC, Claes R, Drollman A, Wulfrank D, Parizel PM, Germonpre P, De Backer W. 2010. Validation of computational fluid dynamics in CT-based airway models with SPECT/CT. Radiology. 257:854-862. Doi:10.1148/radiol.10100322/-/DC1.

de Luzan Cf, Oren L, Maddox A, Gutmark E, Khosla SM. 2020. Volume velocity in a canine larynx model using time-resolved tomographic particle image velocimetry. Exp Fluid. 61:63. Doi:10.1007/s00348-020-2896-x

Derksen FJ, Stick JA, Scott EA, Robinson NE, Slocombe RF. 1986. Effect of laryngeal hemiplegia and laryngoplasty on airway flow mechanics in exercising horses. Am J Vet Res. 47:16–20. PMID:3946898

Dinis PB, Haider H. 2002. Septoplasty: Long-term evaluation and results. Am J Otolaryng. 23:85-90. Doi: 10.1053/ajot.2002.30987.

Dixon PM, Railton DI, McGorum BC. 1993. Temporary bilateral laryngeal paralysis in a horse associated with general anesthesia and post anesthetic myositis. Vet Rec. 132:29-32. Doi:10.1136/VR.132.2.29

Dixon PM, McGorum, Railton DI, Hawe C, Tremaine WH, Pickles K, McCann J. 2001. Laryngeal paralysis: a study of 375 cases in a mixed-breed population of horses. Eq Vet J. 33:452-458. Doi:10.2746/042516401776254790

Dixon PM, McGorum BC, Railton DI, Hawe C, Tremaine WH, Pickles K, McCann J. 2002.Clinical and endoscopic evidence of progression in 152 cases of equine recurrent laryngeal neuropathy (RLN). Eq Vet J. 34:29-34. Doi:10.2746/042516402776181169.

Dixon PM, McGorum BC, Railton DI, Hawe C, Tremaine WH, Dacre K, McCann J. 2003a. Long-term survey of laryngoplasty and ventriculocordectomy in an older, mixed-breed population of 200 horses. Part 1: Maintenance of surgical arytenoid abduction and complications of surgery. Eq Vet J. 35:389-396. Doi:10.2746/042516403776014172.

Dixon PM, McGorum BC, Railton DI, Hawe C, Tremaine WH, Dacre K, McCann J. 2003b. Long-term survey of laryngoplasty and ventriculocordectomy in an older, mixed-breed population of 200 horses. Part 2: Owner's assessment of the value of surgery. Eq Vet J. 35:397-401. Doi:10.2746/042516403776014217.

Dixon PM, Robinson NE, Wade JF. 2004. Havemeyer workshop on equine recurrent laryngeal neuropathy. In: Proceedings; 2004:96.

Draper ACE, Piercy RJ. 2018. Pathological classification of equine recurrent laryngeal neuropathy. J Vet Intern Med. 32:1397-1409. Doi:10.1111/jvim.15142

Ducharme NG, Horney FD, Partlow GD, Hulland TJ. 1989. Attempts to restore abduction of the paralyzed equine arytenoid cartilage I. Nerve-muscle pedicle transplants. Can J Vet Res. 53:202-209. PMID:2713785.

Ducharme NG, Hackett RP, Ainsworth DM, Erb HN, Shannon KJ. 1994. Repeatability and normal values for measurement of pharyngeal and tracheal pressures in exercising horses. Am J Vet Res. 55:368-374. PMID: 8192260

Ducharme NG, Cheetham J, Sanders I, Hermanson JW, Hackett RP, Soderholm LV, Mitchell LM. 2010. Considerations for pacing of the cricoarytenoideus dorsalis muscle by neuroprosthesis in horses. Eq Vet J. 42:534-540. Doi:10.1111/j.2042.-3306.2010.00115.x

Ducharme NG, Rossignol F. Larynx. In: Auer JA, Stick JA, Kummerle JM, Prange T. 2019. eds. Equine Surgery. 5th ed. St Louis: Elsevier Saunders; 734-770. Doi:10.1016/B978-0-323-48420-6.00046-6

Duncan ID, Griffiths IR, McQueen A, Baker GO. 1974. The pathology of equine laryngeal hemiplegia. Acta neuropath. 27:337-348. Doi:10.1007/BF00690698

Duncan ID, Brook D. 1985. Bilateral laryngeal paralysis in the horse. Eq Vet J. 17:228-233. Doi:10.111/j.2042-3306.1985.tb02479.x

Duncan ID, Reifenrath P, Jackson KF, Clayton M. 1991. Preferential denervation of the adductor muscles of the equine larynx II: Nerve pathology. Eq Vet J. 23: 99-103. Doi:10.1111/j.2042-3306.1991.tb02729.x

Duncan ID.1992. Determination of the early age of onset of equine recurrent laryngeal neuropathy. 2. Nerve pathology. Acta Neuropathol 84:316-321. Doi:10.1007/BF00227825

Dyce KM, Sack WO, Wensing CJG. 2010. Textbook of Veterinary Anatomy, 4th ed. St. Louis, MO: Saunders Elsevier; 2010.

Elad D, Liebenthal R, Wenig BL, Einav S. 1993. Analysis of air flow patterns in the human nose. J Med Biol Eng Comput. 31:585-592. Doi:10.1007/bf02441806

Elliot S, Cheetham J. 2019. Meta-analysis evaluating resting laryngeal endoscopy as a diagnostic tool for recurrent laryngeal neuropathy in the equine athlete. Eq Vet J. 51:167-172. Doi:10.1111/evj.12987

Erath BD, Plesniak MD. 2006a. An investigation of jet trajectory in flow through scaled vocal fold models with asymmetric glottal passages. Acoust Soc Am. 41:735-748. Doi:10.1007/s00348-006-0196-8.

Erath BD, Plesniak MW. 2006b. The occurrence of the Coanda effect in pulsatile flow through static models of the human vocal folds. Acoust Soc Am. 120:1000-1011. Doi:10.1121/1.2213522.

Evans DL, Rose RJ. 1988a. Cardiovascular and respiratory responses in Thoroughbred horses during treadmill exercise. J Exp Biol. 134:397-408.

Evans DL, Rose RJ. 1988b. Cardiovascular and respiratory responses to submaximal exercise training in the thoroughbred horse. Pflugers Arch. 411:316-321.

Faizal WM, Ghazali NNN, Khor CY, Badruddin IA, Zainon MZ, Yazid AA, Ibrahim NB, Razi RM. 2020. Computational fluid dynamics modelling of human upper airway: A review. Comp Methods Programs Biomed. 196 (105627): 1-22. Doi:10.1016/j.cmpb.2020.105627

Faizal WM, Ghazali NN, Khor CY, Zainon MZ, Badruddin IA, Kamangar S, Ibrahim NB, Razi RM. 2021a. Computational analysis of airflow in upper airway under light and heavy breathing

conditions for a realistic patient having obstructive sleep apnea. Comp Modeling Eng Sci. 128:583-604. Doi:10.32604/cmes.2021.015549.

Faizal WM, Ghazali NN, Khor CY, Zainon MZ, Ibrahim NB, Razif RM. 2022. Turbulent kinetic energy of flow during inhale and exhale to characterize the severity of obstructive sleep apnea patient. [Preprint (Version 1)]. 2021b. [Posted 2021 December 16; cited 2022 Jan 26] available from Research Square Doi:10.21203/rs.3.rs-1102041/v1

Fernandez-Parra R, Pey P, Zilberstein L, Malve, M. 2019. Use of computational fluid dynamics to compare upper airway pressures and airflow resistance in brachycephalic, mesocephalic, and dolichocephalic dogs. Vet J. 253:105392. Doi:10.1016/j.tvjl.2019.105392

Fitzharris LE, Franklin SH, Allen KJ. 2015. The prevalence of abnormal breathing patterns during exercise and associations with dynamic upper respiratory tract obstructions. Eq Vet J. 47:553-556. Doi:10.1111/evj.12325

Fossa M, Guglielmini G. 2002. Pressure drop and void fraction profiles during horizontal flow through thin and thick orifices. Exp Therm Fluid Sci. 26:513-523. Doi:10.1016/S0894-1777(02)00156-5

Fulton IC, Derksen FJ, Stick JA, Robinson NE, Walshaw R. 1991. Treatment of left laryngeal hemiplegia in standardbreds, using a nerve muscle pedicle graft. Am J Vet Res. 52:1461-1467. PMID:1952334

Fulton IC, Anderson BA, Stick JA, Robertson JT. 2012. Larynx. In: Auer JA, Stick JA, eds. Equine surgery. 4th ed. St Louis: Elsevier Saunders, 2012:592–623. Doi:10.1016/B978-1-4377-0867-7.00045-4

Geng B, Pham N, Xue Q, Zheng X. 2020. A three-dimensional vocal fold posturing model based on muscle mechanics and magnetic resonance imaging of a canine larynx. J Acoust Soc Am. 147:2597–2608. Doi:10.1121/10.0001093

Genton M, Robert C, Jerbi H, Huet H, Cordonnier N, Vitte-Rossignol A, Perkins JD, Rossignol F. 2021. Thyrohyoideus muscle innervation in the horse. Vet Surg. 50:53-61. Doi:10.1111/vsu.13536.

Gerber V, Tessier C, Marti E. 2015. Genetics of upper and lower airway diseases in the horse. Eq Vet J. 47:390-397. Doi:10.1111/evj.12289.

Girardin M, Bilgrin E, Arbour P. 1983. Experimental study of velocity fields in a human nasal fossa by laser anemometry. Ann Oto Rhinol Laryngol. 92:231-236. Doi:10.1177/000348948309200304.

Goulden BE, Anderson LG. 1982. Equine laryngeal hemiplegia. Part III. Treatment by laryngoplasty. N Z Vet J. 30:1-5. Doi:10.1080/00480169.1982.34857

Gray SM, Gutierrez-Nibeyro SD, Secor EJ. 2019. Partial arytenoidectomy in 14 standing horses (2013-2017). Vet Surg. 48:473-480. Doi: 10.1111/vsu.13192.

Gray SM, Gutierrez-Nibeyro SD, Couetil LL, Horn GP, Kesler RM, McCoy AM, Stewart MC, Schaeffer DJ. 2021. Evaluation of the airway mechanics of modified toggle laryngoplasty constructs using a vacuum chamber airflow model. Vet Surg. 50:1409-1417. Doi:10.1111/vsu.13690.

Guillemot A, Rouvre G, Autefage A, Etchepareborde S. 2015. Changes in rima glottidis area and lack of laryngeal epiglottic-glottic seal after unilateral cricoarytenoid lateralization ex vivo. Vet Surg. 44:236-241. Doi:10.1111/j.1532-950X.2014.12300.x.

Guyton AC, Hall JF. Textbook of Medical Physiology. Saunders: Philadelphia, PA. 1996.

Hahn, CN, Mayhew IG. 2000. Examination of the laryngeal musculature and recurrent laryngeal nerves of zebra (Equus burchelli) for evidence of idiopathic laryngeal hemiplegia. N Z Vet J. 48:20-23. Doi:10.1080/00480169.2000.36152.

Hahn I, Scherer PW, Mozell MM. 1993. Velocity profiles measured for airflow through a large-scale model of the human nasal cavity. J Appl Physiol. 75:2273-2287. Doi:10.1152/jappl.1993.75.5.2273.

Hardcastle MR, Pauwels FET, Collet MG. 2012. Clinicopathologic observations on laryngoplasty failure in a horse. Vet Surg. 41:49-653. Doi:10.1111/j.1532-950X.2012.00975.x.

Hawkins JF, Tulleners EP, Ross MW, Evans LH, Raker CW. 1997. Laryngoplasty with or without ventriculectomy for treatment of left laryngeal hemiplegia in 230 racehorses. Vet Surg. 26:484-491. Doi:10.1111/j.1532-950x.1997.tb00521.x.

Hawkins JP, Couetil L, Miller MA. 2014. Maintenance of arytenoid abduction following carbon dioxide laser debridement of the articular cartilage and joint capsule of the cricoarytenoid joint combined with prosthetic laryngoplasty in horses: An in vivo and in vitro study. Eq Vet J. 199:275-280. Doi:10.1016/j.tvjl.2013.11.027.

Hay WP, Tulleners EP, Ducharme NG. 1993. Partial arytenoidectomy in the horse using an extralaryngeal approach. Vet Surg. 22:50-56. Doi:10.1111/j.1532-950X.1993.tb00368.x

Henderson CE, Sullins KE, Brown JA. 2007. Transendoscopic, laser-assisted ventriculocordectomy for treatment of left laryngeal hemiplegia in horses: 22 cases (1999-2005). J Am Vet Med Assoc. 231:1868-1872. Doi:10.2460/javma.231.12.1868.

Hostnik ET, Scanson BA, Zielinski R, Ghadiali SN. 2017. Quantification of nasal airflow resistance in English bulldogs using computed tomography and computational fluid dynamics. Vet Rad Ultrasound. 58:542-551. Doi:10.1111/vru.12531

Huang Y, White DP, Malhotra A. 2005a. The impact of anatomic manipulations on pharyngeal collapse: Results from a computational model of the normal human upper airway. Chest. 128:1324-1330. Doi:010.1378/chest.128.3.1324.

Huang Y, Malhotra A, White DP. 2005b. Computational simulation of human upper airway collapse during a pressure-/state-dependent model of genioglossal muscle contraction under laminar flow conditions. J Appl Phys. 99:1138-1148. Doi:0.1152/japplphysiol.00668.2004.8750-7587/05

Huang Y, White DP, Malhotra A. 2007. Use of computational modeling to predict responses to upper airway surgery in obstructive sleep apnea. Laryngoscope. 117:648-653. Doi:10.1097/MLG.0b013e318030ca55

International Organization for Standardization. Measurement of fluid flow by means of pressure differential devices inserted in circular cross-section conduits running full—part 1: general

principles and requirements (ISO 5167). Accessed Mar 17, 2020. https://www.iso.org/standard/28064.html

Ito Y, Cheng GC, Shih AM, Koomulil RP, Soni BK, Sittitavornwong S, Waite PD. 2011. Patient-specific geometry modeling and mesh generation for Obstructive Sleep Apnea Syndrome cases by maxillomandibular advancement. Math Comput Simul. 81:1876-1891. Doi:10.1016/j.matcom.2011.02.006

Jansson N, Ducharme NG, Hackett RP, Mohammed HO. 2000. An in vitro comparison of cordopexy, cordopexy and laryngoplasty, and laryngoplasty for treatment of equine laryngeal hemiplegia. Vet Surg. 29:326-34. Doi:10.1053/jvet.2000.5599.

Jeong SJ, Kim WS, Sung SJ. 2007. Numerical investigation on the flow characteristics and aerodynamic force of the upper airway of patient with obstructive sleep apnea using computational fluid dynamics. Med Eng Phys. 29:637-651. Doi:10.1016/j.medengphy.2006.08.017.

Johnson RA. 2005. Curve fitting. In: Johnson RA, ed. Miller & Freund's probability and statistics for engineers. 7th ed. Upper Saddle River, NJ: Pearson Prentice Hall Inc, 337–357.

Johnstone A, Uddin M, Pollard A, Heenan A, Finlay WH. 2004. The flow inside an idealized form of the human extra-thoracic airway. Exp Fluids. 37:673-689. Doi:10.1007/S00348-004-0857-4.

Kelly JR, Carmalt J, Hendrick S, Wilson DG, Shoemaker R. 2008. Biomechanical comparison of six suture configurations using a large diameter polyester prosthesis in the muscular process of the equine arytenoid cartilage. Vet Surg. 37:580-587. Doi:10.1111/j.1532-950X.2008.00423.X.

Kenny M, Cercone M, Rawlinson JJ, et al. 2017. Transesophageal ultrasound and computer tomographic assessment of the equine cricoarytenoideus dorsalis muscle: Relationship between muscle geometry and exercising laryngeal function. 49:395-400. Doi:10.1111/evj.12561

Khoa ND, Phuong NL, Tani K, Inthavong K, Ito K. 2021. Computational fluid dynamics comparison of impaired breathing function in French bulldogs with nostril stenosis and an examination of the efficacy of rhinoplasty. Conput Bio Med. 134: 104398. Doi:10.1016/j.compbiomed.2021.104398

Kidd JA, Slone DE. 2002. Treatment of laryngeal hemiplegia in horses by prosthetic laryngoplasty, ventriculectomy and vocal cordectomy. Vet Rec. 150:481-484. Doi:10.1136/vr.150.15.481

Kim SK, Na Y, Kim J, Chung SK. 2013. Patient specific CFD models of nasal airflow: Overview of methods and challenges. J Biomech. 46:299-306. Doi:10.1016/j.jbiomech.2012.11.022.

Kimbell JS, Segal RA, Asgharian A, Wong BA, Schroeter JD, Southall JP, Dickens CJ, Brace G, Miller FJ. 2007. Characterization of deposition from nasal spray devices using a computational fluid dynamics model of the human nasal passage. J Aerosol Med. 20:59-74. Doi:10.1089/jam.2006.0531

Kimbell JS. 2009. Application of computational fluid dynamics modeling in the nasal passages for risk assessment and drug delivery. Proc 4th World Eq Airway Symp. Bern,Switzerland. Aug 5-7. Abstractbook 154-156.

King DS, Tulleners E, Martin BB, Parente EJ, Boston R. 2001. Clinical experience with axial deviation of the aryepiglottic folds in 52 racehorses. Vet Surg. 10:151-160. Doi:10.1053/jevt.2001.21389

Kraus BM, Parente EJ, Tulleners EP. 2003. Laryngoplasty with ventriculetomy or ventriculocoredectomy in 104 draft horses (1992-2000). Vet Surg. 32:530-538. Doi:10.1111/j.1532-950x.2003.00503.x

Lane JG. 2004. 5-Point grading system of laryngeal function in horses during quiet breathing. In: Dixon P, Robinson E, Wade JF, editors. Proceedings of a Workshop on Equine Recurrent Laryngeal Neuropathy; 2004 Sept 7-1; Stratford-upon-Avon, UK. Newmarket, Suffolk; 2004 p.24-25.

Lawson MJ, Craven BA, Paterson EG, Settles GS. 2012. A computational study of odorant transport in the canine nasal cavity: Implications for olfaction. Chem Senses. 37:553-566. Doi:10.1093/chemse/bjs039.

Li C, Jiang J, Dong H, Zhao K. 2017. Computational modeling and validation of human nasal airflow under various breathing conditions. J Biomech. 64:59-68. Doi:10.1016/j.jbiomech.2017.08.031.

Lindegaard C, Karlsson L, Ekstrom CT, Feldborg J. 2016. Primary closure of equine laryngotomy incisions: Healing characteristics and complications of 180 cases. Equine Vet Educ. 38:512-519. Doi:10.1111/eve.12570.

Loew FM. 1973. Thiamine and equine laryngeal hemiplegia. Vet Rec. 92:372–373.

Longest PW, Vinchurkar S. 2007. Effects of mesh style and grid convergence on particle deposition in bifurcating airway models with comparisons to experimental data. Med Eng Phys. 29:350-366. Doi:10.1016/j.medengphy.2006.05.012.

Ludke LK, Cheetham J, Mohammed HO, Ducharme NG. 2020. Management of postoperative dysphagia after prosthetic laryngoplasty or arytenoidectomy. Vet Surg. 49:529-539. Doi:10.1111/vsu.13389

Lumsden JM, Derksen FJ, Stick JA, Robinson NE, Nickels FA. 1994. Evaluation of partial arytenoidectomy as a treatment for equine laryngeal hemiplegia. Eq Vet J. 26:125-129. Doi:10.1111/j.2042-3306.1994.tb04350.x.

Luo H, Sin S, McDonough JM, Isasi CR, Arens R, Wootton DM. 2014. Computational fluid dynamic endpoints for assessment of adenotonsillectomy outcome in obese children with obstructive sleep apnea syndrome. J Biomech. 47: 2498-2503. Doi:10.1016/j.jbiomech.2014.03.023.

Lynch NP, Jones SA, Bazley-White LG, Wilson ZF, Raffetto J. Pfau T, Cheetham J, Perkins JD. 2020. Ex vivo modeling of the airflow dynamics and two- and three-dimensional biomechanical effects of suture placements for prosthetic laryngoplasty in horses. Am J Vet Res. 81:665-672. Doi:10.2460/ajvr.81.8.665.

Malhotra A, Huang Y, Fogel RB, Pillar G, Edwards JK, Kikinis R, Loring SH, White DP. 2002. The male predisposition to pharyngeal collapse: importance of airway length. Am J Respir Crit Care Med. 166:1388-1395. Doi:10.1164/rccm.2112072

Marks D, Mackay-Smith MP, Cushing LS, Leslie JA. 1970. Use of a prosthetic device for surgical correction of laryngeal hemiplegia in horses. J Am Vet Med Assoc. 157:157-163. PMID:5463883

Markwell HJ, Mueller POE. 2016. Ex vivo mechanical evaluation of a sternal ZipFix® implant for prosthetic laryngoplasty in horses. Vet Surg. 45:450-455. Doi:10.1111/vsu.12466

Martonen TB, Quan L, Zhang Z, Musante CJ. 2002. Flow simulation in the human upper respiratory tract. Cell Biochem Biophys. 37:27-36. Doi:10.1385/CBB:37:1:27.

Martin BB, Reef VB, Parente EJ, Sage AD. 2000. Causes of poor performance of horses during training, racing or showing: 348 cases (1992-1996). J Am Vet Med Assoc. 216:554-558. Doi:10.2460/javma.2000.216.554.

Massie S. 2015. Tackling the challenges of an equine metabolic mask: validating a computational approach to simulate airflow using 3D printed models. (Unpublished Master's Thesis, University of Calgary, Calgary, Alberta). Doi:10.11575/PRISM/27968

McClellan NR, Santschi EM, Hurcombe SDA, Litsky AS. 2014. An Ex Vivo model to evaluate the effect of cyclical adductory forces on maintenance of arytenoid abduction after prosthetic laryngoplasty performed with and without mechanical arytenoid abduction. Vet Surg. 43:598-605. Doi:10.1111/j.1532-950X.2014.12178.x

McGorum BC, Murphy D, Love S, Milne EM. 1999. Clinicopathological features of equine primary heptic disease: a review of 50 cases. Vet Rec. 145:134-139. Doi:10.1136/vr.145.5.134

Mylavarapu G, Murugappan S, Mihaescu M, Kalra M, Khosla S, Gutmark E. 2009. Validation of computational fluid dynamics methodology used for human upper airflow flow simulations. J Biomech. 42:1553-1559. Doi:10.1016/j.jbiomech.2009.03.035.

Mylavarapu G, Mihaescu M, Fuchs L, Papatziamos G, Gutmark E. 2013. Planning human upper airway surgery using computational fluid dynamics. J Biomech. 46:1979-1986. Doi:10.1016/j.jbiomech.2013.06.016

Neilan GJ, Rehder RS, Ducharme NG, Hackett RP. 1992. Measurement of tracheal static pressure in exercising horses. Vet Surg. 21:423-428. Doi:10.1111/j.1532-950x.1992.tb00075.x

Nerukar NK, Marwah R, Mahajan S. 2012. Role of CT scan in decision making prior to approximation laryngoplasty. Indian J Otolaryngol. 64:201-204 Doi:10.1007/s12070-011-0421-5

Parente EJ, Birks EK, Habecker P. 2011. A modified laryngoplasty approach promoting ankylosis of the cricoarytenoid joint. Vet Surg. 40:204-210. Doi:10.1111/j.1532-950X.2010.0073.x

Passman SN, Cheetham J, Bonassar LJ, Ducharme NG, Rawlinson JJ. 2011. Biomechanical characterization of equine laryngeal cartilage. Eq Vet J. 43:592-598. Doi:10.1111/j.2042-3306.2010.00315.x

Pekarkova M, Kirhcer PR, Konar M, Lang J, Tessier C. 2009. Magnetic resonance imaging anatomy of the normal equine larynx and pharynx. Vet Radiol Ultrasound. 50:392–397. Doi:10.1111/j.1740-8261.2009.01555.x

Perkins JD, Raffeto J, Thompson C, Weller R. 2010. Three-dimensional biomechanics of simulated laryngeal abduction in horses. Am J Vet Res. 71:1003-1010. Doi:10.2460/ajvr.71.9.1003.

Perkins JD, Meighan H, Windley Z, Troester S, Piercy R, Schumacher J. 2011. In vitro effect of ventriculocordectomy before laryngoplasty on abduction of the equine arytenoid cartilage. Vet Surg. 40:305-310. Doi:10.1111/j.1532-950X.2011.00796.x

Pigott J. 2021. A new approach to chondritis-standing medial debridement. In: Southwood LL, Bleedorn J, Monnet E, Morello SL, Thieman K, editors. ACVS Surgery Summit 2021 Proceedings (virtual). Problem solving for upper airway conditions session. Accessed online Mar 8 2022.

Pirnar J, Sirok B, Bombac A. 2017. Effect of airway surface liquid on the forces on the pharyngeal wall: Experimental fluid-structure interaction study. J Biomech. 63:117-124. Doi:10.1016/j.jbiomech.2017.08.014.

Plesniak MW, Peterson SD. 2004. Wall shear stress measurements for conventional applications and biomedical flows (invited). Proceedings of 24th AIAA Aerodynamic Measurement

Technology and Ground Testing Conference, Portland, Oregon. 28 June-1 July. AIAA-2004-2301. Doi:10.2514/6.2004-2301.

Proetz AW. 1951. Air currents in the upper respiratory tract and their clinical importance. Am Oto Rhinol Laryngol. 60:439-467. Doi:10.1177/0000348945106000216

Radcliffe CH, Woodie JB, Hackett RP, Ainsworth DM, Erb HN, Mitchell LM, Soderholm LV, Ducharme NG. 2006. A comparison of laryngoplasty and modified partial arytenoidectomy as treatments for laryngeal hemiplegia in exercising horses. Vet Surg. 35:643-652. Doi:10.1111/j.1532-950X.2006.00202.x.

Rakesh V, Ducharme NG, Datta AK, Cheetham J, Pease AP. 2008a. Development of equine upper airway fluid mechanics model for Thoroughbred racehorses. Eq Vet J. 40: 272-279. Doi:10.2746/042516408X281216

Rakesh V, Datta AK, Ducharme NG, Pease AP. 2008b. Simulation of turbulent airflow using a CT based upper airway model of a racehorse. J Biomech Eng. 130:031011-1-13. Doi:10.1115/1.2913338

Rakesh V, Ducharme NG, Cheetham J, Datta AK, Pease AP. 2008c. Implications of different degrees of arytenoid cartilage abduction on equine upper airway characteristics. Eq Vet J. 40:629-635. Doi:10.2746/042516408X330329.

Rakestraw PC, Hackett RP, Ducharme NG, Nielan GJ. 1991. Arytenoid cartilage movement in resting and exercising horses. Vet Surg. 20:122-127. Doi:10.1111/j.1532-950X.1991.tb00319.x

Reesink HL, Hermanson JW, Cheetham J, Mu L, Mitchell LM, Soderholm LV, Ducharme NG. 2013. Anatomic and neuromuscular characteristics of the equine cricothyroid muscle. Eq Vet J. 45:630-636. Doi:10.1111/evj.12023

Renotte C, Bouffioux V, Wilquem, F. 2000. Numerical 3D analysis of oscillatory flow in the time-varying laryngeal channel. J Biomech. 33:1637-1644. Doi:10.1016/S0021-9290(00)00134-2.

Rhee HS, Steel CM, Derksen FJ, Robinson NE, Hoh JFY. 2009a. Immunohistochemical analysis of laryngeal muscles in normal horses and horses with subclinical recurrent laryngeal neuropathy. J Histochem Cytochem. 57:787-800. Doi:10.1369/jhc.2009.953844.

Rhee JS. 2009b. Measuring outcomes in nasal surgery: Realities and possibilities. Arch Facial Plas Surg. 11:416-419. Doi:10.1001.archfacil.2009.86.

Rhee JS, Pawar SS, Garcia GJM, Kimbell JS. 2011. Toward personalized nasal surgery using computational fluid dynamics. Arch Facial Plast Surg. 13: 302-310. Doi:10.1001/archfacial.2011.18

Rooney JR, Delaney FM. 1970. An hypothesis on the causation of laryngeal hemiplegia in horses. Equine Vet J. 2:35–37. Doi:10.1111/j.2042-3306.1970.tb04149.x.

Rossignol FE, Perrin R, Debrosse F, Elie C. 2006. In vitro comparison of two techniques for suture prosthesis placement in the muscular process of the equine arytenoid cartilage. Vet Surg. 35:49-54. Doi:10.1111/j.1532-950X.2005.00111.x

Rossignol F, Vitte A, Boening J, Maher M, Lechartier A, Brandenberger O, Martin-Flores M, Lang H, Walker W, Ducharme NG. 2015. Laryngoplasty in standing horses. Vet Surg. 44:341-347. Doi:10.1111/vsu.12307

Rossignol F, Brandenberger O, Perkins JD, Marie JP, Mespoulhes-Riviere MC, Ducharme NG. 2018. Modified first or second cervical nerve transplantation technique for the treatment of recurrent laryngeal neuropathy in horses. Eq Vet J. 50:457-464. Doi:10.1111/evj.12788.

Russell AP, Slone DE. 1994. Performance analysis after prosthetic laryngoplasty and bilateral ventriculectomy for laryngeal hemiplegia in horses. J Am Vet Med Assoc. 204:1235-1241. PMID: 8014096.

Sadeghi H, Dollinger M, Kaltenbacher M, Kniesburges S. 2019. Aerodynamic impact of the ventricular folds in computational larynx models. J Acoust Soc Am. 145:2376-2387. Doi:10.1121/1.5098775.

Satoh M, Higuchi T, Inoue, Miyakoshi D, Kajihara A, Gotoh T, Schimizu Y. 2020. External transcutaneous ultrasound technique in the equine cricoarytenoideus dorsalis muscle:

assessment of muscle size and echogenicity with resting endoscopy. Eq Vet J. 52:550-508. Doi:10.1111/evj.13209

Scherer RC, Shinwari D, DeWitt KJ, Zhang C, Kucinschi BR, Afjeh AA. 2001. Intraglottal pressure profiles for a symmetric and oblique glottis with a divergence angle of 10 degrees. J Acoust Soc Am. 109:1616-1630. Doi:10.1121/1.1333420.

Schumacher J, Wilson AM, Pardoe C, Easter JL. 2000. In vitro evaluation of a novel prosthesis for laryngoplasty of horses with recurrent laryngeal neuropathy. Eq Vet J. 32:43-46. Doi:10.2746/042516400777611991

Schroeter JD, Kimbell JS, Asgharian B. 2006a. Analysis of particle deposition in the turbinate and olfactory regions using a human nasal computational fluid dynamics model. J Aerosol Med. 19:301-313. Doi:10.1089/jam.2006.19.301

Schroeter JD, Kimbell JS, Anderson ME, Dorman DC. 2006b. Use of a pharmacokinetic-driven computational fluid dynamics model to predict nasal extraction of hydrogen sulfide in rats and humans. Toxicol Sci. 94:359-367. Doi:10.1093/toxsci/kfl112.

Schroeter JD, Garcia GJM, Kimbell JS. 2010. A computational fluid dynamics approach to assess interhuman variability in hydrogen sulfide nasal dosimetry. Inhal Tox. 22:277-286. Doi:10.3109/08958370903278077.

Schwab RJ, Gefter WB, Hoffman EA, Gupta KB, Pack AI. 1993. Dynamic upper airway imaging during awake respiration in normal subjects and patients with sleep disordered breathing. Am Rev Respir Dis. 148:1385-400. Doi:10.1164/ajrccm/148.5.1385.

Shapiro J, White NA, Schlafer DH, Rowland GN. 1979. Hypertrophic ossification of the laryngeal cartilages of a horse. J Eq Med Surg. 3:370-374.

Sittitavornwong S, Waite PD, Shih AM, Cheng GC, Koomullil R, Ito Y, Cure JK, Harding SM, Litaker M. 2013. Computational fluid dynamic analysis of the posterior airway space after maxillomandibular advancement for obstructive sleep apnea syndrome. J Oral Maxillofac Surg.71:1397-1405. Doi:10.1016/j.joms.2013.02.022.

Speirs VC. 1986. Partial arytenoidectomy in horses. Vet Surg. 15:316. Doi:10.1111/j.1532-950X.1986.tb00234.x.

Speirs VC. 1972. Abductor muscle prostheses in the treatment of laryngeal hemiplegia in the horse. A. Aust. Vet J. 48:251-254. Doi:10.1111/j.1751-0813.1972.tb05148.x

Strand E, Martin GS, Haynes PF, McClure JR, Vice JD. 2000. Career racing performance in Thoroughbreds treated with prosthetic laryngoplasty for laryngeal neuropathy: 52 cases (1981-1989). J Am Vet Med Assoc. 217:1689-1696. Doi:10.2460/javma.2000.217.1689

Strand E, Fjordbakk CT, Sundberg K, Spangen L, Lunde H, Hanche-Olsen S. 2012. Relative prevalence of upper respiratory tract obstructive disorders in two breeds of harness racehorses (185 cases: 1998-2006). Eq Vet J. 44:518-523. Doi:10.1111/j.2042-3306.2011.00517.x.

Sung SJ, Jeong SJ, Yu YS, Hwang CJ, Pae EK. 2006. Customized three-dimensional computational fluid dynamics simulation of the upper airway of obstructive sleep apnea. Angle Orthod. 76:791-799. Doi:10.1043/0003-3219(2006)076[0791:CTCFDS]2.0.CO;2.

Sutton PA, Hornby ST, Vimalachandran, McNally S. 2015. Instinct, intuition and surgical decision-making. Bulletin. 97:345-347. Doi: 10.1308/rcsbull.2015.345

Taherian S, Rahai H, Gomez B, Waddington T, Mazdisnian F. 2017. Computational fluid dynamics evaluation of excessive dynamic airway collapse. Clin Biomech. 50:145-153. Doi:10.1016/j.clinbiomech.2017.10.018.

Tan RHH, Dowling BA, Dart AJ. 2005. High-speed treadmill videoendoscopic examination of the upper respiratory tract in the horse: The result of 291 clinical cases. Vet J. 170:243-248. Doi:10.1016/j.tvjl.2004.06.011.

Tatarniuk D, Carmalt JL, Allen AL. 2009. Induration of the cricoid cartilage complicates prosthetic laryngoplasty in a horse. Vet Surg. 39:128-130. Doi:10.1111/j.1532-950X.2009.00575.x

Tate LP, Little EDE, Bishop BJ. 1993. Experimental and clinical evaluation of Nd:YAG ablation of the laryngeal ventricle and laryngoplasty in horses with left laryngeal hemiplegia. J Clin Laser Med Surg. 11:139-144. Doi:10.1089/clm.1993.11.139

Thomas DP, Freign GF. 1981. Cardiorespiratory and metabolic responses to treadmill exercise in the horse. J Applied Physiol. 50:864-868. Doi:10.1152/jappl.1981.50.4.864

Tucker ML, Sumner D, Reinink S, Wilson DG, Carmalt JL. 2019. Ex vivo evaluation of laryngoplasty, arytenoid corniculectomy, and partial arytenoidectomy for equine recurrent laryngeal neuropathy. Am J Vet Res. 80:1136–1143. Doi:10.2460/ajvr.80.12.1136

Tucker ML, Wilson DG, Reinink SK, Carmalt JL. 2022. Computed tomographic geometrical analysis of surgical treatments for equine recurrent laryngeal neuropathy. Am J Vet Res. 83: 443-449. Doi: 10.2460/ajvr.21.03.0040

Tulleners EP, Harrison IW, Raker CW. 1988a. Management of arytenoid chondropathy and failed laryngoplasty in horses: 75 cases (1979-1985). J Am Vet Med Assoc. 192:670-675. PMID:3372322

Tulleners EP, Harrison IW, Mann P, Raker CW. 1988b. Partial arytenoidectomy in the horse with and without mucosal closure. Vet Surg. 17:252-257. Doi:10.1111/j.1532-950x.1988.tb01009.x

Tulloch, LK, Piercy RJ, Troester S, Carruthers R, Tast V, Grimes L, Perkins JD. 2014. Use of laryngeal computed tomography for noninvasive assessment of laryngeal function in horses with recurrent laryngeal neuropathy In: Clinical Research Abstracts of the British Equine Veterinary Association Congress 2014. Eq Vet J. 46:17. Doi:10.1111/evj.12323_38.

Versteeg HK, Malalasekara W. 2007. An introduction to computational fluid dynamics: the finite volume method, second edition. Essex: Pearson Education Limited.

Vinchurkar S, De Backer L, Vos W, Van Holsbeke C, De Backer J, De Backer W. 2012. A case series on lung deposition analysis of inhaled medication using functional imaging based computational fluid dynamics in asthmatic patients: affect of upper airway morphology and comparison with in vivo data. Inhal. Toxicol. 24:81-88. Doi:10.3109/08958378.2011.644351.

Vollmer J, Mencl R, Muller H. 1999. Improved Laplacian smoothing of noisy surface meshes. Eurographics. 18:131-139. Doi: 10.1111/1467-8659.00334

Weber JM, Dobson GP, Parkhouse WS, Wheeldon D, Harman JC, Snow DH, Hochachka PW. 1987. Cardiac output and oxygen consumption in exercising Thoroughbred horses. Am J Physiol. 253:R890-895.

Weishaupt MA, Kastner BR, Feige K, Schmid M, Auer JA. 1998. Airflow characteristics and alteration of stride-respiration coupling in a Trakehner stallion with intermittent epiglottic entrapment. Eq Vet Ed. 10:172-176. Doi:10.1111/j.2042-3292.1998.tb00873.x

White NA, Blackwell RB. 1980. Partial arytenoidectomy in the horse. Vet Surg. 9:5–12.

Williams JW, Pascoe JR, Meagher DM, Hornof WJ. 1990a. Effects of left recurrent laryngeal neurectomy, prosthetic laryngoplasty, and subtotal arytenoidectomy on upper airway pressure during maximal exertion. Vet Surg. 19:136–141. Doi:10.1111/j.1532-950x.1990.tb01155.x

Williams JW, Meagher DM, Pascoe JR, Hornof WJ. 1990b. Upper airway function during maximal exercise in horses with obstructive airway lesions: effect of surgical treatment. Vet Surg. 19:142–147. Doi:10.1111/j.1532-950x.1990.tb01156.x

Willsallen, H, Heller J, Kark L, Hillbert BJ. 2015. In vitro mechanical testing of braided polyurethane elastic fiber and braided polyester for equine laryngoplasty. Vet Surg. 44:233-230. Doi: 10.1111/j.1532-950X.2014.12184.x.

Witte TH, Mohammed HO, Radcliffe CH, Hackett RP, Ducharme NG. 2009. Racing performance after combined prosthetic laryngoplasty and ipsilateral ventriculocordectomy or partial arytenoidectomy: 135 Thoroughbred racehorses competing at less than 2400m (1997-2007). Eq Vet J. 41:70-75. Doi: 10.2746/042516408X343163.

Witte TH, Cheetham J, Rawlinson JJ, Soderholm LV, Ducharme NG. 2010a. Can J Vet Res. 74:299-304. PMID: 21197230

Witte TH, Cheetham J, Solderham LV, Mitchell LM. Ducharme NG. 2010b. Equine laryngoplasty sutures undergo increased loading during coughing and swallowing. Vet Surg. 39:949–956. PMID: 21197230

Wootton DM, Sin S, Lou H, Yazdani A, McDonough JM, Wagsul ME, Isasi CR Arens R. 2016. Computational fluid dynamics upper airway effective compliance, critical closing pressure, and obstructive sleep apnea severity in obese adolescent girls. J Appl Physiol. 121:925-931. Doi:10.1152/japplphysiol.00190.2016.

Xu C, Sin SH, McDonough JM, Udupa JK, Guez A, Arens R, Wootton DM. 2006. Computational fluid dynamics modeling of the upper airway of children with obstructive sleep apnea syndrome in steady flow. J Biomech. 39:2043-2054. Doi:10.1016/j.jbiomech.2005.06.021.

Zhang Z, Chhetri. 2019. Effect of changes in medial surface shape on voice production in excised human larynges. J Acoust Soc Am. 146: EL412-417. Doi: 10.1121/1.5131044.

Zhao M, Barber T, Cistulli P, Sutherland K, Rosengarten G. 2013. Computational fluid dynamics for the assessment of upper airway response to oral appliance treatment in obstructive sleep apnea. J Biomech. 46:142-150. Doi:10.1016/j.jbiomech.2012.10.033.

APPENDIX A: ARTICLE PERMISSIONS

Chapter 2:

DIANE A FAGEN, LIBRARIAN / COPYRIGHT/PERMISSIONS

AMERICAN VETERINARY MEDICAL ASSOCIATION
1931 N MEACHAM RD - SCHAUMBURG, IL 60173
P: 847-285-6770 F: 847-925-9329 E: DFAGEN@AVMA.ORG

Monday 21 February 2022

Michelle L Tucker, DVM, DACVS-LA
University of Saskatchewan
Saskatoon, Saskatchewan

Dear Dr Tucker:

Thank you for your request, which I have reproduced, below, highlighted in yellow:

I am writing to inquire about the use of an article to be published in *AJVR* . I will use the article in my Ph.D. dissertation with the university I am attending:

Tucker, ML Ex vivo evaluation of arytenoid corniculectomy, compared with three other airway interventions, performed on cadaveric equine larynges with simulated recurrent laryngeal neuropathy. *American Journal of Veterinary Research (AJVR)* 2019; 80:1136

Permission is granted to reproduce the article in print and electronically provided the bibliographic citation will appear in the reference list at the end of the dissertation or in the footnotes (depending on the citation format you use). Please note that the article is reproduced with the permission of the American Veterinary Medical Association.

Best regards,

AMERICAN VETERINARY MEDICAL ASSOCIATION

Diane A Fagen, Copyright & Permissions
Distinguished Practitioner (Veterinary Medicine) – National Academies of Practice

Chapter 3:

DIANE A FAGEN, LIBRARIAN / COPYRIGHT/PERMISSIONS

AMERICAN VETERINARY MEDICAL ASSOCIATION
1931 N MEACHAM RD - SCHAUMBURG, IL 60173
P: 847-285-6770 F: 847-925-9329 E: DFAGEN@AVMA.ORG

Monday 21 February 2022

Michelle L Tucker, DVM, DACVS-LA
University of Saskatchewan
Saskatoon, Saskatchewan

Dear Dr Tucker:

Thank you for your request, which I have reproduced, below, highlighted in yellow:

I am writing to inquire about the use of an article to be published in *AJVR* . I will use the article in my Ph.D. dissertation with the university I am attending:

Tucker, ML Computed tomographic geometrical analysis of surgical treatments for equine recurrent laryngeal neuropathy. *American Journal of Veterinary Research (AJVR)* 2022 Feb 8;1-7. doi: 10.2460/ajvr.21.03.0040. Online ahead of print.

Permission is granted to reproduce the article in print and electronically provided the bibliographic citation will appear in the reference list at the end of the dissertation or in the footnotes (depending on the citation format you use). Please note that the article is reproduced with the permission of the American Veterinary Medical Association.

Best regards,

AMERICAN VETERINARY MEDICAL ASSOCIATION

Diane A Fagen, Copyright & Permissions
Distinguished Practitioner (Veterinary Medicine) – National Academies of Practice